UNIVERSITY OF LONDON THESIS

Degree PhD Year 2006 Name of Author IOANNOU Kyriaki-Karolina

COPYRIGHT

This is a thesis accepted for a Higher Degree of the University of London. It is an unpublished typescript and the copyright is held by the author. All persons consulting the thesis must read and abide by the Copyright Declaration below.

COPYRIGHT DECLARATION

I recognise that the copyright of the above-described thesis rests with the author and that no quotation from it or information derived from it may be published without the prior written consent of the author.

LOAN

Theses may not be lent to individuals, but the University Library may lend a copy to approved libraries within the United Kingdom, for consultation solely on the premises of those libraries. Application should be made to: The Theses Section, University of London Library, Senate House, Malet Street, London WC1E 7HU.

REPRODUCTION

University of London theses may not be reproduced without explicit written permission from the University of London Library. Enquiries should be addressed to the Theses Section of the Library. Regulations concerning reproduction vary according to the date of acceptance of the thesis and are listed below as guidelines.

A. Before 1962. Permission granted only upon the prior written consent of the author. (The University Library will provide addresses where possible).

B. 1962 - 1974. In many cases the author has agreed to permit copying upon completion of a Copyright Declaration.

C. 1975 - 1988. Most theses may be copied upon completion of a Copyright Declaration.

D. 1989 onwards. Most theses may be copied.

This thesis comes within category D.

☐ This copy has been deposited in the Library of UCL

☐ This copy has been deposited in the University of London Library, Senate House, Malet Street, London WC1E 7HU.

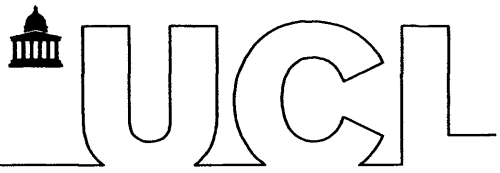

Phase Inversion Phenomenon in Horizontal Dispersed Oil/Water Pipeline Flows

by

Karolina Ioannou

A thesis submitted for the degree of Doctor of Philosophy of the University of London

University College London
WC1E 7JE

October 2006

ProQuest LLC
789 East Eisenhower Parkway
P.O. Box 1346
Ann Arbor, MI 48106-1346

To Jason,
who left us too early

To my family,
for always being there...

Abstract

This thesis reports on experimental and theoretical investigations relevant to the understanding of the phenomenon of phase inversion and its effect on pressure drop during dispersed flow of two immiscible liquids in horizontal pipelines.

Experimental studies of phase inversion and associated phenomena were carried out in the liquid flow facility in the Department of Chemical Engineering at University College London (UCL), and at the Norwegian University of Science and Technology, Trondheim, Norway (NTNU). Detailed local conductivity measurements have been obtained at UCL (using conductivity ring probes, a local needle conductivity probe and a flush probe mounted on the pipe wall), which revealed phase continuity at different locations in the pipe cross section as the system approaches phase inversion and after it. In both systems, pressure gradient was measured and phase inversion identification measurements along the pipe were enabled with the use of the conductivity ring probes. A new probe that enables phase and drop size distribution measurements was designed and developed for use at UCL.

At the UCL facility, velocity ratio of the two phases, the dispersed phase droplet velocity profiles, and phase distribution at the pipe cross section and droplet chord length were also measured. This revealed a significant increase in the dispersed drop size at inversion point. The results also enabled the equal surface energy criterion validation, based on droplet size considerations. The velocity ratio of the two phases was found to have a higher value than unity at all conditions studied, while inversion

from water to oil continuous mixtures results in a decrease in its value. The drop velocity was also becoming lower with increasing dispersed phase fraction and it was found to be affected by the presence of high dispersed phase concentrations.

Various parameters and their effect on inversion were studied. Three types of oil (with viscosities of 1.7, 5.5 and 11 mPa s) were used while different pipe diameters and materials were tested (namely, acrylic with 32 and 60 mm ID, stainless steel with 38 and 60 mm ID and an epoxy coated stainless steel pipe with 60 mm ID). Mixture velocities from 2.5 m/s to 6.2 m/s (depending on the test section) were used, selected so that the mixture away from the inversion was dispersed. Also, two experimental routes were followed, starting from oil continuous and water continuous dispersions to investigate the existence of a possible hysteresis at the occurrence of inversion. It was found that phase inversion is accompanied with significant changes in pressure gradient; it was preceded by a sharp peak when the less viscous oils were used, while no peak was recorded with the use of the more viscous oil. An ambivalent range was seen for the less viscous oil, possibly related to the creation of secondary dispersions.

A mechanistic model that describes the layered structure of the flow during inversion (detected experimentally) was proposed for the prediction of flow characteristics and pressure gradient at the region of inversion. It is suggested that inversion starts when a thin layer of the dispersed phase (that is to become continuous) forms at the top or the bottom of the pipe. A clear layer of the continuous phase may also exist at the bottom or the top of the pipe respectively. Two or three layer models were used for these configurations. Results showed that the two layer model predicts pressure gradient and layer thickness well. The homogeneous model was found to agree well with the experimental results, especially in the water continuous region when considerations for the mixture velocity. The friction factor was modified to compensate for the appearance of the drag reduction in the conducted measurements.

In addition, a commercial feasibility study has been carried out which confirmed the considerable and immediate potential for the commercialisation of the impedance probe developed within this research for phase and drop size distribution measurements.

Acknowledgements

I wish to express my gratitude to my supervisor at University College London Dr Panagiota Angeli for giving me the opportunity to learn from her knowledge and expertise. Her personal sincere involvement, the commitment and genuine enthusiasm in the project made it possible for me to complete it. More significantly, I would like to express my appreciation to her for being there always to provide her advice and guidance in my work, as well as show her personal concern in all aspects of my everyday life. It has been a great learning experience throughout.

I would also like to thank Prof. Ole Jørgen Nydal for giving me the great opportunity of conducting experiments in the Department of Energy and Process Technology at NTNU, Norway. With his experience related to multiphase flow his contribution was invaluable. I would particularly like to thank him however, for making me feel so welcome in their premises.

I would also like to thank Dr Lee Rhyne, whose knowledge has been a source of learning for me. His enthusiasm for the project has been inspiring and his help encouraging, while his suggestions when proof-reading this work invaluable.

Thanks to the members of the electronic workshop, Sarah, Martyn and Marc, and especially our technicians, Martin, John, Alan and John, not only for being such a great and always available help with all practical problems regarding my experimental

work, but mainly for being such great people and enjoyable company. I would also like to thank the technicians at NTNU, Knut and Erling.

Thanks go to the LBS project group for the great collaboration and excellent outcome.

Special thanks to my wonderful colleagues Jonathon, Hu Bin and Talal for always being there to lend me a hand and help out. I really enjoyed working with them! To Jason, special thanks for being the person he was, especially for his admirable optimism and for giving us all a great lesson for life with his -uneven- fight. Jason, I will always look at the bright side of life, as you used to say.

I would like to thank all the people in the department for making it such an enjoyable place to work in and for contributing in their way to the completion of this project: Sarah, for being so patient with me, Sun Jia, Cristina, Andrea, Kit, Nan Shao, Max, Prim, Carlos, Wael, for sharing his knowledge of Mathematica with me, Marta, Giovanna, Marcello, Paolo, Damiano and Tim for his knowledge in pumps, but also Olav, Gael and Monika at NTNU. Best of luck to you all!

On a more personal level, I wish to express my special thanks to Evangelia, Emily and Lia for their unconditional support and friendship throughout this trying time. Thanks for the wonderful time we spent together.

Last but definitely not least, to my beautiful family for always being there to support me, to advise me and to love me...

Contents

List of figures

Chapter 1

Chapter 2

Chapter 3

Chapter 4

Chapter 5

Chapter 6

Chapter 7

Chapter 8

Chapter 9

Appendix A

Appendix B

Appendix C

Appendix E

List of tables

Chapter 2

Chapter 3

Chapter 5

Chapter 6

Chapter 7

Chapter 8

Appendix A

Appendix E

Nomenclature

b	parameter related to k_c and $\overline{k}_c$ (Equation 2.27)
$Birth(d,x,t)$	the rate of number of drop increase per unit volume
c	bending stress coefficient
C'	constant in Equation 2.11.
C''	constant in Equation 7.19
$[C]$	the intrinsic dispersion viscosity
C	parameter in Blasius equation
$\tilde{C}_H$	constant in BRAUNER
d	parameter related to k_c and $\overline{k}_c$ (Equation 2.27)
D	pipe diameter (m)
$Death(d,x,t)$	the rate of number of drop decrease per unit volume
D_{32}	Sauter mean drop diameter (m)
D_H	hydraulic diameter (m)
D_{max}	maximun drop size diameter (m)
$(\tilde{D}_{max})_\epsilon$	dimensionless maximal drop size in a dense dispersion (-)
D_I	impeller diameter (m)
$D(L)$	the number density of drops with diameter D
f	wall friction factor

f_d	modified friction factor by Rozentsvaig (1982)
$f_{effective}$	effective volume fraction of the dispersed phase
Fr_I	Impeller Froude number $Fr_I = N^2 D_I^3 / g$
g	acceleration of gravity
G_E	electrical conductance of a pipe full with liquid
G^M	Gibbs free energy of the system per unit volume
G_{int}	Gibbs free energy of the emulsion
H_L	liquid hold up (-)
j_f	mixture velocity (m/s)
K	constant in Equation 2.3
k	Mooney's crowding factor ($1.35 < k < 1.91$)
k_B	Boltzmann constant
k_1	empirical parameter in Equation 2.13 (reflect the contact perimeter of the wall with the liquids
k_2	empirical parameter in Equation 2.13 (accounts for the flow regime in each of the phases)
k_1'	constant in Equations 2.21 and 2.22
k_2'	turbulence damping factor (Equation 2.21)
k_c	mean elasticity moduli
$\overline{k_c}$	Gaussian elasticity moduli
k_d	constant ($k_d = 1.5-5$), $d_{32} = d_{max} / k_d$
L_{32}	Sauter mean chord length (m)
m'	empirical constant in Equation 2.21
n	parameter from Blasius equation
n_i	concentration of component i
n'	constant in Equations 2.21 and 2.22 (usually equal to 0.6)
N_d	number of droplets

$n(d,x,t)$	the number of drops of size d per unit volume at axial position x and at time t
N	agitation speed (revolutions per second, s^{-1})
N_{Ca}	the capillary number ($N_{Ca} = (\mu_c \dot{\gamma} R)/\sigma$)
P	rate of energy input ($Kgm^{-3}s^{-2}$)
P_{esc}	escape probability of the secondary dispersion fraction
p'	empirical constant in Equation 2.22
$P(L)$	number density of chord lengths of size L
R	radius of the droplets/particles
Re	Reynolds number ($Re_I = \rho_m N D_I^2 / \mu_c$ in stirred vessels)
s	solid surface area per unit volume (in smooth pipes $s = 4/D$) (m-1)
t_{drain}	film drainage time (s)
$t_{contact}$	contact time between the colliding drops (s).
W	width of ambivalent range
We	Weber number
We_I	Weber impeller number ($We_I = \rho_c N^2 D_I^3 / \sigma$)
T	Temperature (K)
T_K	293.15K
t_c	inner droplet circulation time (s)
U_{ws}	water superficial velocity (ms-1)
U	velocity (m/s)
y	Concentration function constant ($0.5 < y < 1.125$ in pipe flows)

GREEK LETTERS

α_{cr}	volume of the critical region (defined as the volume fraction of the droplet outside the critical streamline where escape of the inner droplet is enabled)
α_g	parameter in Equation 7.2.
α	motionless mixer area per unit volume (m2/m3)
α_d	radius of the droplets

α'	constant in Equation 2.2
$\dot{\gamma}$	shear rate
γ	proportionality factor in Equation 7.21
δ	electrical double layer thickness
ΔP	pressure drop (Pa/m)
$\Delta\rho$	density difference between the dispersed and continuous phases
ε_d	dispersed phase holdup
ε_w^I	critical water fraction at phase inversion
ε_o^I	critical oil fraction at phase inversion
η_o	oil viscosity (mPas)
η_r	water viscocity, η_r = 1 mPas
θ	liquid-solid contact angle (degrees)
λ	coalescence efficiency
λ_i	chemical potential
μ	Liquid viscosity (mPa s)
μ_r	water viscosity (= 1 mPas)
$\tilde{\nu}$	kinematic viscosity ratio, $\tilde{\nu} = \nu_o / \nu_w$
ν_w	molecular volume of the continuous medium
$\tilde{\rho}$	density ratio, $\tilde{\rho} = \rho_o / \rho_w$
ρ	density (kgm^{-3})
σ	oil-water interfacial tension (mNm^{-1})
φ	dispersed *in situ* holdup
φ_m	maximum packing of the dispersed phase
φ_o^I	organic phase hold up at inversion
φ_o'	asymptotic phase inversion organic hold up
φ_i	included volume fraction

$\varphi_{effective}$	effective volume fraction of the dispersed phase

SUBSCRIPTS

c	continuous phase
d	dispersed phase
i	interface
K	measured value in Eq 3.1
L	liquid value
m	mixture
o	oil phase
s	superficial
w	water phase

Chapter 1

Introduction

1.1 BACKGROUND

Multiphase flow is defined as the simultaneous flow of two or more phases (gas, solid, and liquid). These flows are encountered in a diverse range of applications, such as in petroleum, chemical, nuclear or geothermal industries. Therefore, the study of multiphase flow is pertinent to the design and operation of industrial processes and of equipment associated with these industries.

Even though there is substantially less amount of work on two phase liquid-liquid flow and most particularly on oil-water flow in pipelines, the applications in industries are wide, especially in the oil field, where water is often produced together with crude oil from the production wells.

When oil is produced from a reservoir, a well is drilled through the ground, vertically at first, then following any slope before it enters the reservoir. The well will normally produce single-phase oil in the first period of its lifetime. At later time, water will often be produced in addition to crude oil. Water production tends to increase as the well ages further. The well though might be economically viable to operate even with extremely high percentages of water production that can reach 98% or more.

The presence of water will obviously influence the transport of oil from the reservoir to the processing unit. Most times wells are connected to a manifold through a pipe called a subsea tie-back. Then the main production and test lines go from the manifold to the producing facility. Often the producing facility, where the separators and compressors are located, is several miles away, sometimes tens of miles away. The more wells can be tied back to a single (expensive) production facility, the more economic the facility gets. Hence, there is a push for longer production lines. An example offshore field design is shown in Figure 1.1. Once the oil is separated from the water and gas, it is moved from the production facility to the refinery, sometimes by tanker, often by an export pipeline. Again, the export pipelines (that might consist of a mixture of oil and water) can be tens of miles long.

Pipeline pressure drop impacts the amount of oil that can be recovered from a reservoir using its pressure (big economic changes with small changes in abandonment pressure). This is the parameter that also impacts the size of the pumps needed to transport the oil, through the production lines (or through the export pipeline).

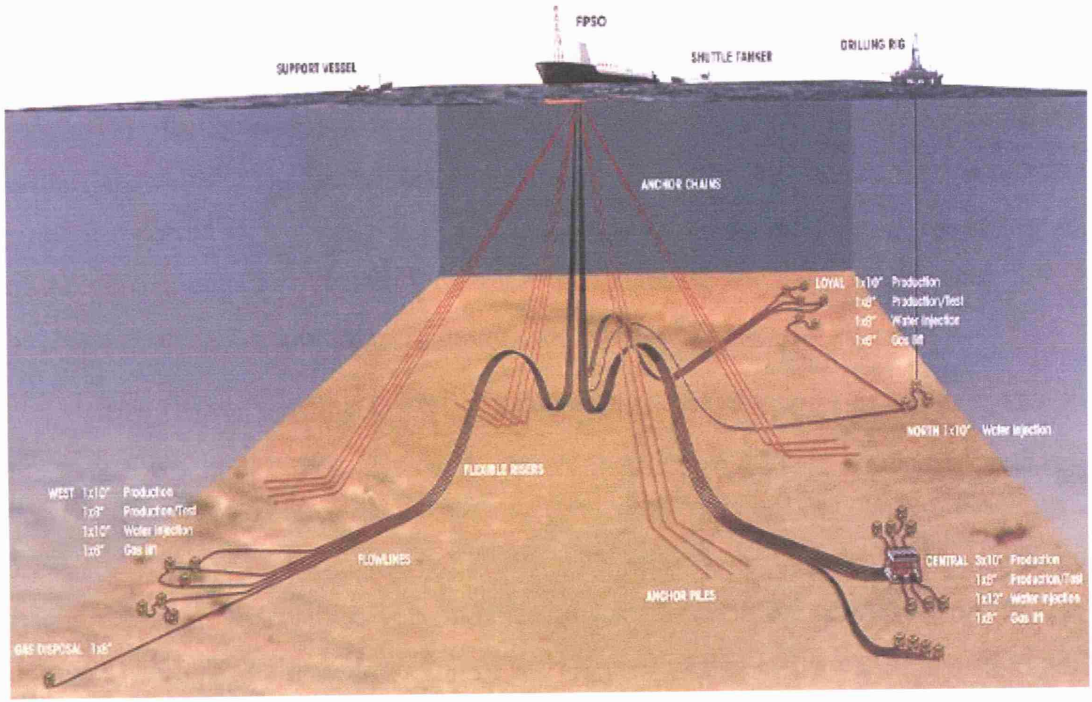

Figure 1.1 Typical Floating Production, Storage & Offtake (FPSO) facility.

The pressure drop thus impacts the distance that can be traversed from wellhead to production facility. So an accurate prediction of viscosity for the entire life of the field (entire viscosity curve as a function of water cut) is *essential* to the economics of the system (e.g. number of production facilities per field, number of manifolds). However, transporting the two phases (oil/water) together is a rather complicated task; the flow mixture will have different characteristics and behaviour than single phase oil. Depending on mixture velocity and water cut, several flow configurations, known as *flow patterns* or flow regimes, will form. The combination of flow patterns and mixture viscosities result in pressure drops that are not predictable by simple mixing rules.

1.2 THE PHASE INVERSION PHENOMENON

When Reynolds number in a two-phase flow mixture is sufficiently high, dispersions of one phase into the other can occur that might lead to *phase inversion*, which is defined as a change in the continuity of the mixture from one phase being continuous to the other. At low water cuts, water will be dispersed as droplets in the continuous oil phase (condition abbreviated as w/o); as the amount of water increases the system will change to a dispersion of oil droplets in a water continuous phase (o/w). The dispersed phase fraction where the continuity of the system changes is called *phase inversion point*. The occurrence of inversion, and thus the inversion point, is reported to be a function of several parameters, such as the physical properties of the oil (i.e. density, viscosity), the pipe wall material and the pipe diameter, and it has been related to abrupt changes in the rheological properties of the system.

The viscosity of the mixture at the phase inversion point has been found to increase compared to the viscosity of the individual liquids (Pal, 1993), often described through exponential correlations (typical correlations are these of Brinkman, 1952, or Krieger and Dougherty, 1959) with respect to dispersed phase volume fraction. Mixture viscosity is very important in determining the pressure drop through a pipe. Therefore, the *understanding* of the parameters that affect phase inversion and the associated pressure drop and their accurate *prediction* is of paramount importance especially to petrochemical industries where important cost savings can be achieved.

Most of the available information on the phenomenon originates from work in stirred vessels. This revealed that for two immiscible liquids, there is a range of volume fractions, the *ambivalent range*, over which either phase can be the continuous one (Selker and Sleicher, 1965; Luhning and Sawistowski, 1971; McClarey and Mansoori, 1978; Arashmid and Jeffreys, 1980; Davies, 1992; Efthimiadou and Moore, 1994). For a particular system, the exact phase inversion point within the ambivalent range will depend on a number of parameters, such as fluids properties, operational (i.e. impeller speed) and initial conditions (i.e. position of impeller, aqueous or organic continuous initial dispersion) and wetting characteristics of the vessel material.

It should be also noted that liquid-liquid dispersions are usually formed with application of external energy. Depending on their behaviour after the energy supply is discontinued, they can be divided into stable dispersions or emulsions usually formed with the use of surfactants and unstable dispersions. In the latter case, the phases start separating as soon as the supply of external energy is stopped. These are the systems considered in the current work.

Despite the extensive work that has been conducted in stirred vessels regarding phase inversion, the actual mechanism of phase inversion is not yet understood. Only limited studies have been conducted and to date, the phase inversion point cannot be predicted.

1.3 OBJECTIVES

The work presented in this thesis reports on studies of the phase inversion phenomenon in oil/water dense dispersions in horizontal pipelines. Experimental work has been conducted in the Department of Chemical Engineering at University College London (UCL) and at the Norwegian University of Science and Technology, Trondheim, Norway (NTNU). The main purpose is an improved understanding of phase inversion: to elucidate how the phenomenon is occurring and to investigate the parameters that affect phase inversion in pipelines. To this end, a significant number of experiments were conducted, while theoretical investigations were undertaken in the light of the experimental findings.

OBJECTIVES OF THE EXPERIMENTAL WORK

- To investigate phase inversion at the pipe cross sectional area and the whole length of the pipe by using a variety of conductivity probes in order to better illustrate phase continuity changes during inversion.
- To conduct detailed flow analysis around the phase inversion point by investigating a number of parameters such as pressure gradient, velocity ratio, drop size, phase distribution.
- To develop new tools for the measurement of the local parameters such as drop size and local phase fractions in highly dispersed and dense systems.

OBJECTIVES OF THE THEORETICAL WORK

- To validate existing models regarding the prediction of the phase inversion point and the ambivalent range.
- To develop a new mechanistic model to predict pressure drop during phase inversion which takes into account the layered structure of the flow that the experimental work suggests exists.

1.4 THESIS STRUCTURE

This thesis is divided into nine chapters. After Introduction, the most important features on liquid-liquid two phase flow are reviewed in Chapter 2. The main focus in Chapter 2 is on previous research regarding the phenomenon of phase inversion both in stirred vessels and in pipe flows, and on the suggested mechanisms for the occurrence of the phenomenon and the existing predictive models. The phenomenon of drag reduction in liquid-liquid dispersions is also introduced.

Chapter 3 focuses on the description of the experimental facilities and instrumentation used. Two experimental facilities were used; one in the Chemical Engineering Department at UCL and the other at NTNU. Emphasis is placed on instrumentation used in both facilities, while the experimental methods are also described in detail. In Chapter 4 the occurrence of inversion is discussed. The interest is on the identification of inversion. More specifically, the conductivity experiments

are described and the obtained results regarding the change of conductivity in the pipe cross sectional area at the point of inversion are presented, along with the observed instability at the point of the inversion and the effects this may cause to the operational system. Based on the experimental findings a mechanism of phase inversion is then introduced.

Chapter 5 is a detailed flow analysis for dense oil/water dispersions in a horizontal stainless steel pipe; parameters such as velocity ratio, phase and drop size distributions are studied pre- and post- inversion at different mixture velocities. Theoretical models for inversion prediction that involve a droplet size parameter were compared against experimental data.

Chapter 6 describes experimental results regarding the effect of various parameters on the occurrence of phase inversion and the inversion point. Pressure gradient was measured for different mixture velocities, pipe material of construction and pipe diameter, and fluid properties. Two experimental routes were investigated: starting from oil continuous or from water continuous mixtures and slowly decreasing oil or water fraction respectively, while keeping the mixture velocity constant. These could reveal any hysteresis effects (ambivalent range) on phase inversion. Empirical correlations regarding the prediction of phase inversion point were compared with the experimental results.

Chapter 7 discusses the role of emulsion viscosity on pressure gradient prediction using the homogeneous model for oil/water dispersions. These considerations combined with the conductivity results are used to construct a mechanistic model for the prediction of pressure drop at/around the inversion point in horizontal pipes by taking a layered structure into consideration.

Reported in Chapter 8 is a commercial feasibility study to assess the business opportunity for the impedance probe developed in this study that can obtain phase and drop size distribution. The options for the commercial application especially for the oil industry and academia were studied while other markets were considered as well.

Conclusions and recommendations are summarized in Chapter 9.

Chapter 2

Literature review

2.1 OVERVIEW

This chapter presents a summary of the significant developments in the study of liquid-liquid pipeline flow (Section 2.2) and those of the phenomenon of phase inversion (Section 2.4). More specifically, liquid-liquid studies and the published flow pattern maps are reviewed in detail in Section 2.2.1. The main flow patterns are then briefly presented in turn in Sections 2.2.2 (Stratified flow), 2.2.3 (Dual Continuous flow) and 2.2.4 (Dispersed flow). Available literature on drag reduction in liquid-liquid dispersions in pipelines without additives is discussed in Section 2.3, since the drag reduction phenomenon was observed in most experiments conducted in the present study. In Section 2.4 the phase inversion phenomenon is introduced; definitions regarding change of continuity in the system can be found in Section 2.4.1. Separate discussion is conducted regarding the ambivalent range, defined as the range of volumes over which either of the two immiscible phases can be the continuous one, in Section 2.4.3. Summarised in Section 2.4.4 is the literature regarding the parameters that have been reported to affect phase inversion, while correlations and methods that can be used as predictive tools are categorized and presented in Section 2.4.5. Finally, the two prevailing theories suggested related to the mechanism of phase inversion are

discussed in turn in Section 2.4.6, including both thermodynamical and kinetic approaches.

2.2 LIQUID-LIQUID STUDIES

Liquid-liquid flow can occur in many chemical industries (namely food industry, pharmaceutical industry, cosmetics etc.), and it is also prevalent in petrochemical industry, where oil and water are often produced together from an oil well or transported together onshore from offshore facilities (Russell and Charles, 1959). More often, this is a necessity imposed by deep water oil fields with long tie-backs to production facilities. During co-current liquid–liquid flow in a pipe, deformable interfaces can acquire a variety of characteristic distributions, known as *flow patterns* (or *flow regimes*). The results of investigations of the two phase flow in horizontal pipes (Russell *et al.*, 1959; Charles *et al.*, 1961; Guzhov *et al.*, 1973; Oglesby, 1979; Arirachakaran *et al.*, 1989; Brauner and Maron, 1992; Nädler and Mewes, 1995a&b; Trallero, 1995; Angeli, 1996; Soleimani, 1999; Lovick and Angeli, 2004) indicate that pressure drop and slip in pipeline flow strongly depend on the flow regime (i.e. the distribution of the two liquids through the pipe cross sectional area). It is therefore necessary to understand how the different flow patterns form, so that accurate predictions regarding the related pressure drop or associated phenomena can be made. Even though the main focus in multiphase flow literature is on liquid-gas flows, the aforementioned authors attempt to understand the main underlying phenomena in liquid-liquid flows. The observed flow patterns are usually delineated in terms of areas on a graph with axes of two independent system parameters (most commonly mixture velocity vs. water velocity), yielding the *flow pattern maps.*

2.2.1 Flow pattern maps

The interest on flow pattern maps arises from the fact that each flow regime has certain hydrodynamic characteristics that can be used for more accurate modelling.

Most flow pattern classifications in literature are based on visual observations in transparent pipes. This imposes a degree of subjectivity on the experimental results and different terminology that has been used for describing similar flow patterns; thus generating a generalised flow pattern map is quite difficult, further complicated by the

fact that investigators have used different fluids and set ups (i.e. pipe diameters and materials). Furthermore, flow patterns might be dependant on the wettability of the pipes and therefore results obtained in acrylic pipes might not be valid in steel pipes.

Based on visual observations as well as a combination of a novel local impedance and a conductivity probe, Lovick and Angeli (2004) have classified oil/water flow patterns using a stainless steel pipe of 38 mm ID and a model oil of 5.5 mPa s as follows:

- *Segregated flow*, which consists of stratified flow (ST), where oil flows above water and the interface between the two liquids is smooth, and stratified wavy flow (SW), where the flow is still stratified, but the interface between the two liquids has large amplitude waves. Dual continuous flow is another classification of segregated flow and it includes any flow pattern where both phases remain continuous, but a degree of dispersion of one phase into the other exists. Guzhov *et al.* (1973) has described dual continuous flow as *an emulsion of water/oil and oil/water (o/w and w/o), a separate flow with a thick layer of emulsion at the interface with a lower layer of water and a separate flow with a thick layer of emulsion at the interface with a lower layer of dilute emulsion o/w.*
- *Dispersed flow*, where one phase is completely dispersed into the other, with either the water or the oil phase being continuous. In the water continuous flow patterns there can either be a complete oil in water dispersion (abbreviated as o/w), or a dispersion of oil in water with a layer of water flowing at the bottom of the pipe (Do/w&w). For the oil continuous flow, the possible flow patterns are a complete dispersion of water in oil (abbreviated as w/o), or a dispersion of water in oil with an oil layer on top (Dw/o&o).

Charles *et al.* (1961) were the first to observe the flow patterns that appeared during the flow of equal density water and oil (for oil 998 kgm^{-3}) in a 1 inch ID

cellulose acetate butyrate pipe. Different types of oil with viscosities of 6.29, 16.8 and 65 mPa s were used, resulting in almost identical flow patterns (with an exception of the most viscous oil that appeared to be dissimilar at high oil to water input ratios) plotted in terms of the superficial velocities of the liquids. Two of the obtained flow pattern maps are shown in Figure 2.1a. Flow pattern maps for horizontal flow of oil and water were also provided by Guzhov *et al.* (1973). Here flow patterns are depicted with respect to mixture velocity and water volume fraction as axes. The authors used a type of oil with a 21.7 mPa s viscosity and 896 kg m^{-3} density at 20°C in a 39.4 mm ID pipe.

Among other experiments, Arirachakaran *et al.* (1989) used an oil with viscosity 84 mPa s at 21°C in a 39.3 mm ID stainless steel pipe to observe flow pattern transitions. The map produced by Guzhov *et al.* (1973) was found to be quite compatible to their findings, but the transition lines were slightly different.

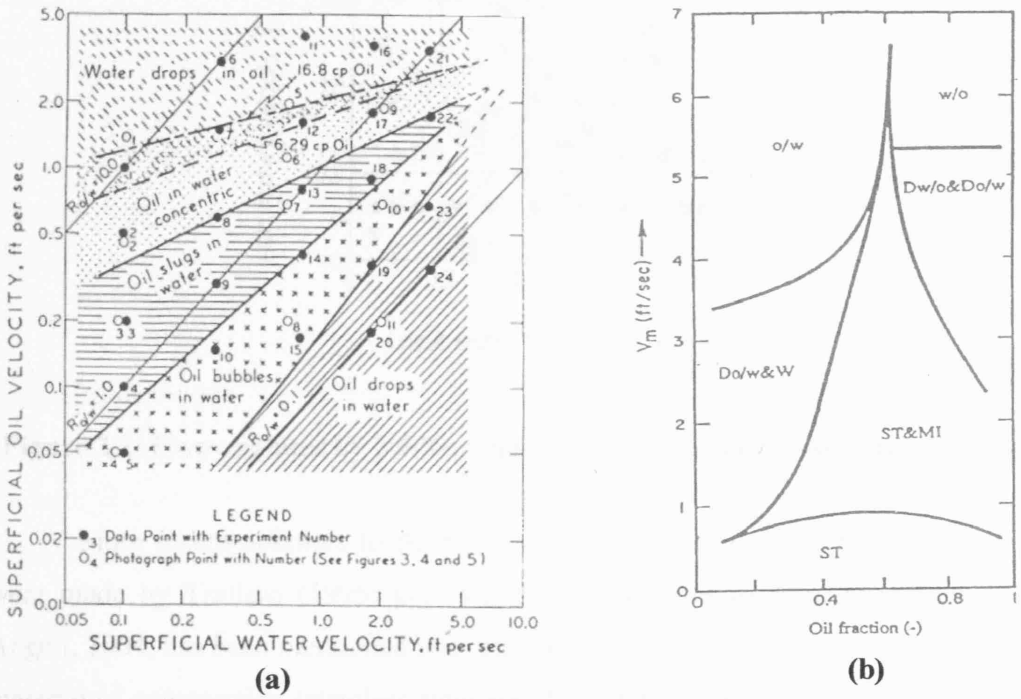

Figure 2.1 Flow patterns as identified by (a) Charles *et al.* (1961) for oils with viscosity of 6.29 and 16.8 mPa s and (b) Guzhov *et al.* (1973) for an oil with viscosity of 21.7 mPa s (reproduction from Arirachakaran *et al.*, 1989).

Nädler and Mewes (1995b) produced a map with axes of mixture velocity and input water volume fraction (Figure 2.2) for the flow of water and oil (viscosity 20 mPa s, density 841 kgm^{-3}) in a 59 mm ID Perspex pipe. By using conductivity probes they were able to observe regions where continuous layers of both phases occurred simultaneously (which is the region of dual continuous flow). These zones appeared between oil continuous and water continuous dispersed flows.

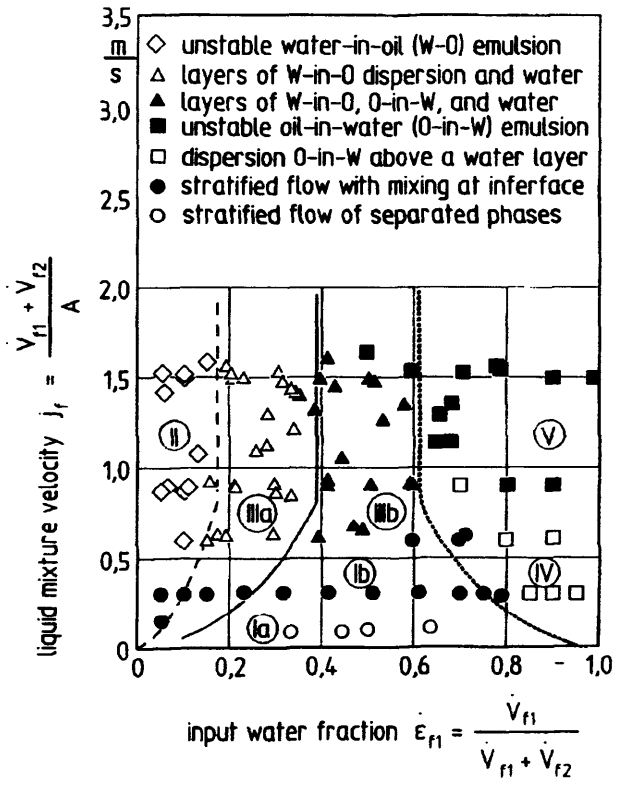

Figure 2.2 Flow regimes by Nädler and Mewes (1995b) (oil viscosity 20 mPa s).

More recent attempts to define the flow patterns in oil/water horizontal flow were made by Trallero (1995) and Angeli (1996) (categorisation from Lovick and Angeli, 2004, has been mentioned above). Angeli (1996) used two pipes with different material of construction (stainless steel and Transpalite ^{TM}) and with almost the same internal diameter (1 inch ID) and obtained results using *EXXSOL^{TM} D80* (density 800 kgm^{-3} and viscosity 1.7 mPa s) as test fluid, while Trallero (1995) used a 50 mm ID acrylic pipe with Crystex AF-M (a naphenic oil with density 884 kgm^{-3} and viscosity

29.6 mPa s). Different flow pattern classification was used and the relations between them are illustrated in Table 2.1. One of the previously reported flow patterns (dispersion of water in oil over a clean water layer Dw/o&w) was not observed by Trallero *et al.* (1997) as it was found that when water was dispersed in oil and there is a free water zone, oil is always present in forms of droplets of different sizes. The identified flow patterns are also illustrated in Figure 2.3.

Table 2.1 Relation between the classification of flow patterns by Angeli (1996) and by Trallero (1995).

ANGELI (1996) OIL VISCOSITY 1.7 MPA S	TRALLERO (1995) OIL VISCOSITY 29.6 MPA S
Stratified wavy (SW)	Stratified flow (ST)
Stratified wavy/drops (SWD)	Stratified with mixing at the interface (ST&MI)
Stratified mixed oil continuous with a layer of water drops (SM/oil)	(-)
Stratified mixed water continuous with a layer of oil drops (SM/water)	Dispersed oil in water over a water layer (Do/w&w)
Dual continuous flow (or three layer pattern, 3L)	Dispersed water in oil and oil in water (Dw/o&Do/w)
Fully dispersed or Mixed (M)	Water in oil dispersion (w/o) Oil in water dispersion (o/w)

Angeli (1996) and Angeli and Hewitt (1998) performed experiments by using both an acrylic resin (Transpalite^{TM}) and a stainless steel test section with *EXSSOL^{TM} D80* and water as test fluids. Even though same sequence of flow regimes was found for both pipe materials, substantial differences existed between the two pipes that are summarised below:

- In the stainless steel pipe the propensity for dispersion formation was greatly increased; mixed flow starts at lower mixture velocities (about 1.3 m/s) compared to the acrylic pipe (about 1.7 m/s). This was attributed to the different roughness; the higher roughness of the steel pipe (Figure 2.4a) compared to that of the acrylic (Figure 2.4b) could

result to a higher degree of turbulence and more disturbed flow patterns for the same flow velocities.

- In the acrylic pipe, oil tended to be the continuous phase for a wider range of flow conditions than in the steel pipe as oil tended to wet the acrylic more than the steel.
- Under all conditions pressure gradients were higher for the steel than the acrylic pipe for the same mixture velocity and volume fractions, the difference being greater than expected due to the difference in the wall roughness.

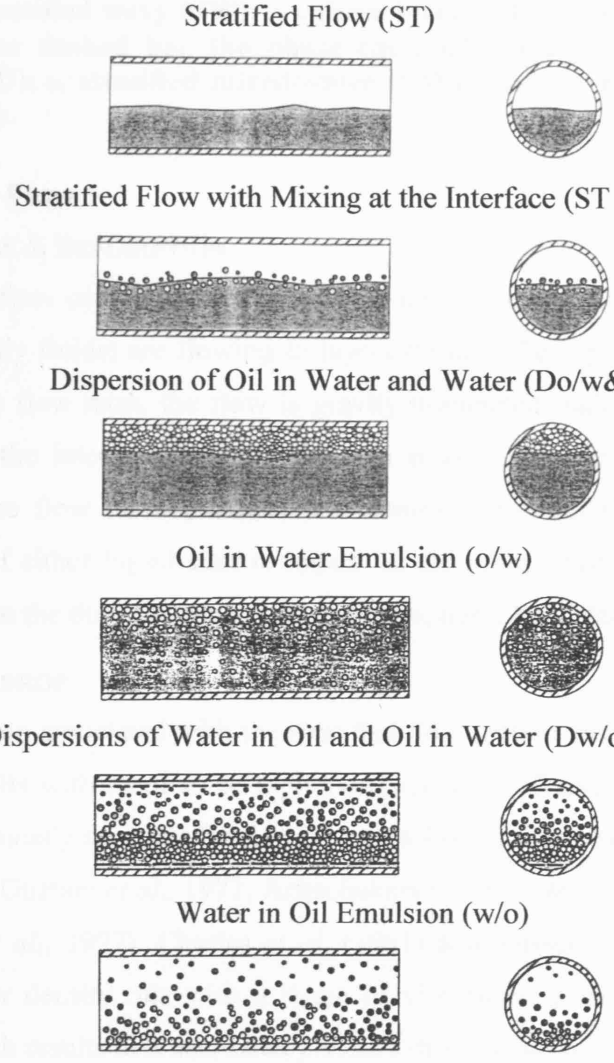

Figure 2.3 Oil-water flow regimes (Trallero, 1995).

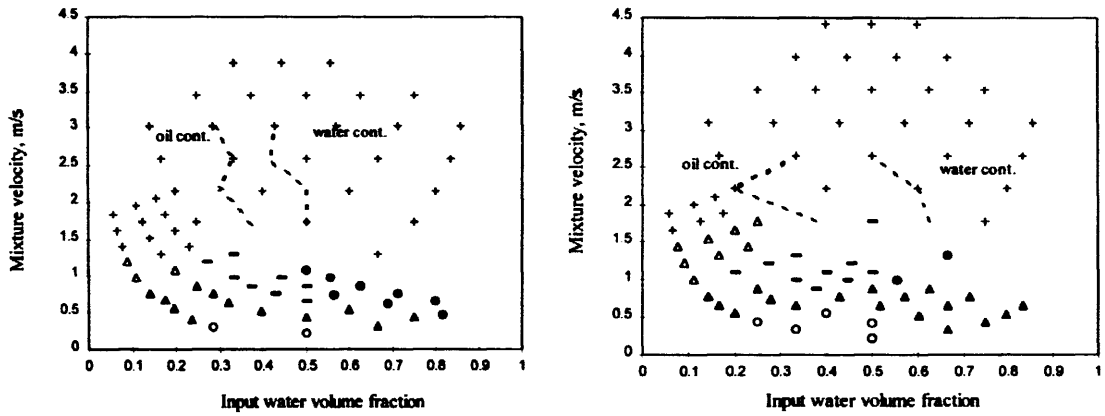

(a) Steel pipe **(b) Acrylic pipe**

Figure 2.4 Flow patterns in (a) the stainless steel test section and (b) the acrylic test section. ○, stratified wavy (SW); —, three layers (3L); △, stratified mixed/oil (SM/oil); with the dashed line the phase continuity boundaries; ▲, stratified wavy/drops (SWD); ▪, stratified mixed/water (SM/water); +, mixed (M) (Angeli and Hewitt, 2000).

2.2.2 Stratified Flow

DEFINITION & DESCRIPTION

Separated flow occurs at the lower flow rates. This is a flow regime where liquids (or generally fluids) are flowing in layers through the pipe according to their densities. At these flow rates, the flow is gravity dominated, rather than inertial. At lower flow rates the interface between the two phases is rather smooth and well defined, but as the flow rates increase, it becomes wavy. As flow rates increase further, droplets of either liquid start to appear in the other phase (entrainment) and there is transition to the dual continuous flow pattern, described later.

PRESSURE DROP

Pressure drop associated with the stratified flow pattern has been studied quite extensively. For oils with medium to high viscosity it was found that pressure drop decreases monotonically as water fraction increases from a single phase oil to a single phase water flow (Guzhov *et al.*, 1973; Arirachakaran *et al.*, 1989; Nädler and Mewes, 1995a; Trallero *et al.*, 1997). Charles *et al.* (1961) and Russell and Charles (1966) found that for low density oils with a range of viscosities, a water annulus forms around them, which results in a decreased pressure drop to that of a single phase oil at the current mixture velocity. Generally, in the laminar flow region, presence of a less

viscous phase together with a more viscous one will result in drop of the pressure gradient values (pressure gradient reduction factor greater than 10; Charles and Redberger, 1962).

2.2.3 Dual Continuous Flow

DEFINITION & DESCRIPTION

At intermediate mixture velocities a combination of both separated and dispersed flow patterns can appear, where both fluids maintain their continuity at the top and bottom of the pipe respectively to their density, while there is a dispersion of one phase into the other to varying degrees. This pattern is called *dual continuous flow* (Lovick, 2004).

The transition from stratified flow to water (or oil, depending on the phase fractions) continuous dispersed flow occurs as follows: During the early stages of the transition (stratified flow), the oil moves along the pipe above the water with a slightly wavy interface. As the velocities increase, vortices that penetrate the interfacial boundary develop at the interface (Guzhov *et al.*, 1973) due to shear forces, causing small droplets of each phase to appear in the other (onset of entrainment and the *dual continuous flow pattern*). There are distinct continuous layers of oil and water at the top and bottom of the pipe respectively but in the interface a layer of drops exists, while drops of each phase could appear within the other (Angeli, 1996). Once a droplet has formed, it is subject to buoyancy forces that tend to return it to its original phase and inertial forces which try to disperse it in the opposite phase. As flow rates increase the inertial forces increase and the dispersion of droplets throughout the pipe increases.

A generalised version of the Kelvin-Helmholtz instability equation may be able to predict the onset of droplet formation, with the instability arising from the different tangential velocity (inviscid case) or viscosity differences across the interface. The kinetic energy of motion causes a wavy disturbance on the interface to grow in amplitude, tending to mix the two fluids. The breakup of the interface can occur even for small shear velocities when the motion of the liquid is laminar. Interfacial tension tends to reduce the unstable growth of the short waves, while viscosity plays a dual

role: it helps dissipate the energy of the instability, but at the same time it is the cause of its appearance (Trallero *et al.*, 1997). Recently, Al-Wahaibi (2006) attempted to predict the onset of entrainment in horizontal oil-water flows in a SS pipe, while he experimentally measured it by flow visualization and by conducting local measurements using an impedance probe. Even though Trallero *et al.* (1997) failed to predict onset of entrainment especially for low viscosity oil, the extended model by Al-Wahaibi (2006) was tested against a range of experimental results from different systems and was found to predict it satisfactorily.

The degree of dispersion of either oil in water or water in oil can be increased when the interface height is located near the top or bottom of the pipe (Valle and Kvandal, 1995) due to the greater differences in velocities of the two phases resulting in higher shear forces.

PRESSURE DROP

There are few reported pressure gradient data in the literature for dual continuous flow. Trallero (1995), Valle and Kvandal (1995) and Nädler and Mewes (1997) observed a reduction in pressure gradient compared to that of single phase oil during dual continuous flow. Guzhov *et al.* (1973), on the other hand, reported that the two-phase mixture pressure gradient, compared to that of single phase oil, increased with the addition of water during 'water/oil and oil/water emulsion' flow at high oil fractions, and reached a peak, but decreased during 'separate flow with emulsion at the interface and a lower layer of emulsion' flow, at medium oil fractions. Angeli and Hewitt (1998) found that pressure gradient depended on the pipe material of construction; in a steel test section two-phase pressure gradient during dual continuous flow was higher than that of single phase oil or water, while in the acrylic test section it was lower than the single phase values.

Changes in pressure gradient trends during flow pattern transitions have been reported by several investigators: Guzhov *et al.* (1973) observed a peak at the transition from water continuous dispersed flow to dual continuous flow (Figure 2.5a), while Nädler and Mewes (1995a&b) also observed pressure gradient peaks at the boundaries of dual continuous flow seen in Figure 2.5b.

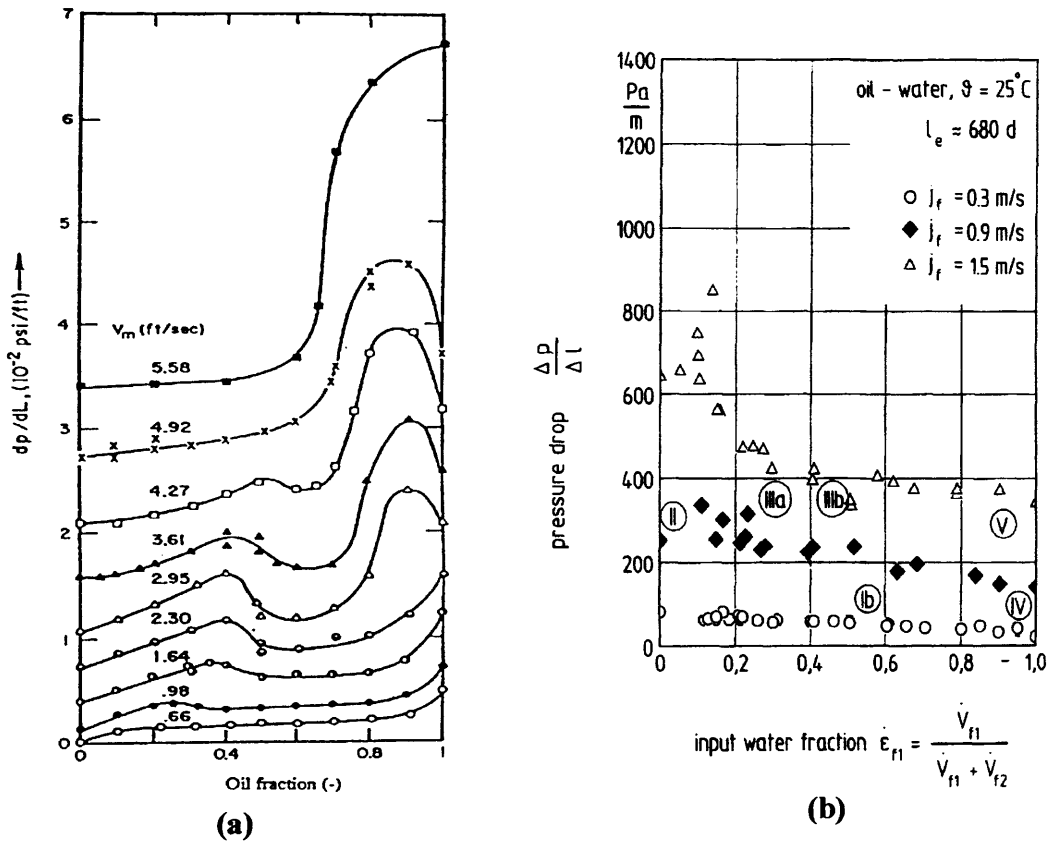

Figure 2.5 Pressure gradient against input oil fraction by (a) Guzhov *et al.* (1973) and (b) Nädler and Mewes (1995a) (j_f is mixture velocity).

2.2.4 Dispersed Flow

DEFINITION

At high mixture velocities, dispersed flows prevail. In dispersed flows two different types of dispersion can exist: water droplets dispersed in a continuous oil phase (w/o) or oil droplets dispersed in a continuous water phase (o/w). In general, horizontal flows have a vertical concentration gradient of droplets due to gravity forces (not expected in vertical pipelines where flow is more symmetric). Only at high velocities or in stable emulsions gravitational effects can be overcome by dynamic forces; then, the dispersion will be homogeneous. The drop size distribution is a function of the fluids' properties, superficial velocities, pipeline configuration, pipe roughness and pipe length (Hinze, 1955; Collins and Knudsen, 1970; Sevik and Park, 1973; Karabelas, 1978; Hanzevack and Demetriou, 1989; Lovick and Angeli, 2004).

PRESSURE DROP

Results obtained in dispersed flows have revealed that the relative mixture viscosity (with respect to the continuous phase) increases for increasing dispersed phase fraction. As a result, there is a gradual increase of the pressure drop towards the phase inversion point for an oil continuous dispersion and a decrease from the phase inversion point to single phase water flow.

Pal (1993) investigated the laminar and turbulent dispersed pipe flow of stable and unstable dispersions. For laminar flow, pressure drop increases gradually to a peak at the phase inversion point and then decreases towards the single phase water flow value, while a different behaviour (reduced pressure drop) was seen in the turbulent flow regime. A peak in pressure gradient was also seen by Angeli (1996), who also observed a dependence of the pressure gradient in dispersed flows (and other flow patterns) on the pipe material (lower pressure gradient in the acrylic than in the stainless steel pipe).

Peaks in pressure drop in dispersed flow have also been observed in many flow pattern transitions. Guzhov *et al.* (1973) found peaks at the boundary of a dispersion of oil in water and water (Do/w & w) with stratified flow with mixing at the interface (ST & MI). After a decrease in the pressure gradient back down to a level comparable to the single phase water, a second, much larger pressure gradient peak is observed around 85% oil fraction, which corresponds to the flow pattern transition from ST & MI to a dispersion of water in oil, over oil in water (Do/w & Dw/o). A similar increase in pressure gradient was also observed by Nädler and Mewes (1995a) during the transition between the Do/w and Do/w & Dw/o, and between Do/w & Dw/o to Dw/o.

In summary, pressure gradient data from different sources show an increase of pressure drop in pipelines towards phase inversion in the conditions studied, while significant changes in pressure gradient are seen to accompany all flow pattern transition.

2.3 DRAG REDUCTION IN LIQUID-LIQUID DISPERSIONS

The term drag reduction connotes an engineering intervention whereby the frictional pressure occurring in a system is (deliberately) lowered. This can be achieved with the addition of a Drag Reducing Agent (DRA) to the fluid in the pipe. DRAs have been used to bring about a reduction in pressure drop at a given flow rate, or correspondingly increase the maximum flow rate attainable for a given pressure (Manfield *et al.* 1999). Even though theory would predict increased pressure drop in dispersed flows in comparison to single phase pressure drop without addition of DRAs, this may not be the case in unstable emulsions; reduced pressure drop or *drag reduction* in both oil and water continuous dispersions has been reported by various researchers. Pal (1993), Valle and Kvandal (1995), Watanabe *et al.* (1996) (at square and rectangular pipes), Beretta *et al.* (1997), Nädler and Mewes (1997), Soleimani *et al.* (1997), Angeli and Hewitt (1998), Watanabe *et al.* (1999) and Lovick and Angeli (2004) and have all observed a reduction in pressure gradient compared to that of single phase oil during dual continuous/dispersed flow, while the degree of reduction appears to be strongly dependant on the type of oil used. However, dependence from the pipe material was also reported (Angeli and Hewitt, 1998); they found that drag reduction appeared in both acrylic and stainless steel pipes in the oil continuous region, whereas only in the acrylic in the water continuous region. In addition to this, most researchers report drag reduction to be more prominent in the oil continuous region. Despite this drop in pressure gradient of highly concentrated dispersions, a peak was still seen around the point of inversion (Soleimani *et al.* 1997; Angeli and Hewitt, 1998).

The early suggested mechanism for drag reduction in the case where a drag reducing agent is added to the system involved a shear-thinning layer at the pipe wall, having an extremely low viscosity, leading to an "effective slip" (Manfield *et al.*, 1999). Other researchers claim that the DRAs function by interfering with the turbulence structure in the fluid. Most recent theories related to drag reduction involve the consideration of the Reynolds stress and the rate of vortex production or the extension of modern turbulence models in which a pulsating sub-layer effect, leads to "bursts" of near wall eddies (Manfield *et al.*, 1999).

Laminar flow data have shown that the viscosity of emulsions increases (forming a peak) as the inversion point is approached. Comparing results obtained from laminar flow data with results from the turbulent region, it is seen that the behaviour of emulsions can be totally different: the relative viscosity obtained from the turbulent data not only decreases as a function of the dispersed phase concentration but also varies with the flow rate, and the difference between laminar and turbulent flow data increases with increasing water concentration. The laminar flow data tend to agree with the Einstein equation for prediction of mixture viscosity:

$$\mu_m = \mu_c(1+2.5\varphi) \tag{2.1}$$

where μ_m is the mixture viscosity, μ_c is the continuous phase viscosity and φ is the dispersed phase fraction.

According to Pal (1993) on experiments conducted in stainless steel pipes, unstable o/w emulsions without any added surfactants exhibit drag reduction behaviour in the turbulent regime; he suggested that this is related to interference of drop breakup and coalescence of the dispersed phase droplets with the turbulence of the continuous phase. The degree to which drag reduction occurs depends on the nature of the oil, since different oils will have different stability characteristics and on the dispersed phase concentration as it becomes stronger with increasing concentration. Drag reduction was found to be more prominent in w/o dispersions. However, o/w dispersions still exhibit drag reduction but to a lesser degree.

Still the exact mechanism of drag reduction is not fully understood. On the basis of the suggested mechanism from Pal (1993), one would expect a significant decrease in drag reduction upon the addition of a surfactant to the same system, because the surfactant would inhibit coalescence and breakup, which was indeed confirmed by his experimental results, also observed from Watanabe *et al.* (1999) for laminar flow in rectangular pipes with highly water-repellent wall.

According to Pal (1993), drag reduction seems to depend also on pipe diameter. The smaller diameter pipe gives larger drag reduction when comparison is made for the same Reynolds number. This agrees with the drag reduction behaviour of dilute polymer solutions. The author doubted that drag reduction in emulsions might be due to viscoelastic effects like in the case of dilute polymer solutions because stable emulsions are expected to have much smaller droplets.

Serizawa and Kataoka (1992) showed that the dispersed phase drops and the turbulent eddies of the continuous phase can interact in many ways that depend on their relative sizes; their interactions affect not only the drops but also the eddies. Owen (1986) observed some turbulence damping in the gas core of annular gas-annular film. He based his explanation on the experimental values of the von-Karman factor k. Turbulence damping occurred when these k values were lower than 0.4.

Opposite to the drag reduction findings, results by Kvandal and Søntvedt (1995) and Valle and Utvik (1997) showed that pressure gradient in oil continuous stable emulsions increased with increasing dispersed water fraction, not only in laminar, but also in turbulent flow when using an oil with a viscosity close to water viscosity.

Drag reduction has been thus reported to depend on pipe diameter, oil type, concentration of the dispersed phase (higher drag reduction for more dispersed phase fraction), type of dispersions (higher for w/o emulsions than o/w in SS pipes), pipe material of construction and the addition of surfactants (drag reduction diminishes upon addition of surfactants, Pal, 1993). However, further experimental findings are needed in order to draw safe conclusions regarding appearance of the phenomenon and its resulted reduction of pressure drop in pipeline flows.

2.4 THE PHASE INVERSION PHENOMENON

One of the most complex phenomena occurring in multiphase flows including two liquids is that of phase inversion. At high oil/water mixture velocities, dispersed flows will prevail, causing formation of water or oil dispersions depending on the dispersed phase fraction. The drops of a dispersed phase continuously coalesce and break up in a turbulent field, either in pipeline flow or in stirred vessels. At low

dispersed phase holdups, the two events always reach a dynamic equilibrium; however, it is postulated that at large holdups, the coalescence events overwhelm the breakage events and eventually lead to phase inversion where the previously continuous phase becomes dispersed and vice versa. As it is complicated and undesirable, phase inversion becomes a key phenomenon in the design of oil/water pipelines and facilities, as well as other operations since it is in the vicinity of inversion that changes in the mixture rheological characteristics might occur, often causing extremes in pressure gradient.

2.4.1 Phase Inversion - Definitions

Phase inversion in oil-water flow systems corresponds to the transition boundary between o/w and w/o dispersions. It refers to the phenomenon, where, *with a small change in the operational conditions, the continuous and dispersed phases spontaneously invert* (process depicted in Figure 2.6 by Arirachakaran *et al.*, 1989).

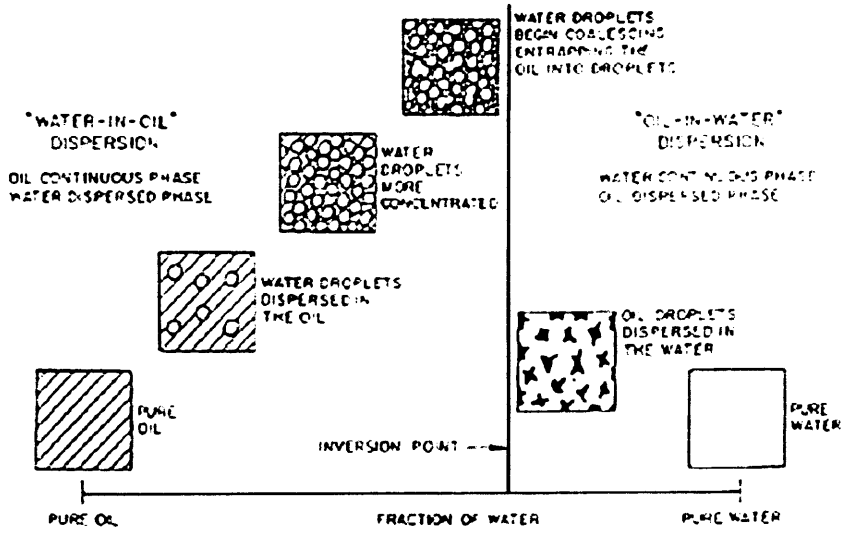

Figure 2.6 Phase inversion process for an oil/water dispersion system (Arirachakaran *et al.*, 1989).

This transition is usually associated with an abrupt change in the rates of momentum, heat and mass transfer between the two phases involved and between the

dispersion and the system solid boundaries. Typically phase inversion will take place at a characteristic dispersed phase fraction: for stirred vessels at a certain impeller speed, while in pipelines at a given mixture velocity. This characteristic phase fraction is commonly found in literature as "*critical*" holdup or most often as the *phase inversion point.*

Phase inversion can be regarded as a form of system instability, with the stability of the system being least at the phase inversion point. Knowledge of the phase inversion point and its characteristics is also essential in the preparation of dispersions in order to achieve desired properties.

2.4.2 Phase Inversion in Pipelines

Extensive investigations of phase inversion have been conducted in stirred vessels, whilst little information is available regarding its occurrence in pipelines either in horizontal (Russell *et al.*, 1959; Charles *et al.*, 1961; Guzhov et *al.*, 1973; Martinez *et al.*, 1988; Arirachakaran *et al.*, 1989; Nädler and Mewes, 1997; Valle and Utvik, 1997; Angeli and Hewitt, 1998; Soleimani, 1999) or in vertical flows (Govier *et al.*, 1961; Luo *et al.*, 1997; Liu *et al.*, 2004; Liu *et al.*, 2006a; Liu *et al.* 2006b; Hu and Angeli, 2006), while some work on three-phase flow (gas-liquid-liquid) has been done as well.

Many researchers have seen a significant increase in pressure drop before the occurrence of inversion in pipes (Martinez *et al.*, 1988; Valle and Utvik, 1997; Nädler and Mewes, 1997; Soleimani *et al.*, 1997, results seen in Figure 2.7; Angeli, 1996), while in other studies the maximum in the pressure gradient graphs does not always represent the inversion point (Pan *et al.*, 1995; Hu and Angeli, 2006). The increased pressure gradient at inversion is attributed to the increase in the mixture viscosity, since relative viscosity (with respect to the continuous phase) increases for increasing dispersed phase fraction. Valle and Utvik (1997) found that for higher flowrates, the increase in the relative pressure gradient towards the inversion point is less pronounced as compared to the lower flowrates.

In the existing published findings, the possible effect of the dispersion initialization condition on the rheological characteristics and the pressure drop around

inversion has not been considered and most experiments have been conducted starting from one phase as the continuous only.

Nädler and Mewes (1995a&b) are distinguishing between inversion that occurs from initially separated layers of water and oil, where maximum pressure drop is registered in case of total emulsification, and phase inversion within the dispersion layers that is occurring at different dispersed phase fraction. In the latter case, higher pressure drop values are registered. In the flow regime map of Figure 2.2, the region of phase inversion is associated with regions IIIa and IIIb. In any case maximum pressure drop appears for input water fractions between 0.1 and 0.2. It has been suggested that the decreased pressure gradient for water continuous mixtures just after the inversion point implies that the inverted mixture might be flowing on top of a water layer (Nädler and Mewes, 1995a; Gillies *et al.*, 2000).

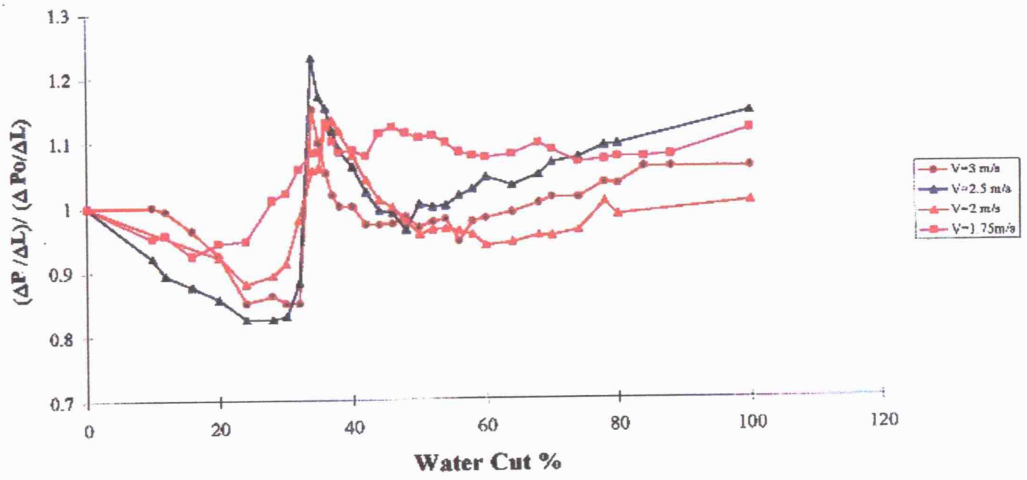

Figure 2.7 Pressure gradient data from Soleimani *et al.* (1997) showing peak at phase inversion for different mixture velocities studied.

Soleimani *et al.* (2000) revealed inhomogeneity in the vertical spatial distribution of the phases (with more water towards the pipe wall due to wetting effects and more dispersed oil droplets in the core); they postulated that this might cause phase inversion to occur locally in the cross section, even at different overall

dispersed phase fractions. Zones of oil and water continuous mixtures were seen before inversion. They, thus, considered the phenomenon to be a gradual process, since the mixture may shift from oil to water continuous within the cross sectional area and within a small change of water fraction. Similar conclusions were drawn by Liu *et al.* (2006a), who used a laser-induced florescence (LIF) technique to visualise the evolution of droplets and the internal flow structure in concentrated liquid-liquid dispersions, where complex secondary and multiple structures as the ones seen in Figure 2.8 were encountered.

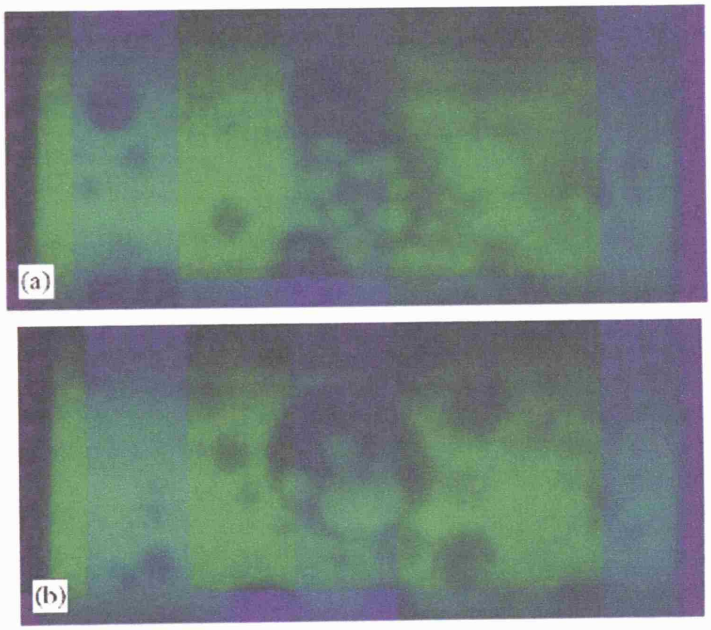

Figure 2.8 w/o/w secondary dispersions at mixture velocity 1.5 m/s and input oil holdup 31%. The dark coloured region designates the organic phase, while the light coloured region designates the aqueous phase (Liu *et al.*, 2006a).

Other researchers have studied inversion in vertical pipes (Luo *et al.*, 1997; Hu and Angeli, 2006). Luo *et al.* (1997) used a SS pipe of 44 mm ID and an oil with viscosity 452.6 mPa s in upward oil-water flow. They found that phase inversion is affected by the mixture velocity, where emulsion becomes unstable probably due to inversion when the mixture velocity exceeds 0.8 m/s. Hu and Angeli (2006) have obtained results in upward and downward vertical flows; no difference in the phase

inversion point was seen when inversion was approached from oil continuous or from water continuous mixtures (no ambivalent range). Furthermore, an interesting increase in dispersed droplet size was seen just before the inversion point, supporting increased coalescence as the mechanism for inversion, where oil droplets before inversion were much bigger than water droplets after inversion. Using a combination of conductivity probes at different locations in the pipe cross section, they also found that phase inversion in vertical pipes initially appears at the pipe centre accompanied by the formation of complex structures (possibly like the ones observed by Liu *et al.*, 2006a) before it finally reaches the wall and spreads through the whole cross section.

There are also few limited studies on the effect of emulsification in the three-phase flow of oil, water and gas (Nädler and Mewes, 1995b; Pan *et al.*, 1995; Utvik *et al.*, 1998). According to their results there does not seem to be a distinct water fraction where phase inversion occurs. The values of the water volume fraction reported for phase inversion in three phase flow vary between 0.15 and 0.77, since in addition to the liquid superficial velocity, the inversion point is a strong function of gas superficial velocity, and thus, a large ambivalent range can be obtained. Utvik *et al.* (1998) noted that the inversion point depends on the gas to liquid ratio, shifting towards higher water holdup with increasing gas-liquid ratios at high flowrates where the bubble concentration in the liquids becomes high. This might explain the increased dispersed fraction needed in 3–phase flows for inversion, since the entrained air bubbles will strongly interfere with the coalescence of the dispersed liquid droplets.

2.4.3 The Ambivalent Range

For two immiscible liquids, there is a range of volume fractions over which either component can be the dispersed phase (Selker and Sleicher, 1965; Luhning and Sawistowski, 1971; McClarey and Mansoori, 1978; Arashmid and Jeffreys, 1980; Efthimiadu and Moore, 1994; Pacek *et al.*, 1994; Norato *et al.*, 1998; Deshpande and Kumar, 2003). This range, where phase inversion may occur, is called *ambivalent range* and represents the existence of a hysterisis effect in the appearance of phase inversion. Ambivalent range can expand from 20% to 90% phase fractions, depending on how the dispersion is produced (Arashmid and Jeffreys, 1980) or the physical

properties of the liquids. This range is a metastable region of relatively high stability (Clarke and Sawistowski, 1978) since any disturbance to the system can lead to the instability of phase inversion at the boundaries of the region. Within this region the existing dispersion maintains its configuration with remarkable stability. However, within the ambivalent range and, in particular, close to inversion point, the dispersion is by no means uniform, but it is postulated that localized inversions can take place and re-invert again (Luhning and Sawistowski, 1971).

Phase inversion curves in the case of stirred vessels can be produced by the following two different procedures resulting in upper and lower curves: an upper inversion curve is obtained by keeping the agitator speed and the volume of the aqueous continuous phase constant, while the dispersed organic phase is added to the mixing vessel until the maximum fraction for which phase inversion occurs is reached (Figure 2.9). By shifting the two liquid phases and through similar procedure a second, lower inversion curve can be obtained. The dispersion can only exist as oil continuous above the upper curve and only as water continuous below the lower curve. *The ambivalent range is defined as area between the upper and the lower phase inversion curves.* McClarey and Mansoori (1978) produced an additional intermediate curve (Figure 2.10) by adding certain volumes of both immiscible liquid phases to the mixing vessel and initiating their mixing from rest position for a range of agitator speeds. The initial volume fraction of the phases that would result in phase inversion would be the phase inversion point at this agitator speed.

According to the close packing theory of uniform dispersed phase spheres, the maximum volume fraction of the dispersed phase can not be more that 74.05% (corresponding to a rhombohedral face centred cubic structure). At this volume fraction drops are in contact with each other (close packing) and coalescence will occur, which will lead to phase inversion. In reality though, since the drops in such unstable dispersions are neither necessarily spherical nor do they have uniform sizes, dispersions with higher fractions of the dispersed phase can be obtained and have been reported (Selker and Sleicher, 1965; McClarey and Mansoori, 1978; Arashmid and Jeffreys, 1980; Pal *et al.*, 1986; Guilinger *et al.*, 1988; Liu *et al.*, 2004; Hu and Angeli, 2006).

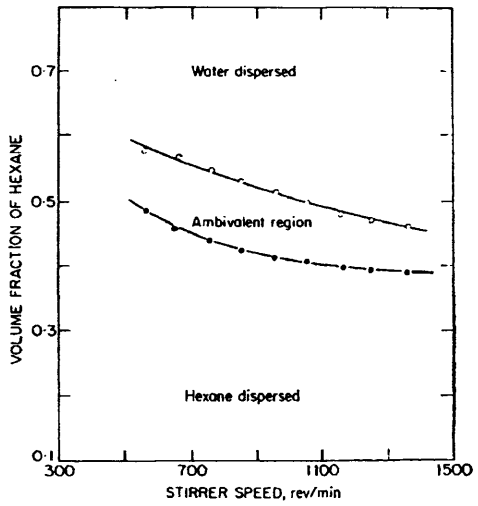

Figure 2.9 Ambivalent range for a hexane-water system (Luhning and Sawistowski, 1971).

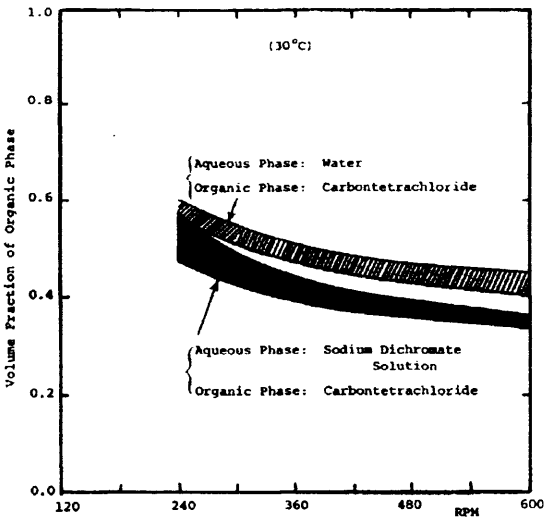

Figure 2.10 Intermediate Inversion Curves by McClarey and Mansoori (1978).

The limits of the ambivalent range vary between systems. Within the ambivalent range a variety of factors, like the volume ratio of the two liquids, density and viscosity ratio, interfacial tension, temperature, mixture velocity, as well as the geometry and the construction material of the dispersion container will determine the exact phase inversion point. Most of the available information in literature regarding the importance of the above factors comes from experiments in stirred vessels.

There are two methods of graphically presenting the ambivalence range. The traditional method of plotting organic phase volume fraction versus agitation speed at phase inversion is useful in that it clearly defines the conditions under which only single dispersion morphology may be maintained. However, an alternative method of displaying ambivalent behaviour (Kumar *et al.*, 1991) plots the volume fraction of the initially dispersed phase at inversion, regardless of which phase was dispersed, versus the agitation speed at phase inversion point (Figure 2.11). This method has great utility in that it explicitly demonstrates the behaviour of the dispersed phase regardless of the initial dispersion morphology, shows the hysteresis effect, and thus the irreversibility of the phase inversion process. In the "cusp" region (intersection of the two inversion

curves), it is possible to cross both ambivalent curves, thus giving the dispersion a locally reversible behaviour with respect to phase inversion.

A primary factor that has been reported to affect ambivalent range seems to be the viscosity ratio of the phases. Selker and Sleicher (1965) found that with increasing oil viscosity, its tendency to be dispersed increases, whereby both the minimum oil volume fraction that it can be continuous and the maximum volume fraction that can be dispersed increase. A similar conclusion was drawn by Arirachakaran *et al.* (1989) in experiments conducted in the laminar and turbulent flow regimes in pipelines with a variety of oil types. However, the widest ambivalent range was obtained for liquids of the same viscosities.

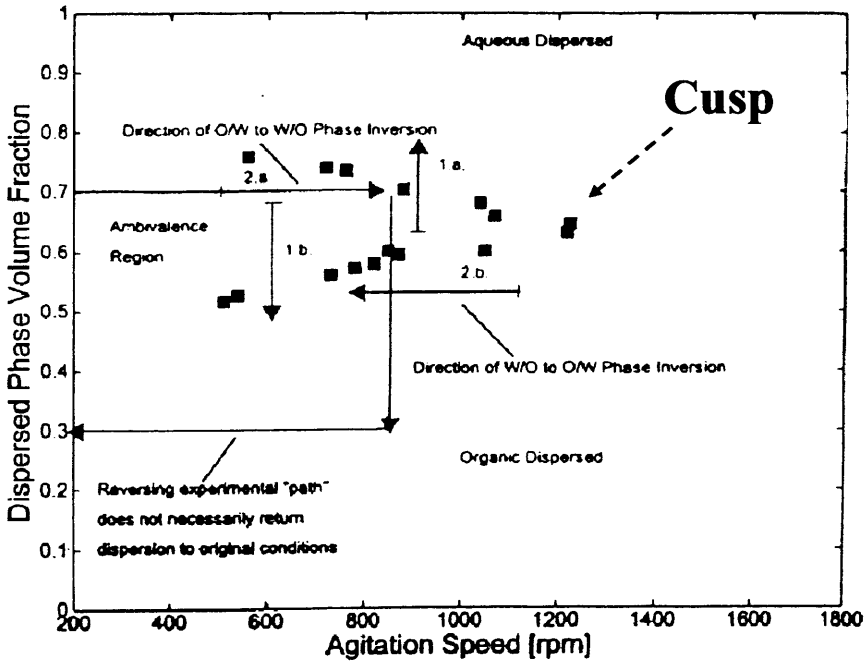

Figure 2.11 Ambivalent range plotted by the method of Kumar *et al.* (1991).

Tidhar *et al.* (1986) observed that in motionless mixer operations, the metastable or ambivalent region is very narrow. Furthermore, in the experiments conducted by Efthimiadu and Moore (1994) in shear plates, approaching phase

inversion by keeping the aqueous phase constant and increasing the organic phase fraction until phase inversion was reached or vice versa, led to the same phase inversion point (no ambivalent range).

The reason for the appearance or absence of the ambivalent range in oil/water dispersions is yet not known, but it is generally attributed to a lack of symmetry between o/w and w/o dispersions. Pacek *et al.* (1994) and Kumar (1996) attributed the phenomenon to the effect of secondary dispersions where the continuous phase becomes entrapped in the dispersed phase (eg. oil in water in oil, o/w/o). Their experiments showed that such structures can only exist in an oil continuous mixture (and not in a water continuous one), leading to an increased effective holdup of the dispersed phase. Pacek and Nienow (1995) have also observed that the volume fraction of dispersed oil in water at phase inversion is much higher than that of dispersed water in oil. So, under the same hydrodynamic conditions and similar physical properties, oil-in-water dispersions are more stable than water-in-oil. This again indicates some lack of symmetry. Kumar (1996) went a step further and also considered differences in the dielectric constants of oil and water. He postulated that dispersed oil droplets are experiencing repulsive forces due to the overlapping of the electrical double layers and thus have low coalescence efficiency; water droplets in an oil continuous environment will not experience them and will consequently have higher coalescence efficiency leading to a hysterisis in the appearance of inversion. Thus, even when the physical properties of the two phases (density and viscosity) are the same, depending on the continuous fluid, the mixture behaviour will be different. This practically explains the appearance of inversion at oil fraction higher than 50%.

2.4.4 Parameters Affecting Phase Inversion

There has been an extensive study, mainly in stirred vessels and less in pipelines, on how different parameters might affect the appearance of phase inversion and the limits of the ambivalent range in an attempt to elucidate the mechanism of phase inversion. In stirred vessels, the impeller speed, position and shape, the geometry of the system, the material of construction, the temperature, density/viscosity ratio and interfacial tension of the fluids are a few of the parameters

that have been postulated to affect the phase inversion point. Similar parameters are found to affect phase inversion in pipelines.

AGITATION SPEED/MIXTURE VELOCITY

Agitator speed in stirred vessels and mixture velocity in pipelines have been identified as a major factor that affects drop coalescence and break-up and thus, the volume fraction of the organic phase at inversion was found to vary with them (Quinn and Sigloh, 1963; Luhning and Sawistowski, 1971; McClarey and Mansoori, 1978). McClarey and Mansoori (1978) concluded that with increase of the impeller speed at constant temperature, phase inversion will occur at higher fractions of the aqueous phase. However, investigators have reported that inversion holdup is independent of stirrer speed at high turbulence intensity for both types of dispersions, i.e. water and oil continuous. More specifically, Quinn and Sigloh (1963), Luhning and Sawistowski (1971) and Deshpande and Kumar (2003) found that at high intensity of turbulence (high agitation speeds), the critical holdup at inversion becomes independent of stirrer speed and reaches an asymptotic value. Selker and Sleicher (1965) found the stirring speed to have no effect on the ambivalent range given that this was high enough to prevent settling, while at low speeds the limits of the ambivalent range were increased. Some effect of the mixture velocity was also found by Norato *et al.* (1998).

Efthimiadu and Moore (1994) found that an increase in rotational speed (and increase in shear rate) led to finer and dynamically more stable dispersions even at higher volume fractions of the dispersed phase, but some dependence on velocity was still obvious in their results.

Arirachakaran *et al.* (1989) who studied the effect of mixture velocity in pipeline flows found it to have little effect on the appearance of phase inversion for the experimental conditions studied.

INTRODUCTION OF ENERGY

Deshpande and Kumar (2003) performed experiments both by producing a dispersion with typical impellers, but also by producing dispersions in a turbulent field generated between two coaxial cylinders that introduced a uniform energy distribution

in the developed turbulent flow, in order to vary the way energy was introduced in the system. No differences were found in the resulting dispersions.

DENSITY

Density difference has shown to have little effect on the ambivalence range (Selker and Sleicher, 1965; McClarey and Mansoori, 1978; Norato *et al.*, 1998). Selker and Sleicher (1965) have shown though that large density differences, i.e. an order of magnitude, might have an affect on the inversion point due to the difficulty in maintaining a complete, uniform dispersion at lower agitation speeds under strong gravitational effects. Systems with large density differences between the two phases have shown a large propensity to invert (Kumar *et al.*, 1991).

Efthimiadou and Moore (1994) found that an increase in the density of the aqueous phase caused a small increase in the volume fraction of the dispersed organic phase at inversion favouring the water-continuous type of dispersion. In their experiments though, other physical properties were altered along with density. However, it should be noted that most types of oil used in experiments and reported in literature have densities very similar to that of water.

INTERFACIAL TENSION

The role of interfacial tension is least understood. Selker and Sleicher (1965) argued that the magnitude of the interfacial tension cannot affect phase inversion, since to suggest otherwise would imply that the interfacial tension between a given pair of fluids is a function of the curvature of the interface. Yeh *et al.* (1964) suggested that interfacial tension plays only a small role on phase inversion behaviour, since in the absence of other forces, it will cause inversion to occur at equivolume mixtures.

However, Luhning and Sawistowski (1971) claimed that interfacial tension is one of the principal factors affecting the ambivalent region. Clarke and Sawistowski (1978) showed that the width of the ambivalence region was critically affect by interfacial tension and the lower the interfacial tension the wider the hysterisis gap, implying an increased difficulty in inducing inversion.

Norato *et al.* (1998) also found that as the interfacial tension decreases, the difficulty in inducing phase inversion increases, and the ambivalent range widens (also

agreeing with results from Luhning and Sawistowski, 1971). Thus, a given dispersion morphology, at a constant agitation speed, will remain stable over a wider range of dispersed phase volume fractions as the interfacial tension is decreased. Decrease in interfacial tension decreases the droplet size and increase the drainage times for the film between the drops in collision; thus, it yields higher droplet breakup and lower coalescence rate according to Coulaloglou and Tavlarides (1977) and the critical dispersed phase fraction needed for inversion to occur should be higher, something that is confirmed by the results of Norato *et al.* (1998).

Efthimiadu and Moore (1994) concluded that low interfacial tension in the liquid-liquid system has the effect of stabilising the type of emulsion favoured by the rest of the properties of the system, while it eliminates any effect of shear rate on the inversion point, even at low shear rates, and reduces the influence of the wettability of the surfaces.

VISCOSITY

The viscosity of either phase, the continuous or dispersed, plays an important role in the ambivalence behaviour of a system. According to the experiments of McClarey and Mansoori (1978) in the absence of viscosity difference between the immiscible liquid phases, the intermediate inversion curve will be located at the equivolume (50% organic phase-50% aqueous phase) line for all the impeller speeds reported in agreement with the claims of Selker and Sleicher (1965). Accordingly, they concluded that any deviation of the intermediate inversion curve from the equivolume location is due only to the viscosity difference between the phases.

Treybal (1951) noted that in immiscible liquid mixtures, high viscosity of one of the liquids favoured its forming the continuous phase. This agreed with Efthimiadu and Moore (1994) who found that a dispersion preferentially formed with the more viscous phase as the continuous one (especially if it tends to wet the shearing surfaces). They attributed this to the increase of the dynamic stability of the type of dispersion with the viscous liquid as the continuous phase. Also, findings from Norato *et al.* (1998) imply that increase in the viscosity of either phase, widens the ambivalent range in stirred vessels. This behaviour was postulated to be the result of the lower

coalescence rates caused by longer film drainage times (also, in agreement with Groeneweg *et al.*, 1998). Indeed, higher viscosity of the continuous phase results in larger film drainage time of the continuous phase between two colliding droplets as found by Coulaloglou and Tavlarides (1977) and Calabrese *et al.* (1986).

However, experiments conducted in pipelines from Arirachakaran *et al.* (1989) with different types of oils with various viscosities (namely 4.7, 58, 84 and 115 mPa s in a 1.5 inch pipe and 237 and 2116 mPa s in a 1–inch pipe) have shown that more viscous oils have a greater tendency to be dispersed. Similar conclusions were drawn by Selker and Sleicher (1965) in stirred vessels.

Nädler and Mewes (1997) conducted studies on phase inversion in pipes and concluded that changes of viscosity ratio of this degree (viscosities 22, 27 and 35 mPa s) does not affect the flow regime boundaries and thus, the appearance of inversion.

WETTABILITY OF THE DISPERSION CONTAINER

It has been suggested that the wettability of the solid surfaces surrounding the liquid-liquid dispersion influences the type of dispersion formed and the phase inversion point. McClarey and Mansoori (1978) suggested that the discrepancies observed in their inversion curves when the effect of other factors, such as density and viscosity, were eliminated could be due to differences in the wettability of the container surface by the liquid phases, but this was only obvious at lower impeller speeds.

Giulinger *et al.* (1988) by changing the materials used in the mixers from water to organic wetted, found that the construction materials affect the inversion point by promoting the wetting phase to be the continuous one. Davies (1992) and Efthimiadu and Moore (1994) obtained similar results when experiments were performed in Perspex, glass and stainless steel plates: the oil-wetted plates strongly favoured the formation of oil-continuous dispersions. In addition to this, Davies (1992) found that the roughness of the surfaces also had a strong effect on inversion, again due to the change in wettability of the plates caused by roughness.

Kumar *et al.* (1991) however found that if the impeller is preferably wetted by the dispersed phase, the drops could coalesce on it and form a thin film, while if this

film was to break on or around the impeller, the inversion characteristics could be changed. Thus, they suggested an additional mechanism of drop coalescence onto the impeller, while the subsequent breakage of this thin layer either at the impeller or at its outer edge could alter the phase inversion characteristics of the system.

Pettersen *et al.* (2001) conducted experiments using *EXXSOL^{TM} D80* as test fluid in PVC and stainless steel pipes of 100 mm ID. They concluded that the point of the inversion is reached at somewhat lower water fraction in PVC compared to steel pipes for the experimental conditions studied when experiments started from oil continuous mixtures, but no further explanation was given. Results from Angeli and Hewitt (1998) in SS and acrylic pipes of 24 mm ID have also shown inversion occurring for both pipes around 37-40% input water fraction with no strong effect of the wettability of the pipe on the appearance of inversion.

EMULSIFYING AGENTS

The effect of the addition of different types and concentrations of emulsifying agents on phase inversion was studied by Efthimiadu and Moore (1994). They found that the use of increasing amounts of a hydrophilic agent (Tween 80) in the aqueous phase favoured the water continuous dispersion and the effect was stronger at higher impeller rotational speeds. Moreover, increasing the concentration of the additive had the effect of minimizing the influence of rotational speed and gap width. When they used a lipophilic agent (oleic acid), the latter favoured the formation of oil continuous dispersions. It should be mentioned that the effect of the emulsifiers strongly depended on the type of test liquids used for the production of the dispersions, as it was found that for some types of dispersions the addition of the emulsifiers did not have any effect (namely in the dibutyl maleate-water system).

INLET CONFIGURATION

The inlet configuration has not been extensively studied, but it was found to affect the appearance of phase inversion by Efthimiadu *et al.* (1994). They used two different configurations as inlets for the test fluids within the shearing plates; one of the liquids was introduced directly into the glass test section tube through a T-branch, while the other liquid was introduced through a small glass tube of 2.5 mm ID which

entered the main tube horizontally and with its outlet at about 2 cm downstream from the T-branch. By alternating the way the two fluids were fed into the test section different results were obtained.

WAY OF ADDING DISPERSED PHASE/DISPERSION INITIALISATION

Selker and Sleicher (1965) concluded that the way dispersion has started (either water or oil continuous) will have a strong effect on the inversion point in stirred vessels especially when the fluid volumes are within the ambivalent range.

In stirred tank experiments, Bouchama *et al.* (2003) found that the volume $\Delta\varphi$ by which the dispersed phase is added to the mixture has a strong influence on the inversion point. Smaller values of $\Delta\varphi$ were found to lead to larger values of the dispersed phase fraction needed for inversion. For very small quantities of $\Delta\varphi$ (<0.002) the emulsion becomes trapped in its non preferred morphology and the phase inversion point is shifted to much higher volume fractions, independent of the velocity of the impeller and the constant flow rate with which the dispersed phase is added to the mixture. This behaviour was also attributed to the fact that inversion is preceded by the formation of multiple emulsions, which can only be formed if the droplets are sufficiently large, or the forces acting on the droplets are sufficiently strong. No such experiments were conducted in pipelines.

Hu and Angeli (2006) who conducted experiments in a vertical SS pipeline found the dispersion initialisation condition to yield no ambivalent range (no change in the inversion point at different mixture velocities) in the experimental conditions studied.

TEMPERATURE

McClarey and Mansoori (1978) reported the dependence of the intermediate inversion curve on temperature. According to their experiments that involved sodium dichromate aqueous phase and kerosene-carbontetrachloride as the organic mixture, phase inversion occurs at lower fractions of organic phase with increasing temperature for constant impeller speed. Given though that temperature will affect most of the physical properties of the liquids, it is expected that a change in temperature will consequently affect the inversion point.

GEOMETRIC PARAMETERS

Norato *et al.* (1998) studied the effect of changing the ratio of impeller diameter to tank diameter (*D/T*) over a range of agitating speeds but without being able to draw any definite conclusions. As far as the impeller type is concerned Norato *et al.* (1998) and Deshpande and Kumar (2003) found that it does not profoundly affect the width of the ambivalent region at constant *D/T*. Deshpande and Kumar (2003) have also studied the effect of impeller diameter on phase inversion point and found that the critical holdup remained unchanged for higher impeller velocities where a critical asymptotic value was reached, while at lower velocities some differences were seen between larger and smaller impeller sizes. More specifically, they found that smaller impellers reach asymptotic value of inversion holdup at larger stirrer speed, a conclusion that agrees with the findings of Quinn and Sigloh (1963). No effect from geometric parameters was found from Selker and Sleicher (1965).

LOCATION OF IMPELLER

Quinn and Sigloh (1963) and Selker and Sleicher (1965) have observed that when operating in a batch mode, the phase in which the impeller is initially placed generally becomes the continuous phase. According to Guilinger *et al.* (1988) however, the location of the impeller does not affect the inversion point in a continuous mode as long as it is situated in a position that ensures sufficient turbulence generation to prevent settling of the two phases under gravity.

ELECTROSTATIC FORCES

Addition of small quantities of salt in the aqueous phase is known to affect the intrinsic process of coalescence of drops and potentially even change the inversion holdup significantly. Generally, the presence of ions reduces the double layer thickness around the drops to the point that electrostatic repulsive forces are overlapped by van der Waals forces. Norato *et al.* (1998) conducted experiments by dissolving quantities of NaCl at the aqueous phase in the concentration of 1 mol/l, but no conclusions were drawn as far as the inversion point is concerned. According to the authors, the addition of high concentrations of NaCl had effectively negated any surface charge effect and drop coalescence rates were greatly increased. Opposite results were obtained by Deshpande and Kumar (2003) who found that the addition of

0.1 M KI to the aqueous phase changed the critical phase holdup from 0.6 to 0.68 for inversion from oil to water continuous mixtures.

TIME

In transient experiments the conductivity of the dispersions has been followed to gain insight into the time required for the occurrence of inversion. Gilchrist *et al.* (1989) observed that phase inversion of liquid-liquid dispersions in stirred vessels at a particular phase volume fraction was also a function of time. They observed that when a small increment of the dispersed phase, sufficient to cause inversion eventually, was added to the system already close to inversion, inversion occurred some significant time after the addition, the delay period ranging from 5 to 1500 s, depending on the experimental conditions (agitation speed, liquid height, baffle gap and liquid pumping direction). They attributed the phenomenon to the inhomogeneity of turbulence causing different coalescence rates in different regions of the stirred vessel.

Nienow *et al.* (1994) found an increase in the delay time with an increase of the viscosity of the dispersed phase for batch experiments that had started with initial w/o dispersions. Attempts to measure delay time in the case of initially o/w dispersions were unsuccessful (delay time was either zero or no inversion happened).

Norato *et al.* (1998) having conducted some inversion delay time experiments concluded that the actual final catastrophic transient occurred in a time which was of the order of a few seconds. Also, even though the overall phase inversion time delay may be dependant on the experimental path, the time required for the final catastrophic transient was independent of the path.

2.4.5 Models for the Prediction of Phase Inversion

The greatest difficulty related to phase inversion is the purely conceptual problem of a physical mechanism by which phase inversion happens, as there has been very little definitive visualisation of the event. However, the ability to predict the point of phase inversion has been a common pursuit since the beginning of phase inversion research. Some of the attempts are described below for agitated vessels and two phase pipeline flows.

RULES OF THUMB

Simple "rules of thumb" have been developed to define the boundaries of the ambivalent range and attempt to predict inversion (Chapman and Holland, 1966) in agitated vessels. When a phase is present at a volume fraction less than about 0.3, it will form the dispersed phase. This rule clearly leaves a wide range of concentration (wide ambivalent range) in which either phase can be dispersed, depending particularly on how the dispersion is produced. Furthermore, the phase in which the agitator is placed initially will become the continuous phase (Chapman and Holland, 1966; Gilchrist *et al.*, 1989).

Luhning and Sawistowski (1971) agreed with this latter assumption only in case the volume fraction of the system corresponds to a value within the ambivalent range, whereas in case this is outside the ambivalent range, then the positioning of the impeller will not prevent the system from an opposite continuous configuration. Also, phase inversion for very viscous oils has been found to occur at values even smaller than 0.3 phase fraction, both in stirred vessels and in pipelines.

EMPIRICAL MODELS IN AGITATED VESSELS

Quinn and Sigloh (1963) were among the first investigators to attempt a prediction of the phase inversion point for agitated vessels, since they found that the phase inversion holdup observed in oil-in-water (o/w) dispersions decreases with increasing agitation speed and reaches a constant value at higher agitation speeds. Thus, they proposed that the phase inversion curves follow a relationship whereby the organic phase volume fraction at inversion, φ_o^I, is inversely proportional to the power input, P (W):

$$\varphi_o^I = \varphi_o^{'} + \frac{a'}{P} \tag{2.2}$$

where a' is a constant and $\varphi_o^{'}$ is the asymptotic phase inversion holdup value at high impeller speeds (constant). From dimensional considerations, the rate of energy input, P, is given by the following relationship for turbulent mixing:

$$P = K\rho_m N^3 \tag{2.3}$$

where K is a constant and N is the agitation speed, ρ_m is the volume fraction mean mixture density (kgm^{-3}) and is given by:

$$\rho_m = \rho_d\varphi + \rho_c(1-\varphi) \tag{2.4}$$

In this equation ρ_m, ρ_c and ρ_d are the mixture, continuous and dispersed phase densities respectively (kgm^{-3}) and φ is the *in situ* holdup of the dispersed phase which is equal to the input dispersed phase holdup if no-slip between the phases is assumed.

Luhning & Sawistowski (1971) experimentally investigated the effect on the phase inversion and ambivalent range of various parameters, such as interfacial tension and agitation speed. According to the authors, localised inversions take place quickly and re-invert again. They assumed that there is some energy barrier which has to be exceeded before the inversion can spread spontaneously. Immediately prior to inversion, the system must possess an excess of energy with respect to the system after inversion. Since phase inversion is considered a spontaneous process, it must be accompanied by a decrease in the total energy of the system. Their results showed that the inversion curve tends asymptotically to a constant value with increasing agitation speed. The organic phase holdup at phase inversion, φ_o^I, was found to be a linear function of impeller Weber number, We_I. Therefore they correlated the curves of the ambivalent range as follows:

$$\varphi_o^I = 0.160 + 6.0*10^{-5}(We_I) \quad \text{for the upper inversion curve} \tag{2.5}$$

$$\varphi_o^I = 0.470 + 2.0*10^{-5}(We_I) \quad \text{for the lower inversion curve} \tag{2.6}$$

where We_I is defined by:

$$We_I = \frac{\rho_c N^2 D_I^3}{\sigma} \tag{2.7}$$

where D_I is the impeller diameter (m) and σ is the oil/water interfacial tension (N/m).

They also found that interfacial tension is one of the principal factors affecting the width of ambivalent range, W, which was correlated by their experimental data as:

$$W = (0.094N - 64.0)\sigma^{-(0.82+0.66*10^{-3}N)} \tag{2.8}$$

MINIMISATION OF ENERGY CRITERION

Fakhr-Din (1973) noticed a reduction in the interfacial energy when inversion appeared. The magnitude of surface energy change was found to be close to the change of the system energy, while the kinetic energy variation was considered negligible. Taking into account that inversion was a spontaneous phenomenon, he suggested that the system energy should be at its lowest at the inversion point. Thus, he correlated the curves of the ambivalent region to the appropriate dimensionless numbers:

$$\varphi_o^I = 1.32*10^6 \left(\frac{\mu_d}{\mu_c}\right)^{0.32} \left(\frac{\Delta\rho}{\rho_c}\right)^{-0.11} Fr_I^{0.71}\, \mathrm{Re}_I^{1.06}\, We_I^{-0.25} \tag{2.9}$$

$$\varphi_o^I = 12.2*10^6 \left(\frac{\mu_d}{\mu_c}\right)^{0.31} \left(\frac{\Delta\rho}{\rho_c}\right)^{-0.04} Fr_I^{0.13}\, \mathrm{Re}_I^{0.22}\, We_I^{-0.03} \tag{2.10}$$

at the upper and lower inversion curves respectively, where $\Delta\rho$ is the density difference between the dispersed and continuous phases, Fr_I is the impeller Froude

number (defined as $Fr_I = N^2 D_I / g$ where g is the acceleration of gravity) and Re_I is impeller Reynolds number (defined as $Re_I = \rho_m N D_I^2 / \mu_c$).

EMPIRICAL MODELS IN PIPELINES

Based on a number of experimental studies on oil-water dispersed flows that covered a wide range of oil viscosities, the empirical model suggested by Arirachakaran *et al.* (1989) (Equation 2.11) confirms the importance of viscosity on phase inversion:

$$\varepsilon_w^I = \left(\frac{U_{ws}}{U_{ms}}\right)_I = 0.5 - 0.1108 \log_{10}\left(\mu_o / \mu_r\right) \qquad (2.11)$$

where ε_w^I is the critical water fraction for phase inversion, μ_r = 1 mPas is the water and μ_o is the oil viscosity, and U_{ws} and U_{ms} are the water and mixture superficial velocities respectively (ms^{-1}).

Arirachakaran *et al.* (1989) observed that mixture velocity had little effect on the phase inversion point as long as there was no transition in the flow regime. They also noted that Eq. 2.11 was developed for oils with interfacial tensions of $(30\pm2)*10^{-3}$ N/m and caution should be taken in using it for oils with interfacial tensions outside this range.

NEGLIGIBLE SHEAR AT THE INTERFACE

Investigators agree that the viscosities of the phases play an important role on the phase inversion point. Yeh *et al.* (1964), by concluding that inversion, promoted by rapid coalescence and breakup of droplets, is controlled by viscous rather than inertial forces, developed an equation for predicting the phase inversion point from the viscosities of the two phases, assuming that at the point of the inversion, the shear at the interface of the two phases is zero (and so there is no tendency to mix or create a new surface) and the momentum transfer between the phases at the interface is zero:

$$\frac{\varphi^I}{1-\varphi^I}=\left(\frac{\mu_d}{\mu_c}\right)^{1/2} \tag{2.12}$$

where φ^I is the dispersed phase volume fraction at the inversion point. Yeh *et al.* (1964) suggested however that the above predictions could be improved if the interfacial viscosity, μ_i (mPa s), is used in place of the continuous phase viscosity.

The equation was developed with reference to a configuration of stratified layers in laminar flow, however, it was tested against critical holdup data obtained in a flask (dispersion prepared by manual vigorous shaking of specified volumes of organic and water phases).

Nädler and Mewes (1995a) in their work on flow in horizontal pipes proposed that phase inversion is a function of the oil-water mixture velocity, also supported by the results of Russell *et al.* (1959), Guzhov *et al.* (1973) and Nädler and Mewes (1994). They also suggested a correlation (Equation 2.13) based on the momentum equations of the phases in stratified flow and assuming a negligible interfacial shear and no-slip between the two phases:

$$\varphi_w^I=\frac{1}{1+k_1\left[\frac{C_o}{C_w}\,\frac{\rho_o^{(1-n_o)}}{\rho_w^{(1-n_w)}}\,\frac{\mu_o^{n_o}}{\mu_w^{n_w}}(DU_m)^{n_w-n_o}\right]^{1/k_2}} \tag{2.13}$$

where D is the pipe diameter, ρ_o and ρ_w are the oil and water density respectively, C and n are the parameters in the Blasius equation for the friction factor, CRe^{-n} and k_1, k_2 are empirical parameters, while the subscripts o and w refer to pure oil and pure water respectively. It was suggested that k_1 reflects the contact perimeter of the wall with the liquids, as determined by the *in situ* flow configuration, and k_2 accounts for the flow regime in each of the phases. For laminar flow in both phases $k_1 = 1$, $k_2 = 2$, the above equation is identical to Yeh *et al.* (1964) model for the phase inversion point:

$$\varepsilon_w^I = \frac{1}{1+\left(\frac{\mu_o}{\mu_w}\right)^{0.5}} \qquad (2.12)$$

EQUAL SURFACE ENERGY

More recently phase inversion has been suggested to occur at the point where the surface energy of the two possible dispersions, oil continuous and water continuous, within the ambivalent range, is equal (Tidhar *et al.*, in motionless mixers, 1986; Brauner and Ullman, 2002; Yeo *et al.*, 2002; Decarre and Fabre, 2003).

Tidhar *et al.* (1986) studied phase inversion in motionless mixers. Based on their observations that phase inversion is a spontaneous phenomenon, they assumed that the total energy of the system does not change with the inversion and predicted that the organic volumetric fraction at the phase inversion point is:

$$\varphi_o^I = 0.5 + C' We^{-0.5} \mathrm{Re}^{0.15} (aD_H) \cos\theta \qquad (2.14)$$

where C' is a constant, a is the motionless mixer area per unit volume (m^2/m^3), D_H is the hydraulic diameter of the mixer (m), θ is the contact angle between the drop and the wall surface, *We* and Re are the Weber and Reynolds numbers respectively defined for motionless mixers by:

$$We = \frac{\rho_m U^2 D_H}{\sigma} \qquad (2.15) \qquad \text{and} \qquad \mathrm{Re} = \frac{\rho_m U D_H}{\mu_m} \qquad (2.16)$$

where U is the velocity of the dispersion (mixture velocity, ms^{-1}).

According to Brauner and Ullmann (2002) the total free energy consists of the sum of the continuous phase free energy, the dispersed phase free energy and the free energy of the interfaces (formed between the oil and water phases and between the continuous phase and the solid surfaces). Under conditions where the composition of

the oil and water phases and the system temperature do not change with phase inversion, the free energies of oil and water phases remain the same. Thus, only the free energies of the interfaces have to be considered. Based on this the critical oil holdup for phase inversion is given by (Brauner and Ullmann, 2002):

$$\varepsilon_o^I = \frac{[\sigma / D_{32}]_{w/o} + \frac{s}{6}\sigma\cos\theta}{[\sigma / D_{32}]_{w/o} + [\sigma / D_{32}]_{o/w}} \tag{2.17}$$

where θ is the liquid-solid surface contact angle with $0 \le \theta < 90°$ denoting a surface preferentially wetted by water (hydrophilic surface) and $90° < \theta \le 180°$ denoting a surface wetted by oil (hydrophobic surface); s=4/D is the solid surface area per unit volume (m^{-1}) and D is the pipe diameter (m), σ is the interfacial tension (N/m) and D_{32} is the Sauter mean drop diameter. The Sauter mean diameter can be scaled with reference to the maximum drop size (m), $D_{32} = D_{\max} / k_d$ where k_d is a constant that depends on the fluid system used, k_d=1.5-5. $D_{\max}$ can be found from the following correlation (Brauner and Ullmann, 2002):

$$\left(\tilde{D}_{\max}\right)_{\in} = \left(\frac{D_{\max}}{D}\right)_{\in} = 2.22\tilde{C}_H \left(\frac{\rho_c U_c^2 D}{\sigma}\right)^{-0.6} \left[\frac{\rho_m}{\rho_c(1-\varphi)} f\right]^{-0.4} \left(\frac{\varphi}{1-\varphi}\right)^{0.6} \tag{2.18}$$

where $(\tilde{D}_{\max})_{\in}$ is the dimensionless maximum drop size in a dense dispersion, $\tilde{C}_H$ is a tunable constant and f is the wall friction factor, ρ_c and ρ_m are the continuous phase and mixture density respectively and U_c is the continuous phase velocity.

For systems where the surface energy between the solid wall and the continuous phase can be ignored, the phase inversion point is given by (Brauner and Ullmann, 2002):

$$\varepsilon_o^I = \frac{\tilde{\rho}\tilde{\nu}^{0.4}}{1+\tilde{\rho}\tilde{\nu}^{0.4}} \tag{2.19}$$

where $\tilde{\nu}$ is the kinematic viscosity ratio, $\tilde{\nu} = \nu_o / \nu_w$.

Yeo *et al.* (2002) following the same assumption suggested the following equation for the prediction of the critical holdup in stirred vessels:

$$\frac{\varphi_o^I}{1-\varphi_o^I} = \frac{D_{32_{o/w}}}{D_{32_{w/o}}} \tag{2.20}$$

where the Sauter mean diameter, D_{32}, can be predicted by the following correlations for dilute and dense systems:

For dense systems: $$D_{32} = k_1^{'}\left(1+k_2^{'}\varphi^{m'}\right)We_I^{-n'}D_I \tag{2.21}$$

For dilute systems: $$D_{32} = k_1^{'}We_I^{-n'}D_I\left(\frac{\mu_d}{\mu_c}\right)^{p'} \tag{2.22}$$

where $k_1^{'}$ is an empirical constant, $k_2^{'}$ is the turbulence damping factor and n' is a parameters usually assumed equal to 0.6, while p' and m' are parameters obtained empirically.

A similar approach by Decarre and Fabre (2003) has yielded:

$$\varphi^I = \left[1+\left(\frac{\mu_c}{\mu_d}\right)^{1/6}\left(\frac{\rho_c}{\rho_d}\right)^{5/6}\right]^{-1} \tag{2.23}$$

All the above mentioned models only predict one phase inversion point for a particular system and do not give an ambivalent range. Brauner and Ullmann (2002) attributed the hysteresis in the appearance of phase inversion to the time needed by the new continuous phase to wet the tube material after phase inversion. A hydrophilic wall will yield the upper inversion curve, while a hydrophobic wall will yield the lower in Figure 2.12.

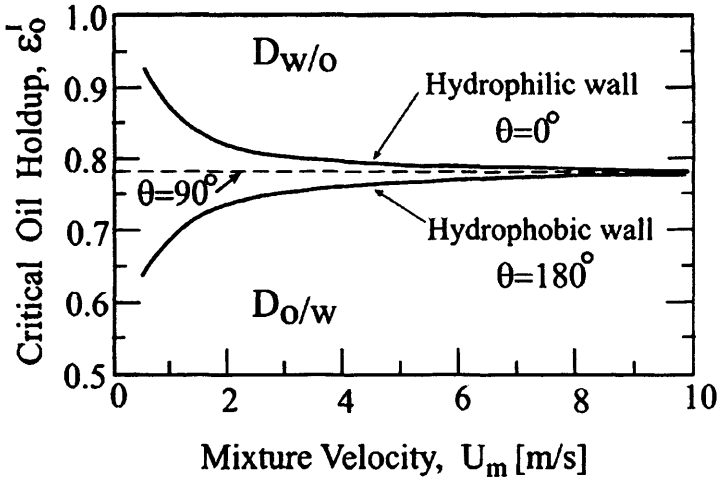

Figure 2.12 Region of ambivalence as predicted by a change in the liquid/wall (Brauner and Ullmann, 2002).

Also, the difference in interfacial tension in the new surfaces created after phase inversion compared to those existing before, where contaminants may have accumulated could lead to hysterisis.

POPULATION BALANCE EQUATION (PBE) MODELS

Population balance equation models have been widely used to predict drop size distributions in liquid-liquid dispersions formed in agitated vessels and pipeline flows. Different models for drop breakage (due to turbulent flow field) and drop coalescence (due to collisions between drops) can be used. Recently Hu *et al.* (2006) developed a model for unsteady state drop size distribution in pipes:

$$\frac{\partial n(d,x,t)}{\partial t}+U_m\frac{\partial n(d,x,t)}{\partial x}=Birth(d,x,t)-Death(d,x,t) \qquad (2.24)$$

where $n(d,x,t)$ represents the number of drops of size d per unit volume at axial position x and at time t, U_m is the mixture velocity. *Birth* and *Death* are the rate of number of drop increase and decrease per unit volume, respectively due to break up and coalescence. When the PBE was combined with a phase inversion criterion, the model could predict the phase inversion point reasonably well. Two alternative criteria were used to identify phase inversion in their model: the first assumes minimum interfacial energy at inversion, while the second one postulates that the breakage rate at inversion is equal to the coalescence rate. Their results show good agreement with experimental measurements of droplet size and illustrated the feasibility of PBE models to study phase inversion.

2.4.6 Phase Inversion Mechanisms

There is still no agreement on the mechanism of phase inversion. Little is really known about the actual mechanism, even though so many extensive studies have been conducted.

To date there are two main approaches: the thermodynamic and the new kinetic based mechanism. The former approach is mostly applicable on emulsions and micro-emulsions. However it is the latter, originating from kinetic phenomena behind phase inversion that is accumulating greater support. Nonetheless, there is currently no unified approach.

Even though the thermodynamic theory could not be employed in the current work, the main theories and correlations will still be presented (Rice, 1960; Ross and Kornbrekke, 1981; Dickinson, 1981; Dickinson, 1982; Overbeek *et al.* 1987; Vaessen and Stein, 1995; Ruckenstein, 1998), along with the main findings regarding the kinetics approach that are mainly divided into the drop breakup and coalescence rates, the delay time mechanism and the secondary/multiple dispersions formation (Pacek *et al.*, 1994; Kumar, 1996; Vaessen *et al.*, 1996; Groeneweg *et al.*, 1998; Gilchrist *et al.*, 1998).

THERMODYNAMIC MODELS

Phase inversion in emulsions (where an emulsifier is added to the system) is divided into two categories according to the mechanism that induces it: *transitional* and *catastrophic* (Salager, 1983). Transitional inversion is induced by changing factors that affect the distribution of the emulsifier over the phases, such as temperature and salinity of the aqueous phase. The term catastrophic phase inversion was first introduced by Salager (1983) to describe the inversion induced by increasing the fraction of the dispersed phase and has the characteristics of a *catastrophe* (a sudden change in behaviour of a system as a result of gradually changing conditions). The applicability of catastrophe theory to emulsion phase inversion was first suggested by Dickinson (1981). The assumption was based on the fact that phase inversion induced by increasing the volume fraction of the dispersed phase displays the qualitative characteristics of the so-called *cusp catastrophe*, one of the elementary catastrophes –a mathematical framework– developed by Thom (1972) (from Vaessen and Stein, 1995). The most outstanding characteristic (apart from bimodality, sudden jumps and divergence) was the occurrence of the *hysteresis*, which could not be explained by other theories at that time.

Vaessen and Stein (1995) tried to deduce the catastrophic behaviour from a description of the Gibbs free energy (suggested as the appropriate optimisation function) of an emulsion system as a function of a relevant morphology parameter, and so thermodynamically explain the mechanism of phase inversion. The authors used the suggestion of Dickinson (1981) who chose the curvature of the interface, defined as the reciprocal radius of the emulsion droplets and of Overbeek *et al.* (1987) that gave the description of the Gibbs free energy of the system per unit volume, G^M, of a droplet-type emulsion in terms of curvature:

$$G^M = \sum n_i \lambda_i + n_d \frac{4\pi a_d^{\,2}}{3} \times \left(\sigma + \frac{2c}{a_d} + \frac{3k_B T}{4\pi a_d^{\,2}} f_{w/o}(\varphi_w, a_d) \right) \qquad (2.25)$$

with

$$f_{w/o}(\varphi_w, a_d) = \ln\varphi_w - 1 + \varphi_w\left(\frac{4-3\varphi_w}{(1-\varphi_w)^2}\right) - \frac{3}{2}\ln\frac{16a_d^3}{v_w} \qquad (2.26)$$

where for a w/o emulsion, φ_w is the volume fraction of the aqueous phase and σ is the interfacial tension at zero curvature (infinite radius of the curvature), v_w is the molecular volume of the continuous medium, a_d is the radius of the droplets, n_d is the number of droplets, k_B is the Boltzmann constant, T is the temperature, n_i is the amount of component i, λ_i is the chemical potential of component i, and c is the bending stress coefficient, defined by Overbeek *et al.* (1987) as:

$$c = -b + \frac{d}{a_d} \qquad (2.27)$$

where the b and d are parameters related to the mean and Gaussian elasticity moduli k_c and $\bar{k}_c$. Bending stress is the interfacial energy that is dependent on the curvature and is expressed by the bending stress coefficient c.

According to Vaessen and Stein (1995) $b = 2k_c / a_0$ and $d = 2k_c + \bar{k}_c$, while some typical values that can be used in calculations are $b \approx 10^{-12}$ N and $d \approx 10^{-20}$ J. According to the authors, the first term of Equation 2.25 represents the chemical potential of the components of the emulsion, the second term $(4\pi a_d^2/3)\sigma$ represents the interfacial energy and the third term accounts for the bending stress. The last term of the equation stands for the entropy of the dispersed droplets. Eliminating the number of droplets from Equations 2.25 and 2.27 results in an expression for the interfacial contribution to the Gibbs free energy of the emulsion G_{int} :

$$G_{\text{int}} = \varphi_w \left(\frac{\sigma}{a_d} - \frac{2b}{a_d^2} + \frac{2d}{a_d^3} + \frac{3kT}{4\pi a_d^3} f_{w/o}(\varphi_w, a_d) \right) \qquad (2.28)$$

Through calculating G_{int} according to the above equation, hysterisis in emulsion can be visualised by means of a "ball-in-hole" analogy, which shows immediately one of the most important prepositions of the catastrophe theory: the *perfect delay convention*, according to which the system remains always at a local optimum (Figure 2.13).

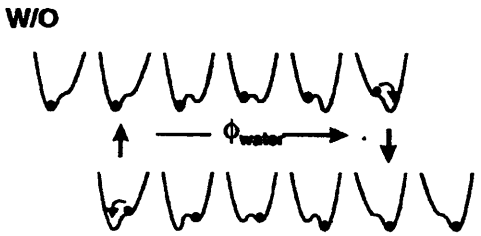

Figure 2.13 Ball-in-hole analogy to explain the hysterisis in phase inversion.

Although this approach has been successfully applied to describe the qualitative features of phase inversion, it failed as a predictive model, when applied to describe the quantitative features; thermodynamic models have been introduced in order to predict inversion in microemulsions *only*, while for values of the interfacial tension $\sigma \geq 10^{-3}$ N/m the emulsion system tends to separate and only a steep minimum at zero curvature appears. Thus, catastrophic inversion cannot occur, which means that the curvature of the system (as suggested) might not be the appropriate behaviour parameter for inversion and so the catastrophe theory is not applicable to phase inversion in coarse emulsions. Thus, Vaessen and Stein (1997) proposed a kinetic approach as a basis for the catastrophic inversion theory.

DROP BREAK-UP AND COALESCENCE

It is often assumed that enhanced coalescence of the dispersed phase compared to its break-up leads to the occurrence of phase inversion. In stirred tanks, the breakage of drops is due to the energy introduced to the system and turbulence created

by the impeller. In column contractors and in pipe flows, the breakage forces are due to turbulent and viscous shear in the flow. For stable liquid dispersions, dynamic equilibrium between the two competing phenomena of drop breakage and coalescence should be maintained. For coalescence to occur, the intervening continuous phase film separating the colliding drops has to drain to a critical film rupture thickness, thus the contact time between the colliding drops must exceed the film drainage time to the critical thickness. Of course not every collision results in coalescence. According to Coulaloglou and Tavlarides (1977) the coalescence rate depends on the coalescence efficiency as well as the collision frequency, where the coalescence efficiency, λ, is described as:

$$\lambda = \exp\left(-\frac{t_{drain}}{t_{contact}}\right) \tag{2.29}$$

where t_{drain} is the film drainage time (s) and $t_{contact}$ is the contact time between the colliding drops (s). During their contact but before they coalesce, the droplets might separate due to turbulent eddies. The dispersed phase holdup and the viscosity of the continuous phase liquid are also two important parameters for coalescence.

The coalescence frequency/rate is calculated based on the number of the collisions of the droplets and the coalescence probability, which is defined as the fraction of the collision that eventually leads to coalescence:

Coalescence rate = Collision rate x Coalescence Probability

On the other hand, drop breakup in a turbulent flow can be described with the following expression given by Prince and Blanch (1990):

Breakup rate = (Eddy-drop Collision Frequency) x Breakage Efficiency

Drop breakup and coalescence are controlled by a number of mechanisms. Thus, drop elongation in a shear flow, turbulent intensity, drop-eddy interaction and interfacial tension all affect the drop breakup.

At low volume fractions, the collision rate is proportional to the volume fraction squared and to the shear-rate. For high volume fractions this correlation is not known but it is expected to be proportional to a higher power of the volume fraction, as droplets are more closely packed. Adding an emulsifier increases the drainage time and so a considerably higher volume fraction of the dispersed phase is required for inversion to occur (Groeneweg *et al.*, 1998).

Kolmogoroff (1949) and Hinze (1955) calculated the maximum stable drop diameter by using the concept of the opposite acting forces of turbulent inertial stresses that tend to deform the droplet and the surface tension stress that tends to restore it to its original shape. As the diameter of the drop decreases, the deforming stress across it also decreases and the restoring stress increases. A diameter is finally reached where the deforming stress is unable to break the droplet. D_{max} is the maximum droplet diameter that can be reached and was calculated to be :

$$\frac{D_{\max}}{D} = C_1 We^{-0.6} \tag{2.30}$$

The model of Vaessen *et al.* (1996) tried to apply the idea of Arashmid and Jeffreys (1980) that inversion in stirred vessels takes place when every collision of drops results in coalescence. This model however, is applied in emulsions and not dispersions, since their behaviour is different: emulsions that are formally unstable may display metastable behaviour over considerable time, because the surfactant layer around the droplets delays the drainage process of the film between two collided droplets considerably, resulting in a very low coalescence efficiency. The situation in liquid-liquid dispersions is different; this retarding mechanism is absent, coalescence efficiency is high, and dispersions usually separate within a short time after agitation has stopped. However, their model has some drawbacks: there is no allowance for

polydispersity of the system, the turbulent energy dissipation is assumed to be uniform at the whole vessel (which is not correct, since around the impeller break up dominates and further away coalescence is the determining phenomenon), the equipment is considered to be completely wetted by the continuous phase and also, a coalescence possibility of 100% is not a realistic assumption.

A good synopsis of all breakage and coalescence models can be found in Hu (2005).

Groeneweg *et al.* (1998) suggested that there is substantial evidence that phase inversion is governed by the balance between break-up and coalescence and is caused by the increase of the effective volume fraction of the continuous phase, resulting from inclusion of droplets from the continuous phase into the dispersed phase. As Brooks and Richmond (1994) suggested when multiple emulsions occur, the effective volume fraction of the dispersed phase is much higher than the actual volume fraction of that component. This phenomenon is counteracted by the escape of these enclosed droplets to the continuous phase. This balance determines whether inversion will take place.

According to Tidhar *et al.* (1986) the mechanisms of coalescence and breakup of droplets (governed by surface wettability) were revealed to govern inversion when conducting experiments in motionless mixers at lower velocities, while turbulence is the controlling parameter at higher velocities.

Groeneweg *et al.* (1998) postulated that the actual inversion process starts when the effective volume fraction required for inversion is approached. At that stage the droplet size increases rapidly and inversion occurs subsequently, while elongated structures were seen before inversion. These very large droplets/structures can only be formed when there is such a large coalescence frequency that the increase in diameter due to coalescence can no longer be completely compensated by droplet break-up events. Variation of the stirring speed will affect the inversion point as it is connected to the coalescence rate of the dispersed droplets. Larger speed leads to more collisions and to a faster increase of the effective volume fraction due to inclusion of the continuous phase. This agrees with the findings of Gilchrist *et al.* (1989) who found that inversion will occur faster at higher speeds. Large droplets prior to inversion were

also seen by Pacek *et al.* (1994) in a different system (water-in-chlorobenzene). The authors postulated there is no evidence that an emulsion of small droplets suddenly inverts to an opposite emulsion of small droplets, but instead the original emulsion is first converted into an extremely coarse emulsion before inversion occurs.

Deshpande and Kumar (2003) proposed that at high dispersed phase holdups when the drops are in contact with each other, break up and coalescence of the drops do not occur independently of each other, but the ratio of the rates at which the two events occur in turbulent flow field is decided by the average relative separation between the drops and the physical properties of the two liquids, and becomes independent of the intensity of the turbulent flow field for sufficiently intense turbulence.

To this end, Liu *et al.* (2006a) applied a non-intrusive dye tracing technique and obtained pictures at the phase inversion point of immiscible organic-aqueous liquid dispersions in stirred vessels. Their experiments revealed that inversion is a gradual phenomenon that occurs over 1-2 s, and may not occur globally, but it depends on the local phase distribution. The mechanism of breakup and coalescence of the dispersed droplets can be seen in Figure 2.14.

The inversion process is thus, driven by the coalescence of the dispersed phase leading to larger drops. However, the continuous coalesce and breakup in a turbulent environment might lead to the inclusion of some continuous phase, within the dispersed phase droplets, giving rise to complex emulsions, i.e. drops within drops.

SECONDARY/MULTIPLE DISPERSIONS

Secondary/multiple dispersions are a common phenomenon for dispersed flows and have been observed by several investigators (Quinn and Sigloh, 1963; Luhning and Sawistowski, 1971; Pal 1993; Pacek *et al.* 1994; Pacek and Nienow, 1995; Kumar, 1996; Sajjadi *et al.*, 2002; Agterof *et al.*, 2003; and Liu *et al.*, 2006a).

Secondary dispersions (where drops of the continuous phase are incorporated into drops of the dispersed phase) have been identified close to inversion point by Luhning and Sawistowski (1971) from visual observations. At phase inversion from

o/w to w/o the mean drop diameter decreased, while the reverse was true for inversion from w/o to o/w, implying that secondary dispersions might be enhanced in the latter.

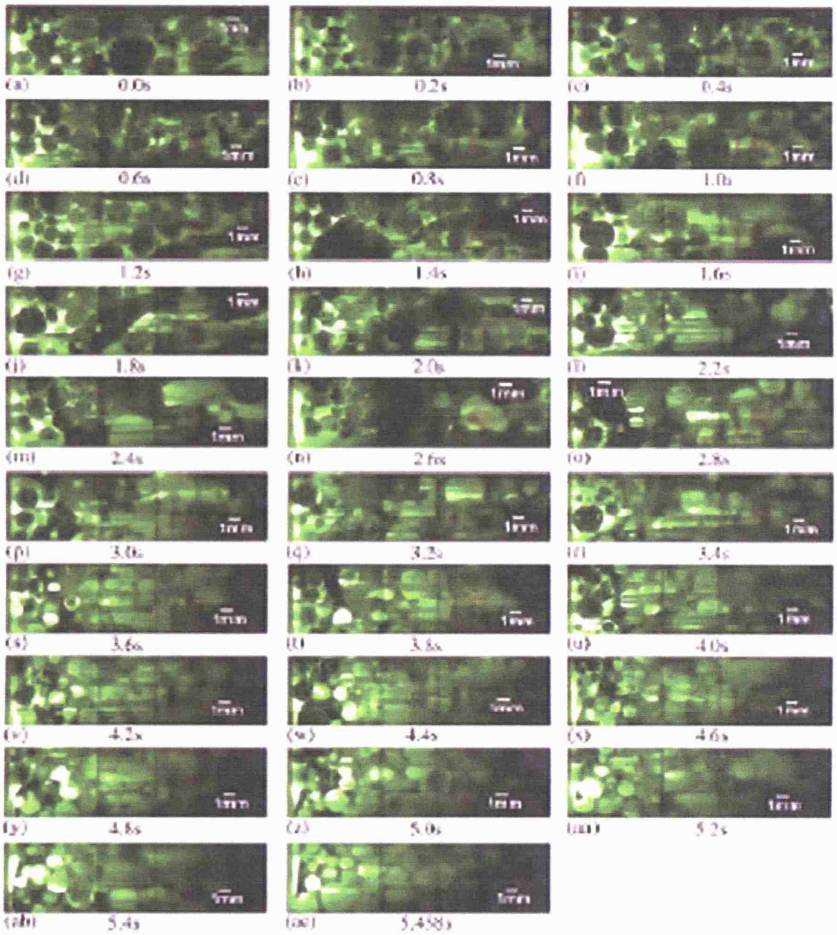

Figure 2.14 Time series of photographs taken over 5.458 s, showing the dynamic evolution of an o/w emulsion (45% aqueous holdup) to a w/o emulsion using laser induced florescence. The black regions designate the organic phase, whereas the light coloured region designate the aqueous phase (Liu *et al.* 2006a).

Pacek and Nienow (1995) made the same observations in agitated systems, while some preliminary experiments conducted in pipe flow using water-kerozene have shown the same two-phase structure, namely oil droplets in water drops in an oil continuous system and the absence of water droplets in oil for a water continuous system. The observation that water drops in water-in-oil dispersions contain oil

droplets inside them but the opposite was not seen was explained by Kumar (1996). He said that successive coalescence of drops easily gives rise to drops containing more than one droplet in them. There are two requirements: the coalescence efficiency should be high enough so that the drops should coalesce simultaneously and the droplets trapped in inside the drop should experience some stabilization, else they would coalesce with each other and with the external phase and the droplet-in-drop configuration will be lost.

According to Kumar (1996) both requirements are met for water-in-oil dispersions and therefore drop-in-drops structures begin to appear. For oil-in-water dispersions such structures are unlikely because oil drops in water have low coalescence efficiencies which prevent simultaneous coalescence and the trapped water droplets, if any, have high coalescence efficiencies and leave oil drops quickly. Recent findings in agitated vessels, have shown that oil drops in oil-in-water dispersions can contain drops of the continuous phase inside them (Liu *et al.*, 2006a) but oil droplets in w/o dispersions are more likely to occur. This was not true for pipeline experiments (Liu *et al.*, 2006a) where both o/w/o and w/o/w secondary dispersions could appear in the same experiment. Also some multiple dispersions, both o/w/o/w and w/o/w/o were found (Figure 2.15 and Figure 2.16), and the formation of those was quite similar to that of secondary dispersions, where the included droplets into the host drop were secondary dispersions rather than drops.

Pacek *et al.* (2004) suggested that phase inversion occurs as a result of development of multiple emulsions, where the volume fraction of droplets of the continuous liquid enclosed in the dispersed liquid has reached a critical value close to the limit of closed packing of these droplets.

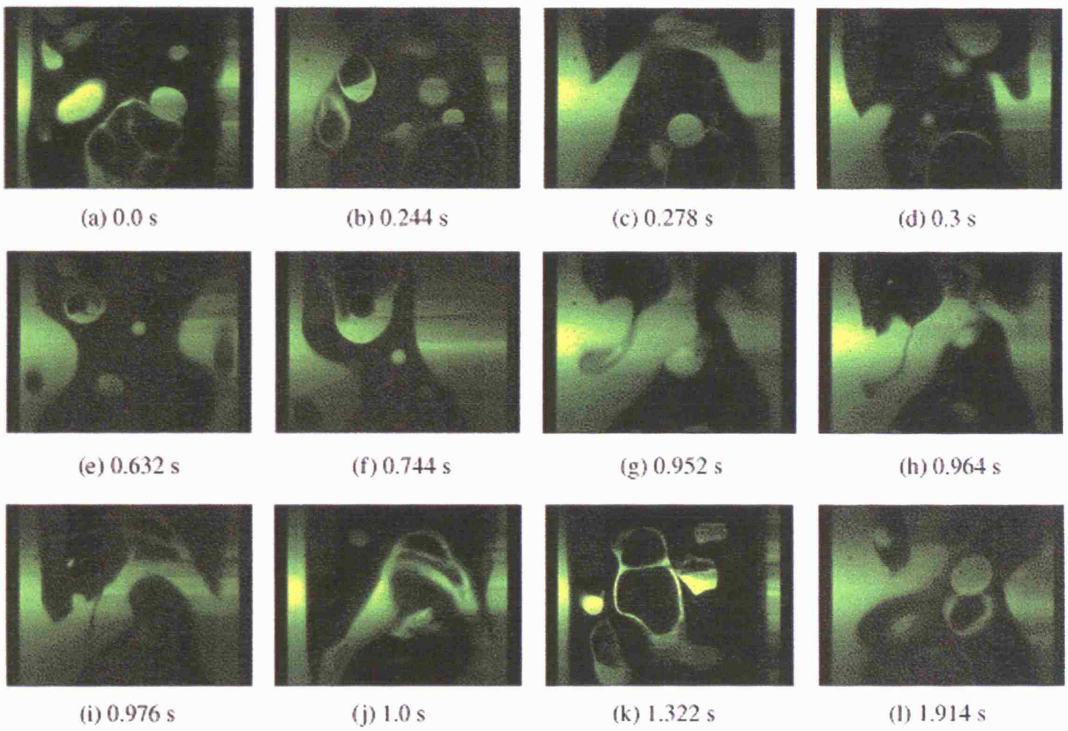

Figure 2.15 A time-series of photographs of the annular flow observed with water dispersion in the oil core. The mixture velocity is 0.0572 m/s. The black regions designate the organic phase, whereas the light coloured regions designate the aqueous phase (Liu *et al.* 2006a).

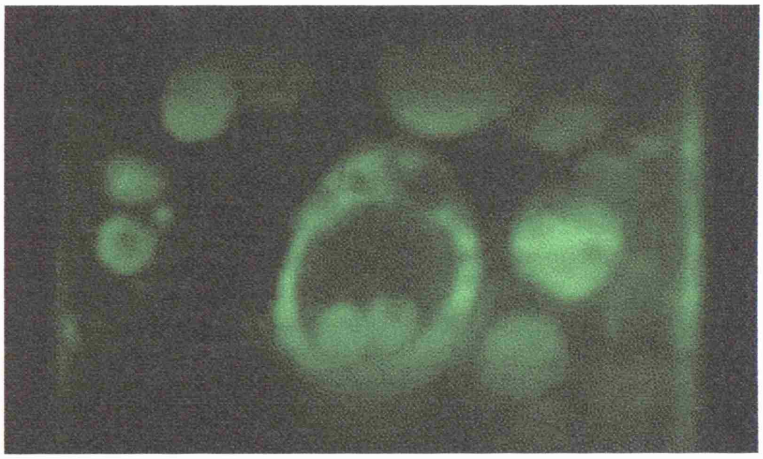

Figure 2.16 Complex drop structures at mixture velocity 1.11 m/s and 71.9 % input oil fraction. The black regions designate the organic phase, whereas the light coloured regions designate the aqueous phase (Liu *et al.* 2006a).

INCLUSION AND ESCAPE OF SECONDARY DROPS

The phenomenon of secondary dispersions and the entrapment of the continuous phase within the dispersed droplets is counteracted by the escape of these enclosed droplets to the continuous phase. The escape process has been speculated to happen because of two mechanisms; either the surrounding droplet of dispersed phase is strongly deformed by the flow, -so that the film between the enclosed droplet and the continuous phase ruptures-, or the enclosed droplet is able to move within the surrounding droplet, -so that the film between the enclosed droplet and the continuous phase ruptures. According to Sajjadi *et al.* (2000) the rate of escape is controlled by the size and volume of the internal droplets. Groeneweg *et al.* (1998) postulated that this balance between the escape of the enclosed droplets to the continuous phase and the inclusion of droplets from the continuous phase in the dispersed phase determines whether inversion takes place. According to their model, escape of enclosed droplets is promoted by a high viscosity of the continuous phase and a low viscosity of the dispersed phase.

Klahn *et al.* (2002) postulated that probably the origin of the included droplets is the formation and the breakage of a dimple during film drainage in the coalescence process. The included "internal" droplets are subjected to internal flow, which is generated by the external flow around the droplet complex, since the outer droplet itself is a fluid and its interface is not rigid. For the inner droplets to escape, they should be pushed by the inner motion towards the surface of the outer drop and "touch" it. There exists a streamline along which an inner drop will come in contact with the surface of the outer drop. Droplets inside this critical streamline will never be able to escape. Droplets outside this streamline will have an opportunity to escape twice per their period of circulation in the drop. The authors manage to construct a predictive model about the escape process using a Computational Fluid Dynamics model. The basis of the model is the following equation:

$$\frac{d\varphi_i}{dt} = -\frac{2P_{esc}}{t_c \alpha_{cr}}\left[\varphi_i - (1-\alpha_{cr})\varphi_{io}\right] \qquad (2.31)$$

where φ_i is the volume fraction of the inclusion, P_{esc} is the escape probability (analogous to the coalescence probability), t_c is the inner droplet circulation time, α_{cr} is the volume of the critical region, defined as the volume fraction of the droplet outside the critical streamline where escape of the inner droplet is enabled, φ_{io} is the initial volume fraction of the inclusions. In this case, the coalescence probability will be given by the general coalescence probability correlation.

DELAY TIME

Gilchrist *et al.* (1989) proposed that the measurement of the delay time during phase inversion might provide insight into the dynamics of the process. They observed that over a quite narrow concentration range, time delay varied from 5 sec (instantaneous inversion) to infinity. The delay time depended on a variety of fluid dynamic features and liquid physical properties. Video pictures during the delay period showed a significant increase of the number concentration of the dispersed larger drops (water drops in oil) with time. They postulated this growth is controlled by the relative rates of droplet break-up and coalescence and that inversion occurs once a critical concentration of large drops is reached. They also reported that within the larger drops of the dispersed phase (water) very small drops of the continuous phase could be seen and this was considered to play an important role in phase inversion mechanism. Once inversion was detected, the whole phenomenon would take place instantaneously (0.5-1 s), with no separation of the dispersed phase. At the same time, there was a change in droplet size to much smaller and uniform.

Nienow *et al.* (1994) found that for an aqueous phase dispersed in oil (a/o) a delay time may be observed before phase inversion to o/a. During this delay, increase in the number of large drops and droplets-in drops are seen in batch experiments. The number of small droplets was barely changing. For o/a dispersions, delay time and droplets-in-drops were not observed. More specifically in wash-out (semi-batch) experiments droplets of oil phase were always seen in droplets of aqueous phase when oil was continuous for concentrations of the aqueous phase from about 0.2 volume fraction up to phase inversion. After phase inversion to o/a these droplets-in-drops

disappeared. Conversely, for initially o/a these droplets-in-drops were never seen, though immediately after phase inversion, a droplets-in-drop structure developed.

The presence of droplets-in-drops is postulated to be the cause of time delay during phase inversion from a/o to o/a. The delay arises because of the time taken for the continuous phase droplets to be incorporated into the dispersed phase so that the critical "effective" volume fraction required for phase inversion can be reached. The presence of these structures also suggests that both continuous phase break-up as well as dispersed phase coalescence are mechanisms involved in phase inversion. These structures are considered to be responsible for the higher dispersed phase concentrations where phase inversion happens in case of dispersions of o/a than in case of dispersions of a/o dispersions, where secondary droplets form.

Kato *et al.* (1991) also reported a time delay of 1.2 minutes for an o/w dispersion to invert in their experiments. When reversing the experiment, the w/o dispersion inverted within 3.4 minutes.

It is generally postulated that the time delay decreases with increasing dispersed phase fraction. Some attempts have also been made for defining the time required for inversion to occur. The cause of time delay is not well understood though. Gilchrist *et al.* (1989) attributed the time delay to the inhomogeneity of turbulence causing variations of coalescence rates in different regions of the stirred vessel. Pacek *et al.* (1994) postulated that it is the secondary dispersions that are responsible for such behaviour. They did not observe any time delay or secondary dispersion when inverting from o/w to w/o dispersions where no secondary dispersions were present.

2.5 SUMMARY

This chapter attempted to report on all significant developments on liquid-liquid pipeline flows, with a focus on the parameters affecting flow patterns and pressure gradient, while the reported drag reduction in unstable emulsions without additives was also reviewed. More importantly findings regarding the phenomenon of phase inversion both in stirred vessels and in pipelines were summarised. While there are many experimental and theoretical findings and hypotheses no definite conclusions can be drawn with regards to the parameters that affect inversion and particularly its

mechanism relative to this matter. In many cases, observations have been contradictory, and results vary depending on the system used.

However, few of the most important conclusions can be summarised in the following:

- The ambivalent range defines the limits of the possible continuity of the two immiscible liquids. Phase inversion must occur within the ambivalent range.
- Inversion in stirred vessels and pipelines is affected by a large number of parameters, some of which are the geometry of the system and the material of its construction, the experimental conditions, the initial continuous/dispersed phase and the fluid properties. Most important of these appear to be the physical properties of the two immiscible liquids, and especially the viscosity ratio.
- A number of predictive tools have been suggested. The ones applied in pipeline flows depend on the physical properties of the liquids, while some of them include a pipe diameter dependence as well.
- There is no unified approach regarding the mechanism of phase inversion. However, the appearance of secondary dispersions appears to be very important in the occurrence of the phenomenon and the existence of the hysteresis during phase inversion.

Despite the extensive work on stirred vessels, more effort is needed towards the general understanding of the phase inversion mechanism, especially regarding the occurrence of the phenomenon in pipelines. The objective of the current study is to enhance the understanding of phase inversion in horizontal pipelines. In the following chapters after experimental conditions are explained, results on phase inversion appearance and its effects on the operational system will be introduced, while flow characteristics of concentrated dispersions will also be presented. Detailed

conductivity experiments in different points in the pipe cross sectional area are also described in detail. The effect of various parameters on phase inversion, namely fluid properties, pipe material and diameter, dispersion initialisation conditions and mixture velocity, will be examined, while based on experimental observations a model is suggested for the prediction of flow characteristics around the area of phase inversion in horizontal pipelines.

Chapter 3

Flow facilities, instrumentation and experimental methods

3.1 OVERVIEW

Experimental work was carried out both at University College London (UCL) and at the Norwegian University of Science and Technology (NTNU), Trondheim, Norway. Hence, the differences in test facilities allowed greater variation of parameters. The purpose of this chapter is to describe both experimental facilities (Section 3.2), together with the instrumentation used, to provide information on the test liquids and explain the experimental methods in detail. Instrumentation is described according to the results obtained (Pressure gradient, Section 3.3, Holdup measurements Section 3.4, Phase continuity, Section 3.5 and Phase and drop size distribution, Section 3.6). The properties of the test fluids are also given.

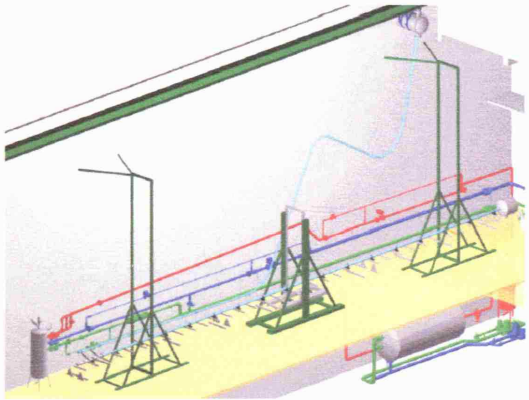

Figure 3.1 Experimental flow facility at NTNU designed in AUTOCAD.

3.2 EXPERIMENTAL FLOW FACILITIES

Two experimental facilities and a variety of test sections have been used and will be discussed further. Both facilities were used with two-phase liquid-liquid mixtures and all experiments were conducted in horizontal flow (zero degree inclination).

3.2.1 Experimental Flow Facility at NTNU

The experimental work at NTNU was carried out in the Multiphase Flow Laboratory in the Department of Energy and Process Technology. The facility (seen in Figure 3.1 and Figure 3.2) was capable of working with three phase flow of gas-liquid-liquid (gas-water-oil) and any inclination angle within +/- 15 degrees. For the purposes of the present work, two phase oil-water horizontal flow was used, while an air supply was used for drying the test section after each experiment so that the pipe wall would be kept clean and dry.

The test loop was made of three main components: oil/water handling facilities, test section (Figure 3.5 as well) and separation equipment. It also incorporated a data acquisition system. A detailed description of the test facility follows.

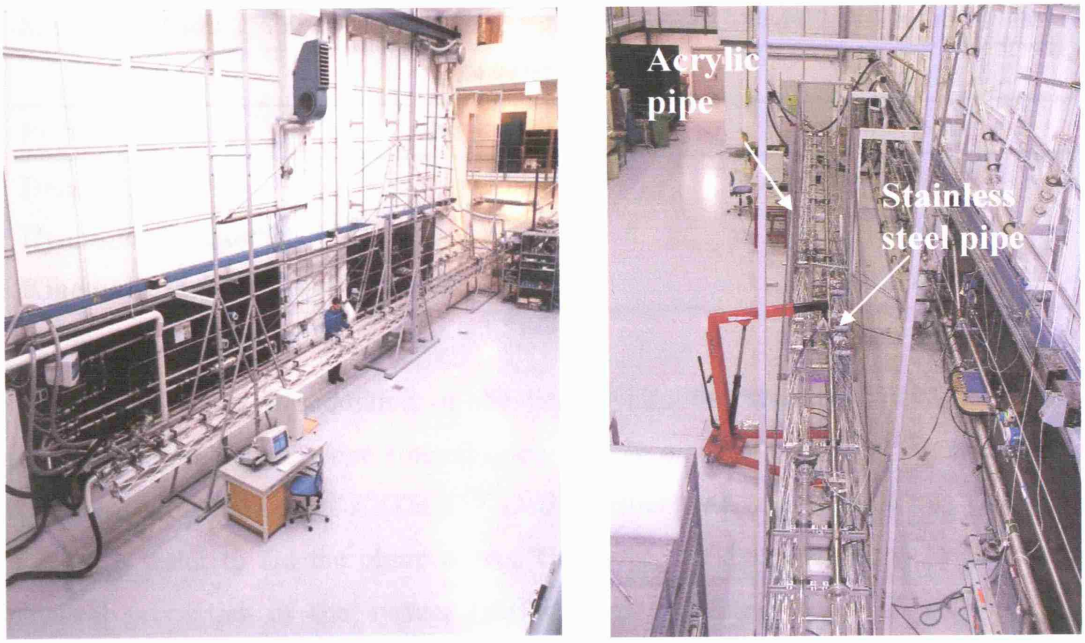

Figure 3.2 Experimental flow facility in NTNU.

WORKING FLUIDS

The test liquids used in the experimental facility at NTNU are tap water and two different model oils: *EXXSOL™ D80* (Dearomatized Aliphatic Hydrocarbon), which is a light hydrocarbon condensate (C11-C15) selected for its innocuity and fast separation ability, and *MARCOL™ 52* (purified mixture of liquid saturated hydrocarbons). The latter is a crystal clear, water-white product that contains non-toxic impurities. It is obtained from petroleum by vacuum distillation with subsequent refining stages including an ultimate purification by catalytic hydrogenation. The properties (viscosity, density and surface tension) of both *EXXSOL™ D80* and *MARCOL™ 52*, as specified by the manufacturing companies Exxon Mobil Chemicals and Exxon Mobil respectively are shown in Table 3.1:

Table 3.1 *EXXSOL™80* and *MARCOL™52* physical properties as specified by the manufacturing companies.

EXXSOL™ D80		
PROPERTY	**TYPICAL VALUE**	**TEST METHOD**
Density @ 15°C	796 kg m^{-3}	ASTM D 4052
Viscosity @ 25°C	1.7 mPa s	ASTM D 445
Kinematic viscosity @ 25°C	2.19 $mm^2 s^{-1}$	ASTM D445
Surface tension @ 25°C	26.3 mN m^{-1}	EC-M-F02 (Wilhelmy Plate)
MARCOL™ 52		
PROPERTY	**TYPICAL VALUE**	**TEST METHOD**
Density @ 20°C	835 kg m^{-3}	ASTM D 4052
Dynamic viscosity @ 20°C	11 mPa s	(Calculated)
Kinematic viscosity @ 40°C	7.5 $mm^2 s^{-1}$	ASTM D 445

Prior to the introduction of the liquids into the separator tank, water was filtered a through stand-alone filter (Figure 3.3). In a set of visualisation experiments conducted with the use of *EXXSOL™ D80* together with tap water, a dye was used diluted in water to aid the observations. However, the dye was found to affect the physical properties of the system (surface and interfacial water/oil tension) and

therefore all other experiments were conducted with the use of clean tap water without added dye.

Temperature was maintained at ambient which was within +/- 5°C. Pressure at the test section outlet was atmospheric throughout the experimental procedure. Effect of temperature, T, on liquid viscosity, μ_L, was estimated by the Lewis-Squire correlation:

$$\mu_L^{-0.2661} = \mu_K^{-0.2661} + \frac{T - T_K}{233} \tag{3.1}$$

where μ_K is the measured liquid viscosity at $T_K = 293.15$ K, T and T_K are in K and is in mPa s. Considering now a +/- 5K variation in temperature the respective variation in water and oil viscosity does not exceed +/- $3*10^{-5}$ Pa s and +/- $5*10^{-5}$ Pa s for *EXXSOL*^{TM} *D80* and +/- $5.5*10^{-5}$ Pa s for *MARCOL*^{TM} *52* respectively.

Figure 3.3 Water stand-alone filter at the NTNU experimental facility.

Apart from the given in Table 3.1 properties a new series of measurements was carried out in order to confirm the given values and to obtain some more information on the fluids' physical properties. Further analysis involved measurements of oil and water density, oil surface tension and oil/water interfacial tension for a variety of conditions for the test fluids (clean/used). For *EXXSOL*^{TM} *D80* the Du-Nouy ring tensiometer was used, while for *MARCOL*^{TM} *52* both the Du-Nouy ring tensiometer and the pendant drop method were used. Measurements were performed in the Chemical Engineering Department at NTNU. The principle and descriptions of the apparatuses used are described in greater detail in Appendix A, while the following two paragraphs summarise the preparation and performance of measurements along with the results obtained.

➢ ***EXXSOL™ D80***

Surface and interfacial tensions of *EXXSOL™ D80* and filtered tap water were measured, while density was provided from the manufacturing company. For the surface tension measurements 4 different water samples were used: clean/filtered tap water, clean coloured tap water (with added dye), water from the lower part of the separator where the water was pumped from and supplied in the test section (this was a sample of water that has been already used and gone through the system), and a rather "dirty" water, quite oily, sampled close to the oil/water interface of the separator that resembles very much the quality of water during an experimental run. The oil sample was taken from the separator tank close to the oil/water interface. These samples are called "*in situ*" samples hereafter. The liquids were not expected to have reached 100% separation soon after an experimental run; rather fine dispersion of o/w and w/o were formed especially at high mixture velocities, which would need long separation time to fully separate. Oil/water interfacial tension was then measured both with clean filtered tap water and clean oil, and water and used oil from the separator. The purpose of using different samples was to find out how much surface and interfacial tension of both liquids was influenced when fluids have gone though the flow loop. Thus the deviation from having absolutely clear and fresh samples of both test liquids could be investigated. Solid samples were prepared especially for this purpose by the construction material of the pipes in order to obtain information on contact angles. The methods used for this purpose are extensively discussed in Appendix A, while Table 3.2 below summarizes the results.

Water appeared to have lower surface tension than that of pure water (typical literature value 72.8 mN/m) which probably resulted from contamination by surface active agents coming either from the oil phase (in the case where water has been in contact with oil), or small amounts of organisms living in water (since this was not de-ionised).

Chupin (2003) has conducted very detailed contact angle measurements on the materials used in these experiments, where static contact angle, but also advancing (where the droplet is moved forward over the solid surface) and receding (where the droplet is moved backward over the solid surface) contact angles have been measured.

Several combinations of solid materials (acrylic, bare stainless steel and epoxy coated steel), liquids (water and *EXXSOL™ D80*) and surrounding media/solvent (air, water and *EXXSOL™ D80*) were considered in his measurements.

Table 3.2 *EXXSOL™ D80* physical properties. Surface and interfacial tension measured with the Du-Nouy ring method.

SURFACE TENSION	
In situ oil (interface at separator)	24.60 mN/m
Clean tap water	70.57 mN/m
Coloured tap water	63.46 mN/m
In situ clean water (bottom of separator)	60.77 mN/m
In situ dirty water (interface at separator)	51.80 mN/m
INTERFACIAL TENSION	
Clean tap water/oil	31.21 mN/m
In situ water from separator/oil (from separator)	30.12 mN/m
CONTACT ANGLE	
In situ clean water on SS	71°
In situ clean water on acrylic	84°
Oil on acrylic	0°
Oil on SS	0°

The fluid samples were taken directly from the separation tank. No special preparation was made for the surfaces used, other than washing them with pure acetone. To perform the contact angle measurements, short lengths of test section pipe were opened in two-halves, the pipe was cut lengthwise and droplets of liquid were deposited with a syringe on the pipe inner surface. Table 3.3 summarises the results of 10 separate angle measurements for each solid/liquid/media system at ambient conditions of pressure and temperature (performed by Chupin, 2003). Measurement accuracy is estimated at +/- 1 deg. His measurements for the respective measurements mentioned above are slightly lower, while it was found that oil is wetting oil surfaces when measurements were taken in air.

Table 3.3 Contact angles of *EXXSOL™ D80* as measured by Chupin (2003).

SOLID	TYPE	LIQUID/SOLVENT			
		WATER/AIR	OIL/AIR	WATER/OIL	OIL/WATER
Acrylic	No pre-wetting	53	0	113	71
Steel	No pre-wetting	61	0	127	105
Coated	No pre-wetting	60	0	117	97
Acrylic	Water pre-wetting	51	0	72	71
Steel	Water pre-wetting	26	0	51	105
Coated	Water pre-wetting	23	0	55	97
Acrylic	Oil pre-wetting	52	0	115	0
Steel	Oil pre-wetting	60	0	127	0
Coated	Oil pre-wetting	66	0	117	0
Acrylic	Advancing	72	0	117	-
Steel	Advancing	86	0	115	-
Coated	Advancing	63	0	96	-
Acrylic	Receding	33	0	68	-
Steel	Receding	19	0	37	-
Coated	Receding	34	0	26	-

➢ ***MARCOL™ 52***

For density measurements a standard densitometer was used (METTLER TOLEDO DENSITO 30P). The densities of used fluids (samples for both *MARCOL™ 52* and water taken from the separator after a complete experimental run) were found to be equal to that of pure liquids. More specifically, the density of water was found to be 997 Kg m^{-3}, while that of *MARCOL™ 52* was 827 Kg m^{-3} at 22.7°C which is slightly lower than the minimum value provided by the company (829 Kg m^{-3}). This is attributed to the fact that the measuring temperature was lower than the one provided from the company. For interfacial tension measurements two different samples were used: clean/filtered tap water was tested against clean oil taken from the oil drums ("clean" fluids) and water and oil from the separator (*in situ* samples taken from the interface) that had gone through some runs.

The methods used for these interfacial tension measurements are discussed extensively in Appendix A. Table 3.4 summarises the results obtained from the Du-Nouy ring method:

Table 3.4 *MARCOL™ 52* physical properties measured using the Du-Nouy ring method.

SURFACE TENSION RESULTS	
Clear oil	27.05 mN/m
In situ oil	26.87 mN/m
INTERFACIAL TENSION RESULTS	
Clear water/oil	43.54 mN/m
In situ water/oil	39.57 mN/m

The pendant drop method was also used and the obtained values were slightly higher; it looks that even though the oil/water sample was left for about 1.5 hrs to settle, steady state has not been achieved (see Appendix A). This could be attributed to the fact that either the sample needs more time to reach steady state, or there was some deformation/change of the oil drop formed into the water sample and thus, constant changing of interfacial tension value. The values shown in Table 3.5 are the last obtained values.

However, in order to be consistent with the measurements obtained for the other test liquids with use of the Du-Nouy ring method, values obtained from the same method will also be used for *MARCOL™ 52*.

Table 3.5 *MARCOL™52* properties measured using the pendant drop method.

INTERFACIAL TENSION RESULTS	
Clear water/oil	48.89 mN/m
Used water/oil	44.40 mN/m

OIL -AND WATER- HANDLING SECTION/AIR SUPPLY

Oil and water were pumped directly from the separator. There were four permanently connected centrifugal pumps available. Two for pumping the oil and

another two for pumping water depending on the flow rate demands of the experiments. For the needs of the current experimental work only the water and oil large pumps were used to achieve high flow rates and adequately high velocities for dispersed flow and phase inversion occurrence. Flow rates are controlled by controlling the frequency of the pumps. The specifications of the pumps used in the experiments are given in Table 3.6:

Table 3.6 Specifications of the pumps at the NTNU experimental facility.

PUMP	LARGE WATER PUMP	LARGE OIL PUMP
BRAND	Gustavsberg	Grundfos
MODEL	C100-35	CR 64-1
CONNECTION	DN100 flange	DN100 flange
REVOLUTION	2875 r/min	2900 r/min
MAX EFFECT	7.5 kW	5.5 kW
CURRENT	15 A	12 A

The pumps were equipped with an emergency shut-down switch that protected them from excessive current. As the pumps were located in the basement below the level of the test section, the two liquids and the air reach the test section via pipes, bends and other connections made from acid-proof steel, AISI 316L. The valves were made from treated brass resistant to corrosion. The length of the piping before the test section inlet was approximately 20 m.

Four different flowmeters measured liquid flow rates downstream of the pumps and right before the test section inlet. Water and oil could be directed to either a large diameter (60.3 mm) or a small diameter (21.3 mm) tubing where the flow rate was metered. For the purposes of this research only the flowmeters for high flow rates were used. The air supply was connected to the central high pressure supply, which could give air with pressure 6-7 bar.The specifications of the flow meters can be seen in Table 3.7. The accuracy of the water and oil flowmeters was 0.5% and 0.20 % full scale respectively.

Table 3.7 Specifications of the flowmeters at the NTNU experimental facility.

INSTRUMENT	PRODUCT SPECIFICATION	FLOW RANGE
LARGE WATER VOLUME FLOW METER	Fisher & Porter COPA-XM	$83x10^{-5}$-$16x10^{-3}$ m^3s^{-1}
LARGE OIL MASS FLOW METER	MicroMotion T150	1.1-2.4 kgs^{-1}
LARGE AIR VOLUME FLOW METER	Endress&Hauser flowirl 77A	$8.6x10^{-3}$ -10^{-2} m^3s^{-1}

TEST SECTION

Different test sections could be easily connected to the flow loop (L-riser, S-riser, straight section). In this work only the horizontal straight section was employed.

The support beam of the *straight test section* could support two pipes of 16.5 m length each; the ones mainly used were made from stainless steel and transparent acrylic, seen in Figure 3.2. The internal diameter for both pipes was about 60.0 mm (detailed specifications are given in Table 3.8). A third pipe of the same diameter made from epoxy coated stainless steel was also available.

The maximum mixture superficial velocity was 5.0 m/s for the lighter oil used, while with the heavier oil mixture velocity could only go up to 4.5 m/s. The liquid outlet/return to the separator from each test section was a 20.32 cm ID hose. The straight section was mounted on a support beam that can be tilted around its central axis using pre-defined anchors (upward or downward to the horizontal up to ± 15 degrees).

Two pipes could be mounted in parallel at all times and the inlet could be easily fitted to either one of them giving the possibility of interchanging between the two. Both outlet parts end in the first separator tank. The acrylic test section was assembled out of 2 m long pipe sections. The steel test pipes (bare stainless steel and epoxy coated steel) were made of 6 m long sections, cut into 2.5 m long sections for the coated pipe. Pipe sections were joined with a male/female flange junction in order to ensure smooth transitions.

In addition to the 60 mm ID pipes, a transparent acrylic pipe with a 32 mm ID was used that allowed comparisons between pipes of the same material of construction, but of different internal diameter.

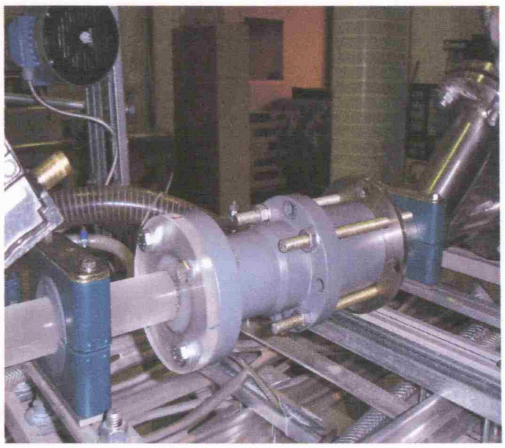

Figure 3.4 Inlet adaptor for the 32 mm ID acrylic pipe at the NTNU experimental facility.

This pipe was mounted on the same support beam (in the place of the steel pipe with special support adaptors seen in Figure 3.4). A larger range of superficial mixture velocities could thus be achieved with the new pipe, reaching 6.2 m/s with the light *EXXSOL™ D80* and 5.3 m/s with the heavier *MARCOL™ 52*. In order to study the possibility of an impact of internal coatings on the phenomenon of phase inversion, experiments have been performed in an internally coated pipe with the use of *MARCOL™ 52*.

A diagram of the test section for the large acrylic pipe that was used for the experiments conducted with *EXXSOL™ D80* is given in Figure 3.5. Similar configurations have been used for all different test sections in these experiments both for *EXXSOL™ D80* and *MARCOL™ 52*.

The two liquids joined at the beginning of the test section via a modified Y-junction that minimized turbulence and interpenetration of the phases. As shown in Figure 3.6, the three inlets were positioned to ensure gentle introduction of the phases; hence, the fluids were introduced such that they were stratified in a density-stable configuration. By using a special reducing adapter the same inlet section was used with the smaller acrylic pipe, as shown in Figure 3.4 and Figure 3.6.

Both pipes were equipped with Quick Closing Valves (QCVs) that could allow holdup and other types of experiments (i.e. pigging experiments). The QCVs were located far apart (approximately 5 m in the acrylic pipe and 4.4 m in the steel pipe), so measurements of holdup were avoided in this experimental set up because of the

potentially disastrous effects of water hammer, due to the long distances between QCVs and the high mixture velocities used.

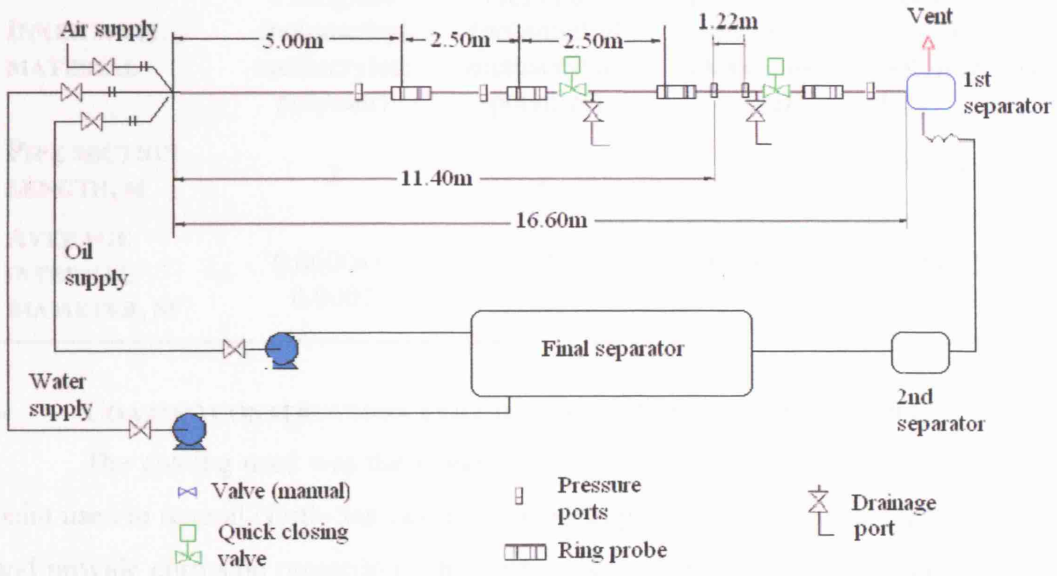

Figure 3.5 Test section of the 60 mm ID acrylic pipe at the NTNU experimental facility with the use of *EXXSOL™D80*.

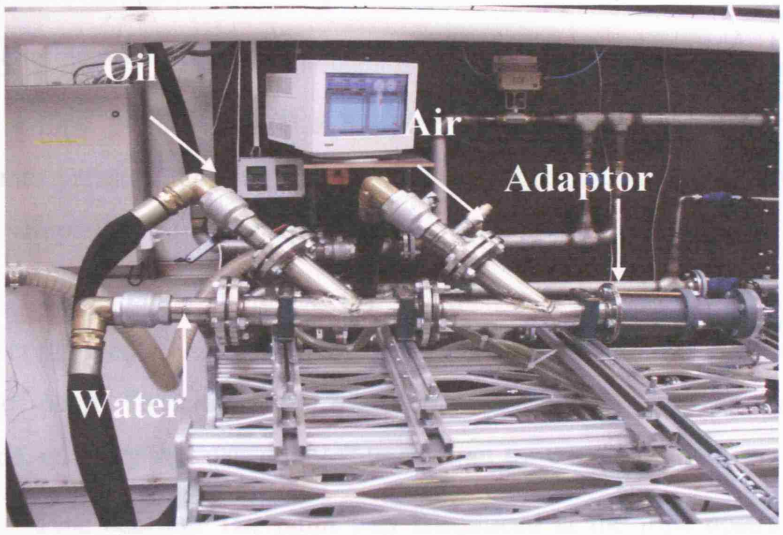

Figure 3.6 Inlet section at the NTNU experimental facility.

In Table 3.8 a summary of the test section specifications can be seen:

Table 3.8 Summary of the test section specifications.

SPECIFICATION	60 MM ID ACRYLIC	32 MM ID ACRYLIC	60 MM ID STEEL	60 MM ID COATED STEEL
INNER WALL MATERIAL	Plexiglass (polumethyl methacrylate polymer)	Plexiglass (polumethyl methacrylate polymer)	Stainless steel (min.10% chromium-nickel)	Epoxy resin (epoxy polymer+diamine)
PIPE SECTION LENGTH, M	2	2	6	2.5
AVERAGE INTERNAL DIAMETER, M	0.0600+/-0.0007	0.0320+/-0.0002	0.0604+/-0.0001	0.0601+/-0.0001

➢ COATING CONSTRUCTION AND COATING CONTROL (CHUPIN, 2003)

The coating used was the Copon EP 2306. This was a two-component epoxy paint used in several North-Sea gas transportation pipelines to mitigate pipe roughness and provide corrosion protection. The coating was applied to the same stainless steel pipe as used in other experiments. Due to the small pipe ID, it was not possible to spread the coating using the normal industrial method that involved a rotating nozzle. The coating was thus applied manually.

The coating application was performed in three steps:

1. Pipe preparation. The SS pipe was cut in maximum 2.50 m long sections, 2 mm pressure tapp ings were drilled and plugged with foam and the inner surface was scraped with fine sand paper.

2. Epoxy preparation. The epoxy quantity was computed for each section, and the two components were mixed and stirred. The objective was to apply a 125 μm thick layer of paint. To achieve this film thickness, 28 g of paint per meter of pipe were required, quantity that was doubled to account for contingency.

3. Pipe coating. The paint was introduced at the pipe upstream end and spread by manual rotation of the pipe until complete wetting of the pipe circumference. Excess paint was drained and the pipe was centrifuged at 125 rpm for 5 min. Drainage and centrifugation was repeated twice until an average of 20 g/m of

excess paint was collected to achieve a film thickness as close as possible to specifications. The pipe section was finally dried for 24 hours in slow rotation on an electric motor and for a further 7 days on a bench.

Further information on the coating process and control can be found in Chupin (2003).

SEPARATION PROCESS

The liquids from the test section are led back to the first water/oil separator (Figure 3.7a). This is a small air trap that is located directly after the test sections and is used to vent out the air and maintain atmospheric pressure without any further treatment. Following that, a second and slightly bigger separator promotes initial separation further (Figure 3.7a), but also, together with the small first separator, is absorbing pressure transients and liquid slugs so that the upstream flow remains unaffected. The second separator acts as a surge tank.

The liquids are then finally led to the main and 3rd separator where they are also stored and from where they are pumped (Figure 3.7b). This is a 3 m^3 acid proof steel tank placed in the basement below the flow loop. The tank can be filled from the ground floor with the liquids. The separator contains plastic baffles that promote coalescence and help the separation process, since they reduce vortices in the flow and create a less turbulent environment in the separation vessel. For the purposes of these experiments some extra baffles have been added to enhance coalescence of the smaller droplets formed. The tank has a cylindrical shape with an observation window. The two fluids enter at one end of the separator above the mid-height of the tank, go through the baffles and the larger drops that are thus formed, settle under gravity in the compartment of the separator after the baffles. The separated fluids are then pumped from the other end of the tank. The tank is not completely filled with liquids; there is also a layer of air on top of the oil. The oil is taken out from the top half. There are two available outlets for the oil; depending on the level of the oil/water interface either the top or the bottom one is used. The bottom one is placed at the middle of the separator, while the top one is about 20 cm above it. The oil is then pumped to the test section. Water is pumped from the bottom of the separator.

The fluids in the separator can be observed through an observation window. It has been detected that during the experiments a biological contamination at the interface appeared. The exact origin of this contamination however could not be determined. Preliminary analysis showed that it was neither bacterial nor fungal but probably resulted from an algae thriving in water and finding its nutrient in oil (Chupin, 2003).

(a) (b)

Figure 3.7 a) Air trap/initial and b) final separation/storage at the NTNU experimental facility.

When slower mixture velocities were employed, the algae colony did not spread and stayed at the interface region. The separator was therefore cleaned twice during the experimental procedure with *EXXSOL™ D80*, while during the experiments with *MARCOL™ 52* oil/water separation under gravity was more rapid, the condition in the separator was less turbulent and the algae formations in the separator were less obvious.

DATA ACQUISITION

The experimental information was logged into a PC using the LabView software. This enabled data recording from most of the instruments connected to the test sections and the continuous storage of data that can then be kept for further processing at the desired sampling rate. The data acquisition was done via one

computer and two different data acquisition cards. It was possible to log the signal of most of the instruments used simultaneously. All instruments connected to the permanent infrastructure produce a 4-20 mA signal output. These signals were sent to the signal cabinet for further distribution and conversion.

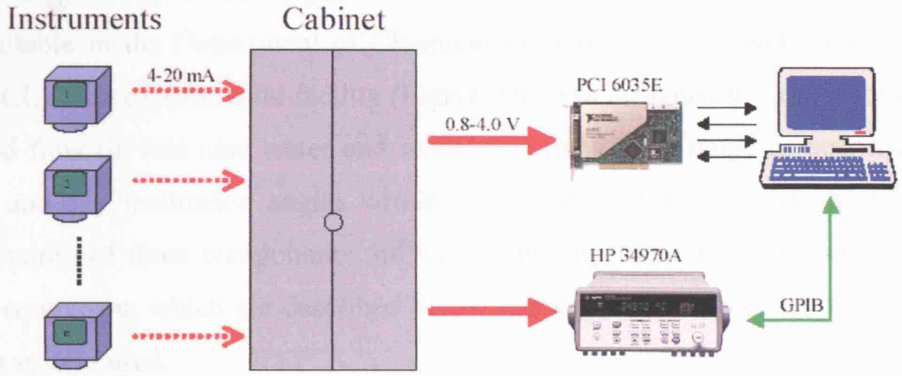

Figure 3.8 Procedure from instruments to saved data at the NTNU experimental facility.

The signal cabinet also supplied the instruments with power. All the signals in the cabinet had their own terminal block, which was then marked. The 4-20 mA signals were then converted through a 200 Ω resistor, to produce a signal of 0.8-4.0 V signal, which was fed to either an external data logging instrument (HP 34970 switch unit) or a Data Acquisition Card (DAQ Card by national Instruments, PCI 6035E MIO) (Lilleby, 2001).

➢ **HP LOGGER**

The HP logger has a lot of built-in electronics for smoothing, averaging etc. suitable for slow changing values, like flow rates. The scan rate was quite slow and depending on the number of the channels in a single scan can be 0.4 s. In these experiments the sampling frequency used was 1 Hz. The logger was connected to the PC via a General Purpose Interface Bus (GPIB) (Lilleby, 2001).

➢ **DAQ BOARD**

The data acquisition board was a PCI card installed inside the PC with a scanning rate of 200 ks/s (kilo samplings per second). Signal conditioning was to be done post processing.

3.2.2 Experimental Flow Facility at UCL

The biggest part of the experimental work was conducted in the oil-water facility available in the Department of Chemical Engineering at University College London (UCL). The experimental facility (Figure 3.9) was designed to run one or two phase liquid flow (in this case water and model oil) for a wide range of operational conditions and any inclination angles within the range -10° to +10°. The test loop consisted mainly of three components: oil/water-handling facilities, test section and separation equipment, which are described below together with a short description of the logging system used.

WORKING FLUIDS

The two test liquids used in the experiments were tap water and a model oil (*EXXSOL^{TM} D140*) supplied by Exxon Chemicals. Its viscosity was measured for a range of temperatures using a Contraves 155 Rheometer (detailed description in Appendix A). Surface and oil/water interfacial tension were measured using a Kruss Processor Tensiometer K-12 (oil properties are shown in Table 3.9). The properties of the oil have been monitored closely and discrepancies were found with time for different oil samples due to possible oil degradation.

Table 3.9 *EXXSOL^{TM} D140* physical properties.

EXXSOL^{TM} D140		
PROPERTY	**TYPICAL VALUE**	**TEST METHOD**
Density	828 kg m^{-3}	Exxon Chemicals
Viscosity @ 25 °C	5.5 mPa s	Contraves 155 Rheometer
Surface tension @ 25°C	27.6 mN/m	Kruss Tensiometer K-12
Interfacial tension @ 25°C	39.6 mN/m	Kruss Tensiometer K-12

Furthermore, it was found that viscosity is strongly dependant on temperature which implies slight fluctuations of oil viscosity during the experimental procedure. An indication of these values is given in Table 3.10.

Table 3.10 Variations of *EXXSOL™ D140* viscosity with temperature.

TEMPERATURE	20 °C	25 °C	30 °C
AS DEFINED FROM EXXON CHEMICALS (mPa s)	7.28	6.19	5.06
NEW OIL (mPa s)	(-)	5.5	(-)
RANDOM (*IN SITU*) SAMPLE (mPa s)	7.01	5.72	4.95

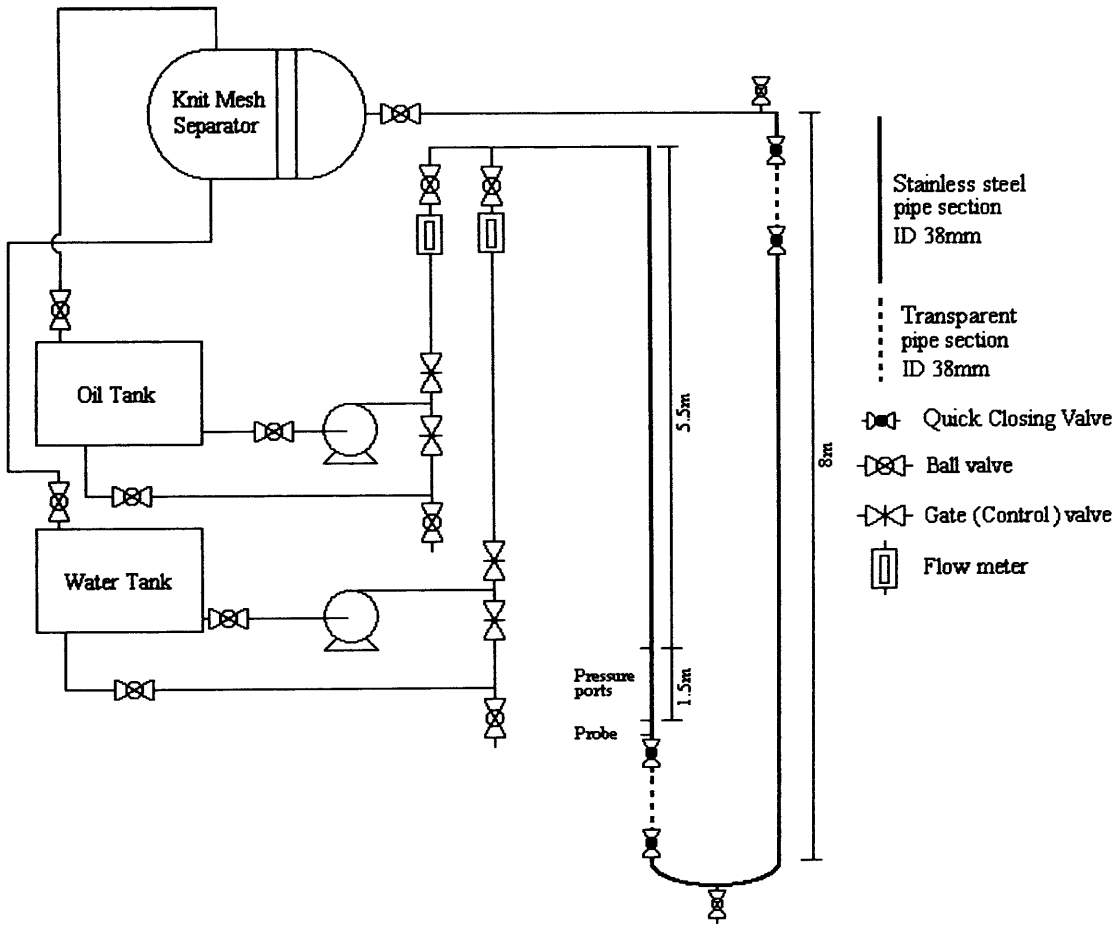

Figure 3.9 Experimental liquid-liquid facility at the UCL experimental facility.

OIL -AND WATER- HANDLING SECTION

Both oil and water handling sections consisted of a fibre-glass storage tank with a total volume of approximately 880 l, a centrifugal pump and a variable area flowmeter. Each storage tank contained baffles to reduce vortexing that might affect the flow exiting to the liquid pump. Furthermore, in case of "intrusion" of one liquid into the storage tank of the other liquid, mostly because of creation of fine dispersions of w/o or o/w due to experimental conditions and the use of high shear centrifugal pumps, baffles were placed in such a way that would stop the entrained phase from escaping to the pump inlet.

The centrifugal pumps (Ingersoll-Dresser CPX200) were capable of generating flow at 240 l/min each and 450 kPa. Pipe connections allowed them to recycle part of their output back to the respective tanks to enable more accurate flow regulation. The normal operational temperature was approximately 20°C (+/- 5°C). Water temperature was maintained by continuously draining and re-filling the water tank with fresh tap water during the experimental procedure. This process also helped to remove any excess heat from the oil during the mixing of the two phases in the pipe, while also keeping the water as fresh and clean as possible (again fine dispersions could form because of experimental conditions and the use of centrifugal pumps).

Finally, two armoured variable area flowmeters (ABB Instrumentation 10A5400) with a 1% full scale accuracy and a range of 20-240 l/min were connected to a PC for data logging. In case there was need for smaller flow rates two similar flowmeters, one for oil and one for water, that cover lower ranges were available (these were not used in the present experimental work).

TEST SECTION

The test section was made from stainless steel 316 and had an internal diameter (ID) of 38 mm. It was a 16 m long pipe which comprised of two, eight-meter long "legs". Each leg was made from two-metre and one-metre long sections connected with tri-clamp fittings which provide a near seamfree connection.

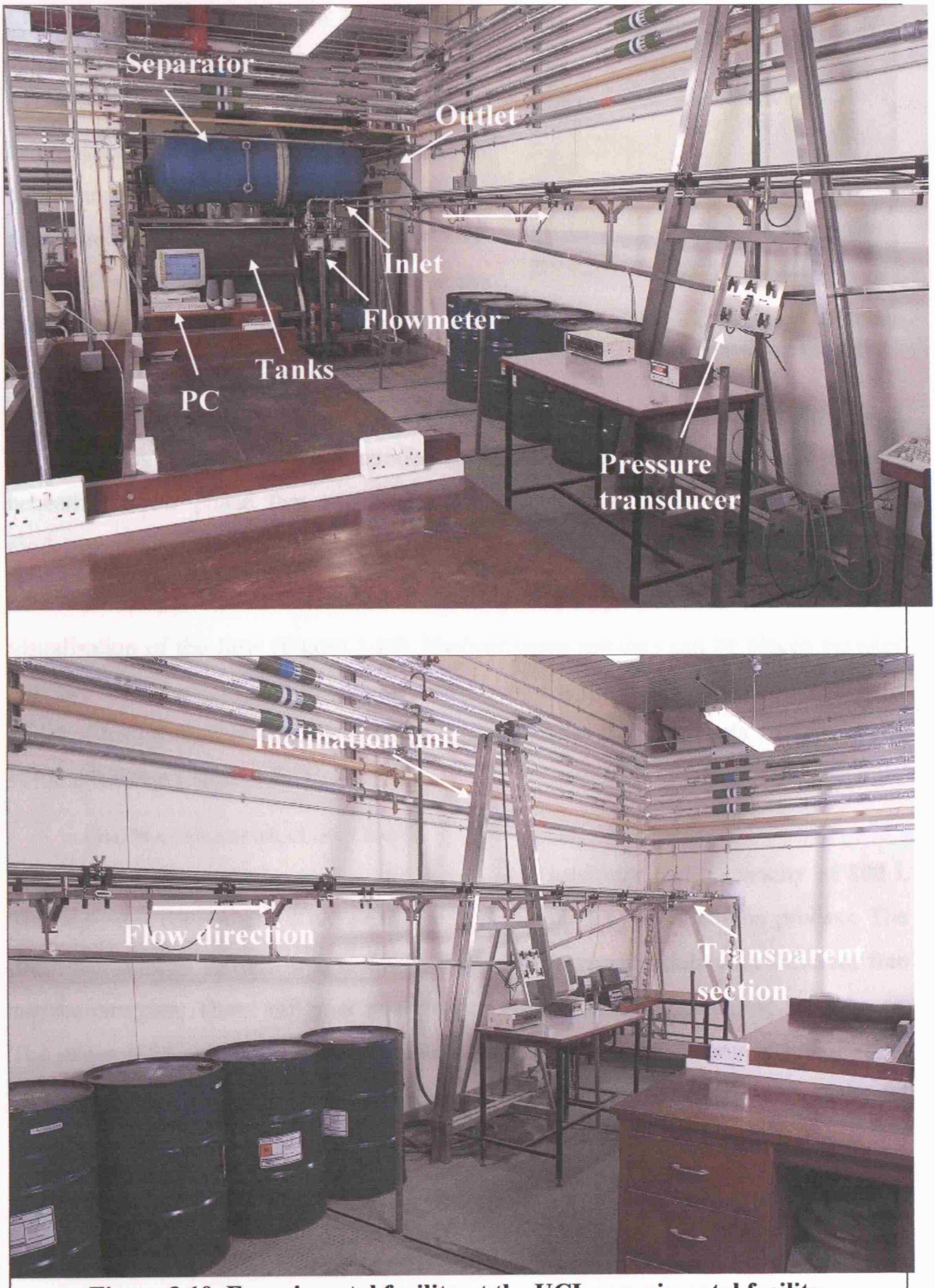

Figure 3.10 Experimental facility at the UCL experimental facility.

The way each leg was built provided the ability to rapidly alter the total length of the test section and move around any instrumentation in order to allow measurements at different locations along the pipe. The individual legs were joined by a U-turn. All measurements were performed at the end of the front leg, since the length was sufficient to ensure full flow development and the effect of the bend on the flow pattern was thus, avoided. The inlet configuration of the two fluids was a modified T-junction (Figure 3.11), with the water phase entering beneath the oil phase that results in low mixing (as confirmed also by CFD modelling).

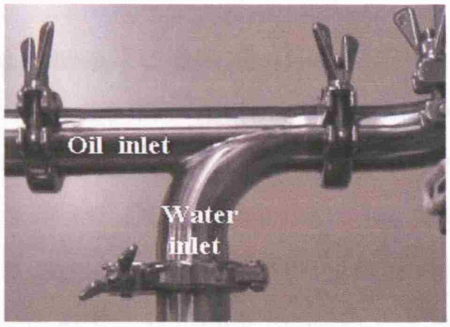

Figure 3.11 Test section inlet at the UCL experimental facility.

Both legs had a one-metre long acrylic transparent section that allowed visualisation of the flow (Figure 3.14). Each of these sections can be placed between any two steel sections, while both of the acrylic compartments were equipped with Quick Closing Valves (QCV) at their ends enabling measurements of the *in situ* volume fraction (Section 3.4).

OIL/WATER SEPARATOR VESSEL

The horizontal two phase (kerosene/water) separator had a capacity of 800 l. The separator contained a KnitMesh coalescer that aided the separation process. The mesh had a large surface area and was made from two materials with different free surface energies. These different materials promoted coalescence of the two phases. The larger drops that were thus formed settled under gravity in the compartment of the separator after the KnitMesh coalescer. The coalescer also helped the flow in the separator tank to be less turbulent and more uniformly distributed. The tank had exit pipes to each of the two storage tanks. The exit pipe for oil was at the top of the separator tank, while the exit for water was at the bottom.

DATA ACQUISITION

The experimental information was logged into a PC that used the HPVee software. This way it was possible to record data from the flow meters, the pressure transducer and the local conductivity probe simultaneously at a sampling rate of 10 Hz. Another computer with custom-made software in MS-DOS was used to log the data from the impedance and the dual impedance probes, which will be described later. The logging frequency varied and was the same as the sampling frequency. The flush probe results were recorded in a separate system that controlled the hot film configuration (DANTEC Dynamics Ltd., described in detail in Hu, 2005).

3.3 PRESSURE GRADIENT MEASUREMENTS

Pressure gradient measurements were performed for all test sections, but different pressure drop measuring devices were employed depending on the anticipated pressure drop along the pipeline and on availability. The distances provided below regarding the measurements were estimated to the first of the two of the pressure ports used in each test section, while the distances over which pressure gradient was measured varied depending on the experimental test section and are stated below.

3.3.1 Measurements at NTNU

Different pressure transducers and configurations were used for the 60 mm ID (bare stainless steel, epoxy coated stainless steel and acrylic) and 32 mm (acrylic) ID test pipes, but also for different sets of experiments, depending mainly on the availability and the range of the instrumentation.

MEASUREMENTS IN THE 60 MM ID PIPES

Throughout the set of experiments that were conducted using the *EXXSOL™ D80* in the two pipes of 60 mm ID (only the acrylic and bare SS pipe were used in this case) the same differential pressure transducer was used. This was a FCX-A series differential pressure transmitter (by Fuji Electrics) which transmitted a proportional 4-10 mA signal. The transmitter utilized a micromachined silicon sensor with state-of-art micropressure technology to provide good performance and functionality. The instrument had 0.07% full scale accuracy and had been calibrated to measure

differential pressure up to 5.50 kPa. The pressure transducer was connected through 6 mm nylon tubings to in-house made pressure taps glued on the pipe outside wall. Pressure ports were located on top of the pipe with tubing filled with air (Figure 3.12 a and b) for the 60 mm ID pipes. A system of quick-connect couplings had been devised for easy and fast changes of the measuring points allowing complete flexibility in the location along the pipe of the pressure drop measurement.

Slightly different equipment was used for the experiments conducted using *MARCOL™ 52*. A differential pressure transducer of the same type but with different specifications was used. This was a FCX-AII Series transmitter, a smart type transmitter equipped with communication function as a standard. Fuji and HART (Highway Addressable Remote Transductor) protocol were supported on FCX-AII Series transmitter. Remote setting/display was possible by using the Fuji Hand Held Communicator (HHC) or HART compatible HHC. Dead time of FCX-AII Series transmitter was approximately 200 msec, that was smaller compared to the previous model FCX-A (300 msec). In this case the HART communicator was used according to the experimental demands to reset the range of the transducers. The DP cell (called DP3 hereafter) had a capacity to measure differential pressure up to 500 kPa, but was re-calibrated for both the bare SS and acrylic 60 mm pipes to measure up to 5 kPa, while for the epoxy coated pipe up to 10 kPa as the pressure ports were located slightly further apart and higher pressure drop was thus expected, even though the same range of pressure gradient was anticipated. The transducer was connected to the pipes by the same 6 mm air-filled nylon tubings.

Due to restricted time and additional equipment, pressure drop for the 60 mm ID pipes was measured in only one location along the pipes. The rest of the existing pressure ports that were not used in the experimental procedure were carefully sealed with screws. Since the tubing connecting the transducer with the pressure ports was transparent, visual observation of the fluid in them was easy and it was possible to check whether there was any intrusion of liquid in the air-filled tubing. In that case, high pressure air could be supplied in them through a loop that has been made especially for this purpose to ensure the tubing was free of liquid at all times. This was

preferably done at the beginning of the experiment in order to avoid introducing potential shift of the zero of the instrument while the experiment was running.

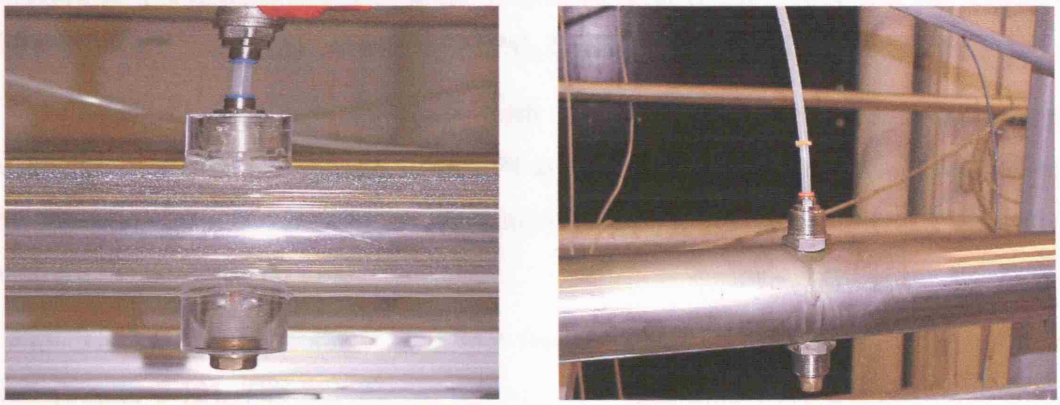

(a) (b)

Figure 3.12 Pressure port in the (a) acrylic and (b) steel pipes at the NTNU experimental facility.

➢ **EXPERIMENTAL PROCEDURE**

For the experiments conducted with *EXXSOL*^{TM} *D80* in the SS pipe, pressure drop was measured at approximately 9.5 m (158*D*) from the inlet section and the pressure ports were located 1.7 m apart, while in the 60 mm acrylic pipe pressure drop was measured at approximately 11.4 m (190*D*) from the inlet section and the pressure ports used were located 1.2 m apart.

For the experiments conducted with *MARCOL* ^{TM} *52* and for the acrylic pipe, differential pressure was measured approximately 10.5 m (175*D*) from the inlet with the pressure ports located 1.2 m apart and at 9.5 m (158*D*) on the SS bare pipe over a 1.67 m distance, while in the epoxy coated pipe pressure drop was measured at approximately 10 m (167*D*) from the inlet over a distance of 2.6 m.

The preparation for the experiments was common in all cases: the zero of the pressure transducers was checked before each series of measurements. This was done by checking the output of the instrument when it was open to atmosphere (zero pressure drop equals 0.8 V output signal). Drift from the zero value was easily corrected by an external adjustable screw.

MEASUREMENTS IN THE 32 MM ID PIPE

For the measurements in the 32 mm acrylic pipe with *EXXSOL™ D80*, a different pressure transducer was used with larger range necessary for the increased pressure drop expected and measured. This transducer (FCX-AII series) can measure differential pressure up to 1.3 bar (130 kPa). This will be called DP4 hereafter.

For the experiments conducted with *MARCOL™ 52* two pressure indications were taken for each experiment from DP4 and DP3 to check the pressure drop along the pipeline. DP3 was re-calibrated using the HART communicator to differential pressure range up to 100 kPa.

The same quick connect couplings have been used for the small acrylic pipe as well (Figure 3.12). The transparent tubing of the transducer for the DP4 was filled with water and pressure ports were located at the bottom of the pipe, while for DP3 pressure ports on top of the pipe and tubing filled with air were used instead.

➢ **EXPERIMENTAL PROCEDURE**

Before each experiment, the pipe would be filled with water and the drain of the DP4 transducer would be left open long enough to get rid of the air bubbles trapped in the tubing and/or oil drops especially found on the tubing walls. When there was no air/oil remaining, the instrument was zeroed to give a signal of 0.4 Volts with static water. Static water would give a signal of 0.4 Volt for zero differential pressure. The maximum value for DP4 would be equivalent to 2 Volts. Similarly, DP3 was open to atmosphere and the zero was checked.

Pressure drop was measured in one location in the small acrylic pipe using DP4 for experiments conducted with *EXXSOL™ D80* approximately 11.0 m (344*D*) from the inlet and the pressure ports were located over a distance of 1.35 m apart.

For the *MARCOL™ 52* experiments pressure drop was measured in two locations using DP4 and DP3 over 1.35 m at 6.5 m (203*D*) from the test section inlet and further downstream at 11.0 m (344*D*) from the inlet. The locations of the two pressure transducers were altered in order to check the measurements obtained.

3.3.2 Measurements at UCL

In the experimental facility at UCL, pressure drop was measured with a FP2000 wet/wet differential pressure transducer (RDP Electronics Ltd). The pressure transducer was connected to the stainless steel pipe of the test section by hard nylon tubing. A system of quick connect couplings has been devised for easy changing of the measuring points to allow flexibility of pressure drop measurement location along the test section (Figure 3.13).

As mentioned above in the description of the experimental test section, each 8 meter leg had one and two meter pipe sections with pressure tapping ports where the male adaptors of the quick connect couplings were fitted, while on the end of the nylon tubing of the pressure transducers were the female adaptors were fitted. These were special auto shut-off, flat face connectors that do not allowed any air to enter the tapping line during connection and disconnection. The dimensions of the ports were carefully designed with the port openings in the test section having a bore size no more that $1/8^{th}$ of the total pipe diameter (Perry, 1997).

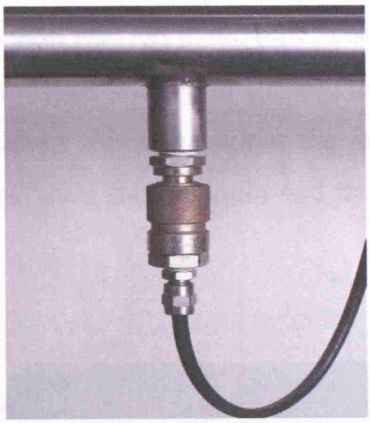

Figure 3.13 Pressure ports in SS pipe at the UCL experimental facility.

The pressure transducer was connected to a type E308 transducer conditioner (RDP electronics) which had been calibrated to give pressure drop.

EXPERIMENTAL PROCEDURE

The tubing of this transducer was filled with water and the pressure ports were located at the bottom of the stainless steel pipe. They could be drained so that no air bubbles or oil drops would remain trapped in them. The zero was checked by measuring static pressure in the pipe which would give a zero signal and any offset would be recorded. Most of the results were taken at 5.5 m from the inlet (145*D*) and over 1.5 m, but different combinations of pressure ports and distances have been tested at times.

3.4 HOLDUP MEASUREMENTS

The average *in situ* phase fraction and slip ratio was measured with the use of the Quick Closing Valves (QCVs) (Figure 3.14). The transparent sections were fitted with the QCVs at each end allowing a specific volume of liquid to be trapped and measured (total volume 800 ml). These sections were fitted with two holes: one was used as vent while the other one was equipped with a small valve to allow quick draining of the trapped liquid. Once the desired flowrates have been set, time was allowed to ensure steady-state (about 2 min) and then the pumps and the QCVs were shut simultaneously. The top hole of the transparent section would be opened to allow draining of the mixture through the valve at the bottom of the section. The test sections was inclined to ensure that no -or negligible amount of- liquid was left in the pipe. The liquid was drained into a glass graduated cylinder and some time was again allowed to ensure good separation of the two phases before the reading was taken. Once the *in situ* volume of the two phases was measured, the pumps were started again and the next experimental conditions were set.

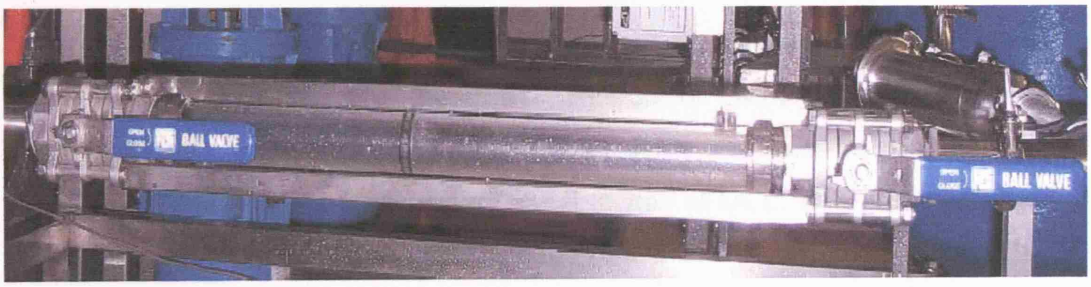

Figure 3.14 Transparent acrylic pipe section used for holdup measurements and visualisation at the UCL experimental facility.

3.5 PHASE INVERSION IDENTIFICATION

The most important feature of this study was the accurate and precise identification of the phase inversion point and of the ambivalent range. Measurements of this kind were conducted in both labs, while a variety of instrumentation, made in-house in its majority, was employed. At NTNU phase inversion was identified through the monitoring of the continuous phase at the whole pipe cross section with ring

probes that were flush-mounted to the pipe wall. Apart from the ring probes, a new probe (called the "wetting probe") was also used to obtain information on the conductivity of the phase wetting the pipe wall. At UCL phase inversion was identified with a combination of measuring devices, such as the local conductivity probe, a flush hot-film probe and the impedance ring probes, all of which were made in-house. The ring probes and a new impedance probe were also self-designed. All instrumentation is described below in detail.

3.5.1 Local Conductivity Probe (LP)

A local probe is a point sensor, whose shape is usually similar to that of a needle. In two-phase flow the probe emits a two-state signal indicating which phase surrounds its sensitive tip, based on the detection of differences between the physical properties of the two phases. Local probes may discriminate between the phases based on a variety of properties (i.e. thermal conductivity, refractive index, electrical resistance or electrical impedance). Due to the large differences in the electrical properties between oil and water electrical probes are widely used to obtain measurements in two phase oil/water flow.

In the dispersed flow regime, the continuous phase is not readily identified. In the present work, since one phase was conductive (water) and the other non-conductive (oil), a conductivity probe (Figure 3.15) was used to determine phase continuity (Lovick, 2004) at the experimental facility at UCL. This probe consisted of two copper needle-conductivity wires of 0.5 mm diameter that were placed 10 mm apart, a distance chosen so that it was bigger than the largest expected dispersed drop to ensure that the probe was monitoring the conductivity of the continuous phase (Lovick, 2004). Each wire was insulated with a wire sleeve leaving only a bare tip (of about 3 mm when straight and about 10 mm when bent) exposed to the flow. The needles were mounted normal to the direction of the flow and could be moved across a vertical pipe diameter together. The tips of each wire were at times bent by 90° in opposite directions along the flow direction; this was shown to increase the sensitive area and made their response clearer (Ioannou *et al.*, 2004).

As both wires were placed at the same height in the pipe they indicated phase continuity at that particular height. Scanning along a vertical pipe diameter could therefore indicate whether phase inversion happened simultaneously in the whole pipe cross section or whether gravitational effects resulted in different phase inversion points. When an electric current was applied to the needles, there would be a voltage output when the needles were immersed in a water continuous mixture and no signal when the needles were immersed in an oil continuous mixture. The probe was located 7.0 m from the test section inlet (equal to 184D), in order to avoid inlet effects.

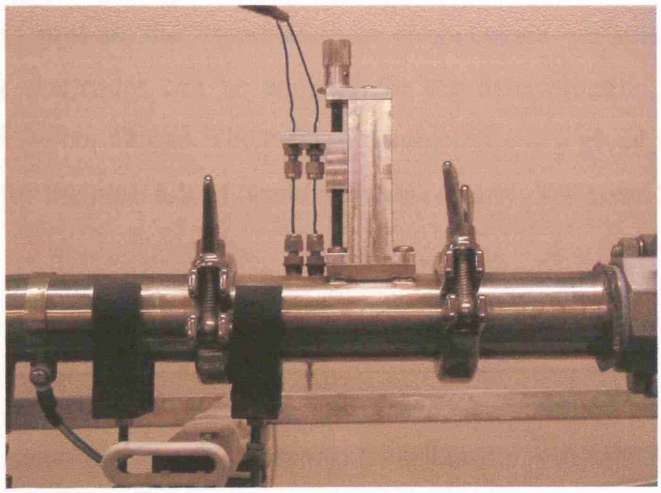

Figure 3.15 Local conductivity probe mounted on the 38 mm ID SS pipe at the UCL experimental facility.

3.5.2 Impedance Ring Probes (RP)

To identify phase continuity, impedance ring probes were located (at 0.5 m, 3.5 m, 8.0 m and 12.0 m away from the inlet) along the pipeline in both acrylic pipes (32 mm and 60 mm ID) at NTNU, while similar configurations were later constructed at UCL. Each probe consists of two electrode pairs placed in the internal wall of a cylindrical duct made from acrylic, flush to the pipe surface. The electrodes were stainless steel rings; the length of the rings was therefore equal to the pipe circumference πD. This is a non-intrusive measurement system since the sensor does

not disturb the flow. The technique is based on the measurement of the electrical impedance between two electrodes which in this case are the rings of the same pair. By placing electrodes at the perimeter of the pipe and measuring the bulk impedance between a pair, it is possible to distinguish between oil and water phases that have different electrical properties. An electrical field is formed between the electrodes when current is supplied. This field is dependent on the conductivity of the fluid that is flowing in the pipe and between the two rings. When the pipe is filled with water, the output voltage will be maximum and when there is oil or air in the pipe the output voltage is minimum (zero).

According to Andreussi *et al.* (1988) who conducted studies in liquid/gas flows for these types of probes, the capacitance or conductance are related to the liquid holdup, and ring electrodes can be adopted for the determination of liquid holdup under dispersed flow conditions. The ratio of conductance at a given liquid holdup and the conductance for the pipe full of liquid (expressed as G_E) is given by:

$$G_E = H_L^{3/2} \tag{3.2}$$

where H_L is the liquid holdup. This can also be applied in oil/water flows where water is the conductive liquid and oil is the non- conductive phase. It is recommended that static calibration curves should be used in case a precise measurement of holdup is required, while according to Andreussi *et al.* (1988) when the distance between the electrodes is greater than $2.5D$, where D the diameter of the pipe, the holdup is linearly related to conductance. For the experimental conditions employed in this study it was not possible to obtain holdup results in the oil continuous region since the output voltage signal would be zero, independent of the watercut in the mixture. However, this was attempted for the water continuous region after thorough static calibrations at the UCL facility.

Figure 3.16 shows the basic dimensions of an impedance ring probe mounted in an acrylic tube section used in the experimental facility at NTNU. The length of the acrylic pipe section was 50 cm. The distance between the rings in a pair was 18 mm

while the thickness of each ring was 5 mm. The distance between two successive pairs of rings was 125 mm. The acrylic mounting can also be seen in Figure 3.17a.

Each pair of rings at NTNU was connected to one channel of the analyser. The connection between the ring and the electronic box was via a double coaxial cable. On the impedance ring probe side, both rings were connected to signal cables. The signal cable from one of the rings was connected to the conductor of the coax, while the one from the other ring was connected to the shield (sheath) of the coax. This means that a single signal comes from the combination of two rings as a pair.

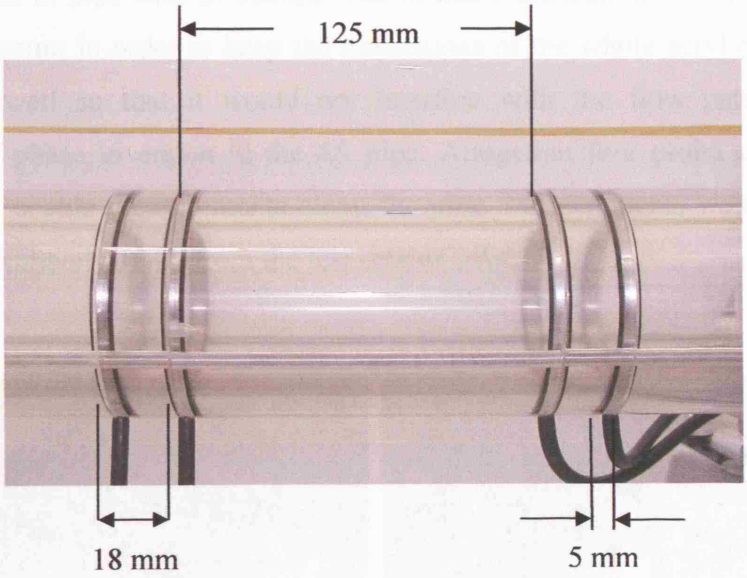

Figure 3.16 Impedance ring probe dimensions at the NTNU experimental facility.

The probes were run through a two-point oil-water calibration before starting each experiment. The probe signal was set to 1 for single-phase water in the pipe and 0 for single-phase oil (Ioannou *et al.*, 2004). In most cases the graphs obtained are interpreted as indicative only. The probe can be used to identify the continuous phase in fully dispersed flow, since the signal of the probe is zero in case of oil continuous flow (non-conductive), while if water is the continuous phase, the signal is somewhere between 0 and 1 depending on the percentage of water in the pipe cross-section.

Due to a special adaptor the ring probes (RP) could be used with the SS and the epoxy coated pipes as well (Figure 3.17b) for experiments conducted with *MARCOL ™ 52*. The probe sections when used with a test section of different material were located downstream close to the pipe outlet, and more specifically at approximately 200*D* from the test section inlet for SS and the epoxy coated SS sections) so that the flow pattern and the appearance of phase inversion point would not be affected by this change of material.

Similar configurations were constructed for use at UCL (Figure 3.18). These were of smaller dimensions in order to match the smaller SS test section and were fitted to the rest of pipe with tri-clamps. The distance between the rings of a pair was kept to a minimum in order to keep the dimensions of the whole acrylic section to a minimum as well so that it would not interfere with the flow pattern and the appearance of phase inversion in the SS pipe. Altogether four probe sections were constructed to enable measurements along the pipe. Measurements were most times taken at approximately 184*D* from the test section inlet.

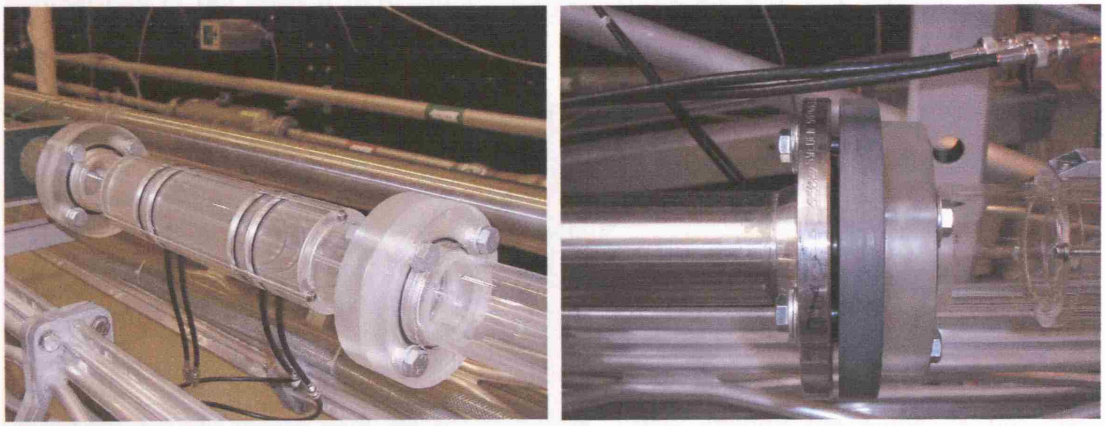

(a) **(b)**

Figure 3.17 a) Impedance ring probe (RP) section in the acrylic pipe and b) adaptor for use of ring (RP) and wetting probes (WP) with SS and epoxy coated SS test sections at the NTNU experimental facility.

Figure 3.18 Impedance ring probes (RP) at the UCL experimental facility.

3.5.3 Wetting Probe (WP)

This was a design very similar to that of the ring probes, but with much smaller rings (Figure 3.19). More specifically, it consisted of one pair of fine rings (with rings' width 0.2 mm) placed 0.1 mm apart. This probe could enable the identification of the phase that was wetting the pipe wall (similar to the flush probe, described in the following section). This is because the sensitivity of the probe is increased in comparison to the normal impedance ring probes, giving a higher voltage output for the same water fraction since the two rings were placed very close to each other. The circuit was thus, more easily bridged and this would allow even small amounts of a water continuous layer in the pipe cross section to be detected. The connection to the conductivity box was exactly the same as the one described for the impedance ring probes at NTNU. The probe was only used for the set of experiments in SS and epoxy coated pipe with *MARCOL*^{TM} *52*. The wetting probe

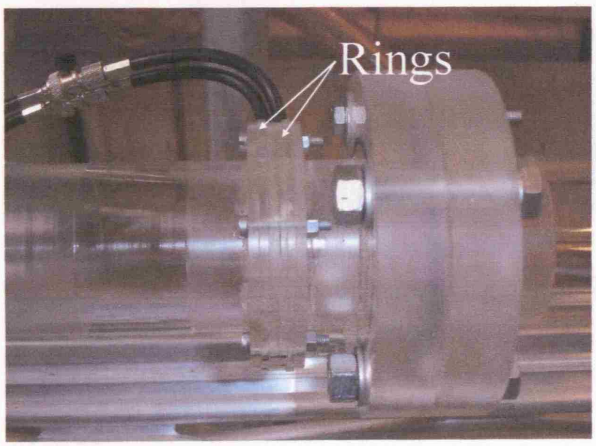

Figure 3.19 Wetting probe (WP) used with the epoxy coated and bare SS pipes at the NTNU experimental facility.

was placed close to the outlet of the test sections so that the change of wall material would not affect the other experimental results.

3.5.4 Flush Probe (FP)

The identity of the continuous phase that was wetting various parts of the pipe was determined also by a glue-on hot-film probe that was located on the pipe wall to monitor the phase continuity in the area very close to it (Figure 3.20).

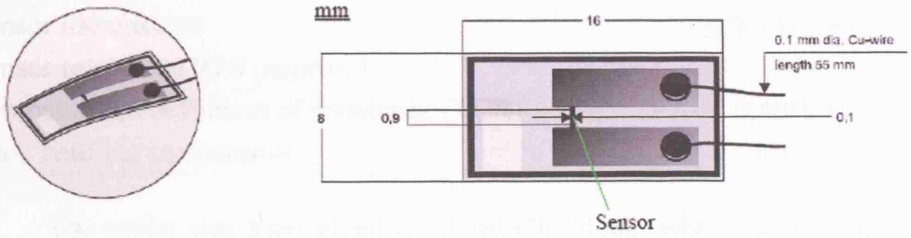

(a) Schematic of the probe

(b) Side view of probe mounting

(c) Top view of probe mounting

Figure 3.20 Flush probe (FP) used with the 38 mm ID SS pipe at the UCL experimental facility.

This probe (55R47 supplied by Dantec Dynamics Ltd.) was employed and linked to a computer-controlled hot film anemometer (HFA, Dantec 99C10) further discussed in Hu (2005). In the glue-on hot-film probe, as shown in Figure 3.20, the sensor was deposited on a Kapton™ foil, which is 50 μm thick. The sensor was 0.9

mm ×0.1 mm and connected to gold-plated lead areas. Copper wires soldered to the leads constitute the electrical connection between probe cable and probe. The sensor was oriented perpendicular to the flow direction. The details of the technical data (Hu, 2005) for this probe are listed in Table 3.11.

Table 3.11 Technical data for the flush hot-film probe DANTEC 55R47.

PROPERTY	TECHNICAL DATA
Thickness of quartz coating	0.5 μm
Medium	Air
Sensor material	Nickel
Sensor dimensions	0.9 × 0.1 mm
Sensor resistance R20 (approx.)	15 W
Temperature coefficient of resistance (TCR)	0.40%°C
Max. ambient temperature	120°C

The probe was then glued to an acrylic block, which, as seen in Figure 3.20 b&c, had a surface flush with the inner wall of the pipe and was inserted into a 10 cm long SS section. The whole section was sealed at the ends with rubber O-rings. The probe once glued could not be removed. The glue-on hot-film probe is primarily designed for measurements in air flows and has never been used before for monitoring the phase continuity. However, even in this work (also in Hu, 2005) useful results were obtained; experiments were performed by placing the probe at the bottom, middle or top of the pipe. The probe was mostly used to obtain results at 7 m from the test section inlet (184*D*).

3.6 PHASE AND DROP SIZE DISTRIBUTION: THE IMPEDANCE PROBES

Phase and drop size distribution measurements in a pipe cross section were enabled in the experimental facility at UCL through a local impedance probe made in-house. Results obtained from this probe combined with conductivity measurements taken from all different measuring devices can indicate whether the flow pattern is homogeneously dispersed or if gravitational effects have resulted in a stratification of the dispersed drops. Stratification of drops may be responsible for initiating phase inversion. In total, two different probes have been used, based on the same principle.

The first one was made previously (Lovick, 2004). The second one was designed, constructed and tested as part of this work to reduce the required maintenance, and improve precision, especially at high flowrates, compared to the original design.

3.6.1 Phase Distribution - Local Impedance Probe (LIP)

Phase distribution was measured with one local impedance probe. Impedance probes measure the differences in capacitance and/or the resistance between the two phases. Similar to the conductivity probes they consist of 2 sensors. If the sensors are in contact with oil (or alternatively air) the resistance value is large and no signal can be recorded. These probes are used extensively in research in different configurations.

A common configuration is to have one probe in the form of a wire placed at a known distance across the pipe diameter and a second probe in the form of a small plate attached to the pipe wall. With this configuration Barnea (1980) identified flow patterns in gas-liquid flow. Having the electrodes far apart means that only phase continuity can be measured. The other approach that is also widely used is to have both electrodes on a single coaxial wire. The shape of the probe tip is very important in this case, since it will pierce the droplets and identify them.

In such applications the tip geometry can affect the electrical field around the probe and is important especially when the tip is close to the pipe wall. A sharp pointed tip (Figure 3.21) will have a spread electrical field that is prone to errors by wall effects but will be able to pierce droplets of water or oil and increase the chances of recording even the smallest droplets, while at the same time the deformation of the droplets is kept to a minimum. A blunt tip has non-spreading electrical field and is therefore less prone to errors caused by the wall effect (pipe wall), but will pierce the dispersed drops with greater difficulty.

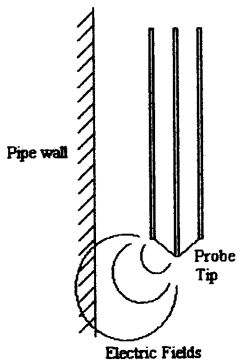

Figure 3.21 Electrical fields around a probe tip.

The first probe (see Lovick, 2004) was based on the work of Das & Pattanayak (1993). The probe is able to detect the difference in electrical impedance between oil

and water and obtain results that when processed give phase distribution. The electronics have a variable AC frequency. Alternating current is used to avoid polarisation and electrolysis effects. Furthermore, alternating current minimizes the chance of an electro-attack on the tip. The measurements are made when current is flowing in one direction only to avoid directional effects (Das & Pattanayak, 1993). More specifically, the electrode used for the probe was a semi-rigid coaxial wire (EZ34 Huber - Suhner) with a solid copper outer conductor and a silver coated copper inner conductor separated by an insulator. The inner electrode had a diameter of 0.2 mm and the outer electrode had a diameter of 0.9 mm (Figure 3.22). The whole wire was coated with a heat shrink insulator which made the total outside diameter equal to 1.4 mm. For phase fraction measurements the tip was cut short with the inner conductor protruding approximately 0.5 mm so that the distance between the two conductors was kept to minimum. This configuration allowed measurements to be made close to the pipe wall.

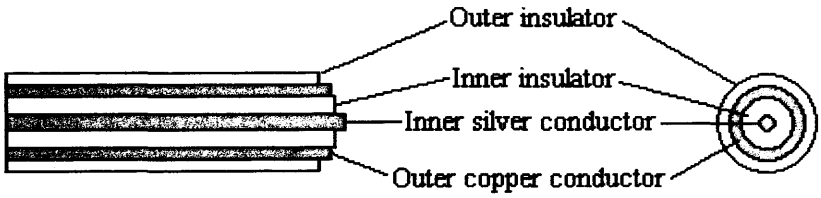

Figure 3.22 Local impedance probe electrode design used at the UCL experimental facility.

Minimum distance between the two conductors should be obtained so that measurements could be obtained close to the wall. The smallest droplet that could be measured was 0.2 mm, since this was the diameter of the inner conductor.

At the beginning of each experiment the counts for 100% oil and 100% water were determined. The water value was found by placing the probe in water and adjusting the signal (band) of the oscilloscope so that it was minimum. To measure the oil count the probe was placed in oil and the oscilloscope signal was set to maximum. The band width controlled the maximum count possible, and allowed a greater

difference between the impedance of the phases to be achieved. This way it was made possible to calculate the percentage oil present each point of the pipe cross section by comparing the count recorded to the range of 100% water and 100% oil. For each alternating current cycle, a count was given that represented the time in which the probe was in oil. As the duration of the total cycle was known the percentage of oil for that cycle could be calculated. Further details can be found in Lovick (2004).

Experiments on phase distribution were carried out at the highest possible sampling rate of 45,000 Hz and 120,000 samples were collected. Both values were chosen based on previous work (Lovick, 2004) and were considered suitable for the high mixture velocities employed. The time counter was turned on and off depending on the state of a capacitor rather than by a predetermined value of impedance. The capacitor was charged quickly when the probe tip was in a low impedance water environment, and slowly when it was in high impedance oil environment. When the probe was in oil, the capacitor was not charged and the time counter was initiated. This count continued until the probe was surrounded by water which caused the capacitor to be charged and the time counter to stop (Lovick, 2004).

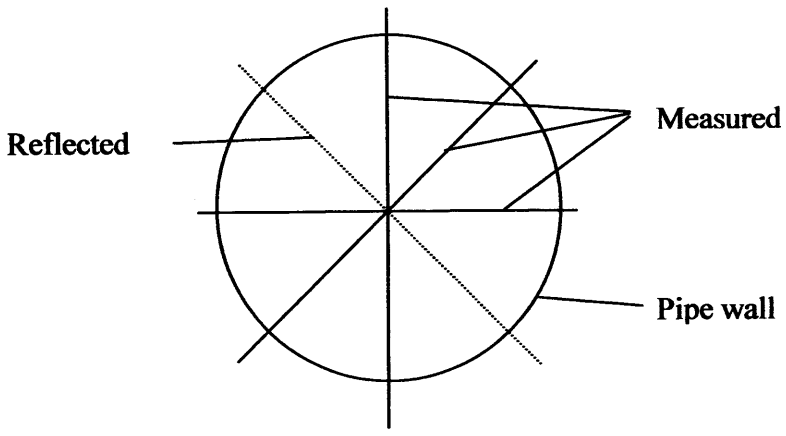

Figure 3.23 Sampling points in the pipe cross section for the impedance probe at the UCL experimental facility.

Measurements were made in the horizontal, vertical and 45° diagonal diameter, at intervals of 2 mm (Figure 3.23). Assuming symmetry in the flow, the volume fraction values at 135° were considered the same as those at 45°. In total, 50 locations

were sampled. Also, by integrating the phase distribution data over the pipe area, the average volume fractions of the two phases in that cross section could be found. This can be done using a FORTRAN program (Lovick, 2004). These results could be compared with those by QCV results. The phase distribution graphs were then plotted using MATLAB.

Phase distribution measurements with the impedance probe were performed in a slightly different way than previous experiments since each measurement for one set of conditions (oil fraction and mixture velocity) lasted longer than a normal pressure drop and conductivity measurement. For this reason and in order to avoid overheating of the fluids, phase distributions were only obtained at a few phase volume fractions around the phase inversion point. To achieve conditions as similar as possible to those of the conductivity and pressure drop measurements, runs were performed in the same way; the experiment would start with 100% oil or 100% water according to the condition and the fraction of the other phase would be gradually increased. Impedance measurements would only be taken at certain volume fractions. At each of these fractions, the oil-water percentage was kept constant until all 50 locations within a pipe cross section were sampled with the impedance probe; this required about 1 h. After all locations in the cross section had been sampled, flow rates were changed again (allowing about 5 min between every change) until the new required volume fraction was reached. Measurements were usually taken at $184D$ away from the test section inlet.

3.6.2 Drop size distribution – Dual impedance probe (DIP)

An impedance probe with two sensors (*dual impedance probe*) was used for drop velocity and drop size distribution measurements in the two-phase mixtures. The probe consists of two coaxial wires -instead of just one used for obtaining phase distribution data- in a single mounting. Each of the two electrodes was the same as that described for the impedance probe. The probe mounting was the same as that used for the conductivity probe (Figure 3.15 and Figure 3.24 respectively).

The specially designed mounting allows the two sensors to be moved together and at the same height inside a pipe, aligned with the flow direction at a distance of 10

mm apart. This distance was found to be greater that the largest expected drop and at the same time cross-correlation diagrams with clear peaks could be obtained (Lovick and Angeli, 2004).

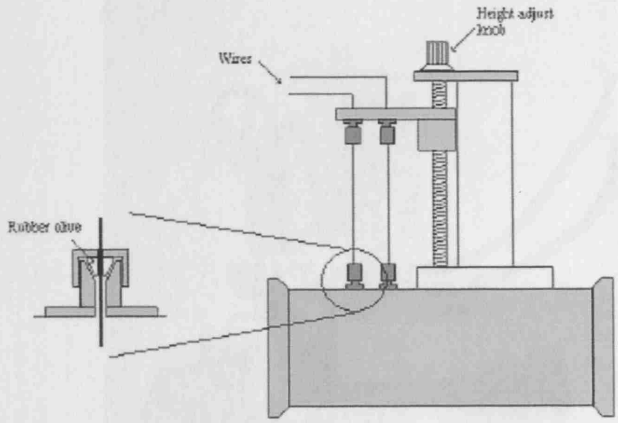

Figure 3.24 Dual impedance probe (DIP) at the UCL experimental facility.

One of the drawbacks of this type of probe is the fact that the charged tip would be quickly electro-attacked by the flowing liquids during the long time of the drop size measurements and would become less sensitive, so a new tip had to be cut for each experiment. A new configuration was thus made (Figure 3.25): instead of a single coaxial silver/copper wire the new electrode consisted of an inner platinum conductor (Platinum-Rhodium alloy , Hogsett and Ishii, 1997, with a diameter of 0.15 mm) and an outer SS tubing with an ID of 0.51 mm (second conductor), isolated with a plastic wire sleeve from each other. The SS tubing was isolated with a heat shrink from a second SS tubing with a bigger diameter (1.19 mm), that would act only as a sheath. The latter was insulated completely from the flow with the use of another heat shrink and only a tip of the inner and outer conductors was exposed to the flow, giving signals according to the phase that was in contact with it, while both stainless steel tubings were acting as the ground of the system. The distance between the two sensors was brought down to 5 mm. The new sensors were then inserted in a traversing mechanism (similar to the one used for the previously designed dual impedance probe

as seen in Figure 3.24) that can be seen in Figure 3.25. The new probe does not require any maintenance or change of the tips.

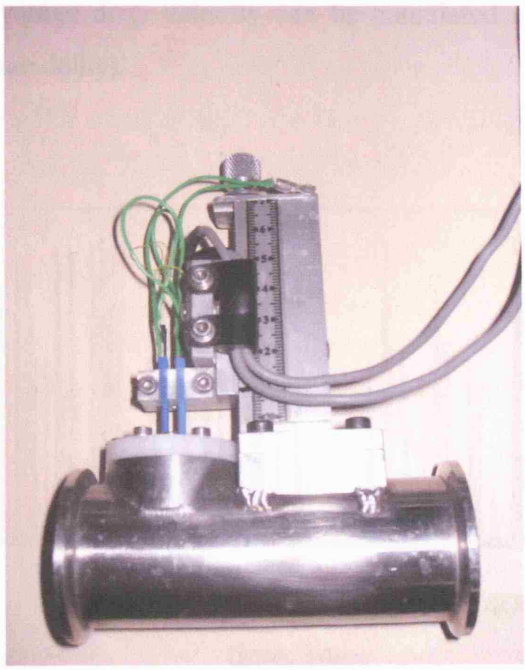

Figure 3.25 New dual impedance probe.

Experimental results with the aforementioned probes were obtained at 7.0 m from the test section inlet. Sampling frequency was again high at 45 kHz. For precise drop size measurements, each dispersed drop should be represented by more than one points in the output signal, thus higher frequency resulted in more accurate results. Measurements were taken every 2 mm in the vertical direction to give a total of 20 sample locations. The resistance data output signals from the two probes are then saved in a PC at a total number of 120,000 from each location. An example of a time series (raw signal) from the dual impedance probe is presented in Figure 3.26, where the signal (E) has been divided with single phase oil signal (Emax).

It is assumed that the drops detected from the first upstream sensor would be then detected from the second sensor for both designs. Drop velocity can be estimated by the time and the distance between the sensors. Thus, the data from the two probes

were cross-correlated (the cross correlation function for the signals shown in Figure 3.26 can be seen in Figure 3.27) to obtain the average time delay for the drops passing through the distance between the two probes. Since the distance between the two sensors is known, the average drop velocity can be calculated as a result (distance divided by the average time delay).

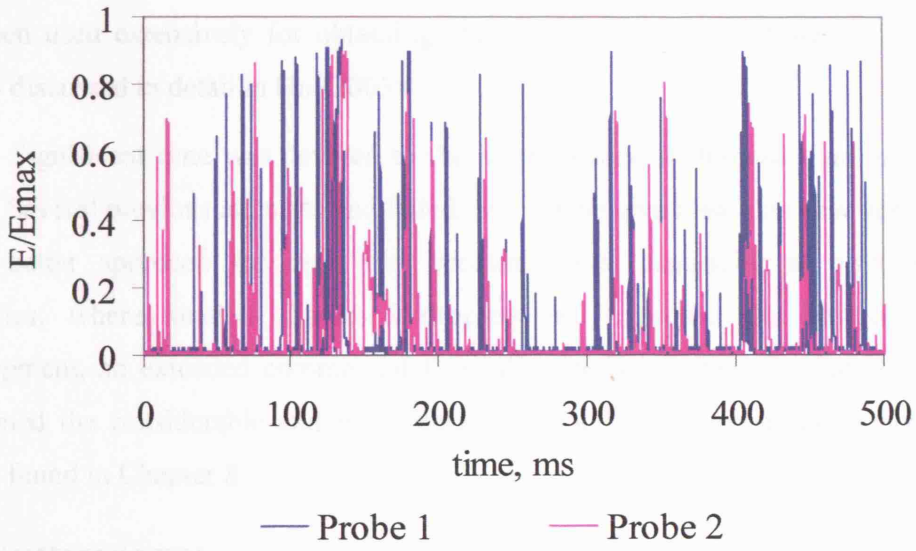

Figure 3.26 An example of the raw signal obtained from dual impedance probe.

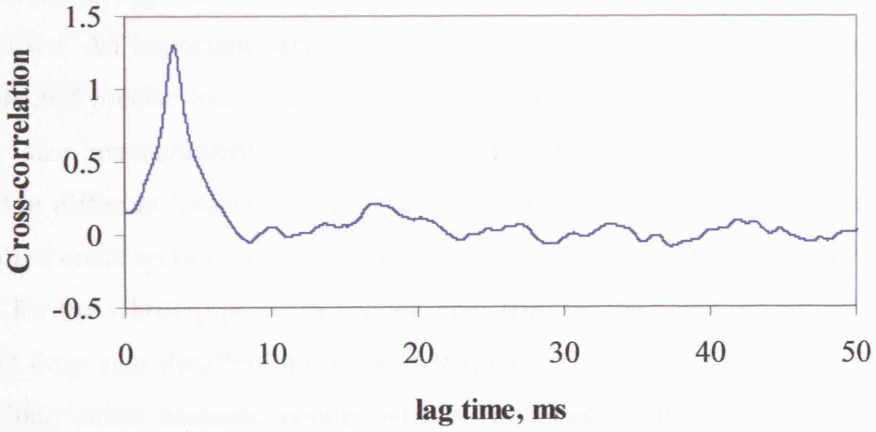

Figure 3.27 Cross-correlation function against lag time showing a peak at the time needed by a drop to travel between the two sensors of the probe.

Following the determination of the drop travelling velocity, the chord length can be found from the signals of either sensor by multiplying this average drop velocity by the duration of each drop passage. To obtain the durations of each dispersed drop passage, a square wave model based on level and slope threshold values developed by Lovick (2004), was used. Finally, chord length distributions for each location were found by summarising all the drops detected in the recorded signals. An improved programme and algorithm has been developed by Hu (2005) and has been used extensively for obtaining chord velocity and chord size distribution. This is discussed in detail in Hu (2005).

Significant time was devoted to the development of the new dual impedance probe. Several previous attempts had failed, but it is believed that this new version is a much better approach for drop size measurements, especially at high mixture velocities, where smaller dispersed droplets are expected. In addition to its development, an extended commercial feasibility study has been carried out, which confirmed the considerable and immediate potential for its commercialisation. This can be found in Chapter 8.

3.7 SUMMARY

In Chapter 3 the experimental flow facilities and the instrumentation used and the experimental procedures followed were discussed in detail. The working principles and experimental applications were presented. Pressure drop was measured in all test facilities used. An important part of this work was the development and employment of suitable and precise instrumentation for identification of phase continuity but also for drop size measurements. The conductivity of the continuous phase can be measured at different locations along the test section either locally at different points inside a pipe cross section (local conductivity probe), at the wall with a flush hot-film probe or for the whole pipe cross section area (ring probes, wetting probe). Finally, phase and drop size distributions were measured with impedance probes, while it is believed that more accurate results will be obtained with the use of the newly developed dual impedance probe.

Chapter 4

At the occurrence of inversion

4.1 OVERVIEW

Oil/water dispersions and the change of the continuity of the system (*phase inversion*) have been studied in two flow facilities with horizontal test sections at UCL and NTNU, using a combination of different oil types, pipe materials and pipe diameters. The change of the continuous phase and the phase fraction where inversion appeared were identified with a variety of instrumentation, namely a local conductivity probe (LP), a flush hot-film probe (FP), a wetting probe (WP) and impedance ring probes (RP), enabling measurements that elucidated the mechanism of inversion in horizontal pipes. Phase inversion identification through detection of the electrical properties of the dispersion and the resultant changes in pressure drop at different systems will be described first in Section 4.2. The observed oscillations around and at the inversion point, obtained by different instrumentation will then be discussed in detail (Section 4.3). The effects of inversion on the operating system of the flow facility in NTNU will be also investigated (Section 4.4). Finally, the change of the conductivity of the system in the cross sectional area around and at the point of inversion at the UCL flow facility is presented in Section 4.5. Based on these experimental findings, an inversion mechanism will also be proposed (Section 4.5).

Experiments were carried out at different mixture velocities. At the NTNU facility the range was 2.5 - 4.5 m/s (with steps of 0.5 m/s) for the pipes with nominal ID 60 mm, while in the 32 mm ID acrylic pipe the mixture velocity was 3.5, 4.0, 4.5 and 5.3 m/s. At the UCL facility mixture velocities varied between 3.0 to 4.5 m/s (with steps of 0.5 m/s). Two types of experiments were carried out: either starting from oil continuous mixtures or single phase oil where possible, and gradually increasing the water flowrate while decreasing that of the oil ("Type I", o→w), or starting from water continuous mixtures or single phase water where possible, and gradually decreasing the water flowrate while increasing the oil one ("Type II", w→o). In this way the dispersed phase fraction is increased towards inversion and beyond but the mixture velocity is kept constant. It should be noted that inversion in a specific system at a given mixture velocity does not always occur at exactly the same input oil fraction, but it slightly shifts from one experimental run to the other (± 3% input oil fraction), especially at lower mixture velocities. As a result, some of the characteristic peaks in pressure gradient for example during phase inversion became smoother when averaging more than one data sets. Hence, results from single runs that show better the variations of the variables close to phase inversion point will be presented in this chapter.

It should be noted that comparison of the results obtained at the UCL and the NTNU facilities is not straightforward; different instrumentation for the identification of phase continuity was used in each flow facility, yielding different type of information regarding the same phenomena. Mainly, local probes were used at UCL, while the probes at NTNU gave measurements averaged over the whole cross sectional area. Results from all experimental facilities will be presented.

4.2 PHASE INVERSION POINT: IDENTIFICATION AND ASSOCIATED PRESSURE DROP

Mixture conductivity and the pressure gradient along the pipe were measured at all experimental test sections during phase inversion experiments. Results from NTNU will be presented for the 60 mm ID stainless steel (SS) pipe with the use of *MARCOL™ 52* and tap water as test fluids. Along with the ring probe (RP), the wetting probe (WP), described in Section 3.5.3, is employed. The WP can detect the

phase that is wetting the pipe wall, because even though it has the same construction as the RP, due to its dimensions it has increased sensitivity in comparison to them. Since the two probes were mounted on acrylic sections, the probe sections were located after the pressure ports (same set up for the epoxy coated SS pipe), so that the change of material would not interfere with the inversion point and the flow characteristics, and just before the first separator (RP at $225D$ and WP at $233D$ downstream the test section inlet). Both Type I and Type II experiments were carried out.

For the experiments that have started with water as the continuous phase (Type II), the signal obtained from both probes is initially very high (Figure 4.1a). The signal from the WP is much higher than that from the RP as the pair of rings for the WP is located much closer to each other than the rings in the RP, yielding a higher voltage. The trend of both curves, however, obtained from averaging the signal of each probe over 30 s is similar. As the percentage of oil in the mixture increases, the conductivity decreases, with the decrease being more prominent for the RP. This is due to the fact that the WP cannot detect quantitative changes in the whole mixture, since it will always yield a high voltage as long as it is wetted by water, regardless of its percentage in the flow. At approximately 65% input oil fraction, the signal by the WP starts decreasing sharply (a decrease that becomes bigger with mixture velocity), while the rate of decrease also changes for the RP. This could potentially signify a change in the flow characteristics of the mixture; the formation of an oil layer on the top of the pipe could account for such a decrease in the conductivity signal. Between 75% and 78% input oil fraction the signal of both probes reduces to zero. This is interpreted as a change in the bulk mixture continuity from water to oil continuous. After this decrease, and with further increase of the input oil fraction, the signals of both probes remain at zero since they are now wetted by oil. It should be mentioned that these probes are very much influenced by the continuity of the system close to the wall. If there is an oil continuous mixture close to the wall then the signal obtained is zero, while if both oil and water continuous mixtures wet the wall a non-zero signal will be obtained.

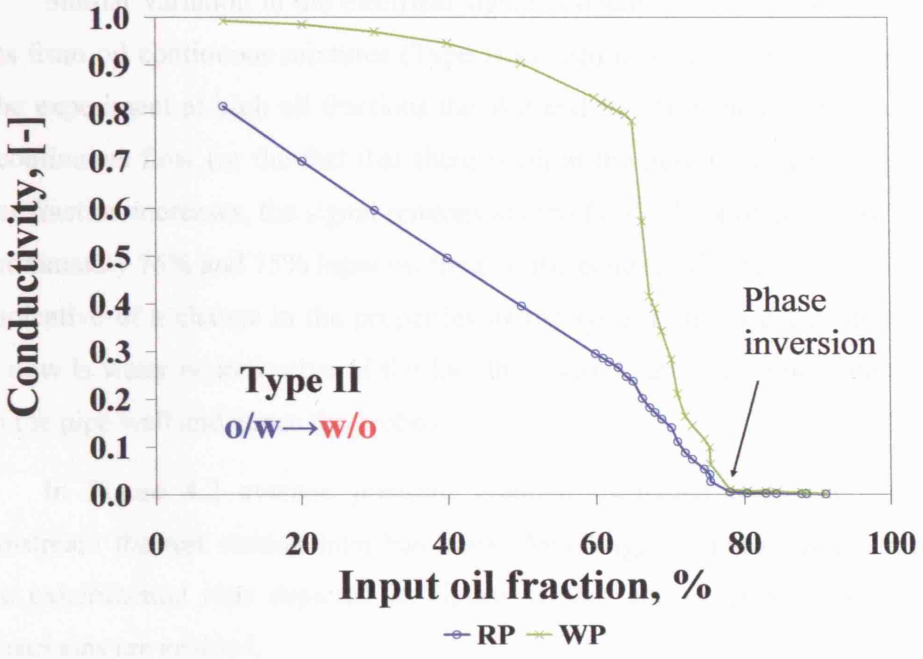

(a)

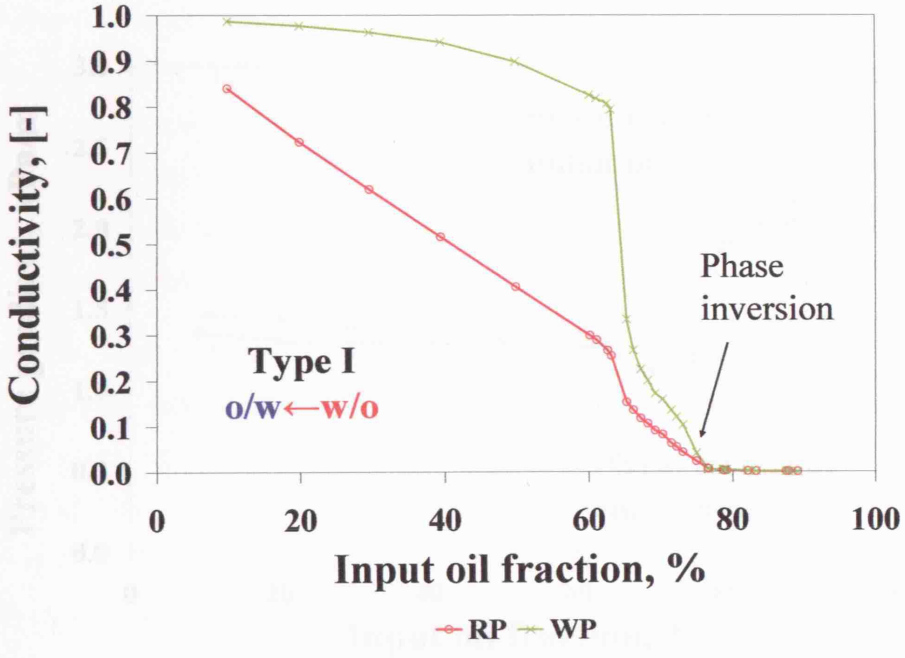

(b)

Figure 4.1 Normalised to single phase water value conductivity signal obtained by the ring (RP) and the wetting (WP) probe for (a) a Type II and (b) a Type I experiments at 3.5 m/s mixture velocity conducted in the 60 mm ID SS pipe with the use of *MARCOL*^{TM} *52* (NTNU). The RP and the WP are located at 225*D* and 233*D* downstream the test section inlet respectively.

Similar variation in the electrical signal is obtained in the case the experiment starts from oil continuous mixtures (Type I) as seen in Figure 4.1b. At the beginning of the experiment at high oil fractions the WP and the RP signals are zero indicating oil continuous flow (or the fact that there is oil at the perimeter of the pipe). As the water fraction increases, the signal remains at zero (still oil continuous flow). Between approximately 76% and 75% input oil fraction the conductivity becomes positive. This is indicative of a change in the properties of the system and in the continuous phase that now is water or indicative of the fact that there is at least some water in contact with the pipe wall and hence the probes.

In Figure 4.2 average pressure gradient measured over 1.67 m at 158*D* downstream the test section inlet has been plotted against input oil fraction for the same experimental runs depicted in Figure 4.1a&b and described above, so direct comparisons are enabled.

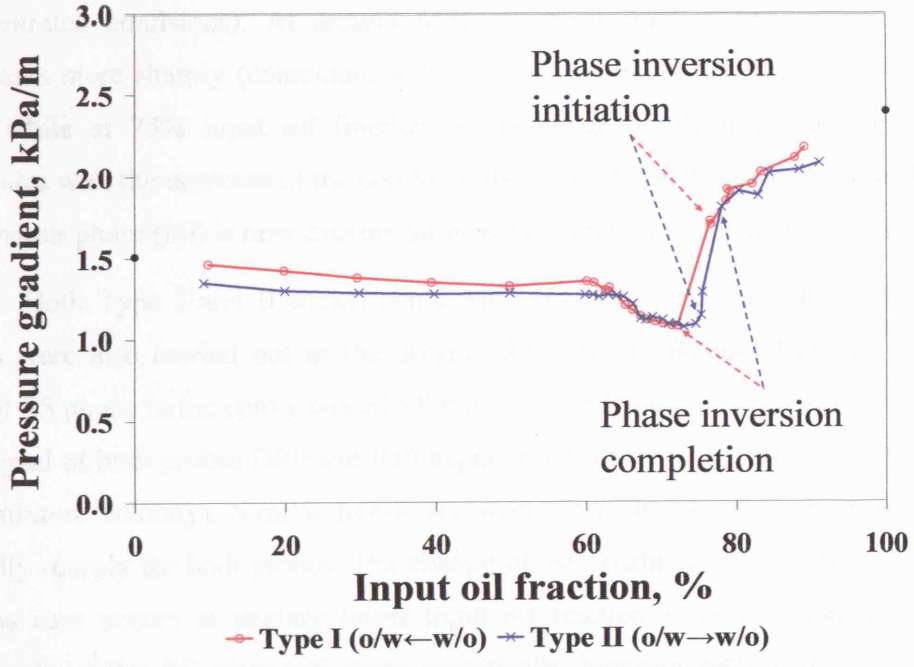

Figure 4.2 Pressure gradient measured at 158*D* downstream the test section inlet against input oil fraction for a Type I and a Type II experiments at 3.5 m/s mixture velocity. Experiments were conducted in the 60 mm ID SS pipe with the use of *MARCOL*^{TM} *52* (NTNU).

Single phase pressure drop values, ΔP, as predicted by the Blasius equation for a smooth pipe can be seen (with the closed symbols) on the vertical axes. These are given by Equation 4.1:

$$\frac{\Delta P}{l} = \frac{2 f \rho U^2}{D} \tag{4.1}$$

where U is the average velocity, l is the length over which pressure drop is measured, f is the Fanning friction factor, ρ is the fluid density and D is the pipe diameter.

Both Type I and II experiments give similar trends in pressure drop with changing dispersed phase fraction. By comparing the conductivity with the pressure gradient data, it can be seen that for the Type II experiment, for example, the initial gradual decrease in conductivity within the water continuous region coincides with a slight decrease in the pressure gradient curve (due to drag reduction[4.1] in highly concentrated emulsions). At around 65% input oil fraction the pressure gradient decreases more sharply (coinciding with the decrease recorded from the WP and the RP), while at 75% input oil fraction, it increases significantly, an increase that coincides with the decrease of the conductivity values by both probes to zero. The new continuous phase (oil) is now causing an increased pressure drop along the pipe.

Both Type I and II experiments with *MARCOL*^{TM} *52* and tap water as test fluids were also carried out in the acrylic (32 mm and 60 mm ID) and the epoxy coated SS pipes. In the epoxy coated SS pipe and for Type I experiments the change in the signal of both probes (WP and RP) happens simultaneously (see Figure 4.3 for 3.5 m/s mixture velocity). Similar trends are seen when the signal from zero increases initially sharply for both probes. The change of the conductivity, and phase inversion, in this case occurs at slightly lower input oil fraction in comparison to the value obtained for the SS pipe and more specifically between 68% and 71% input oil fraction.

[4.1] Drag reduction is discussed in detail in Section 6.8.

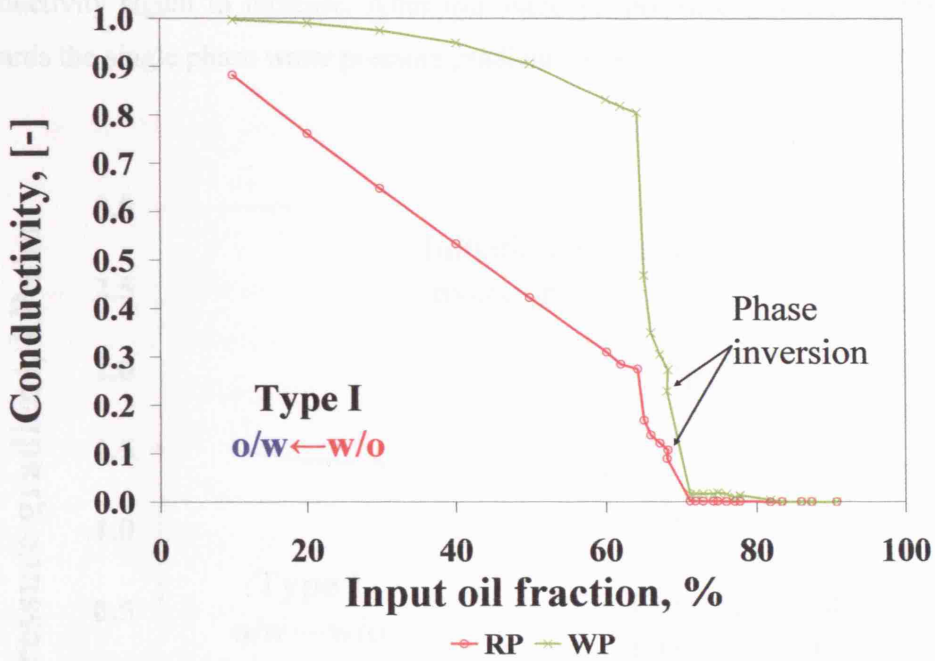

Figure 4.3 Normalised to single phase water conductivity signal obtained from the ring (RP) and the wetting (WP) probe for a Type I experiment at 3.5 m/s mixture velocity conducted in the 60 mm ID epoxy coated SS pipe with the use of *MARCOL*^{TM} *52* (NTNU). The RP and the WP are located at 225*D* and 233*D* downstream the test section inlet respectively.

This can be attributed to the different wettability of the pipe, as SS is preferably wetted by water, hence inversion from oil to water continuous mixtures will occur sooner in the SS pipe. However, these differences are not large. Inversion is occurring at about the same input oil fraction for Type II experiments as for Type I for each test section, so it can be concluded that water continuous mixtures were favoured in the SS in comparison to the epoxy coated SS pipe.

The respective measured pressure gradient at the epoxy coated SS test section is shown in Figure 4.4 against input oil fraction. Pressure gradient is high at the beginning for the oil continuous mixtures and decreases significantly at the point of the occurrence of inversion towards water continuous flows; after inversion it increases initially. This increase, and more specifically the point where pressure gradient appears to have a peak, coincides with the increase in the signal from both conductivity probes. It is possible that at this fraction any residual oil layer is completely consumed by the water continuous phase which could cause the

conductivity signal to increase. After this increase, pressure gradient slightly varies towards the single phase water pressure gradient value.

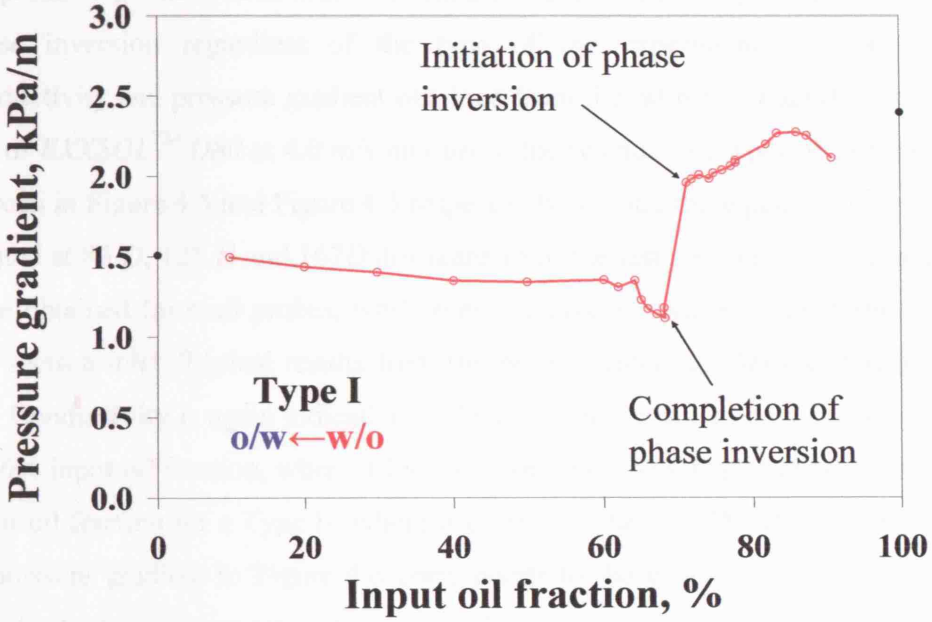

Figure 4.4 Pressure gradient measured at 158*D* downstream the test section inlet against input oil fraction for a Type I experiment at 3.5 m/s mixture velocity. Experiments were conducted in the 60 mm ID epoxy coated SS pipe with the use of *MARCOL*^{TM} *52* (NTNU).

Similar results to the epoxy coated SS section were obtained with the use of the 60 mm ID acrylic pipe. Generally, in the experiments conducted with *MARCOL*^{TM} *52* in all test sections used, the resulted pressure drop was significantly less in the water than in the oil continuous mixtures and this difference was larger for the acrylic than for the SS or the epoxy coated SS test sections [4.2]. Especially with the acrylic, both the 60 mm and the 32 mm ID pipes, and less with the epoxy coated SS pipe with the use of *MARCOL*^{TM} *52,* pressure gradient curves are showing that pressure drop is almost independent of the oil percentage in the oil continuous region, and in the water continuous region away from inversion. This agrees with results from Arirachakaran *et*

[4.2] Differences between the different pipe materials used will be discussed extensively in Section 6.7.

al. (1989) that has shown that for viscous oils, the viscosity of the mixture remains very close to single phase oil viscosity.

When the less viscous oil (*EXXSOL™ D80*) was used in the same test sections the pressure gradient trend was different and a prominent sharp peak was seen around phase inversion regardless of the type of the experiment. Typical results of conductivity and pressure gradient obtained from the 60 mm ID acrylic pipe with the use of *EXXSOL™ D80* at 4.0 m/s mixture velocity and both types of experiments can be seen in Figure 4.5 and Figure 4.6 respectively. In total three pairs of RPs were used, located at 83 *D*, 125 *D* and 167*D* downstream of the test section inlet and same results were obtained from all probes, while pressure gradient was measured 190*D* from the test section inlet. Typical results from the probe located at 83*D* are shown in Figure 4.5. Conductivity is again indicative of the continuity of the system showing inversion at 56% input oil fraction, where it increases sharply, for a Type I experiment and 65% input oil fraction for a Type II, where it decreases sharply. The maximum of the peak in pressure gradient in Figure 4.6 corresponds to the exact point of inversion in the pipe for both experimental routes. Comparing Figure 4.4 with Figure 4.6 it can be seen that the different types of oils used result in totally different pressure gradient behaviour at the inversion point in the same test sections[4.3].

This can be explained considering that for the same mixture velocity the less viscous *EXXSOL™ D80* (viscosity 1.7 mPa s as opposed to 11 mPa s for *MARCOL™ 52*) results in much higher Reynolds numbers which would lead to finer dispersions. The peak in pressure gradient actually agrees with findings in emulsions although in the current cases drag reduction is still seen away from the inversion point [4.3].

Peak at the inversion point with the use of the same type of oil (*EXXSOL™ D80*) was seen by Angeli and Hewitt (1998) in a SS and an acrylic 1 inch ID pipes and Soleimani *et al.* (1999), who used the same experimental facility, but also by Pettersen *et al.* (2001) who used the same experimental fluid but conducted experiments in 100 mm ID acrylic and SS pipes.

[4.3] The effect of oil properties on phase inversion are discussed further in Section 6.3.

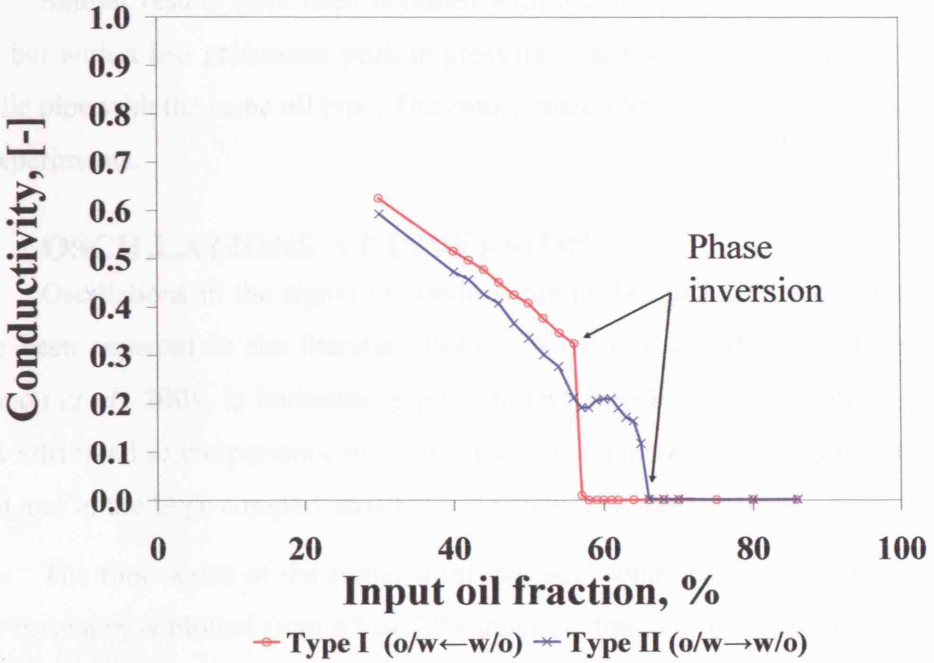

Figure 4.5 Normalised to single phase water conductivity signal obtained by the ring probe (RP) for Type I and II experiments at 4.0 m/s mixture velocity conducted in the 60 mm ID acrylic pipe with the use of *EXXSOL™ D80* (NTNU). The RP is located 83*D* downstream the test section inlet.

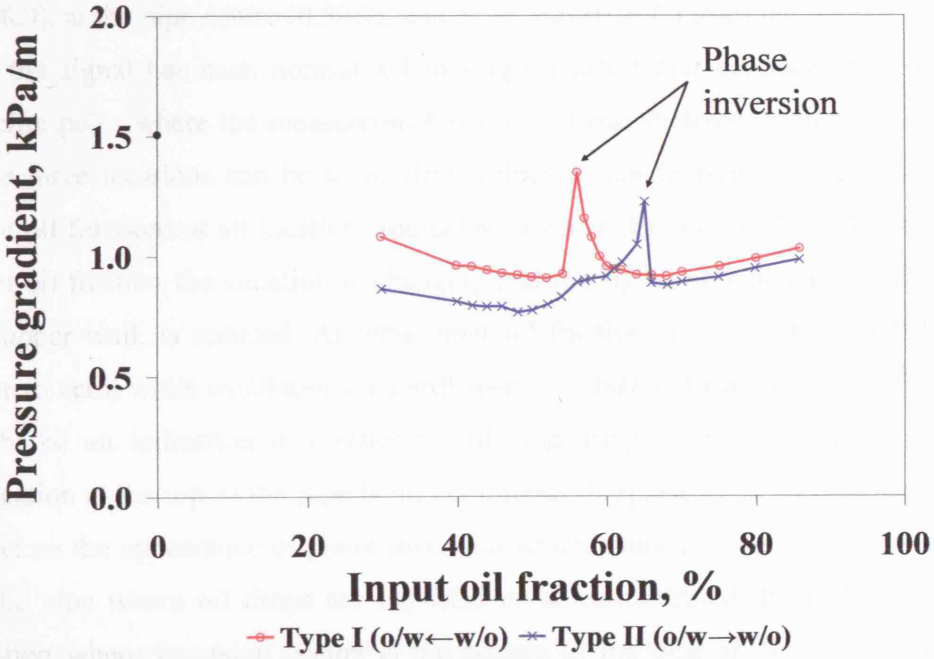

Figure 4.6 Pressure gradient measured at 190*D* downstream the test section inlet against input oil fractions for Type I and Type II experiments at 4.0 m/s mixture velocity. Experiments were conducted in the 60 mm ID acrylic pipe with the use of *EXXSOL™ D80* (NTNU).

Similar results have been obtained with the use of *EXXSOL*^{TM} *D80* in the SS pipe but with a less prominent peak in pressure gradient, but also with the 32 mm ID acrylic pipe with the same oil type. The epoxy coated SS pipe was not used in these set of experiments.

4.3 OSCILLATIONS AT INVERSION

Oscillations in the signal of conductivity probes just before or after inversion have been reported in the literature before (Norato *et al.*, 1998, in stirred vessels; Ioannou *et al.*, 2004, in horizontal pipes; Hu and Angeli, 2006, in vertical pipes) and were attributed to the presence of secondary dispersions in the region of the inversion point and to the large complex structures frequently encountered.

The time series of the signal from the local conductivity probe at oil fractions near inversion is plotted from 67 to 72% input oil fraction in Figure 4.7 for a Type II experiment (w→o) conducted at the experimental facility at UCL (appearance of inversion at about 70% input oil fraction). The mixture velocity is 3.5 m/s. Conductivity was measured at three positions along a vertical pipe diameter: at 3 mm (0.08*D*), at the pipe centre (0.50*D*), and at 30 mm (0.79*D*) from the bottom of the pipe and the signal has been normalised to single phase water conductivity value at the specific point where the measurement is taken. Great differences in the signals from these three locations can be seen. High values of conductivity are recorded at 67% input oil fractions at all locations indicating a water continuous flow. Already at 68% input oil fraction the situation is changing and the signal obtained at 0.79*D*, closer to the upper wall, is reduced. At 69% input oil fraction conductivity at 0.79*D* is very close to zero, while oscillations are still seen at 0.08*D* and especially at 0.50*D*, which might be an indication that water is still appearing in the pipe centre, while the indication at the top of the pipe is oil continuous. It appears that there is some gravity effect on the appearance of phase inversion which happens in this case first at the top of the pipe where oil drops are expected to be concentrated. Interestingly, the next location where inversion occurs is the bottom of the pipe at 71% input oil fraction rather than the centre, indicating perhaps some sort of annular flow with the oil in the annulus. The centre is the last that becomes totally oil continuous.

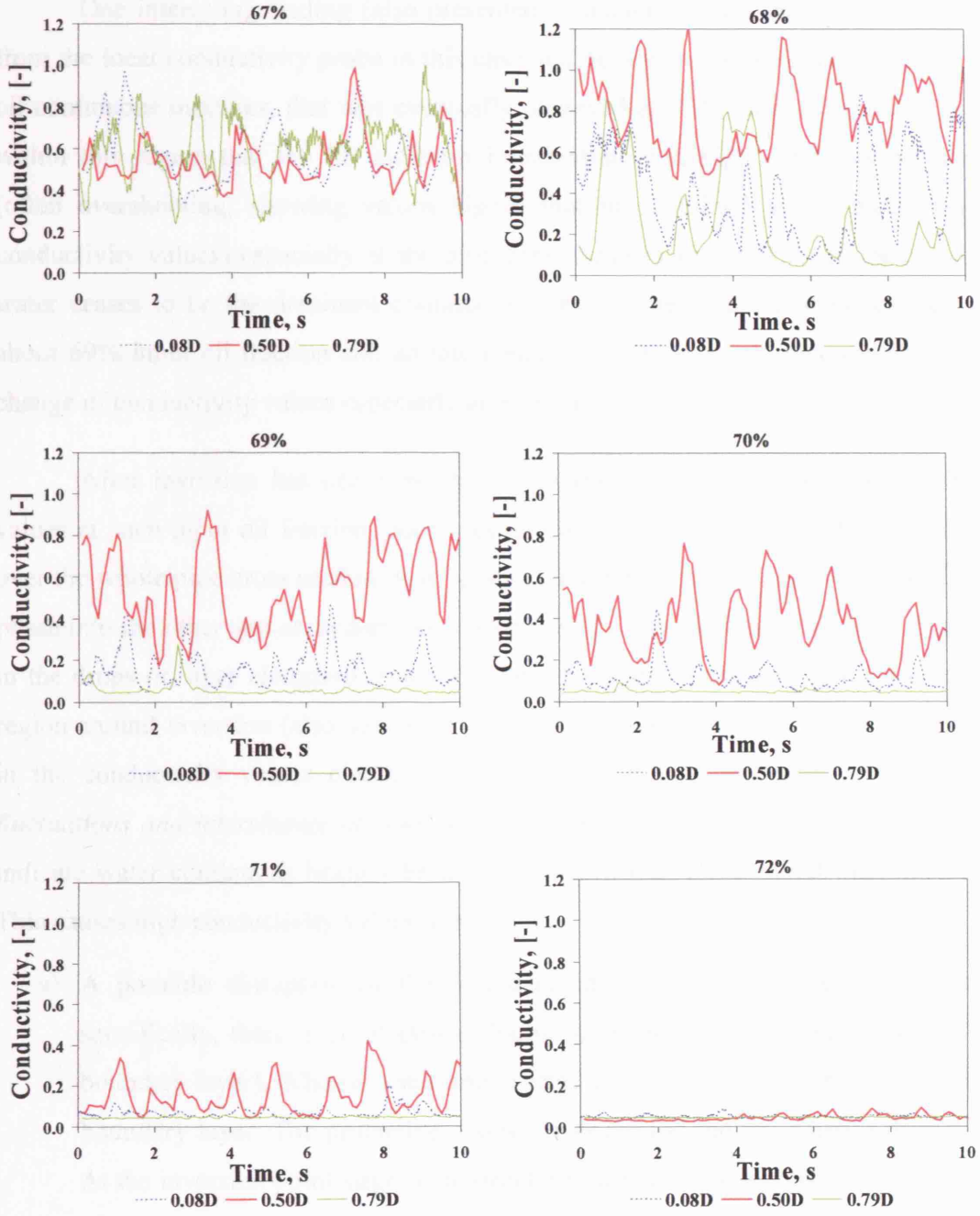

Figure 4.7 Normalised to single phase water value conductivity signals obtained by the local conductivity probe (LP) for a Type II experiment at 3.5 m/s mixture velocity in the 38 mm ID SS pipe with the use of *EXXSOL™ D140*, near and at the inversion point until inversion at the whole pipe cross sectional area has occurred at 72% input oil fraction (UCL). Results obtained from at 3 locations at the pipe cross sectional area, made dimensionless by dividing with pipe diameter. The LP is located 184*D* from the test section inlet.

One interesting finding (also presented in Ioannou *et al.*, 2004) is the results from the local conductivity probe in this case just before and at the inversion point to oil continuous mixtures, that was eventually observed at 72% input oil fraction. It is within this region that the LP indicates intermediate and high conductivity values (often overshooting, showing values higher that the obtained single phase water conductivity values) especially at the pipe core (0.5*D* in Figure 4.7). It appears that water ceases to be the dominant continuous phase in the pipe cross section here at about 69% input oil fraction and an intermediate condition exists that yields a large change of conductivity values especially at the pipe core.

After inversion has occurred, the fluctuations of the measured conductivity values at each input oil fraction, decreases and oil is now the new continuous phase over the whole pipe cross section. It is believed that large continuous structures of one phase into the other and secondary dispersions, where the continuous phase is trapped in the drops or other elongated formations of the dispersed phase, might form at the region around inversion (also seen by Liu *et al.* 2006a and 2006b). The overshooting in the conductivity values obtained from the LP is thus, attributed to the *rapid fluctuations and interchange of continuous phases* in contact with the probe tip that indicate water continuous bridges between the electrodes form, albeit intermittently. This causes high conductivity values due to:

a) A possible disruption of the boundary layer around the electrodes. More specifically, there is an electrical double layer at the tips of the electrodes (a boundary layer). When a water drop comes at the electrode tip, it penetrates the boundary layer. The protective double layer around the tip is hence disrupted. At the inversion point large scale structures are believed to exist, the electrodes are hit by a huge water droplet/formation, then an oil one. As a result, the boundary layer is totally ripped away, then re-established and then hit again, yielding high voltage values and overshooting.
b) The large formations are causing the electronics attached to the sensors to overshoot (opening and closing the circuit rapidly, will cause the meter to swing above the actual current flowing).

At 72% input oil fraction, the conductivity signals from all probes are much flatter, showing that the mixture has now a more uniform distribution of dispersed phase (now water) droplets, re-establishing the values of the LP probe to normal oil continuous values. The fact that the large fluctuations are mainly seen at the pipe core, might be due to the fact that these large, probably elongated structures *can move easily form in the low shear location of the core, while the high shear at the wall will not allow such structures to grow.*

Figure 4.8 shows the signals obtained from the ring probe (RP) for the same experiment. Oscillations are seen here as well, attributed to the same large formations of continuous and dispersed phases, while it appears that inversion of the continuity of the bulk liquid has occurred at 69% input oil fraction.

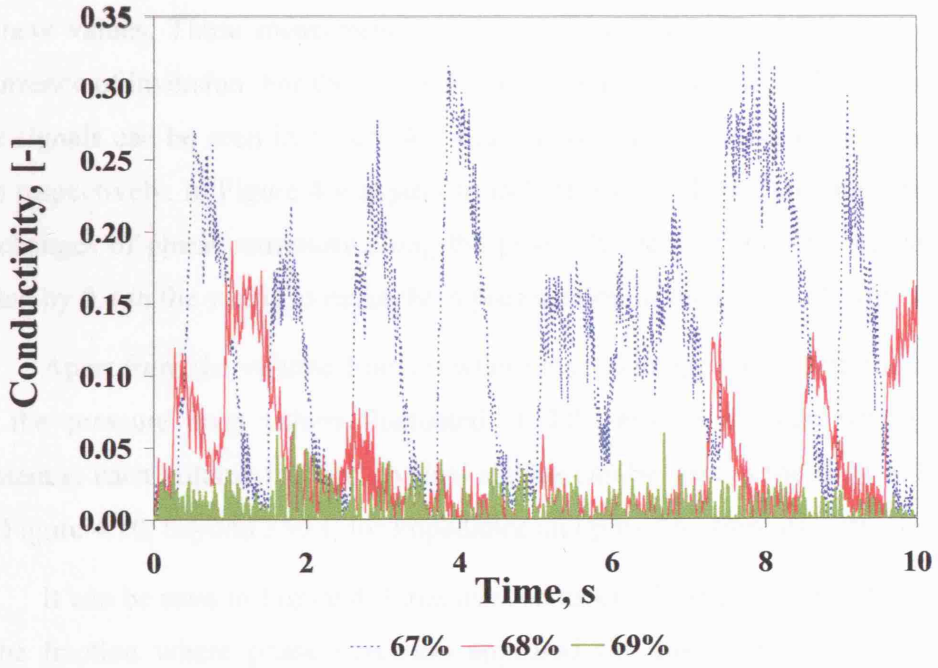

Figure 4.8 Normalised to single phase water conductivity values obtained by the ring probe (RP) at 67, 68 and 69% input oil fractions for a Type I experiment at 3.5 m/s mixture velocity in the 38 mm ID SS pipe with the use of *EXXSOL™ D140* (UCL). The RP is located 184*D* from the test section inlet.

This agrees with results of the LP which shows that close to the wall the mixture becomes oil continuous at a similar fraction (locations 0.08*D* and 0.79*D*). It takes however a further increase of the oil fraction for the signal obtained from the LP at the pipe centre (0.5*D*) to flatten (see Figure 4.7), which indicates that inversion has now happened at the whole pipe cross section.

Oscillations prior to inversion were also seen in the experimental facility in NTNU. A Type I (o→w) experiment will be described for the 60 mm ID acrylic pipe. Results from 2 pairs of RPs (RP1 and RP2) will be presented, located at 5 m and 10 m from the test section inlet (83*D* and 166*D*) respectively, along with results from the pressure cell located right after RP2 (so direct comparisons can be made). *EXXSOL*^{TM} *D80* and water have been used as test fluids, while the mixture velocity was 4.0 m/s. At each volume fraction pressure drop and impedance values were recorded over a period of time starting soon after the flowrates of the two phases had been changed to the new values. These measurements can also reveal a potential time delay at the occurrence of inversion. For the volume fraction where phase inversion appeared these time signals can be seen in Figure 4.9 and Figure 4.10 for conductivity and pressure drop respectively. In Figure 4.9 signals from both RP1 and RP2 are presented to show the changes of phase continuity along the pipe. The zero of the RP2 signal has been shifted by 0.4 in the y-axis to make the representation of the results clearer.

Apart from the volume fraction where inversion appeared, both the impedance and the pressure drop values fluctuated slightly around a mean which remained constant at each volume fraction (typical signals can be seen at the right of Figure 4.9 and Figure 4.10, beyond 350 s, for impedance and pressure drop respectively).

It can be seen in Figure 4.9 that as soon as the flowrates of the phases changed to the fraction where phase inversion appeared (in this case about 57% input oil fraction) the conductivity value, which was almost zero before indicating oil continuous flow, started fluctuating significantly. These fluctuations lasted for about 350 s and during this time the average value of the signal changed from low to high (indicating water continuous phase) for both RPs. After this time the fluctuations

reduced significantly and conductivity values settled to those of a water continuous mixture.

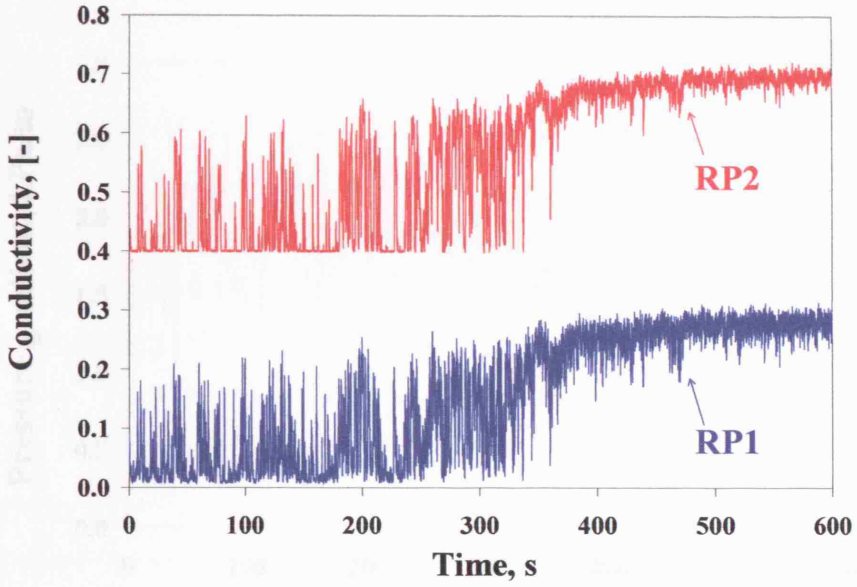

Figure 4.9 Conductivity signals at the inversion point (56% input oil fraction) obtained at 83*D* and 166*D* downstream the test section inlet (RP1 and RP2 respectively) for a Type I experiment at 4.0 m/s mixture velocity in the 60 mm ID acrylic pipe using *EXXSOL™ D80* (NTNU). Large oscillations are seen before the establishment of the new continuous phase (water) at about 350 s after the beginning of logging.

Similar behaviour can be seen in Figure 4.10 for pressure drop. Again soon after the flowrates changed pressure drop fluctuated significantly for about 350 s before settling to a new lower value (since water is now the continuous phase) where the fluctuations were very small. Interestingly, as soon as the new impedance and pressure drop values established the flow rates changed slightly (less than 5 %). However, even when flowrates were set to their initial values (oil fraction where inversion appeared) the impedance value remained to that of a water continuous mixture and the pressure drop also remained low. This means that the mixture did not invert back to oil continuous. The large fluctuations seen are attributed for this system as well to large dispersed structures (about to become continuous) and to secondary

dispersions, while this type of instability of the system (fluctuations of the flowrates) was also observed with the use of *MARCOL™ 52* and will be discussed further in the following Section.

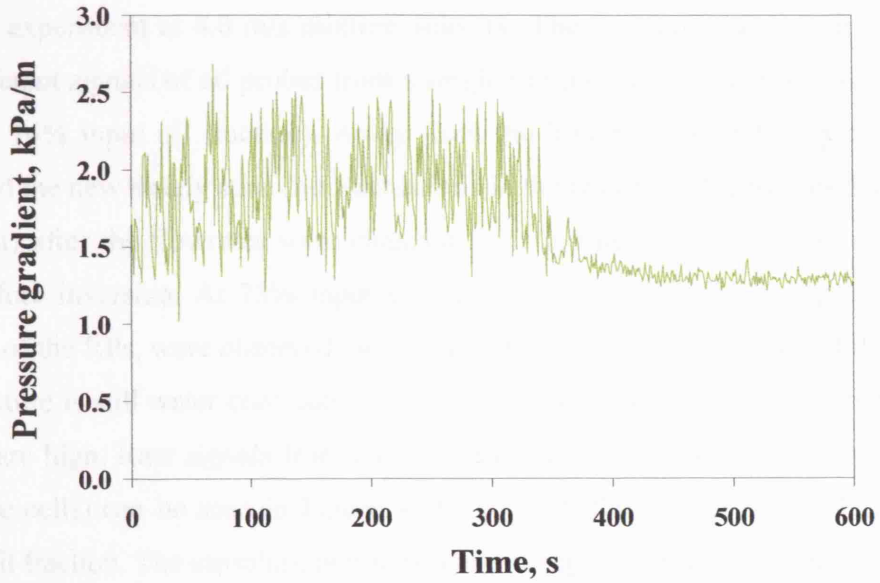

Figure 4.10 Pressure gradient signal at the inversion point (56% input oil fraction) for a Type I experiment at 4.0 m/s mixture velocity in the 60 mm ID acrylic pipe at NTNU, using *EXXSOL™ D80*. Oscillations can be seen up to 350 s.

It should be noted that, as can be seen in Figures 4.7- 4.10, the oscillations at the UCL facility existed over a range of input oil fractions, while they are not so persistent at the NTNU facility. This is believed to be due to the different ways the two systems operate. As will be explain in Section 4.4 it is easier to maintain a condition in the UCL facility, while any rheological change at the NTNU facility will cause further changes to the system.

4.4 INVERSION EFFECTS ON THE OPERATIONAL SYSTEM

The differences in the way the two facilities at UCL and NTNU operate are believed to cause great differences in the way inversion is occurring, or rather, in the effects inversion has on the operational system. To demonstrate this, experiments of both Type I and II were conducted with *MARCOL™ 52* in the 60 mm ID acrylic pipe

at NTNU. Four pairs of ring probes (RP1, RP2, RP3 and RP4) were used for determining phase inversion, located at 0.5 m, 3.5 m, 8.0 m and 12.0 m away from the inlet (8.5 *D*, 58.5 *D*, 133.5 *D* and 200*D*) respectively. Pressure gradient was measured right before RP4 (190*D* from the test section inlet) enabling direct comparisons between signals from these two instruments. The results shown below are for a Type II (w→o) experiment at 4.0 m/s mixture velocity. They are presented as time series of the different signals of all probes from a single run only at the point of inversion (here seen at 74% input oil fraction). Away from the inversion point the system quickly acquired the new steady state (no fluctuations in the readings of flowrates and pressure gradient) after the flowrates were changed. This is true until 72% input oil fraction, just before inversion. At 73% input oil fraction some oscillations, especially in the signals of the RPs, were observed, but the flowrates remained constant; at this fraction the mixture is still water continuous as indicated by the values obtained from all RPs, which are high. Raw signals from all instrumentation used (oil/water flowmeters and pressure cells) can be seen in Figure 4.11 and from the RPs in Figure 4.12 for 74% input oil fraction. The sampling period is 5 min using a sampling frequency of 10 Hz.

It can be seen in Figure 4.11 that absolute pressure (measured just after the test section inlet) and pressure gradient increase significantly, after an initial period, before they acquire new constant values. Flowrates of both liquids at the duration of the logging time after an initial period decrease before they acquire new constant values at this fraction.

Main characteristic in this case is the fact that the initiation of the phenomenon is related to non-steady state in the system. Phase inversion can destabilise the system because it is accompanied by rheological changes (phase continuity, dispersion type and fraction) that affect pressure drop. This is believed to be related to the fact that flowrates (both water and oil) are in this flow facility set by controlling the pump frequency; depending on this frequency the pumps will deliver respective amount of liquid. Any changes in pressure or pressure gradient downstream can therefore affect the flowrates.

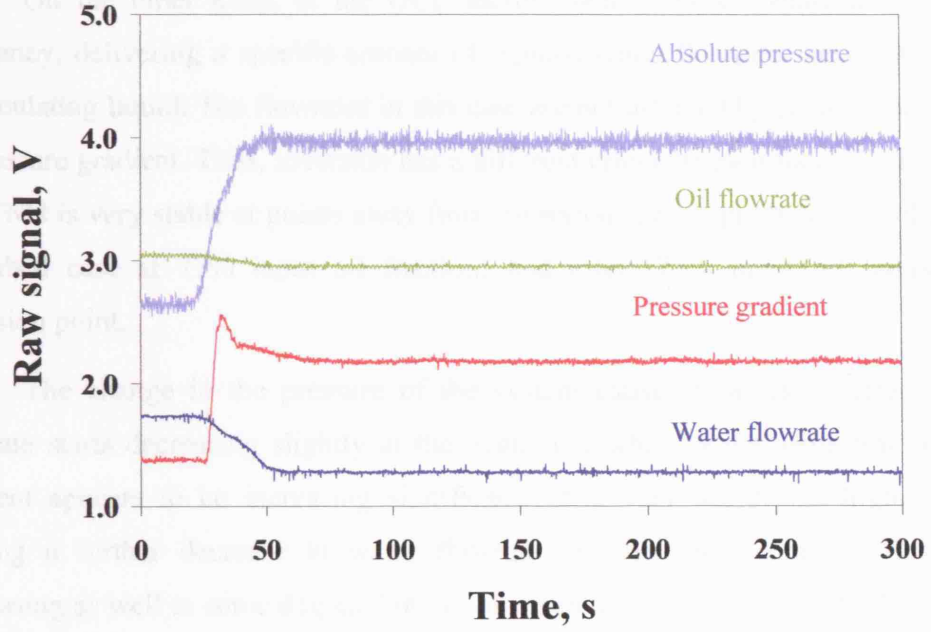

Figure 4.11 Raw signals from all instruments implemented in a Type II experiment at 74% input oil fraction (phase inversion point) at 4.0 m/s mixture velocity in the 60 mm ID acrylic pipe with the use of *MARCOL™ 52* (NTNU).

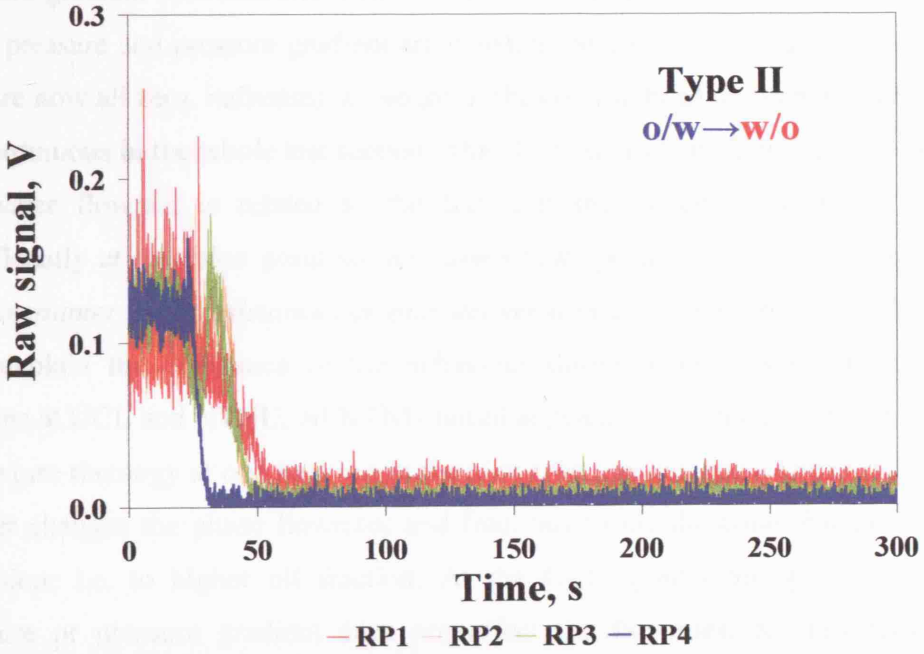

Figure 4.12 Raw signal from the RPs located along the pipe length at the point of inversion for a Type II experiment at 74% input oil fraction (phase inversion point) at 4.0 m/s mixture velocity in the 60 mm ID acrylic pipe with the use of *MARCOL™ 52* (NTNU).

On the other hand, at the UCL facility both pumps operate at a constant frequency, delivering a specific amount of liquids, while flowrates are controlled by re-circulating liquid. The flowrates in this case are not affected by changes in pressure or pressure gradient. Thus, inversion has a different effect on each facility. The system at NTNU is very stable at points away from inversion, even right before (in the above described case at 73% input oil fraction) and after (75% input oil fraction) the inversion point.

The change in the pressure of the system causes a series of effects: water flowrate starts decreasing slightly at the beginning while at the same time pressure gradient appears to be increasing significantly and very sharply to higher values, causing a further decrease in water flowrate. At the same time oil flowrate is decreasing as well to some degree, but not as much as the water flowrate. Between 30 and 40 s pressure gradient appears to form a maximum: it shows first an increase and then a decrease, until a plateau is again reached, while simultaneously a fluctuation to the signals of the RP2 and RP3 is appearing that is matching the behaviour of the pressure gradient (increase and then decrease). At the end of this transient stage (after 60 s) pressure and pressure gradient are constant and so are the signals from the RPs that are now all zero, indicating a change in the continuity of the system from water to oil continuous in the whole test section. This decrease in both flowrates and especially the water flowrate is related to the fact that the system pressure is increasing significantly at inversion point so *the pumps that operate at the same frequency but now encounter more resistance can only deliver a smaller quantity of liquid.* This may also explain the difference in the behaviour during phase inversion between the systems at UCL and NTNU. At NTNU initial appearance of phase inversion or change at mixture rheology at one location in the pipe cross section has a knock-on effect and further changes the phase flowrates and fractions to the direction that favours phase inversion; i.e. to higher oil fraction. At the UCL system though, any change in pressure or pressure gradient does not affect the flowrates; for this reason large structures and multiple dispersions "survive" for many oil fractions (Figure 4.7).

It can also be seen from Figure 4.12 that the signals from the 4 RPs do not change simultaneously at this phase fraction. First the signal by RP4 (located further

downstream) becomes zero at about 25 s after the start of logging, indicating inversion to oil continuous flow at this location, then about 20 s later the signals from RP3 and RP2 become zero, followed even later (within the next 5-10 s) from RP1 which is the probe located closer to the Y-shaped test section inlet. After the change in all the RPs phase inversion at the whole pipe length has occurred and oil has now established as the continuous phase.

It appears that in this case inversion does not happen simultaneously along the whole test section but *it takes time for inversion to spread in it* and *for the experiment that started from water continuous mixtures inversion first happens downstream and then upstream.* However, this behaviour is quite complex considering the instability of the system during inversion as shown in Figure 4.11, and could be due to a flow pattern development along the pipe. In this experiment water is initially the continuous phase and oil is dispersed into it in the form of fine droplets; thus, the mixture conductivity is high at the beginning. As the oil percentage is increased the dispersed droplet size is increasing as well, due to increased drop coalescence, forming a dispersion of larger oil droplets.

Because the two liquids are introduced in a stratified manner through the Y-shaped inlet junction, it is possible that there is some flow stratification close to the inlet. At low oil fractions this may only mean a clear water layer below a water continuous dispersion. At these fractions the amount of water is enough to fully disperse the existing oil. The flow is expected to become more uniform and the drops smaller further downstream in the pipe. As the oil fraction in the mixture increases, a clear oil layer would also form at the top of the pipe (more likely closer to the test section inlet). All these flow configurations would be interpreted as water continuous patterns by the RPs. At the phase inversion fraction the amount of oil is sufficient to now fully disperse the water phase. It would probably take some time for the flow pattern to develop and this happens further downstream the pipe, rather than closer to the inlet where the two phases are introduced in layers; this is in fact indicated by the change first of the signal of the RP4 located further downstream the pipe.

Comparing now Figure 4.11 and Figure 4.12 it can be seen that the initiation of the increase in absolute pressure and pressure drop coincides with the decrease of the signal of the RP4, which indicates phase inversion at this pipe location (the DP cell is located next to RP4 and direct comparisons can be made).

Similar observations for a Type I experiment in the 60 mm ID acrylic pipe can be made from Figure 4.13 for pressure, pressure gradient and flowrates and in Figure 4.14 for the signals of the RPs at 4.0 m/s mixture velocity.

Starting from high oil fractions, where the mixture is oil continuous, steady state is easily achieved when flowrates change away from the inversion point (that is expected around 74% input oil fraction). As soon as the frequencies of the two pumps are adjusted to deliver 74% input oil fraction instability appears. In this case at the phase inversion fraction pressure and then pressure gradient start decreasing after some initial delay, while oil and –particularly- water flowrates start increasing. Because pressure gradient is decreasing, the pumps need to supply less pressure and therefore for the same rotation speed give higher flowrate.

It is obvious that in both cases it is the water flowrate that is affected more than the oil one. This is due to the region within the characteristic curve that the pumps operate; according to characteristic pump curves, in higher flowrates, changes in the head of the pump result in smaller changes of flowrate, while at lower flowrates changes in head will result in larger changes of flowrate. The oil pump is delivering larger quantity of liquid at 74% input oil fraction and is thus less affected by changes in head than the water one.

In contrast to Type I experiments, the signal by RP1, closer to the inlet is first indicating the change in phase continuity for inversion from oil to water continuous. This is followed by the signal for RP3, while the inversion happens last at the furthest downstream position where RP4 is. It is believed that again the stratified manner the two liquids are entering the test section (through the Y-shaped junction) together with the changes in the oil/water flowrares at the inlet, can account for this.

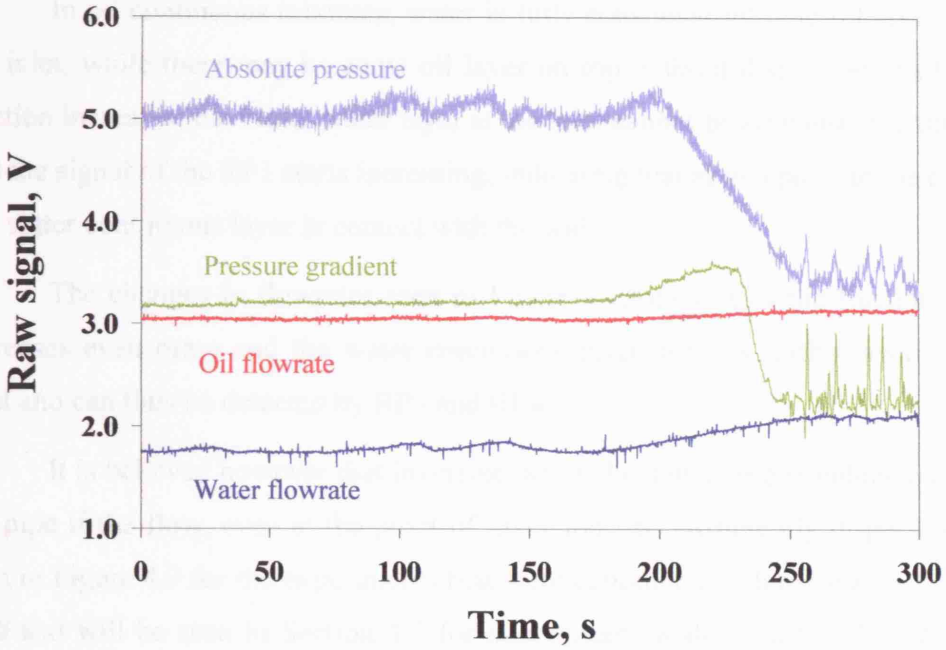

Figure 4.13 Raw signals from all instruments implemented in a Type I experiment at 74% input oil fraction (phase inversion point) at 4.0 m/s mixture velocity in the 60 mm ID acrylic pipe with the use of *MARCOL™ 52* (NTNU).

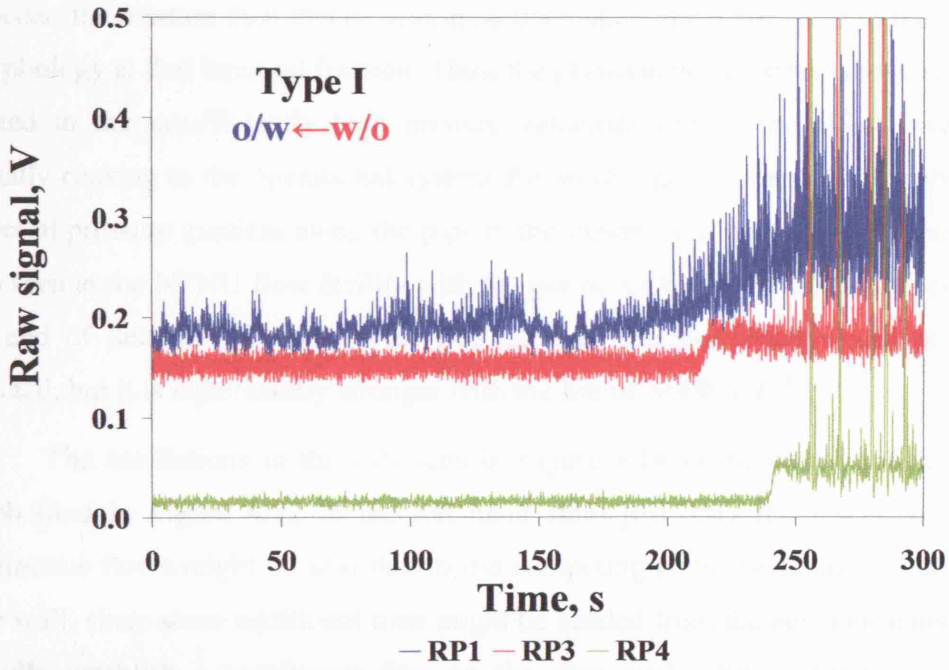

Figure 4.14 Raw signal from the RPs located along the pipe length at the point of inversion for a Type I experiment at 74% input oil fraction (phase inversion point) at 4.0 m/s mixture velocity in the 60 mm ID acrylic pipe with the use of *MARCOL™ 52* (NTNU).

In oil continuous mixtures, water is fully consumed into the oil layer, close to the inlet, while there may be some oil layer on top without dispersion. As the water fraction increases, the initial water layer at the inlet cannot be all consumed into the oil and the signal of the RP1 starts increasing, indicating that at this point in the pipe there is a water continuous layer in contact with the wall.

The changes in flowrates seen in Figure 4.13 mean that the fraction of water increases even more and the water continuous layer spreads further away from the inlet and can thus be detected by RP3 and RP4.

It is believed however that inversion would be happening simultaneously along the pipe if the flow, even at the point of inversion was sufficiently dispersed. This is seen in Figure 4.9 for the experiments that were conducted with the use of *EXXSOL™ D80* and will be seen in Section 4.5 for experiments with *EXXSOL™ D140* that are both less viscous than *MARCOL™ 52*, resulting for the same mixture velocity in much higher Reynolds numbers and thus in less stratification even close to the inlet.

It is interesting that in Figure 4.9 even though it takes some time for inversion to occur, the mixture then inverts within seconds along the whole pipe to the preferred morphology at that input oil fraction. Thus, the phenomena described above are mostly related to the insufficiently high mixture velocities and to the effect inversion is actually causing to the operational system due to changes in rheology. Instability and effect of pressure gradient along the pipe to the flowrates at the point of inversion was also seen at the NTNU flow facility with the use of *EXXSOL™ D80* (see discussion at the end of Section 4.3), where the flowrates at inversion point would be slightly affected, but it is significantly stronger with the use of *MARCOL™ 52*.

The oscillations in the RPs seen in Figure 4.14 in the right hand side of the graph (and in Figure 4.12 in the left hand side) just after the inversion to water continuous flows might be also due to the competing phenomena taking place at the pipe wall, since some additional time might be needed from the new continuous phase to fully establish a continuous film on the pipe wall. This ("wetting") time will strongly depend on wettability effects and is believed that the new phase takes some time to wet the pipe wall at all experimental conditions studied.

4.5 INVERSION IN THE PIPE CROSS SECTION

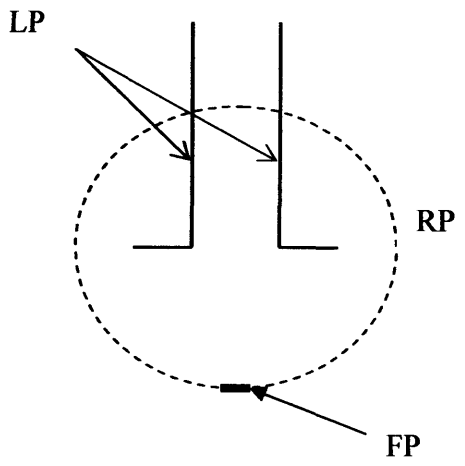

Figure 4.15 Location of the conductivity probes at the cross sectional area at the experimental facility at UCL (38 mm ID SS pipe).

Results from the UCL facility and the 38 mm ID stainless steel pipe will be presented here. *EXXSOL*^{TM} *D140* and tap water were used as test fluids. The graphs that follow refer to single experimental runs to enable direct comparisons between the signals obtained from different instrumentation; using average values from many experiments tends to smooth the trends of the signals, due to the fact that the inversion point slightly varies between different experimental runs. However, experiments were repeated many times (more than 3) with good repeatability. The values shown are the average values over a sampling time of 30 s.

A conductivity Type I experiment (mixture started as oil continuous and inverted to water continuous) is described first. All probes were used in order to identify phase inversion and understand how the phenomenon occurs in the pipe cross sectional area and also along the pipe. Figure 4.15 shows where each one of the probes is located. The local conductivity probe (LP) was recording the conductivity of the mixture at the pipe centre and was also able to traverse along the pipe diameter, the ring probes (RP), shown with the dashed line in Figure 4.15, were recording the conductivity of the mixture in contact with the wall, while the flush hot film probe (FP) was measuring the conductivity of the phase that was wetting a specific point on the wall (in this case, the bottom of the pipe). In total 2 ring probes were used, RP1 and RP2 located at 5.5 m (145*D*) and at 7 m (184*D*) downstream from the test section inlet respectively. All other probes were located at 184*D* from the inlet (the FP first, then the RP2 and last the LP so that the probes flush to the pipe surface would not be

affected by the LP that is interfering with the flow). Each probe section is about 10 cm long.

Mixture velocity was kept at 4.5 m/s. In Figure 4.16 raw signal (voltage) of all probes used are plotted against input oil fractions close to inversion. Voltage has been made dimensionless by dividing each value with the single phase water value from the respective probe at the location where measurements were obtained. In the beginning, the raw signal from for the RPs and the LP is at zero while it has a standard low value for the FP, indicating oil continuous flow.

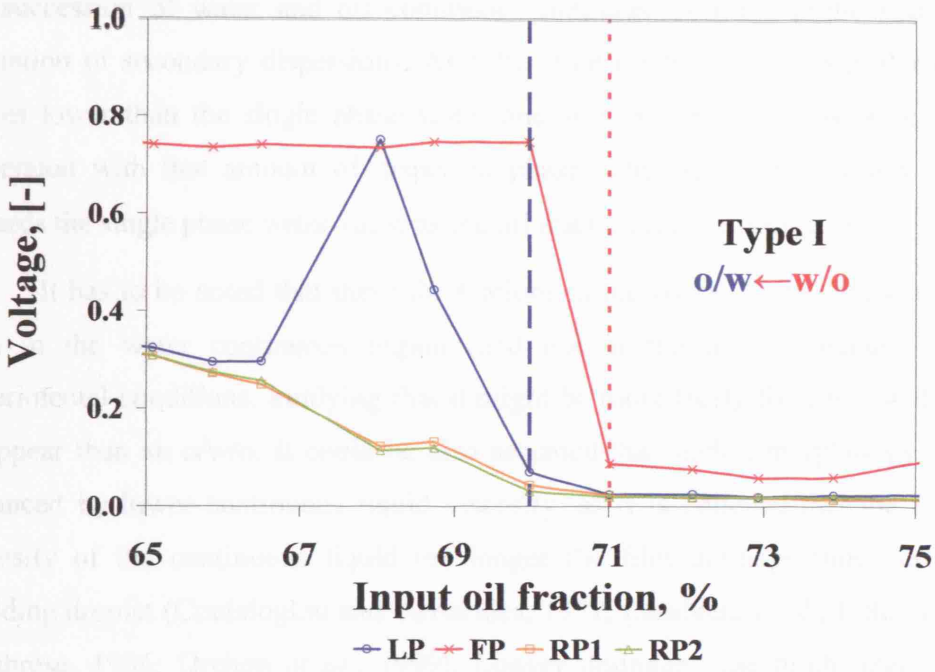

Figure 4.16 Normalised to single phase water voltage around the inversion point obtained from the ring probes, RP1 and RP2, located at 145*D* and 184*D* respectively, the local conductivity probe (LP) located in the pipe centre, and the flush probe located at the bottom of the pipe at 184*D* from the test section inlet for a Type I experiment at 4.5 m/s mixture velocity in the 38 mm ID SS pipe with the use of *EXXSOL™ D140* (UCL).

The obtained values of conductivity remain constant until 71% input oil fraction is reached (red dotted line). At that point all signal values are low. With a further slight decrease of the input percentage of oil to about 70%, indicated in Figure

4.16 by the blue dashed line, the signal from the FP increases significantly, showing that this is now wetted by water which has a fast cooling effect. The signals of the other probes, though, only increase slightly. This indicates that the RPs can detect some water layer that covers part of the wall at the bottom of the pipe as the signal of the FP probe also suggests. The signal of the LP shows that now in the middle of the pipe some large water structures (larger than the 10 mm distance of the two probe sensors) appear. With increased water fraction, the signals of the RPs continue to increase indicating that continuous water phase covers more and more of the pipe wall. The signal of the LP shows a peak which reaches values higher than the single phase water. This "overshooting" was discussed before in Section 4.3 and was attributed to the succession of water and oil continuous mixtures over the probe and possible formation of secondary dispersions. At 67% input oil fraction the signal reduces to values lower than the single phase water one and expected for a water continuous dispersion with that amount of dispersed phase. The signal then slowly increases towards the single phase water value as the oil fraction further decreases.

It has to be noted that these fluctuations in the conductivity values are mostly seen in the water continuous region (and not in the oil continuous) for these experimental conditions, implying that it might be more likely for a w/o/w dispersion to appear than an o/w/o. It could be also assumed that such a morphology might be enhanced by lower continuous liquid viscosity, as it is believed that the higher the viscosity of the continuous liquid the longer the film drainage time between the colliding droplet (Coulaloglou and Tavlarides, 1977; Calabrese *et al.*, 1986; Wang and Calabrese, 1986; Drehen *et al.*, 1999). Longer drainage time might mean reduced coalescence efficiency and reduced number of entrapped (secondary) droplets.

The same experiments were conducted with the use of the flush probe on the top part of the pipe. This indicated that as the water fraction was increased in the flow, high voltage from the FP was only obtained at the point where the highest value from the LP is recorded and not sooner, signifying that it only then that water wets the upper part of the pipe wall.

Similar results were obtained in a Type II experiment in the same experimental facility (starting from a water continuous mixtures and inverting to an oil continuous ones) at 4.5 m/s mixture velocity. In Figure 4.17, dimensionless voltage (as before) for all probes used is plotted against input oil fraction. The flush probe is now located at the top of the pipe indicating the continuity of the phase that is wetting the upper pipe wall and all other probes are at the same locations as before.

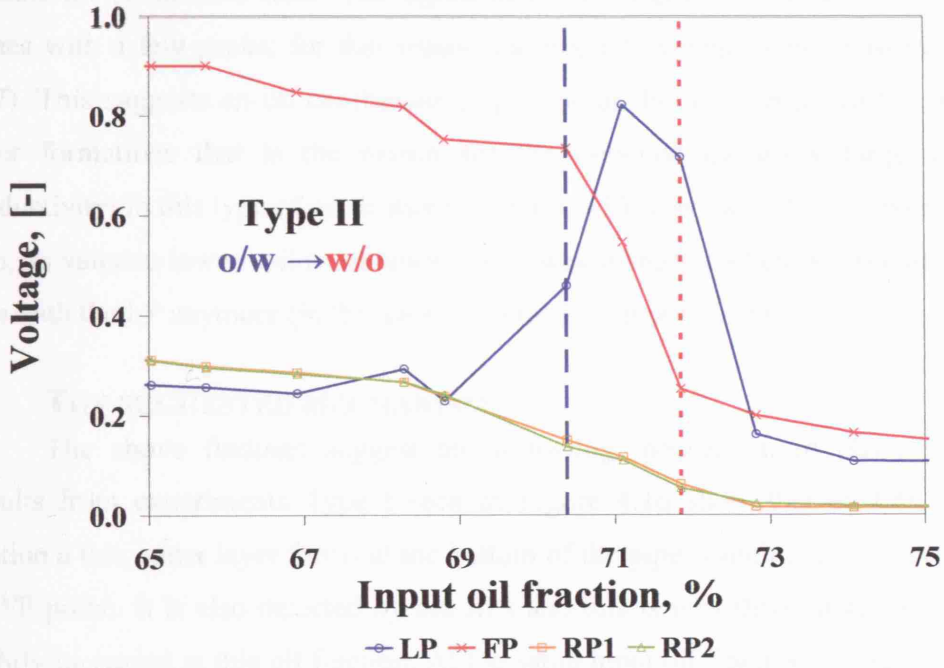

Figure 4.17 Normalised to single phase water voltage around the inversion point obtained from the ring probes, RP1 and RP2, located at 145*D* and 184*D* respectively, the local conductivity probe (LP) located in the pipe centre, and the flush probe (FP) located at the top of the pipe 184*D* from the test section inlet for a Type II experiment at 4.5 m/s mixture velocity in the 38 mm ID SS pipe with the use of *EXXSOL*^{TM} *D140* (UCL).

Initially the signal values from all probes are high, indicating a water continuous flow. As the oil fraction in the mixture is increased, slightly lower voltage values are recorded for all probes while values from the LP remain high indicating water continuous mixture at the pipe centre. At 70% input oil fraction the trends change signifying the onset of inversion (blue dashed line). The values of the LP

fluctuate a lot and their mean value is significantly increased (as discussed before), while the value from the FP decreases significantly and reaches at about 72% input oil fraction, the oil continuous value, indicating that oil is now wetting the upper part of the pipe (red dotted line in Figure 4.17). The RPs are still giving a low but positive value showing that there is some water continuous mixture in contact with the pipe wall.

Once the oil fraction increases further and reaches 73%, the FP and RPs indicate oil continuous flow. The signal of the LP has mainly low (oil continuous) values with a few peaks; for that reason the overall average is not zero (see Figure 4.17). This suggests an oil continuous dispersion at the pipe centre with a few large water formations that is the reason for the obtained transitory large values of conductivity. In this type of experiments, when the FP was located at the bottom of the pipe, its value to lower –oil continuous valus- would change when no oscillations were seen with the LP anymore (in this case at about 73% input oil fraction).

THE SUGGESTED MECHANISM

The above findings suggest the following mechanism of phase inversion. Results from experiments Type I seen in Figure 4.16 show that at 70% input oil fraction a thin water layer forms at the bottom of the pipe, which is clearly detected by the FP probe. It is also detected by the RPs and this is why their values appear to be slightly increased at this oil fraction. At the same input oil fraction the signal from the LP probe shows large fluctuations attributed to the alternating large oil and water structures and possibly formation of secondary dispersions especially in the pipe centre. When input water fraction increases by 1% more, inversion occurs at the whole cross section and the signals of the RPs and the LP increase to high water continuous values. However, the signal from the LP at the pipe centre still fluctuates indicating that large structures of both continuous phases exist at the pipe centre. It will take a further increase in the water fraction for inversion to be completed in such way that a fine, uniform dispersion of oil droplets into water forms (this is the point where the signals from all probes stabilize at high water continuous values) at about 67% input oil fraction. The appearance of an intermediate condition with large oil and water

continuous structures and secondary dispersions in pipelines before the completion of inversion has been seen before (Liu *et al.* 2006a; Hu and Angeli, 2006, in vertical pipes), but the presence of the thin layer of water at the onset of inversion from oil to water continuous mixtures at horizontal pipelines has never been reported before. Its detection was made possible with the use of the flush hot film probe in horizontal pipelines.

Results from Type II experiments lead to the conclusion that a similar mechanism governs inversion from water to oil continuous mixtures; as the oil fraction increases in the mixture more and more oil droplets appear in the water carrier, and coalescence is enhanced against breakup; this results in larger oil droplets. The point is reached where no more oil can be dispersed by the existing water. This is the onset of inversion and it is accompanied by the formation of a thin oil layer at the top of the pipe due to gravity. With further increase in the oil fraction (note that the input oil fraction is changing at very small steps), the system inverts to an oil continuous mixture not only at the wall, but at the whole pipe cross sectional area. Again, the signal of the LP indicates a transitional region in the pipe centre that persists over the intermediate range of oil percentages.

Whether or not there is a layer of oil forming prior to inversion towards oil continuous mixtures in the experimental facility at NTNU in all pipes used cannot be confirmed with the instrumentation used. Further complication is introduced in the NTNU system due to the flow development discussed above.

The same behaviour was seen for inversion from either oil or water continuous mixtures and for all mixture velocities studied; however the experimentally highest mixture velocity achieved was shown above to demonstrate this stratification effect at inversion even at high velocities. The phenomenon is more prominent at lower mixture velocities.

Two potential flow configurations are thus suggested:

a) Just before inversion one type of dispersion occupies the whole pipe cross sectional area. At small increase of the dispersed phase fraction a single thin layer of the phase that is about to become continuous

forms that wets the lower (water layer) or the upper (oil layer) part of the pipe (Figure 4.18b), when inversion occurs from oil or from water continuous mixtures respectively. Once inversion is complete the pipe cross section is occupied by a mixture with the opposite continuity of the initial one and maybe the single phase layer persists (mechanism depicted in Figure 4.18 for a Type II experiment). This will be the 2-layer approach.

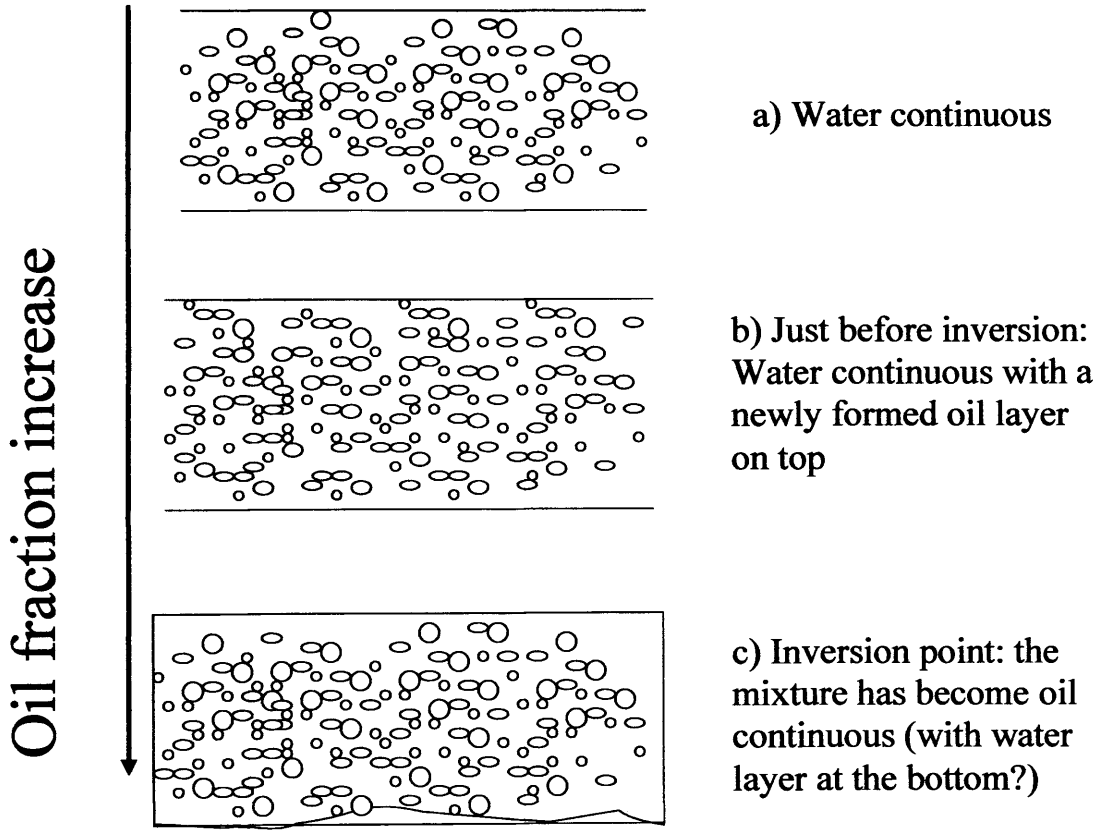

Figure 4.18 Schematic of the suggested phase inversion mechanism for the Type II experiments in horizontal pipelines.

b) If inversion occurs from water to oil continuous mixtures, some water will always wet the bottom of the pipe before inversion happens in the whole cross section. Thus, just before inversion there is a 3-layer structure in the flow: a single phase layer of the continuous phase, a mixed layer that is occupying the biggest part of the pipe (still with some stratification of the dispersed phase droplets depending on gravity) and a single phase fine layer of the phase that is about to become continuous. Just after inversion has taken place, there exist all three layers with the mixed layer now being of the opposite continuity that the initial one, while the single phase layer of the initially continuous phase is receding.

4.6 CONCLUSIONS

Phase continuity and pressure gradient were studied during investigations of phase inversion of oil/water mixtures in two experimental facilities. The following summarise the observations:

- Phase inversion in horizontal pipelines is accompanied by large changes in the recorded pressure gradient along the pipe around the area of the occurrence of inversion. The dispersion viscosity -and as a consequence the pressure gradient along the pipe- behaviour will depend on a variety of parameters, the most important of which is believed to be the oil type.
- It is proposed that the less viscous oils have a greater propensity to form secondary dispersions; this is attributed to the fact that colliding water droplets in a continuous oil environment will require less drainage time for coalescence and thus, lead to higher coalescence efficiency with decreasing oil viscosity. More effective collisions potentially mean that a larger amount of the continuous phase is entrapped within the dispersed droplets. This might be the reason of the appearance of the ambivalent range for *EXXSOL™ D80*, while same behaviour was not seen with the more viscous oils.

- Large oscillations of the signal of the LP and the pressure gradient in some conditions were detected around and especially at the point of inversion. In terms of conductivity this was attributed to an intermediate condition that might exist before inversion has fully occurred; this intermediate condition is characterized by the large/elongated formations of one phase into the other. These formations were mostly detected at the pipe core.
- Oscillations were mostly seen in the water continuous region, implying that it might be easier for a w/o/w dispersion to occur, as opposed to an o/w/o and for large oil formations to exist in a water "continuous" environment.
- It was found that phase inversion occurred simultaneuously at the whole length of the pipe for the less viscous oil, but there was some flow development when the more viscous oil was used that resulted in inversion at different points along the pipe.
- The change of the rheological characteristics of the mixture and thus, the abrupt change in the resulted pressure/pressure gradient in the system affected significantly the operational system and as a result the flowrates of the two liquids.
- Conductivity experiments, at various locations in a pipe cross section at the experimental facility at UCL elucidated that just before inversion, there is a formation of a single phase layer of the phase that is about to become continuous, at the upper or lower part of the pipe depending on the properties of the layer (gravitational effects). This layer was first detected with the hot film probe. This resulted in the suggestion of a mechanism for inversion, where a stratification of two or three layers exists.

It can be concluded that the occurrence of inversion results in great changes in the system, not only in its rheological characteristics, but in its actual operational stability. The detection of the conductivity of the system at different locations in the pipe cross sectional area with the variety of instrumentation available proved very useful as it revealed the complicated nature of the phenomenon and the different morphologies it may take. However, in order to fully comprehend what is happening at inversion in horizontal pipelines, further flow analysis should be conducted, and other parameters such as the velocity profile and the phase and drop size distribution in the pipe cross sectional area should be considered. This is done in the following chapter.

Chapter 5

Flow analysis of inversion and concentrated dispersions in horizontal pipelines

5.1 OVERVIEW

Investigations in highly concentrated dispersions before and after phase inversion point were carried out in the experimental facility at University College London. Pressure gradient and *in situ* phase holdup were measured for both experimental routes starting from oil (Type I) and from water (Type II) continuous dispersions and the velocity ratio was calculated (Section 5.2). Dispersed drop velocity profiles were obtained and comparisons were made to continuous phase velocity and theoretical predictions (Section 5.3). From the drop velocity results and the signal of one of the two sensors of the dual impedance probe chord length distributions of the dispersed drops were found. Phase distribution graphs have also been obtained. Chord length distributions were converted into drop size distributions (with the use of an algorithm proposed by Hu *et al.*, 2006b) (Section 5.4). These were used for the theoretical prediction of phase inversion point based on the equal surface energy criterion.

Drop size measurements were performed for input oil fractions 20 - 80% and mixture velocities 3.0, 3.5 and 4.0 m/s, while pressure drop and holdup were also

measured at 4.5 m/s mixture velocity. All experiments in this Chapter were conducted in the 38 mm ID SS pipe at the UCL facility using *EXXSOL^{TM} D140* and tap water as test fluids. It should be noted that the inversion point at the same conditions might vary slightly for different experimental runs. To enhance discussion only Type II experiments will be considered in the following.

5.2 VELOCITY RATIO

Holdup measurements were obtained for both Type I and II experimental routes with the use of the quick closing valves (QCV) as explained in Section 3.4. Differences due to the different approach of the inversion point are negligible, something that is expected since no ambivalent range was seen when *EXXSOL^{TM} D140* was used (see also Section 6.5), but also due to the way these experiments are performed: the pumps are stopped simultaneously with the closure of the QCV, the entrapped liquid volume fraction is measured and then the pumps are restarted and the flowrates are set to the values required for the next experimental condition. Thus, each measurement is practically independent from the previous. From one set of conditions to the next, however, the dispersed phase fraction changed only by 1% so that the phase inversion point could be captured with accuracy. Type II experiments will be considered. The graphs below are average values for experiments repeated at least 3 times. Velocity ratio, S, defined as the ratio U_o/U_w is calculated by Equation 5.1 below:

$$S = \frac{\varepsilon_o \varphi_w}{\varepsilon_w \varphi_o} \tag{5.1}$$

where ε_o and ε_w is the oil and water input fraction respectively, while φ_o and φ_w are the respective *in situ* values. The average calculated standard deviation for the velocity ratio is 0.20.

In situ holdup measurements against input oil fraction averaged over the two experimental routes are shown in Figure 5.1. It can be seen that for all conditions

studied, the *in situ* measured oil fraction is lower than the inlet one. More specifically, starting from low input oil fractions, the *in situ* measured oil holdup is almost the same for all mixture velocities. This changes at about 70% input oil fraction or slightly less at 3.0 m/s mixture velocity (where the change occurs at 68% input oil fraction) where *in situ* oil holdup is increasing suddenly and reaches values closer to the input oil fractions. The increase is more pronounced for the lower velocities and is related to the occurrence of inversion. Low holdup value is related to the point right before inversion when the mixture is still water continuous, while the increase is related to the point after the occurrence of inversion to oil continuous mixtures for a Type II experiment. After inversion lower holdup values are obtained for increasing mixture velocity. In other words, inversion results in less dramatic changes in the holdup values at the higher mixture velocities where the holdup profiles become "flatter".

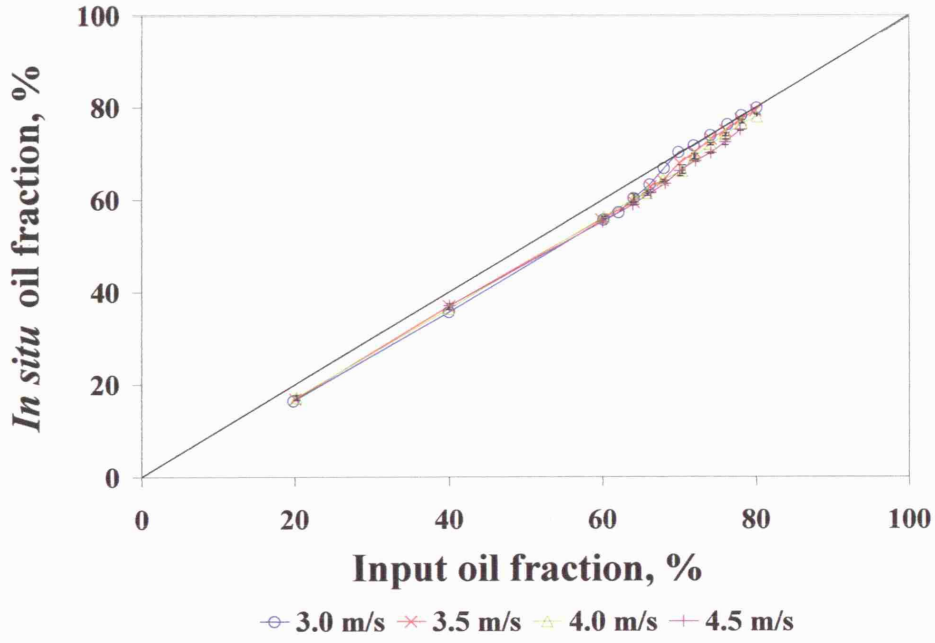

Figure 5.1 Average *in situ* oil fraction against input oil fraction for different mixture velocities.

In Figure 5.2 the calculated slip ratio from Equation 5.1 with error bars is plotted against input oil fraction for different mixture velocities. At low oil fractions

and before inversion, velocity ratio is above unity, indicating that the dispersed oil phase travels faster than the water continuous one. This is supported by the drop velocity measurements (see for example Figures 5.8 and 5.9) that demonstrate that the dispersed oil drops are indeed faster than the single phase velocity. The slip ratio also seems to get closer to unity as the mixture velocity increases.

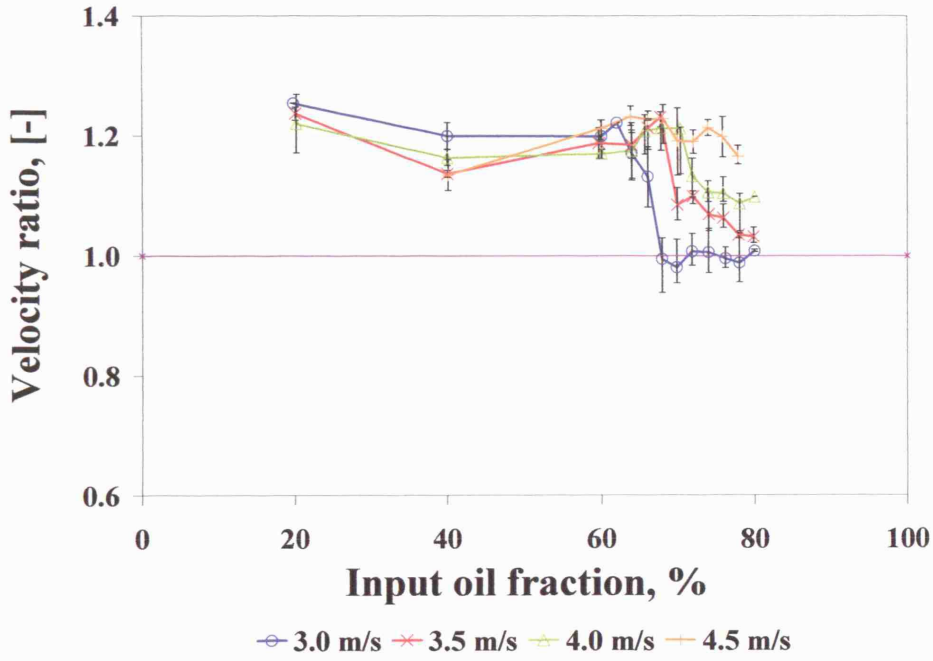

Figure 5.2 Velocity ratio against input oil fractions for different mixture velocities.

After inversion the trend changes and generally S decreases and takes values closer to 1. This means that the oil phase now travels less fast than in the water continuous mixtures which is expected, as oil is now the phase in contact with the wall that experiences more frictional drag.

In this region the effect of mixture velocity is more prominent and S increases with increasing mixture velocity. As a result the higher differences in S over phase inversion are seen at low mixture velocities, while at the highest mixture velocities used there is little variation. This is surprising as with increasing mixture velocity, S is

expected to take values closer to 1. It is possible that as the mixture velocity increases the water droplets are pushed more towards the wall where the flow is slower.

Also, the slip ratio trend becomes flatter with a smoother change at inversion point with increasing velocity. This is expected as before inversion oil is dispersed. Higher mixture velocities and turbulence will result in a more homogeneous dispersion: not only in size but also in number, the dispersed oil droplets in the water continuous mixture are expected to occupy the whole cross sectional area with more homogeneous distribution as velocity becomes higher. More oil droplets will be closer to the wall, so more drops will be experiencing shear from the wall, making the difference in slip before and after inversion less with increasing mixture velocity. Oil becomes continuous after inversion and is in contact with the wall, so more shear is acting on it and the value of S is decreasing.

In Figure 5.3 and Figure 5.4 *in situ* oil fraction and velocity ratio at inversion point are shown respectively against mixture velocity.

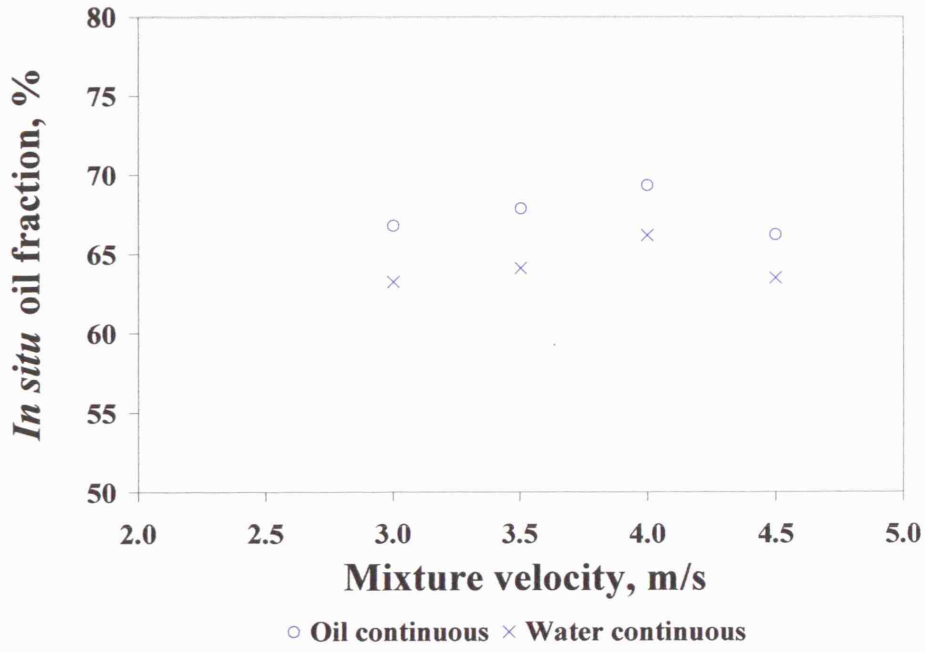

Figure 5.3 *In situ* oil fraction at phase inversion point at different mixture velocities before (water continuous mixtures) and after (oil continuous mixtures) inversion.

Both values just before (in water continuous region, shown as "water continuous" in Figures) and just after (oil continuous region, shown as "oil continuous") inversion are shown. *In situ* oil hold up just after inversion (oil continuous region) is between 66 and 69%. The velocity ratio just after inversion is between 1.0 (at 3.0 m/s mixture velocity) and 1.19 (for higher velocities), and increases slightly with increasing velocity. The velocity ratio just before inversion when the flow is still water continuous (66% input oil fraction at 3.0 m/s and 68% and 70% input oil fraction at higher velocities) is about 1.20-1.23 at higher mixture velocities apart from 3.0 m/s where it is slightly less.

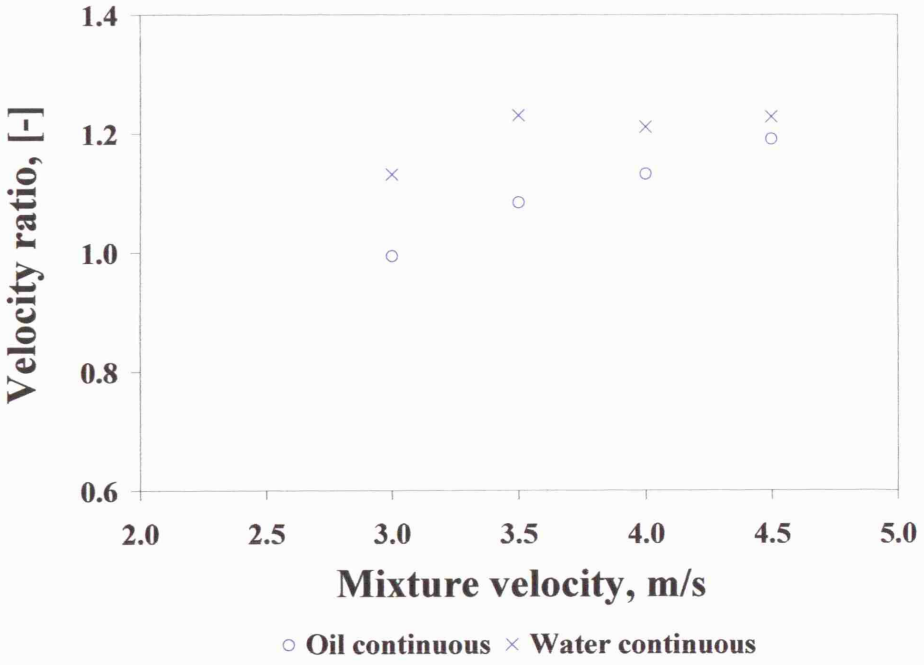

Figure 5.4 Velocity ratio at phase inversion point at different mixture velocities.

It is interesting that as the mixture velocity is increasing the velocity ratio S at inversion (from both oil and water continuous mixtures) seems to converge to one value. Hu and Angeli (2005) made similar observations during phase inversion experiments in vertical flow, even though the value of S they found was significantly less (0.8). This suggests that maybe a mechanism on phase inversion that depends on

the momentum of the phases is relevant. This would agree with the theory proposed by Yeh *et al.* (1964) and Nädler and Mewes (1995b) of zero interfacial shear stresses during inversion.

5.3 VELOCITY PROFILES

With the use of the dual impedance probe dispersed drop velocity profiles can be obtained (as described in Section 3.5.2). More specifically the signal from the two probe tips can be cross-correlated to yield the drop velocity at the point of the measurement within the pipe cross section (Section 3.6). Experiments were conducted for both experimental routes (starting from oil continuous mixtures, Type I, or starting from water continuous mixtures, Type II) and similar results were obtained. Figure 5.5 and Figure 5.6 show drop velocity profiles at 3.0 m/s mixture velocity for water and oil continuous mixtures respectively at different input oil fractions obtained from measurements along the pipe vertical diameter.

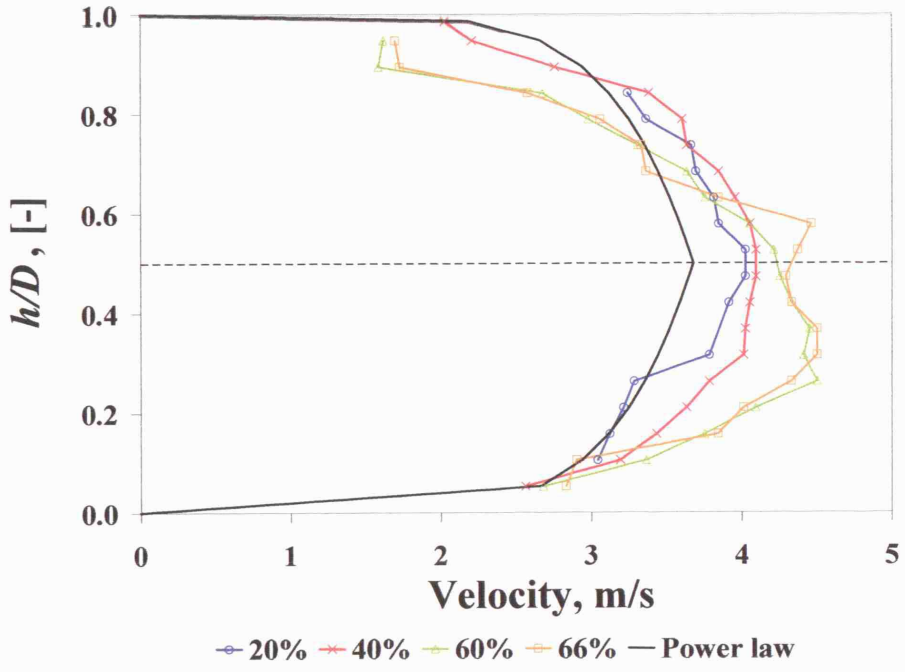

Figure 5.5 Dispersed oil drop velocity profile in the water continuous region at 3.0 m/s mixture velocity for different input oil fractions.

This is of increased interest as gravitational effects might result in a different distribution of dispersed phase fraction and droplet size, thus affecting droplet velocity. Measurements along the diagonal and the horizontal diameters were also conducted (Figure 5.7). Oil droplet velocity is depicted against height from the bottom of the pipe, h, that has been made dimensionless by dividing with the pipe diameter, D. Together with the experimental results the theoretical prediction for single phase velocity profile in turbulent field at the same velocity as the mixture velocity can be seen (solid line) that is calculated by Equation 5.2:

$$u = \frac{60}{49} * U_m * \left(1 - \frac{r}{R}\right)^{\frac{1}{7}} \tag{5.2}$$

where u is the predicted single phase velocity at a specific height r in the pipe cross sectional area of radius R and U_m is the mixture velocity.

It can be seen in Figure 5.5 that at the lower part of the pipe oil drop velocity tends to increase with input oil fraction and is higher than single phase velocity profile. At the part of the pipe closer to the upper wall drop velocity seems to decrease with input oil fraction and is less than the single phase velocity. It is expected that there is some flow stratification with more oil drops in the upper than in the lower part of the pipe. It seems that the drops in the dilute dispersion of the lower part of the pipe travel faster than the single phase, while at dense dispersions at the upper part of the pipe the movement of drops is hindered and drops travel slower than in the single phase. The high concentration of the oil droplets at the top of the pipe is also interfering with the cross correlation signal obtained by the probe.

The results from the QCVs showed velocity ratios above 1 for these conditions, which could be justified as in a large part of the pipe cross section oil drops are faster than single phase predictions. The drop velocity profile is also more symmetrical at low oil percentages indicating that the dispersed phase is more uniformly distributed. This implies that there is a smoother velocity profile for dilute dispersions where the

dispersed phase is travelling without any constraints. The above results which show oil drops to travel much faster than the single phase seem to support the findings of the QCVs that at these conditions S is above one (in Figures 5.8 and 5.9 for some of the conditions studied the dispersed droplets will be shown to go faster than the continuous phase).

In Figure 5.6, drop velocity profiles along the vertical pipe diameter at 68% and 70% input oil fraction (dotted lines) and 3.0 m/s mixture velocity can be seen, along with results in the oil continuous region (at 72, 74, 76 and 78% oil, solid lines) and with the power law prediction (solid line). At 68% input oil fraction at this mixture velocity inversion starts (as described in Section 4.5) and low values of conductivity are encountered in the upper part of the pipe. It can be seen for 70% oil fraction that above 0.7 *h/D* there is a sharp decrease in the drop velocity that coincides with the appearance of dispersed water droplets in the oil continuous flow; this part of the graph now depicts dispersed water droplet velocity.

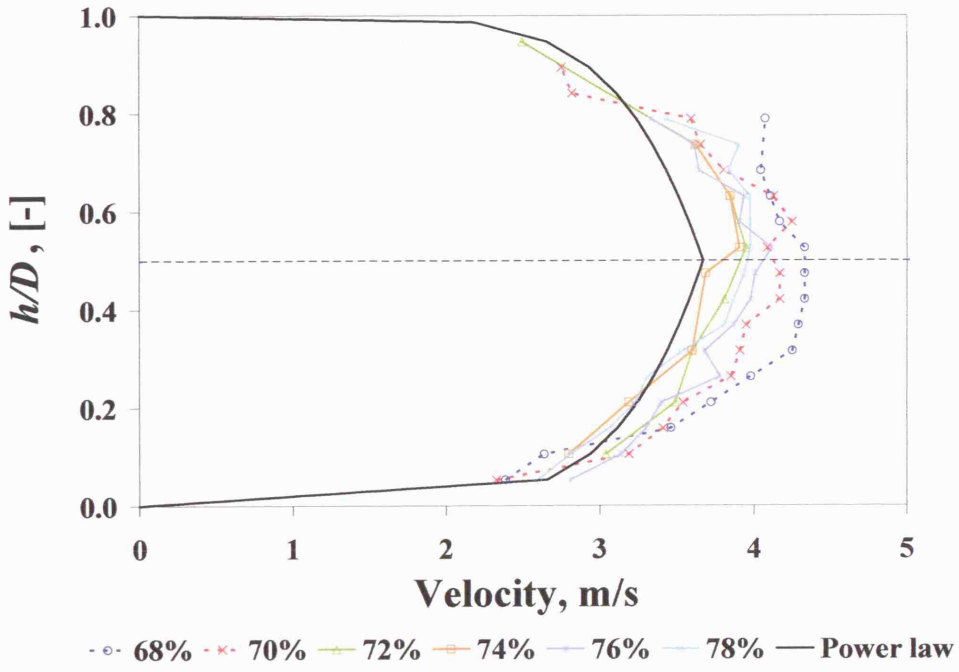

Figure 5.6 Drop velocity profile at the inversion point (dotted lines) and the oil continuous region (solid lines) at 3.0 m/s mixture velocity for different input oil fractions.

At 72% oil fraction inversion has happened in the whole pipe cross section (fully dispersed oil continuous flow). The (water) drop velocity profiles are lower than those in the water continuous flows, but quite similar if comparison is made for respective dispersed phase fraction. The velocity profile remains almost constant with further increase in the input oil fraction, perhaps reflecting the small differences in the input oil fractions. In the oil continuous mixture drop velocities are closer to single phase value and could justify the change of velocity ratio to values closer to unity (see Figure 5.2).

Results are not shown for the upper part of the pipe especially at the higher oil fractions as the cross correlation at these points is not very good, because of the low concentration of dispersed phase at this part of the pipe. More water drops are expected to be concentrated at the lower part of the pipe where indeed good cross correlations were obtained.

Lovick (2004) also found that in an oil continuous dispersion at 2.5 m/s mixture velocity and 80% input oil fraction water droplet velocity was lower than that given by the single phase turbulent velocity profile. Lovick (2004) found suppression (a "dimple") of the parabolic velocity profile at the pipe core at 80% oil and 2.5 m/s that he attributed to the larger water droplets found at that location. Something similar is also seen in the current findings: whenever the dispersed phase appears at a specific location in large concentration, it hinders the full development of the velocity profile.

Similar results were also obtained at 3.5 m/s mixture velocity.

Velocity profile comparisons are also made for measurements obtained along the vertical, diagonal and horizontal diameters in the pipe cross sectional area and results are shown in Figure 5.7 at 70% input oil fractions (phase inversion point, water continuous mixture up to $0.7D$ and then oil continuous for the vertical and diagonal diameters) at 3.0 m/s mixture velocity.

Dispersed drop velocity has a similar distribution along the three directions. However, at the vertical and diagonal diameters the velocity decreases significantly close to the top of the pipe where the flow has already changed to water continuous. This does not happen in the horizontal diameter close to the wall. Generally though,

velocity profiles at these high mixture velocities are quite symmetrical in the whole cross section.

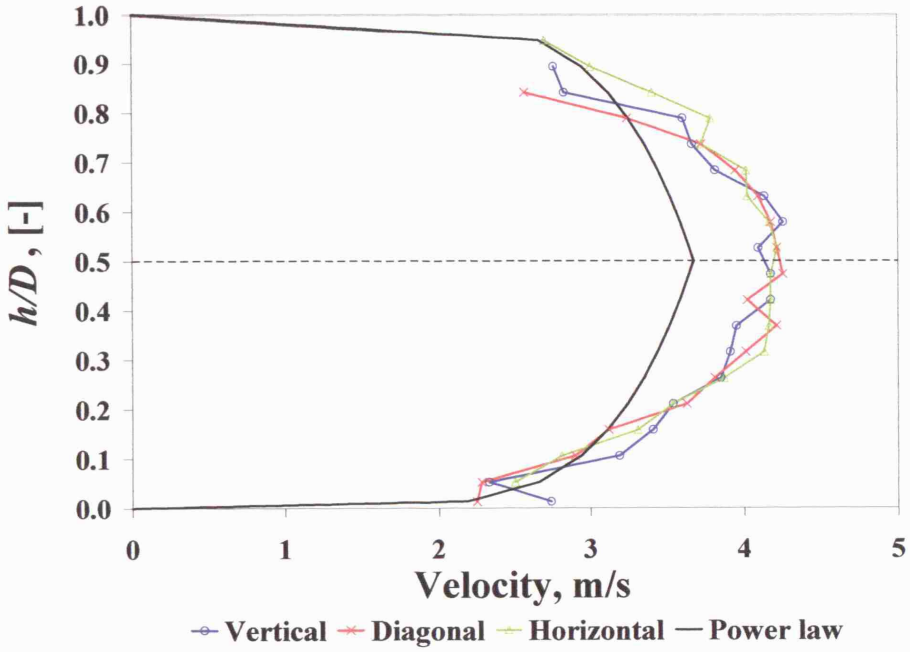

Figure 5.7 Drop velocity profile at the whole cross sectional area at 70% input oil fraction and 3.0 m/s mixture velocity.

Comparisons between dispersed and continuous phase velocities can be made at 3.0 m/s mixture velocity and water continuous mixtures at 20% and 40% input oil fractions. The continuous phase velocity in the same system was obtained by Hu (2005) with the use of a hot film anemometer probe. Further details about the probe can be found in Hu (2005). The comparisons can be seen in Figure 5.8 (dotted lines represent the continuous phase results while solid lines represent the dispersed droplet velocity).

In general, the continuous phase velocity profiles are flatter than for the dispersed phase. Dispersed oil phase velocity is higher when compared with the continuous phase for both oil fractions especially at the pipe core. On the other hand, the velocity of the continuous phase becomes higher than that of the dispersed phase

close to the pipe wall, where the dispersed phase velocity appears to be suppressed. Again, this agrees with the holdup results from Figure 5.2 which showed that at low input oil fractions, oil (now dispersed) is flowing much faster than water (continuous). Furthermore, the difference in continuous and dispersed phase velocities is higher at 20% than at 40% input oil fraction which also agrees with the holdup data (Figure 5.2) that show a decrease in the velocity ratio at 3.0 m/s mixture velocity between 20% and 40% dispersed phase fraction.

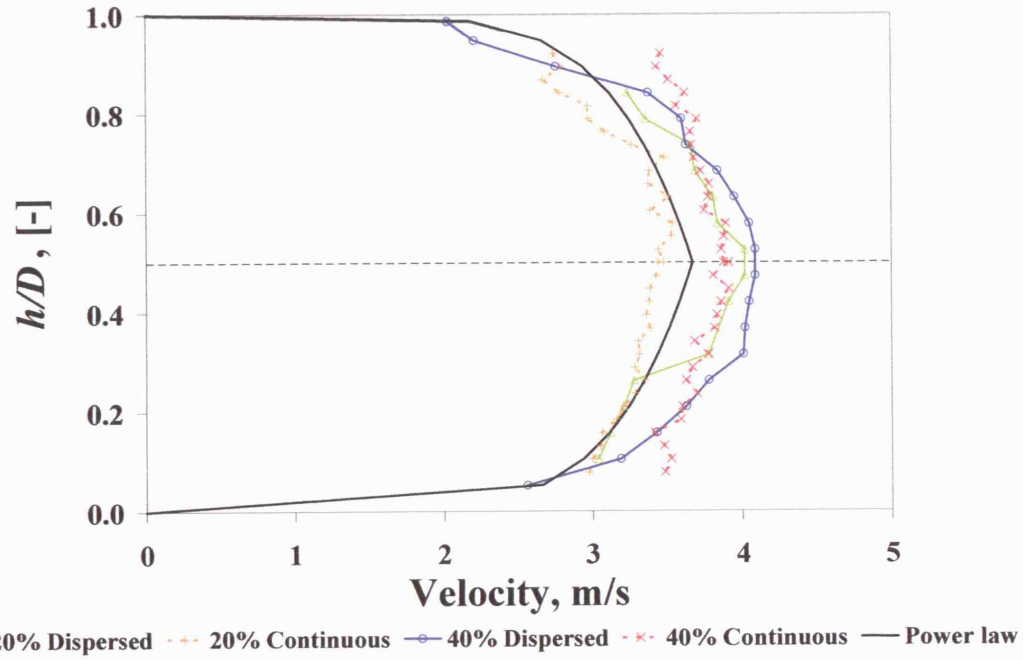

Figure 5.8 Velocity profiles for the dispersed oil droplets (solid lines) and the continuous water phase (dotted lines, obtained by Hu, 2005) at 20 and 40% input oil fraction and 3.0 m/s mixture velocity.

A similar comparison can be made for an oil continuous mixture at 3.5 m/s mixture velocity. This can be seen in Figure 5.9 for 75% input oil fraction. It appears that the dispersed phase (water) is faster than the continuous one (oil) at the lower part of the pipe up to *h/D* equal to 0.5. This agrees with the results in the water continuous flows (Figure 5.8). At the upper part of the pipe however, the continuous phase velocity is higher than that of the dispersed. This is attributed to the fact that the lower

concentration of water droplets at the top of the pipe allows full development of the velocity profile of the continuous (oil) phase. The fact that oil remains the faster phase at a large part of the pipe in oil continuous mixtures (in contrast to water being the slower phase in most of the pipe in water continuous mixtures) explains the holdup results (Figure 5.2) which showed that velocity ratio remained above 1 even after inversion to oil continuous mixtures, although it became closer to 1.

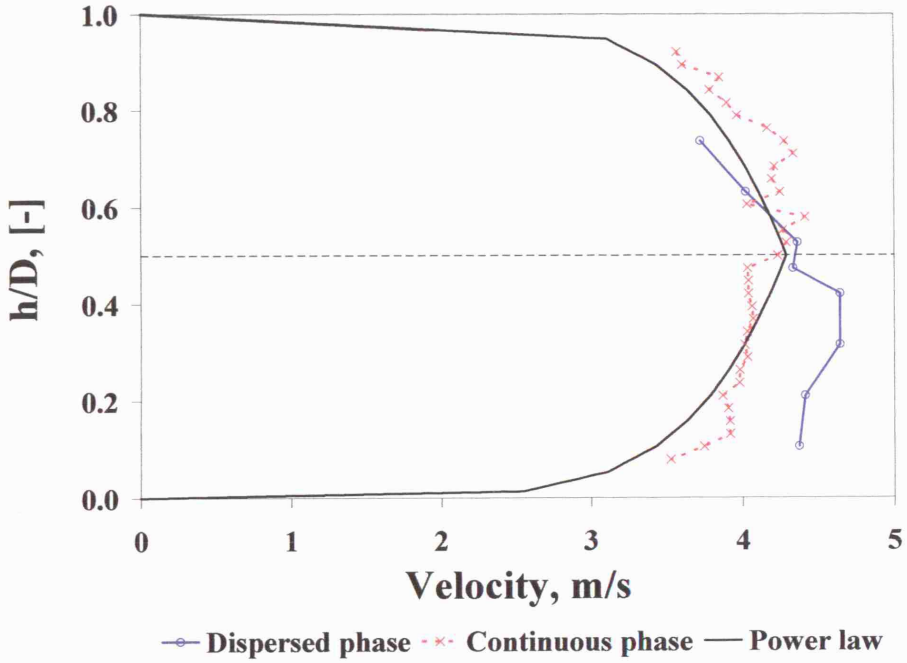

Figure 5.9 Velocity profiles of the dispersed water droplets and the continuous oil phase at 75% input oil fraction and 3.5 m/s mixture velocity.

Dimensionless dispersed phase velocity profiles at 3.0, 3.5 and 4.0 m/s mixture velocity for the same dispersed phase fractions in water continuous dispersions at 40% and 60% input oil fraction and in oil continuous dispersions close to phase inversion are compared in Figure 5.10 and Figure 5.11 respectively. Velocity has been made dimensionless by dividing each value with the respective single phase velocity as predicted by Equation 5.2.

The velocity profiles seem to fluctuate more in water continuous (Figure 5.10) than in oil continuous flows (Figure 5.11) where the values of dimensionless velocity remain closer to unity while in general water droplets seem to have lower velocity than oil droplets. The dimensionless water drop velocity profile is almost uniform along the whole vertical diameter suggesting that water droplets follow closely the single phase parabolic profile. This is expected as in the oil continuous region the dispersed water fraction is small (less than 28%) and at these high velocities and dispersed phase fraction water drops are expected to be small and uniformly distributed in the pipe section. In the water continuous region (Figure 5.10) the dimensionless oil drop velocity at all mixture velocities depends on the dimensionless height and is larger in general at the lower part of the pipe.

The velocities are higher at the lowest part of the pipe and smaller at the top. A stratification of the dispersed phase is expected with less and smaller oil drops close to the bottom of the pipe and more and larger drops close to the top. The large concentration of drops close to the top of the pipe may, hence, hinder their movement.

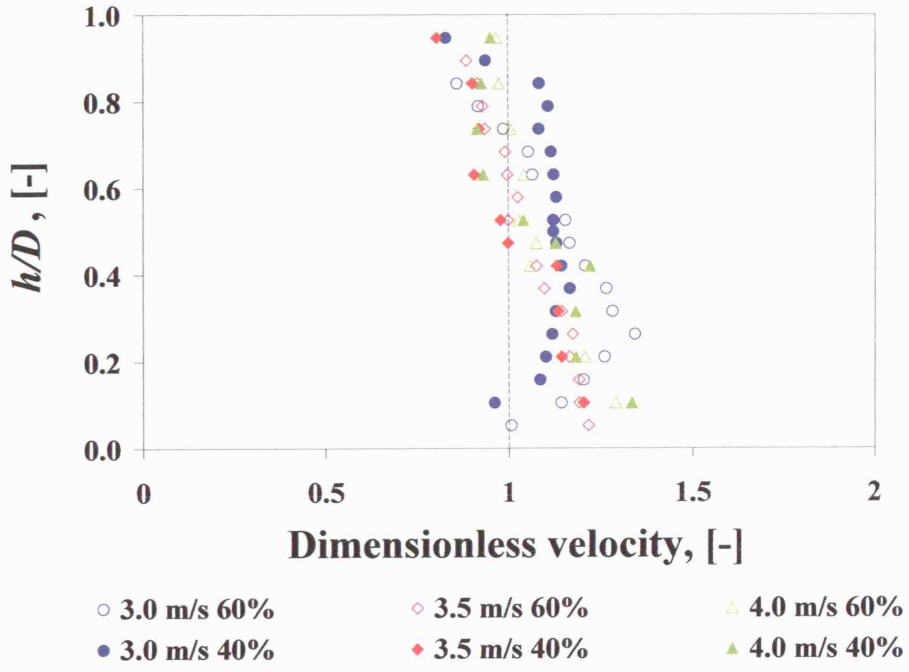

Figure 5.10 Dimensionless dispersed phase velocity for water continuous dispersions at different mixture velocities and input oil fractions in the vertical pipe diameter.

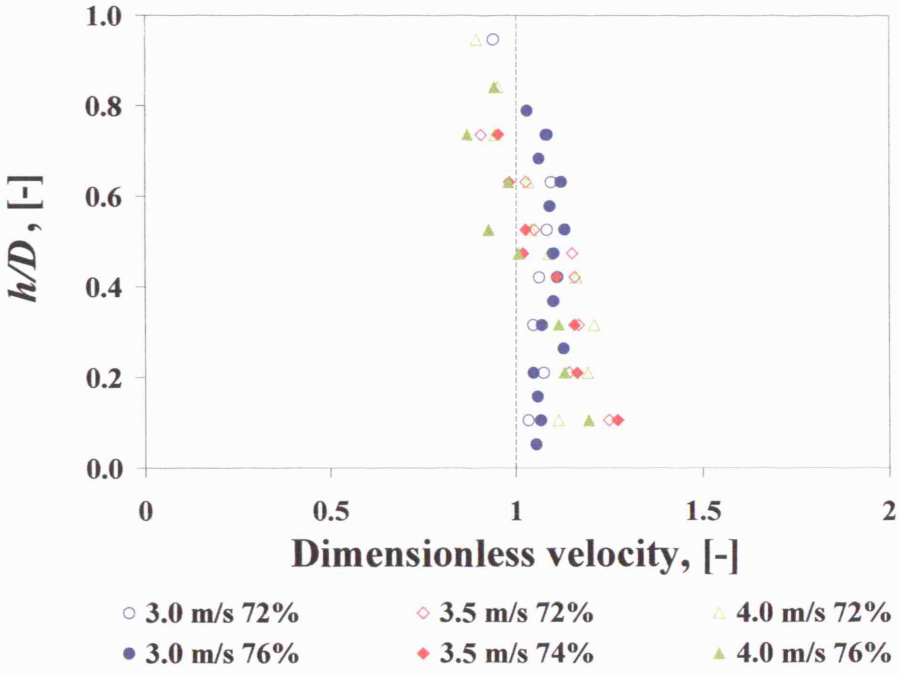

Figure 5.11 Dimensionless dispersed phase velocity for oil continuous dispersions close to inversion at different mixture velocities and input oil fractions in the vertical pipe diameter.

In both graphs the velocity of the dispersed droplets follows the single phase predictions quite well at all mixture velocities. In Figure 5.10 the slight suppression of velocity profile is attributed to the high concentration of oil droplets mostly seen at the upper part of the pipe; this is not seen closer to the bottom of the pipe as the less in number dispersed oil droplets are flowing more freely. Water droplet velocity (shown in Figure 5.11) is lower in comparison to oil droplet velocity (closer to single phase predictions) and fluctuates less.

5.4 CHORD LENGTH/DROP SIZE - PHASE DISTRIBUTION

In the multiphase flow literature the majority of work on drop sizes has been conducted for two-phase gas-liquid flows especially for flows of air and water (Simmons and Azzopardi, 2001). However, knowledge of drop size and distribution is important in liquid-liquid flow, as these are factors that could determine the rheology and stability of a dispersion. Both in stirred vessels and pipelines, drop break-up and coalescence will determine the final drop size distribution in a dispersed flow system.

While most of the works looked at these phenomena separately, a few tried to combine them using population balances (Valentas *et al.*, 1966; Tsouris and Tavlarides, 1994; Hu *et al.*, 2006a). A number of investigators have presented experimental drop size distribution in turbulent pipe flow. Sleicher (1962) found that the maximum drop size decreased as the velocity increased. Ward and Knudsen (1967) investigated drop size and velocity distribution in downward vertical liquid-liquid flow and found that the Sauter mean diameter, D_{32}, (defined in Equation 5.5) varied as the 0.4 power of the dispersed phase concentration. Su and Hanzevack (1988) concluded that the drop size is linearly decreased with the increase in velocity.

Collins and Knudsen (1970) investigated drop size of three different oils in water for vertical downward flow and showed that the length of time for the drops to break-up into their final distribution increases as the viscosity of oil increases. Kubie and Gardner (1977) conducted experiments in horizontal pipes and measurements were taken by photographing the flow through the pipe wall. Karabelas (1978) studied water dispersion in oil in a horizontal pipe. As in other works, coalescence was not present in his study since 0.2% of dispersed phase volume fraction was used.

Angeli and Hewitt (2000) used an endoscope to measure drop size distribution generated from turbulent flow and their results revealed that d_{max} decreased as the continuous phase velocity increased. Furthermore, water drops appeared to have smaller mean drop sizes compared to oil drops in water. Simmons *et al.* (2000) also found a decrease in D_{32} with increasing mixture velocity. Simmons and Azzopardi (2001) used the same laser technique to study drop size distributions for both vertical upward and horizontal flows. They found that the maximum drop diameter agreed with the theory of Hinze (1955) for dilute dispersions but not for concentrated ones.

Lovick and Angeli (2004) measured the chord length distributions in horizontal oil-water flows along a vertical diameter and found that drop size decreased with increasing distance from the interface in dual continuous flow. Hu (2006) studied chord length distributions using the same oil for downward and upward vertical flows with the dual impedance probe developed by Lovick (2004). He found more large oil drops in the pipe central region for both downward and upward flow in comparison to

horizontal flows. Also, smaller water drops in oil compared to oil drops in water were seen, while larger chords were enhanced by increased dispersion fraction.

In the current work once the droplet velocity is found, drop chord length can be calculated from the signal of one of the two dual impedance probe sensors (for details see Lovick, 2004). The time duration that each drop is intercepted by the probe multiplied by the average drop velocity will give the chord length of that drop. From the signal of each probe the volume fraction of the phases at the location of the probe tip can also be found. So, the oil fraction is equal to the time the probe indicates oil, divided by the total time of the experiment at that point.

It was found that the impedance probe would not work well in very dilute dispersions (either water or oil continuous) because not many dispersed droplets are cut by the probe tips, and a cross correlation cannot be obtained. Thus, few results were obtained at 20% input oil fraction and above 78% input oil fraction. Chord length results were obtained at 3.0, 3.5 and 4.0 m/s mixture velocities for input oil fractions between 40 and 80%. Sauter mean chord length, L_{32}, has been calculated as follows:

$$L_{32} = \frac{\sum\left[P(L)L^3\right]}{\sum\left[P(L)L^2\right]} \tag{5.3}$$

where $P(L)$ is the number density of chord lengths of size L. After estimating chord length and chord length distribution, drop size is also calculated for all experimental conditions using an algorithm developed by Hu *et al.* (2006b). The Sauter mean drop diameter, D_{32}, that is calculated by Equation 5.4, is used for making comparisons with literature:

$$D_{32} = \frac{\sum\left[P(D)D^3\right]}{\sum\left[P(D)D^2\right]} \tag{5.4}$$

where *P(D)* is the number density of drops with diameter *D*. Drop size distributions in a pipe cross section and average values are presented and discussed below. The full set of data can be found in Appendix B.

5.4.1 Area weighted averaged chord/drop size distribution

For all mixture velocities local measurements of the dispersed drop chord length were made and area-weighted distributions of the chord length (L) over the pipe cross sectional area were then calculated. Dispersions were treated as oil or water continuous depending on the findings from the local conductivity probe that was able to identify mixture continuity at specific locations in the pipe cross section (Chapter 4). Chords/drops larger than 9 mm were ignored both in the graphs and for the calculation of the Sauter mean chord lengths/diameters. Chords of these dimensions were only measured just before and at the point of phase inversion at all locations in the pipe cross sectional area (including them in the calculation of L_{32} would shift it to very high values around the point of inversion). Chord distribution results at 4.0 m/s are plotted in Figure 5.12 a-h for different input oil fractions and for a Type II experiment that started from water continuous mixtures (40-72% oil fractions) and inverted to oil continuous ones (74-76% oil). Starting from water continuous flows (Figure 5.12 a-f) and increasing the dispersed phase (oil) input fraction, there appears to be a slight shift of the distribution to higher chord lengths due to enhanced coalescence of the dispersed phase; this is not very prominent between 66-68% where the difference in the dispersed phase fraction mixture concentration is not large either, but it is more obvious between 70% and 72% oil, where inversion is about to happen. At 72% the bulk of the mixture is still water continuous and large chord lengths of the dispersed phase are measured by the probe. This increase in the dispersed phase chord length cannot be explained by the small increase in the inlet oil fraction. Information on the shape of these large formations, however, can not be obtained with the current instrumentation. With further change of the input fraction, inversion at the whole cross sectional area occurs and results in the presence of much smaller water droplets at 74% and 76 % input oil fraction (Figure 5.12 g&h) with the distribution shifting to smaller sizes with increasing oil (decreasing dispersed water) fraction.

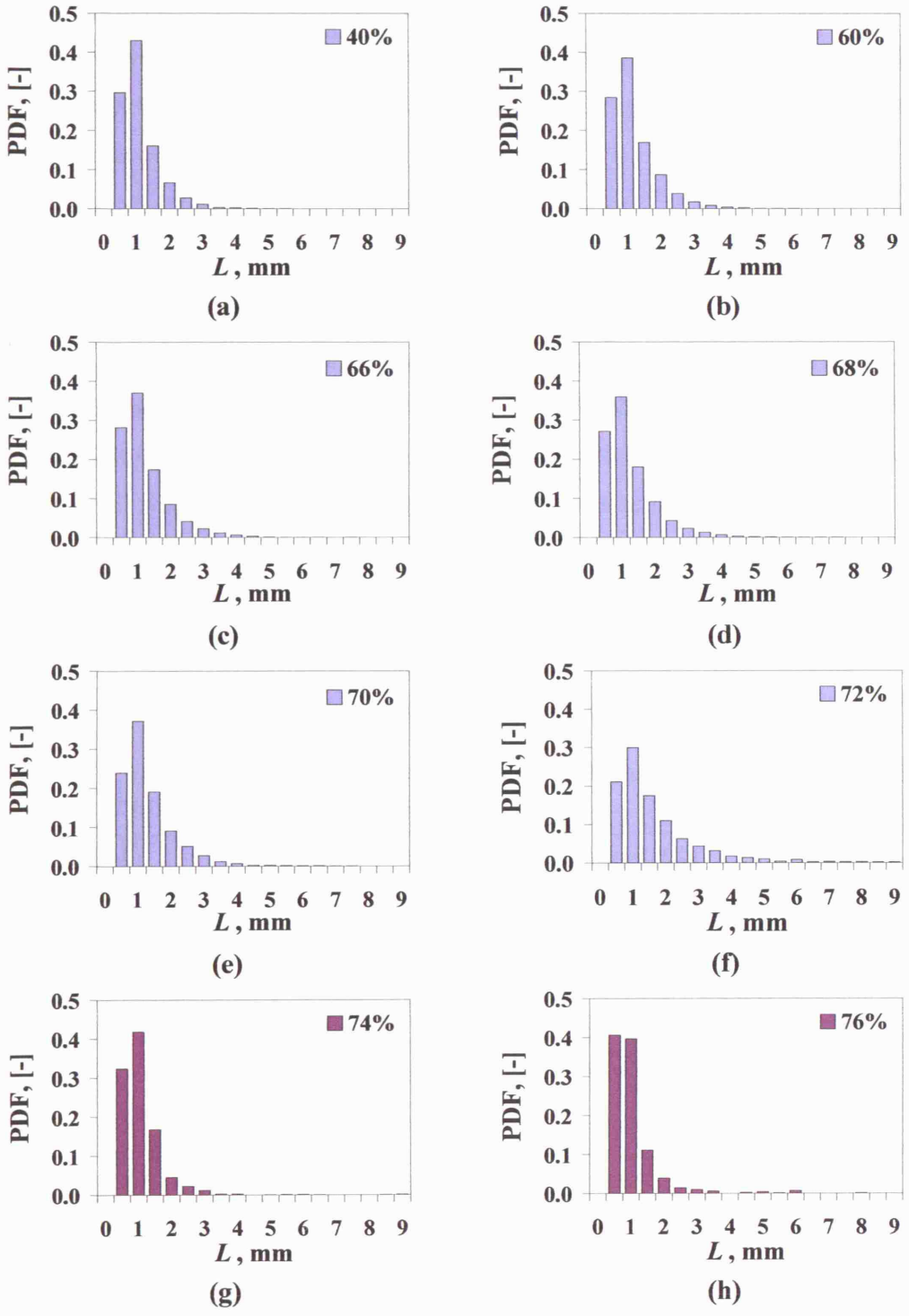

Figure 5.12 Chord length (L) distributions averaged for the whole cross section at 4.0 m/s mixture velocity and for different input oil fractions (40 - 76%) starting from water continuous mixtures. Light (blue) colour represents water continuous flows, while dark (magenta) represents oil continuous flows.

Results at higher concentrations could not be obtained at this mixture velocity (due to low water concentration), but it is expected (in agreement with results obtained at lower mixture velocities) that water droplet chord length would further decrease as its fraction is decreasing.

Measurements for experiments Type I (from oil to water continuous dispersions) yielded similar results. Area weighted average chord length results from all mixture velocities and phase fractions studied can be seen in Table 5.1. In water continuous mixtures, there is a gradual increase in Sauter mean chord length with the increase in the dispersed phase fraction towards the phase inversion point, where a maximum is encountered. The trend is reversed after inversion when now the size of the dispersed water drops due to decrease in the water fraction.

Results obtained at 76% and 80% oil fraction are biased to larger chord lengths as cross correlation could only yield results at the lower part of the pipe (where larger water droplets are encountered), but not at the top of the pipe, where there was not sufficient number of dispersed droplets.

Table 5.1 Values of the cross sectional averaged Sauter mean chord length in mm (L_{32}) at different mixture velocities.

MIXTURE VELOCITY (M/S)	INPUT OIL FRACTION (%)								
	40	**60**	**66**	**68**	**70**	**72**	**74**	**76**	**80**
3.0	2.32	4.1	4.3	4.68[5.1]	5.29[5.2]	4.27[5.3]	3.52	3.33[5.4]	2.4[5.4]
3.5	2.25	2.34	2.8	3.1	3.95[5.1]	5.56[5.2]	2.63[5.3]	2.51	1.66
4.0	1.86	2.08	2.29	2.46	2.55	4.04[5.2]	2.63[5.3]	2.87[5.4]	(-)

Drop size distributions are obtained from the measured chord length distributions. Results at 3.5 m/s mixture velocity can be seen in Figure 5.13 a-i. Starting from water continuous mixtures and 40% input oil fraction, the drop sizes encountered are small and less than 3 mm. As the dispersed phase fraction in the

[5.1] Oil layer appears on top (before inversion).
[5.2] Just before inversion (water continuous region).
[5.3] Just after inversion (oil continuous region).
[5.4] Value biased to bigger droplets as results could not be obtained at the upper part of the pipe due to insufficient number of dispersed droplets.

mixture is increasing, drop sizes are also slightly increasing up to 70% input oil fraction. At 72% input oil fraction based on findings from the conductivity probe the upper part of the pipe is behaving as oil continuous (so dispersed water drop chord lengths are measured by the probe), while the core and lower parts of the pipe remain water continuous. Thus, in Figure 5.13f (depicted with two colours due to the dual continuous pattern), the averaged dispersed phase droplet size that includes both oil and water drops is plotted. Droplet size variations are similar to the above described chord length behaviour (distributions tend to be sharper than chord length and shifted to smaller values) and at the exact point of inversion in the water continuous region (70% input oil fraction at 3.0 m/s and 72% at 3.5 and 4.0 m/s mixture velocity, seen also in Figure 5.12f) droplets as large as 7 mm are found. After inversion to oil continuous mixtures much smaller water droplets are measured (the mixture now contains only 26% dispersed phase fraction as opposed to 72% prior to inversion) and their size decrease with increasing input oil fraction (Figure 5.13 g-i).

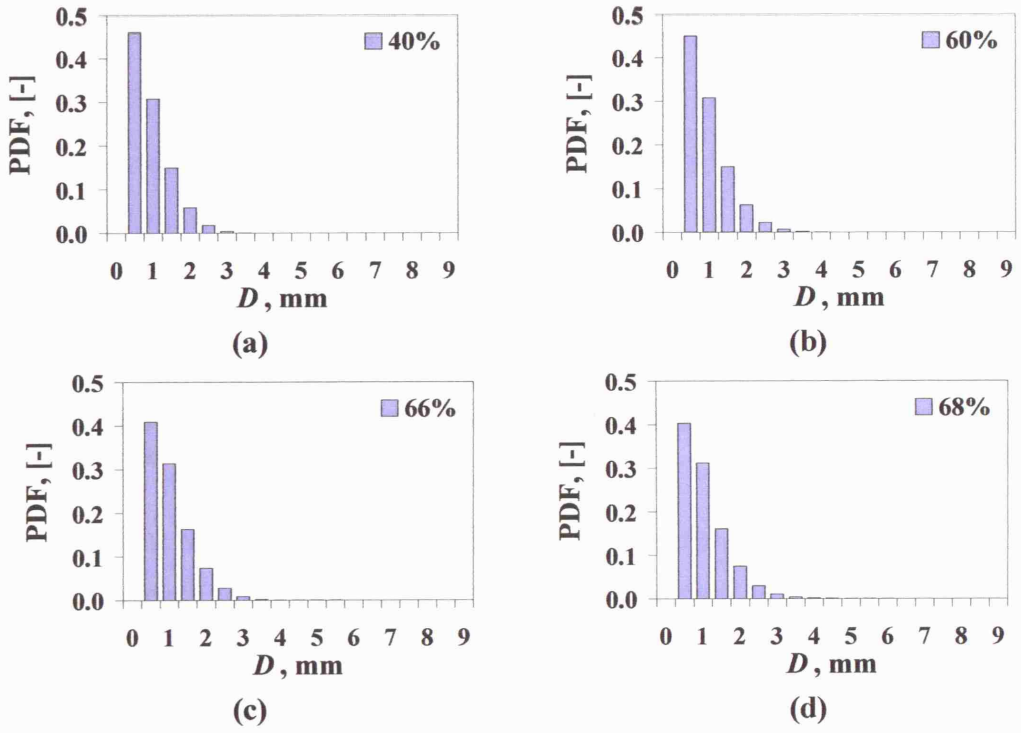

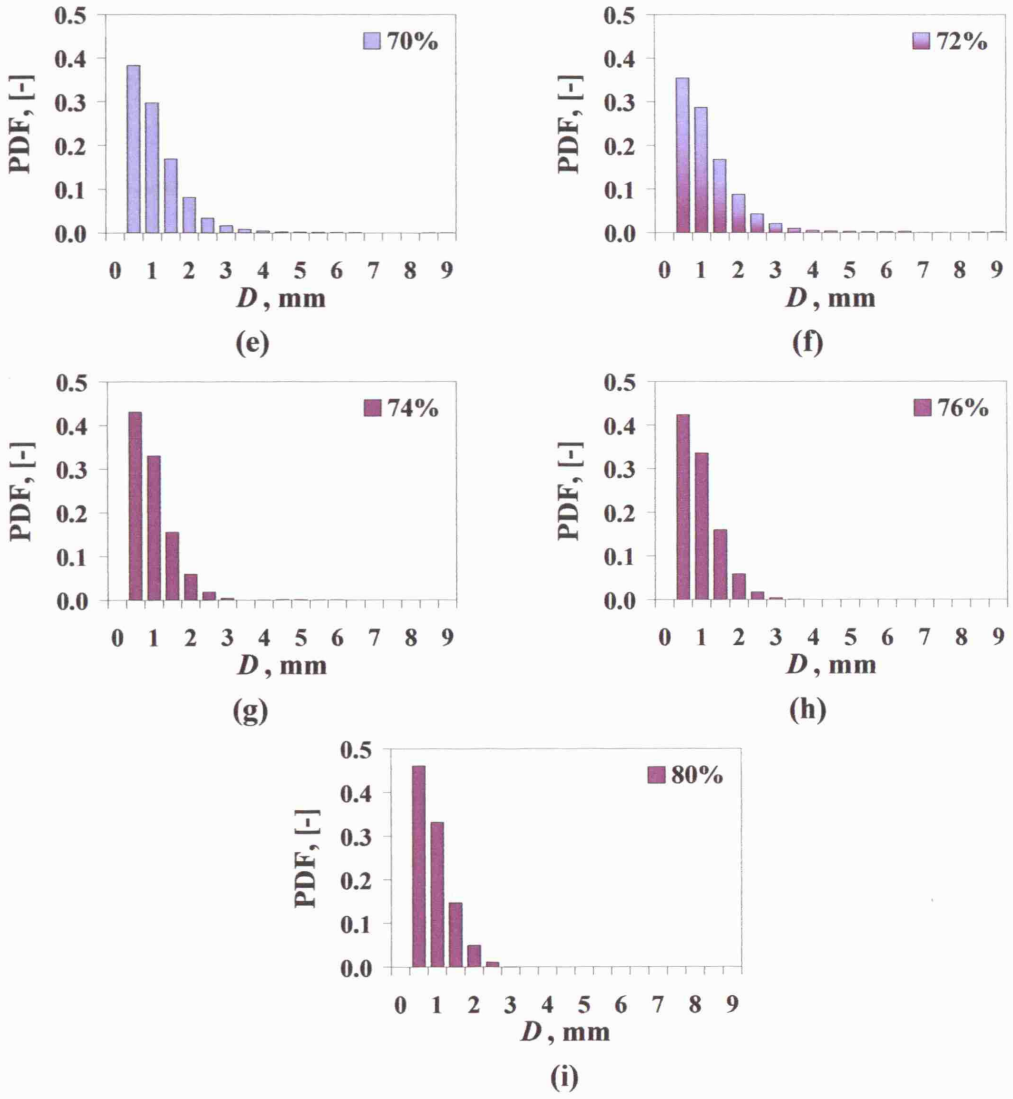

Figure 5.13 Drop size distribution averaged for the whole cross section area at 3.5 m/s mixture velocity and for different input oil fractions (40 - 80%). Light blue colour represents water continuous flows, while dark magenta represents oil continuous flows. The experiment started from water continuous mixtures and inversion was seen at 72%.

Results on drop diameter from all experimental conditions can be seen in Table 5.2: the increase in the Sauter mean drop diameter right before the completion of phase inversion is significant and does not correspond to the slight increase in the dispersed phase fraction.

Table 5.2 Values of the cross sectional averaged Sauter mean diameter (D_{32}) in mm at different mixture velocities.

MIXTURE VELOCITY (M/S)	INPUT OIL FRACTION (%)								
	40	**60**	**66**	**68**	**70**	**72**	**74**	**76**	**80**
3.0	1.7	2.29	2.52	2.98	$3.48^{5.2}$	$2.46^{5.3}$	1.95	2.24	2.1
3.5	1.56	1.65	1.8	1.96	$2.49^{5.1}$	$3.6^{5.2}$	$1.66^{5.3}$	1.57	1.41
4.0	1.51	1.61	1.67	1.72	1.76	$2.27^{5.2}$	$1.51^{5.3}$	1.49	(-)

Making comparisons among different mixture velocities it can be concluded that for the same dispersed phase fraction, chord length and drop diameter become smaller as the mixture velocity increases (this is obvious at the inversion point as well), while generally there are more variations in the drop size with dispersed phase fraction at lower mixture velocities. At 4.0 m/s mixture velocity more uniform distributions are encountered, not only in the pipe cross section in each input oil fraction, but also over the whole range of input oil fractions (as seen in Table 5.1 and especially in Table 5.2 regarding the Sauter mean drop diameter).

5.4.2 Chord length and phase distributions in the pipe cross section

Results of local chord length measurements are shown in Figure 5.14 a-c for different mixture velocities and input oil fractions (40-80%). Solid fine lines represent water continuous flows; thick solid line is the point just before inversion to oil continuous flows, while the dotted lines represent oil continuous conditions. Sauter mean chord length is plotted against dimensionless height (h/D) where h is the distance from the bottom of the pipe. Few results obtained at 20% input oil fraction at 3.0 m/s mixture velocity have shown that more dispersed droplets and larger are seen at the top of the pipe (for example 243 droplets with L_{32}=4.47 mm were counted at $0.10D$ as opposed to 1165 droplets with L_{32}=4.70 mm at $0.84D$).

As mentioned earlier for the area weighted chord lengths over the whole pipe cross section it is obvious that locally chord length is increasing with increasing dispersed phase fraction at the water continuous region due to enhanced drop coalescence.

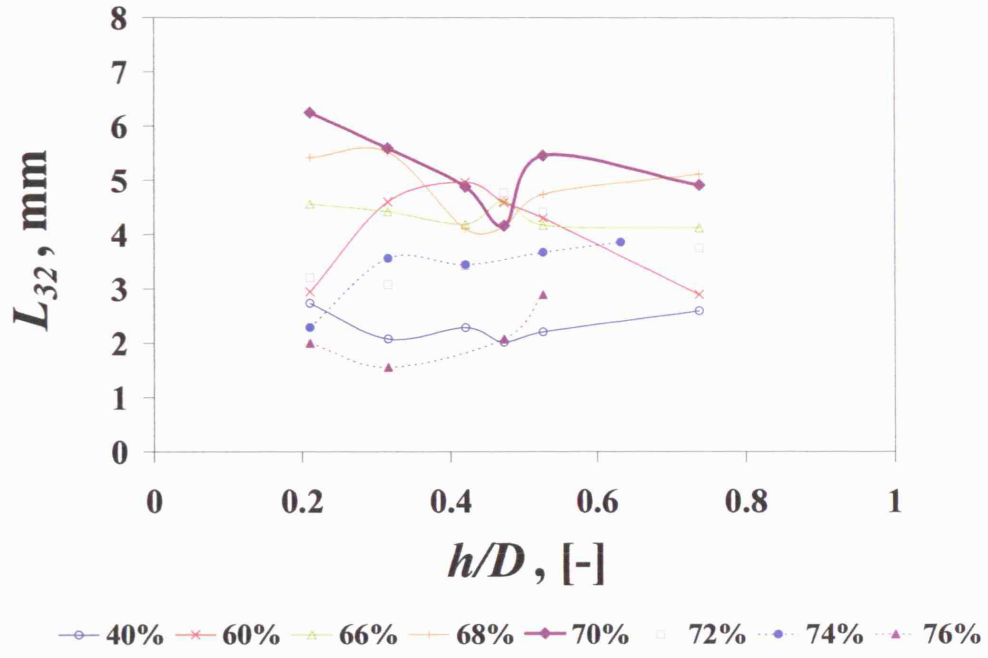
8
7
6
5
4
3
2
1
0
0
0.2
0.4
0.6
0.8
1
L_{32}, mm
h/D, [-]
40%
60%
66%
68%
70%
72%
74%
76%

(a)

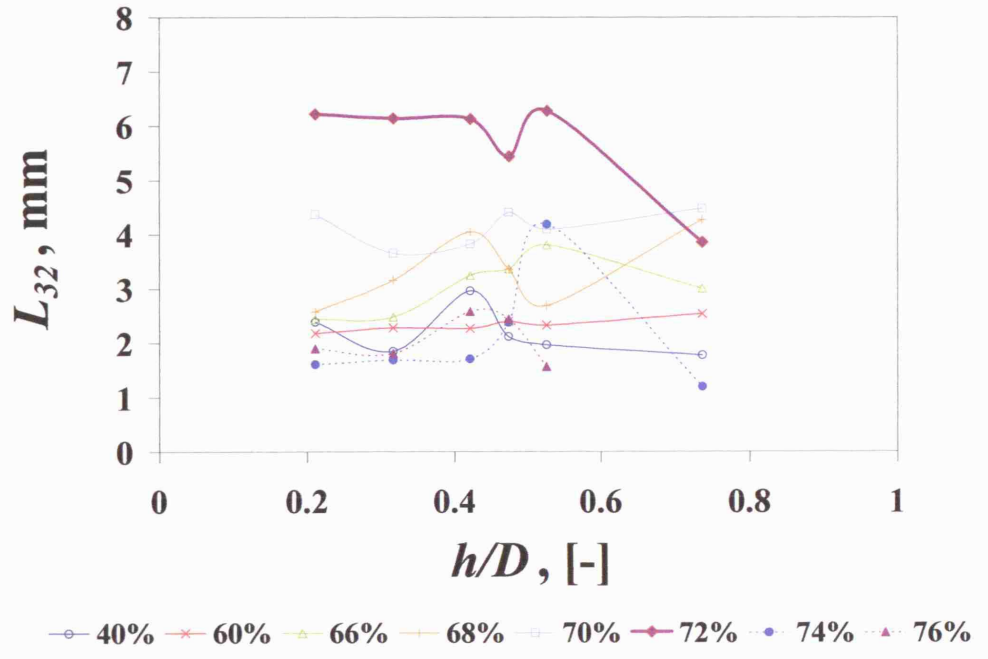
8
7
6
5
4
3
2
1
0
0
0.2
0.4
0.6
0.8
1
L_{32}, mm
h/D, [-]
40%
60%
66%
68%
70%
72%
74%
76%

(b)

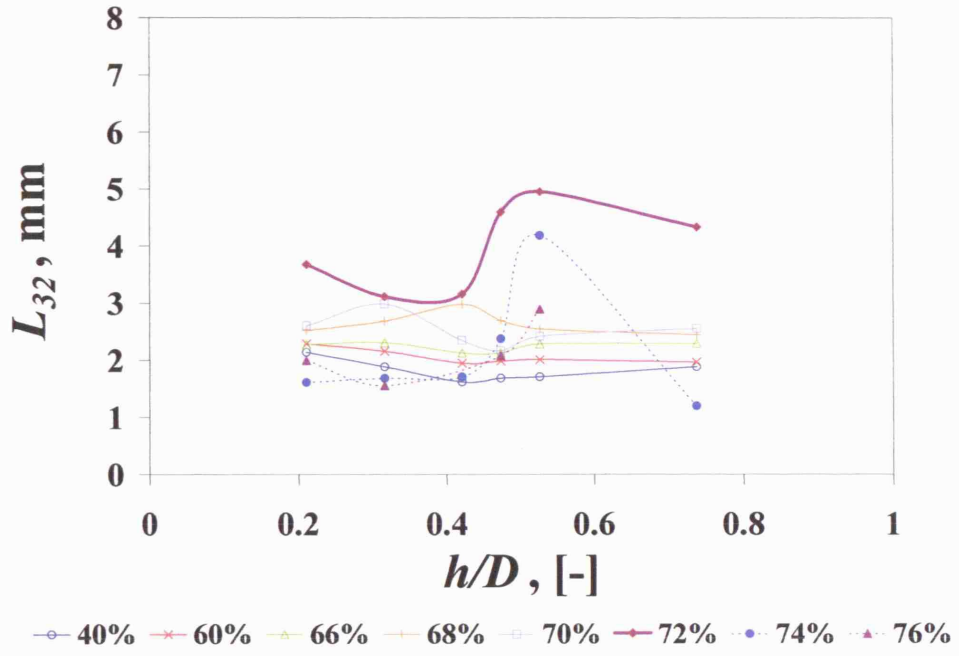

(c)

Figure 5.14 Sauter mean chord length profiles at the pipe cross sectional area at a) 3.0 m/s, b) 3.5 m/s and c) 4.0 m/s mixture velocity and at different input oil fractions (40 – 76%). Open symbols with solid lines represent water continuous flows, while closed symbols with dotted lines represent oil continuous flows. The thick solid line is the inversion point.

As phase inversion is approached (input oil fraction above 60%), there is an increase in the concentration of larger dispersed drops around the core of the pipe and at the upper part of the pipe. This increase will sometimes lead to early localised inversion. The increase in size at the inversion point in the whole cross sectional area is very prominent at all mixture velocities. At 3.0 and 3.5 m/s mixture velocity, the decrease in the chord lengths, and therefore in drop diameter as well, at $0.7D$ is due to the fact that inversion was completed locally and these points represent water droplet chord length. At 4.0 m/s there is a large increase in chord length in the middle and the upper part of the pipe that will eventually lead to inversion at that part of the pipe. After inversion, L_{32} reduces to lower values, reflecting the fact that water droplets have a much smaller size than the oil droplets prior to inversion, but at higher mixture velocities there is a high concentration of larger water droplets at the core of the pipe,

showing that water as the dispersed phase is trapped mostly at the core of the pipe. With further increase of the oil fraction (decrease of water fraction) and at all velocities, water droplet L_{32} decreases. The L_{32} distribution also becomes more uniform at the highest velocity 4 m/s, especially at the lower oil fractions. At this high velocity the distribution of the phases in the pipe cross section is also quite uniform (see also Figure 5.15a). At the lower velocities gravitational effects will be important and will affect the distribution of the phases (see Figure 5.15b for 3.5 m/s mixture velocity) and subsequently the distribution of the drop sizes.

The variation of droplet diameter size in a pipe cross section around the inversion point can be seen in Figure 5.16 and Figure 5.17 at 3.0 m/s (68% and 72% input oil fraction respectively). Figure 5.16 explains the decrease in chord length seen in the middle of the pipe at 68 and 70% as shown in Figure 5.14a: it is at that location that a significant increase in the number of dispersed droplets is seen.

In general it was found that most dispersed droplets of both oil or water are at the core of the pipe. In the water continuous region, more (oil) drops are seen at the top of the pipe than in the bottom, while the opposite is observed for water drops in the oil continuous region (also seen in Figure 5.16 and Figure 5.17). In Figure 5.18 the drop size distribution in the pipe cross section at 40% input oil fraction can be seen. It is obvious that even in more dilute dispersions, most of the dispersed phase is found at the centre of the pipe (explaining the high slip ratios discussed above as most of the dispersed phase will be travelling in the high velocity core).

Similar results regarding the distribution of the droplets were found at all mixture velocities studied, with the difference in the number of dispersed droplets between upper and lower part of the pipe decreasing with increasing velocity.

In Table 5.3 the chord lengths and chord numbers in the pipe centre are depicted at 3.5 and 4.0 m/s mixture velocity and different input oil fractions.

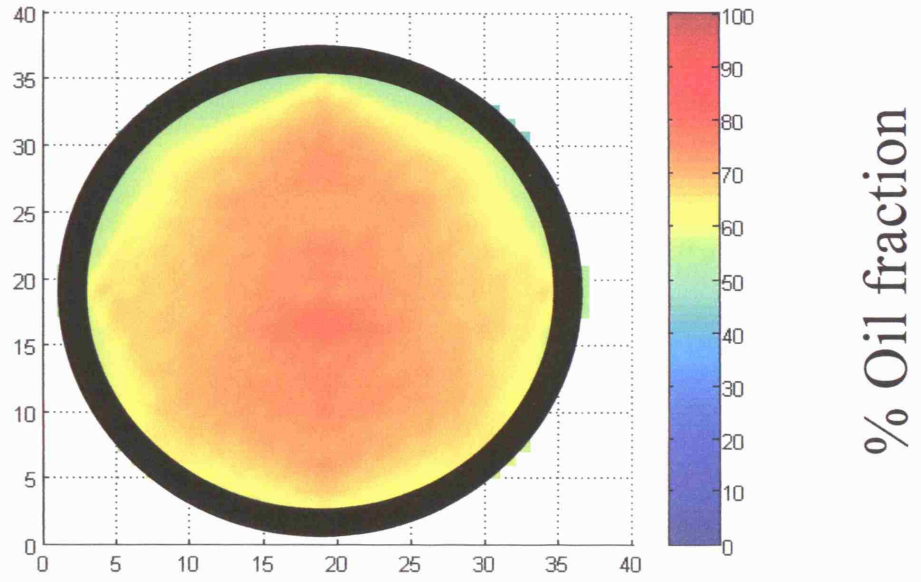

(a)

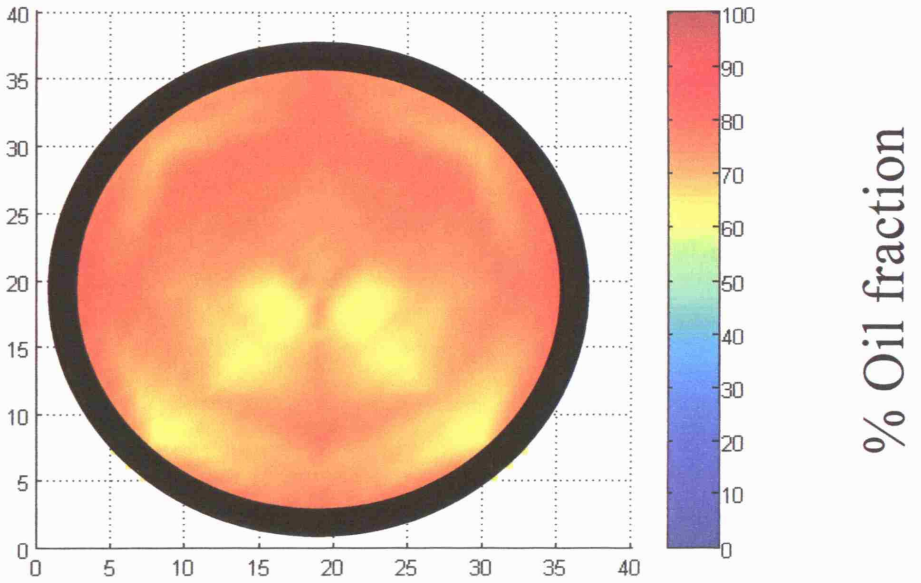

(b)

Figure 5.15 Phase distribution at the pipe cross sectional area at a) 4.0 m/s mixture velocity and 68% input oil fraction and b) 3.5 m/s and 72% input oil fraction.

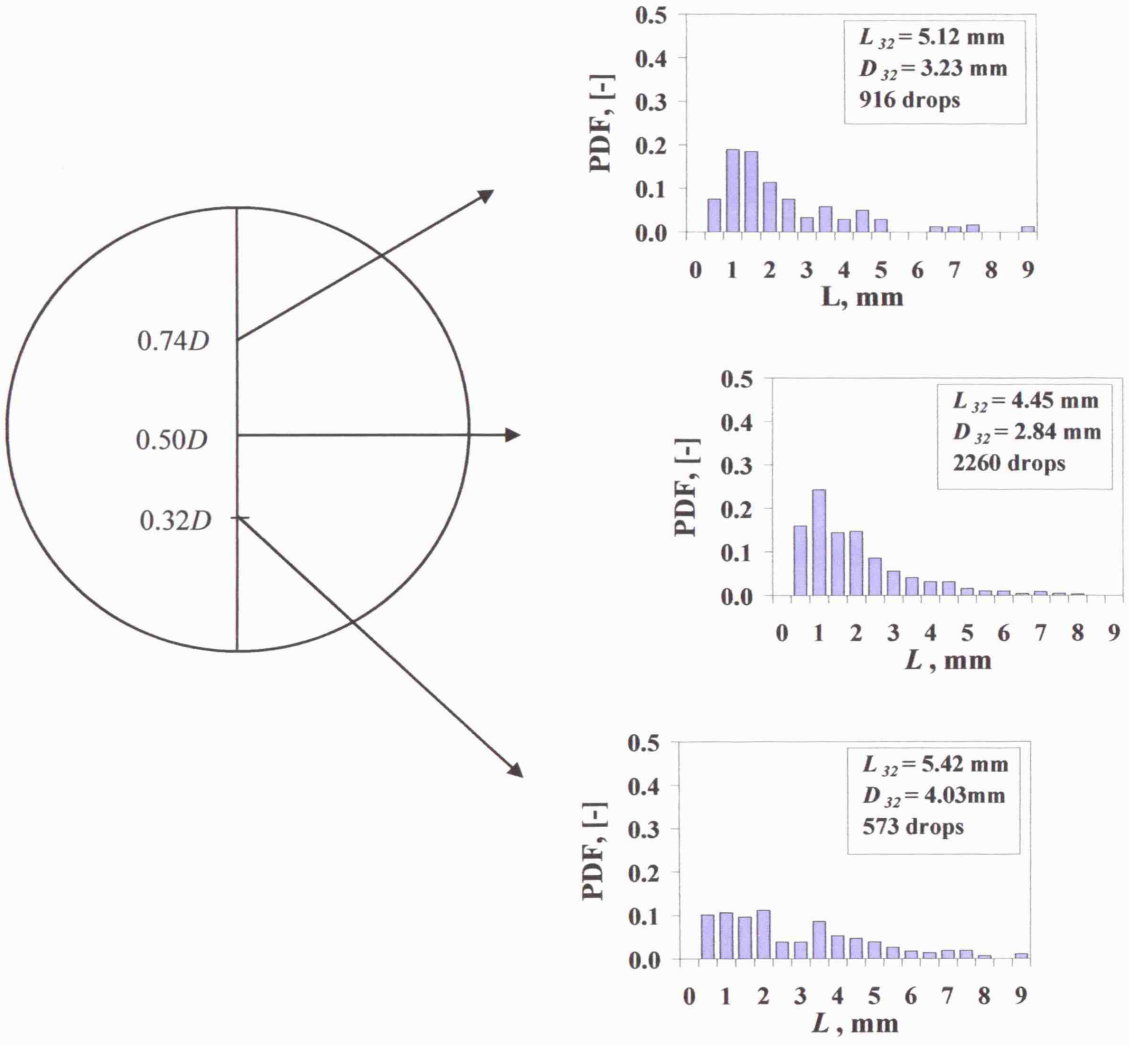

Figure 5.16 Drop size distribution at 3.0 m/s mixture velocity at 68% input oil fraction (close to inversion). Flow is water continuous, so oil droplet chord length is measured. Most of the dispersed oil droplets are in the pipe core.

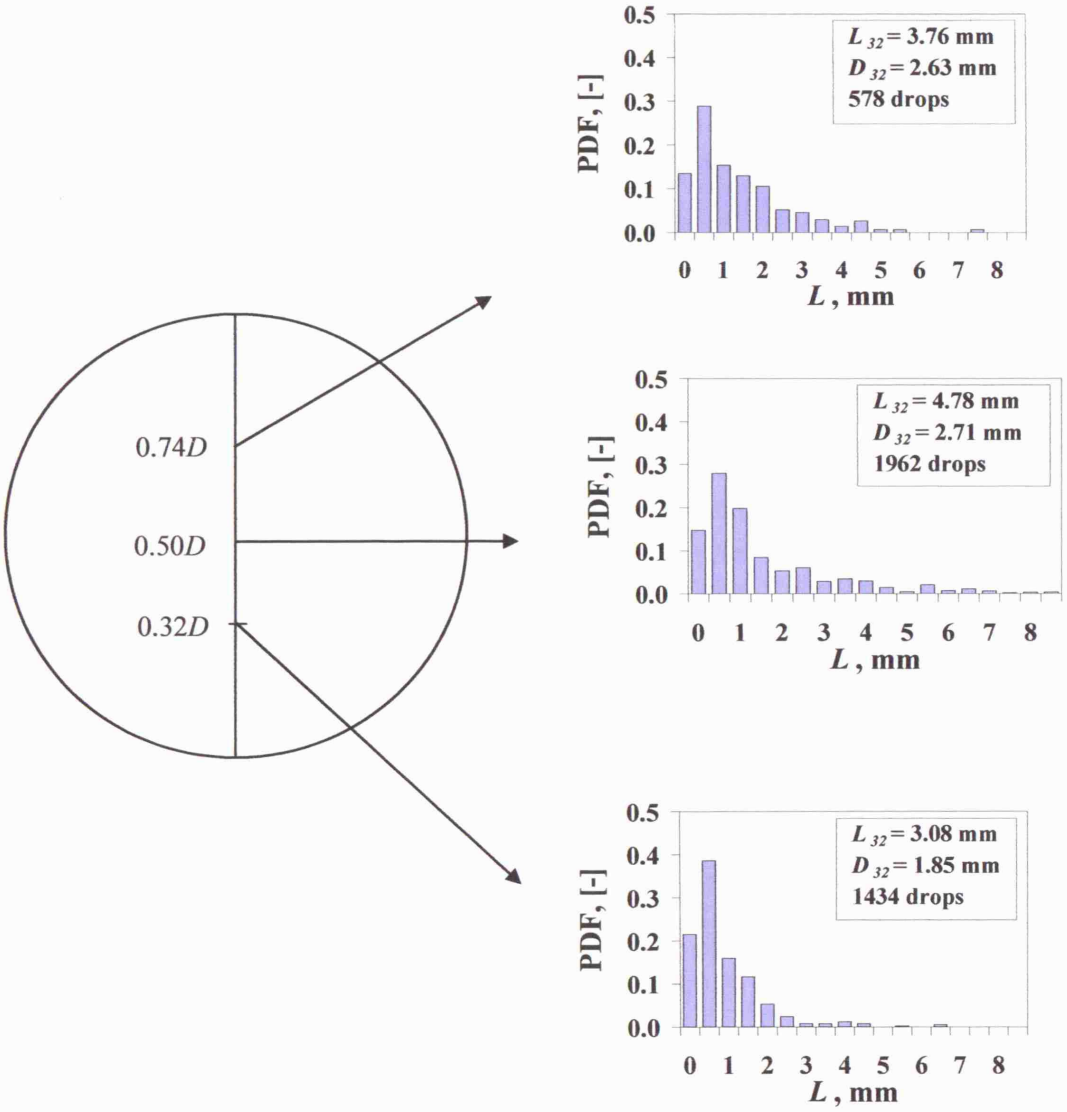

Figure 5.17 Drop size distribution at 3.0 m/s mixture velocity at 72% input oil fraction (after inversion). Flow is now oil continuous, so water droplet chord length is measured. Most dispersed droplets can be found in the pipe core.

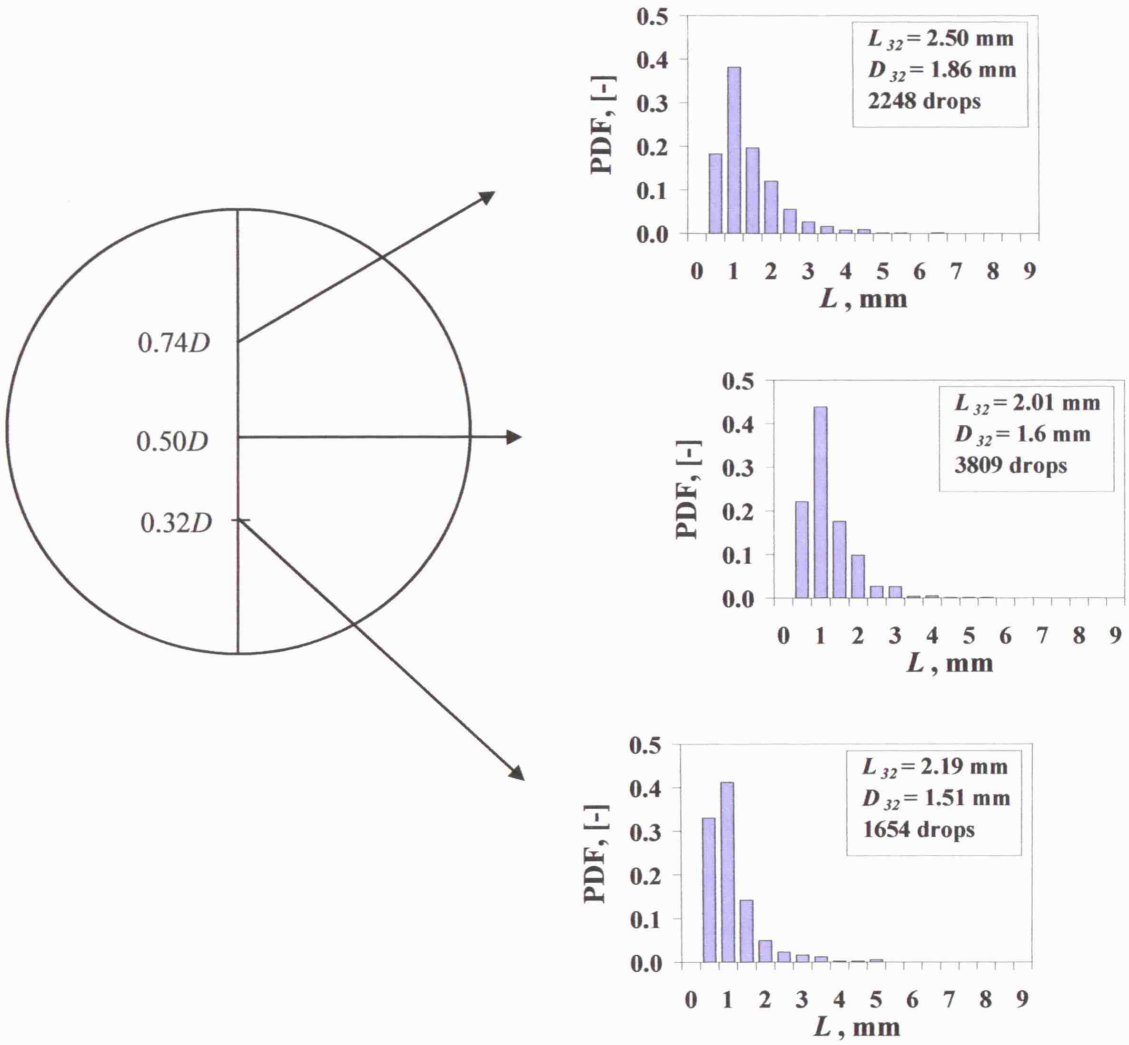

Figure 5.18 Drop size distribution at 3.0 m/s mixture velocity at 40% input oil fraction. Flow is water continuous, so oil droplet chord length is measured. Most of the dispersed oil droplets are in the pipe core.

Going from low to high input oil fractions (also seen in Figures 5.16-5.18), there is an increase in the number and the size of the droplets (also seen in the rest pipe cross section). However, close and at the inversion point (seen in Figure 5.16 and Table 5.3), the number of drops decreases significantly favouring the increase in their size at all mixture velocities studied. After inversion to oil continuous flows, the number of droplets measured drops significantly, justified by the percentage of the dispersed flow that is now much lower (28-30% water in the oil continuous carrier).

Table 5.3 Sauter mean chord length L_{32} measurements (in mm) and number of chords (N_d) at the pipe centre at different input oil fractions and mixture velocities.

	INPUT OIL FRACTION (%)						
MIXTURE VELOCITY (M/S)	40	60	66	68	70	72	74
3.5	L_{32}=2.12 N_d=3407	L_{32}=2.39 N_d=4636	L_{32}=3.37 N_d=3551	L_{32}=3.7 N_d=3319	L_{32}=4.55 N_d=3401	L_{32}=4.93 N_d=1596	L_{32}=2.65 N_d=1191
4.0	L_{32}=1.70 N_d=4214	L_{32}=2.0 N_d=5150	L_{32}=2.21 N_d=5067	L_{32}=2.28 N_d=4844	L_{32}=2.3 N_d=4412	L_{32}=4.6 N_d=2169	L_{32}=2.38 N_d=666

5.5 THEORETICAL CONSIDERATIONS

If phase inversion is a spontaneous phenomenon then, according to literature, a criterion for inversion would be the minimization of the system energy at the inversion point (Luhning and Sawistowski, 1971; Tidhar *et al.*, 1986; Brauner and Ullmann, 2002). Provided that there is no temperature or chemical composition change at inversion this criterion is equivalent to that of equal surface energy of the two possible dispersions, namely oil continuous and water continuous. This criterion was applied by Hu and Angeli (2006) in vertical flows where it was found that it did not agree well with his experimental results. In fact a difference in both upward and downward vertical flows on surface energy existed before and after inversion because drop sizes changed significantly at the inversion point. The system free energy consists of two terms, the liquid-liquid interfacial energy and the surface-solid surface energy given by (Brauner and Ullmann, 2002):

$$E_s = \frac{6\sigma\varepsilon}{D_{32}} + s\sigma_s \tag{5.5}$$

where σ is the oil/water interfacial tension, σ_s is the surface-solid surface energy, s is the solid surface area per unit volume (equal to $4/D$ for smooth pipes) and ε is the dispersed phase fraction. Here, only the interfacial liquid-liquid energy will be considered as the surface-solid surface energy in this system is much smaller at the high mixture velocities used compared to the interfacial energy of the large number of dispersed droplets and can therefore be ignored.

For the estimation of the interfacial energy the Sauter area-weighted average in the pipe cross section will be used (values seen in Table 5.2 and plotted in Figure 5.19), where ε is the *in situ* dispersed phase fraction obtained from holdup experiments. In Figure 5.19 the point of the inversion to oil continuous flows is the point right after the maximum appearing at each mixture velocity. The results obtained with the use of Equation 5.5 at all mixture velocities can be seen in Figure 5.20 where interfacial energy Es/σ has been plotted against input oil fraction.

The open symbols are used to depict water continuous mixtures, while closed symbols are used to depict oil continuous ones. Interfacial energy is significantly decreasing to lower values with the occurrence of inversion and the values just before and right after inversion do not seem to coincide. The difference however becomes less with increasing drop size just before inversion (e.g. results at 3.5 m/s mixture velocity); this means that there might be a condition at lower mixture velocities where the interfacial energy before and after inversion becomes the same. Of course, further considerations of the holdup in such case should be made. Difference in the interfacial energy prior and after inversion has been observed in literature before (Luhning and Sawistowski, 1971, in stirred vessels; Hu and Angeli, 2006, in vertical upward and upward flows).

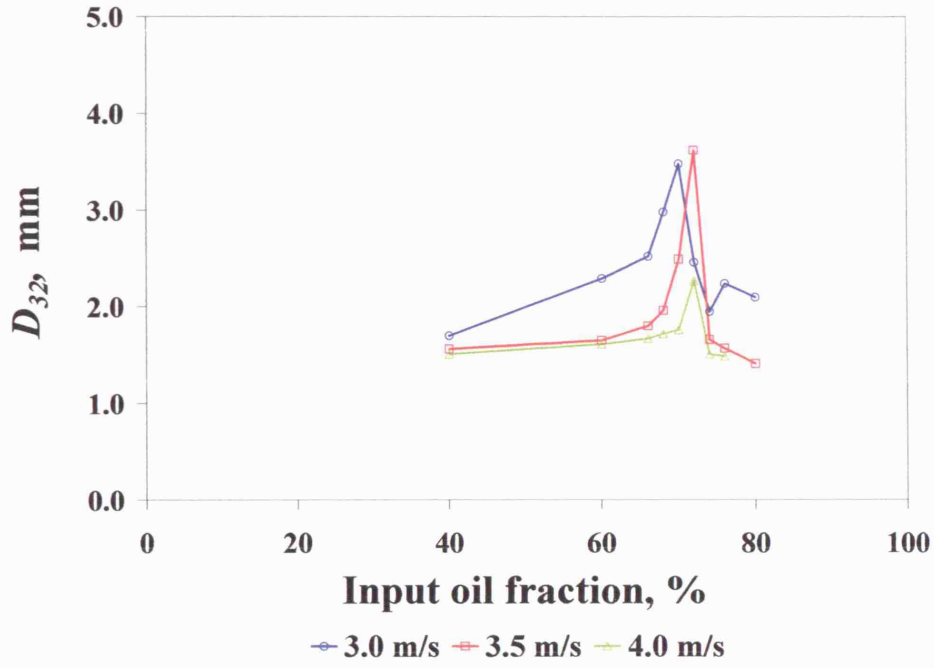

Figure 5.19 Cross sectional averaged Sauter mean diameter (D_{32}) at different mixture velocities with input oil fraction.

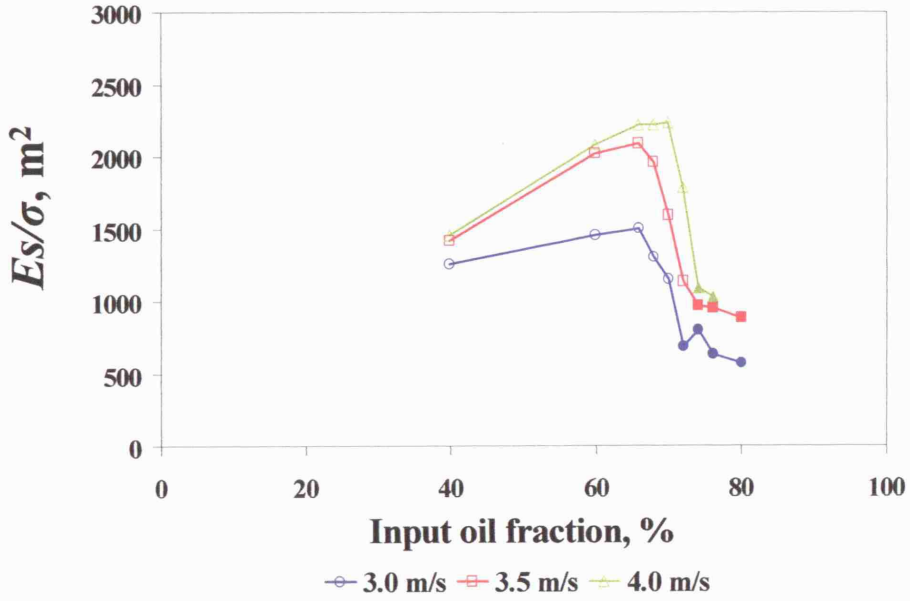

Figure 5.20 Interfacial surface energy (Es/σ) at different mixture velocities plotted with input oil fraction.

5.6 CONCLUSIONS

In the 38 mm ID SS pipe at UCL with *EXXSOL™ D140* as test oil, experiments were carried out to investigate variations of holdup, phase and chord length distributions in a pipe cross section as the system approached phase inversion and after it. Both experimental routes, starting from oil or water continuous dispersions were used. The following summarise the findings of this chapter:

- There is a decrease in the value of velocity ratio after the inversion point in Type II experiments. The difference in velocity ratio before and after inversion becomes less with increasing mixture velocity.
- Velocity ratio for the conditions studied was found to be more than 1 for both oil and water continuous mixtures, indicating that oil is always the faster phase. This was verified from findings of the drop velocity profiles that indicated an increase in the dispersed oil velocity with increased input oil fraction until the occurrence of inversion towards oil continuous flows after which dispersed (water) drop velocity became much lower.
- Dispersed phase velocity profiles showed that oil droplets are faster than water droplets. Droplet velocity profiles became more uniform at lower input oil fractions.
- Most dispersed phase, both in oil and water continuous mixtures, was found at the core of the pipe. If the upper and lower parts of the pipe are compared, in water continuous mixtures more dispersed oil droplets were detected at the upper part of the pipe, while in oil continuous mixtures more water droplets were found at the lower part of the pipe.
- Drop size and phase distributions became more homogenous while smaller droplets were encountered with increasing mixture velocity.
- In Type II experiments, there was a significant increase at the dispersed droplet size at the input oil fraction just before inversion at all mixture

velocities studied, indicating enhanced coalescence just before inversion completes.

- The experimental findings did not agree with the criterion of phase inversion, which stipulates that at the inversion point the surface energies of the two possible dispersions (oil continuous and water continuous) are equal.

These experimental results help towards the understanding of the mechanism of inversion. It is clear from the current findings that inversion must be strongly related to the appearance of increased droplet size that cannot be explained only by the increase in the dispersed phase fraction before inversion. However, the effect of different flow parameters on the inversion phenomenon should also be studied to further understand the mechanism of the phenomenon. This is done in the following Chapter.

Chapter 6

Effect of parameters on phase inversion

6.1 OVERVIEW

The effect of different parameters on the phase inversion point and the accompanying pressure gradient were studied in two experimental facilities and are described below. More specifically, the effect of oil properties (Section 6.3), mixture velocity (Section 6.4), dispersion initialisation conditions (Section 6.5), pipe diameter (Section 6.6) and pipe material (Section 6.7) were investigated. Drag reduction for both oil-in-water and water-in-oil dispersions was seen in all systems used and this is discussed extensively in Section 6.8. The experimental findings were compared with the predictions of empirical correlations on phase inversion (Section 6.9) and the ambivalent range (Section 6.10). Single phase pressure drop considerations were made to obtain information on the experimental friction factors of each test section (Section 6.2).

The graphs in this section are averaged over at least three experimental runs for each condition. The variations in pressure gradient due to changes in mixture properties and the occurrence of inversion tend therefore to appear smoother than when single runs are considered. This is also due to the fact that phase inversion may appear at slightly different oil fraction in the different runs causing significant shifts in

the pressure gradient curve. In some cases the exact point of phase inversion was omitted because of the instability of the system at this point (as described in Section 4.4). In each graph the experimental facility and the type of oil used will be noted in the legend. The experimental error in the pressure drop measurements is approximately 10% in all 60 mm ID test sections used at NTNU, 5% in the 32 mm ID acrylic pipe at NTNU, while the calculated average standard deviation for the UCL pressure gradient measurements is 0.2. The whole set of results can be found in Appendix C.

6.2 SINGLE PHASE EXPERIMENTS

Single phase pressure gradient experiments were conducted for both oil and water in all test sections (acrylic with 32 and 60 mm ID, epoxy coated stainless steel with 60 mm ID and bare stainless steel with 38 and 60 mm ID) to obtain information on pipe roughness and also have the values necessary to non-dimensionalise the two-phase flow results. Single phase velocities were varied from the lowest to the highest possible that could be achieved in each setup (also depending on the properties of the liquids used). A wide range of Reynolds numbers was thus obtained. The flow in the mixture velocities studied is considered turbulent as the lowest Reynolds number encountered in all single phase measurements was approximately 4000, well above the laminar region. Experimental friction factor was calculated from the measured pressure drop with the use of Equation 4.1.

Figure 6.1 and Figure 6.2 summarise the results from the stainless steel (SS) and acrylic sections respectively; the results from the epoxy coated pipe have been plotted together with those from the SS. In the legends, the type of oil used as a test fluid is mentioned as well, since it was found that in certain cases, (e.g. *MARCOL™ 52* in the epoxy coated pipe at high Reynolds numbers and *EXXSOL™ D80* in the acrylic pipe), different oils could yield friction factors lower than those predicted by the Blasius equation. The more viscous oils (both *EXXSOL™ D140* and *MARCOL™ 52*) give results close to Blasius predictions for both, SS and acrylic, pipes.

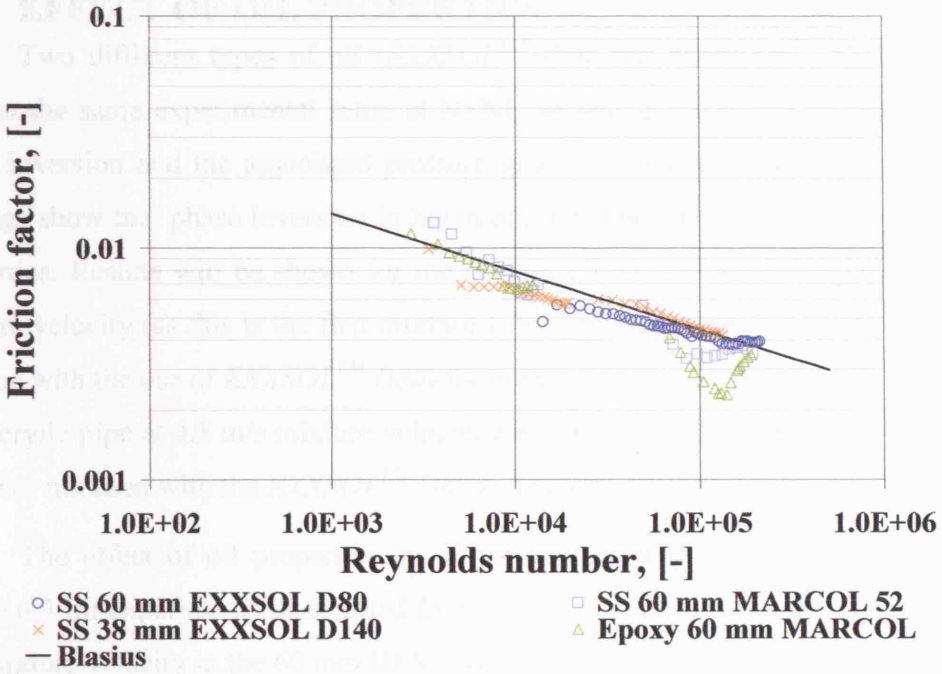

Figure 6.1 Friction factor vs. Reynolds number for single phase (oil and water) flows in the stainless steel and the epoxy coated test sections.

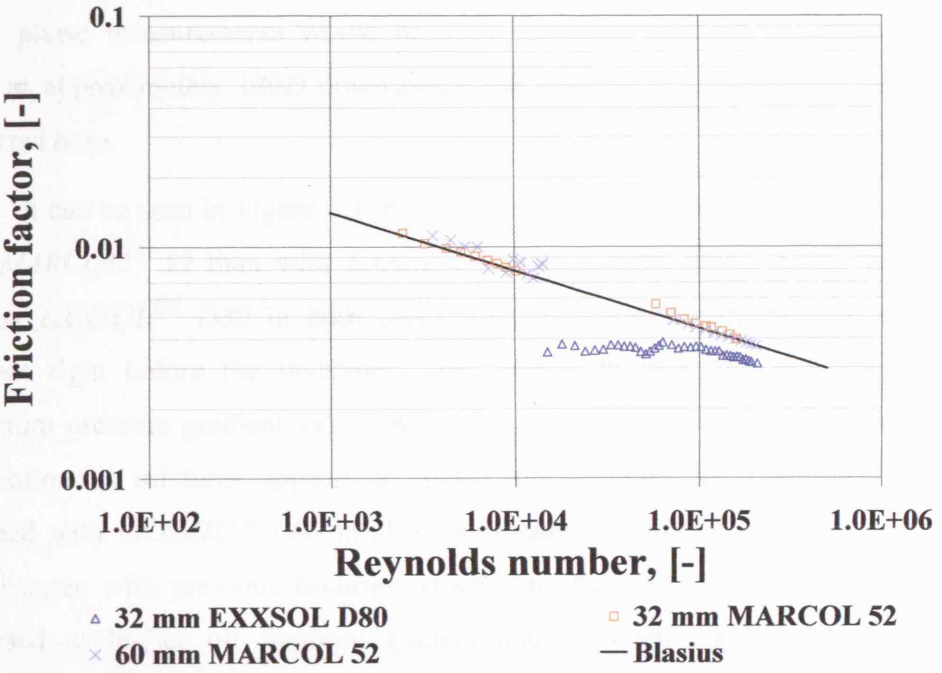

Figure 6.2 Friction factor vs. Reynolds number for single phase (oil and water) flows in the acrylic test sections.

6.3 EFFECT OF OIL PROPERTIES

Two different types of oil (*EXXSOL™ D80* and *MARCOL™ 52*) have been used in the same experimental setup at NTNU so that the effect of oil properties on phase inversion and the associated pressure gradient could be studied. Experimental findings show that phase inversion in horizontal pipelines depends strongly on the oil properties. Results will be shown for the 60 mm ID SS and acrylic pipes at 4.0 m/s mixture velocity (as this is the first mixture velocity where inversion is obvious in the SS pipe with the use of *EXXSOL™ D80*) for both Type I and II experiments and the 32 mm acrylic pipe at 4.5 m/s mixture velocity for Type I experiments; the epoxy coated pipe was not used with the *EXXSOL™ D80* and results are therefore not included.

The effect of oil properties on dimensionless pressure gradient is shown in Figure 6.3 for experiments that started from water continuous mixtures (Type II) at 4.0 m/s mixture velocity in the 60 mm ID SS and acrylic pipes. Pressure gradient has been made dimensionless by dividing the two-phase pressure gradient in each pipe with the respective experimental single phase oil value at the same mixture velocity. When the experimental value could not be directly measured, an extrapolated value based on single phase measurements would be used. Pressure gradient measurements were taken at approximately $180D$ downstream the inlet in all experimental test sections presented here.

It can be seen in Figure 6.3 that dimensionless pressure gradient is much lower with *MARCOL™ 52* than with *EXXSOL™ D80* in both pipes. Also, with the less viscous *EXXSOL™ D80* in both pipes there is a significant increase in pressure gradient right before the inversion point, which in this case coincides with the maximum pressure gradient value. When *MARCOL™ 52* is used, phase inversion to oil continuous mixtures appears at higher oil fractions in comparison to results obtained with *EXXSOL™ D80* in all experimental conditions and test sections. This would agree with previous findings which state that more viscous oils can remain dispersed at higher oil fractions (Selker and Sleicher, 1965, in stirred vessels; Arirachakaran *et al.*, 1989, in pipelines). Also with *MARCOL™ 52* inversion is preceded by a decrease in pressure gradient, followed by an increase for a Type II experiment. In this case though, inversion point is not reached with the use of

MARCOL™ 52 at 4.0 m/s mixture velocity (due to restrictions in the experimental facility).

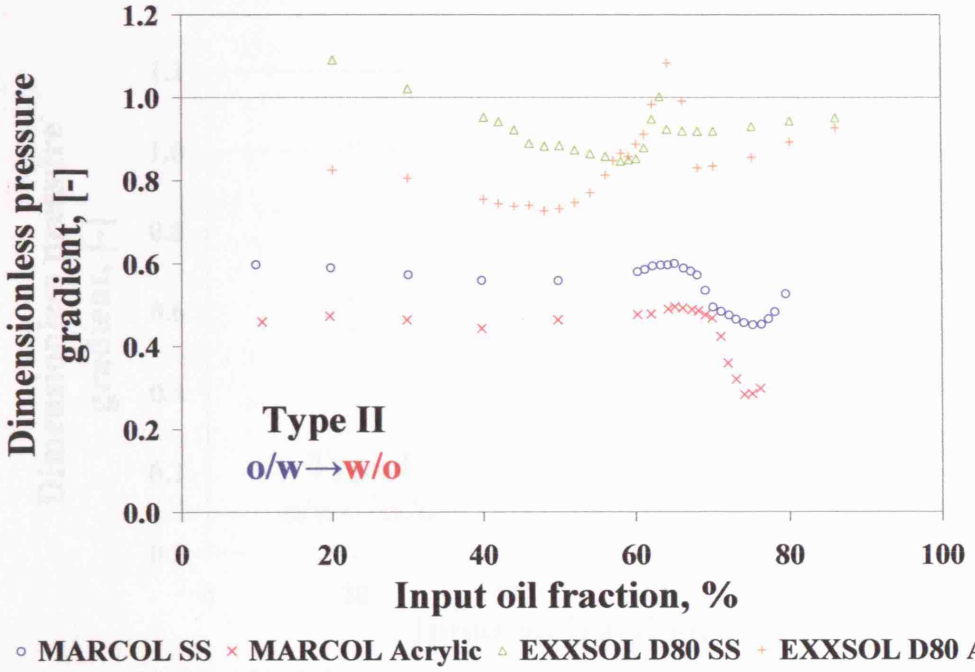

Figure 6.3 Effect of oil properties for Type II experiments at 4.0 m/s mixture velocity for the 60 mm ID SS and acrylic pipes (NTNU).

Results for experiments that started from oil continuous mixtures (Type I) can be seen in Figure 6.4. Again, dimensionless pressure gradient is much lower with *MARCOL™ 52* than with *EXXSOL™ D80*, apart from results obtained in the oil continuous region where results are comparable in all pipes. With *EXXSOL™ D80* dimensionless pressure gradient in both pipes is gradually increasing towards the phase inversion point which is also the point of the maximum pressure gradient. With *MARCOL™ 52* in the acrylic pipe dimensionless pressure gradient shows increased values before inversion and reaches a minimum at the point after inversion (water continuous region). Similar behaviour is seen for the SS pipe with *MARCOL™ 52*, where the minimum in dimensionless pressure gradient is again seen after inversion to water continuous mixtures. Comparing Figure 6.3 with Figure 6.4, it can also be seen

that there is an ambivalent range for *EXXSOL™ D80* (phase inversion points for Type I and II experiments do not coincide), but not for *MARCOL™ 52*. This is discussed further in Section 6.5.

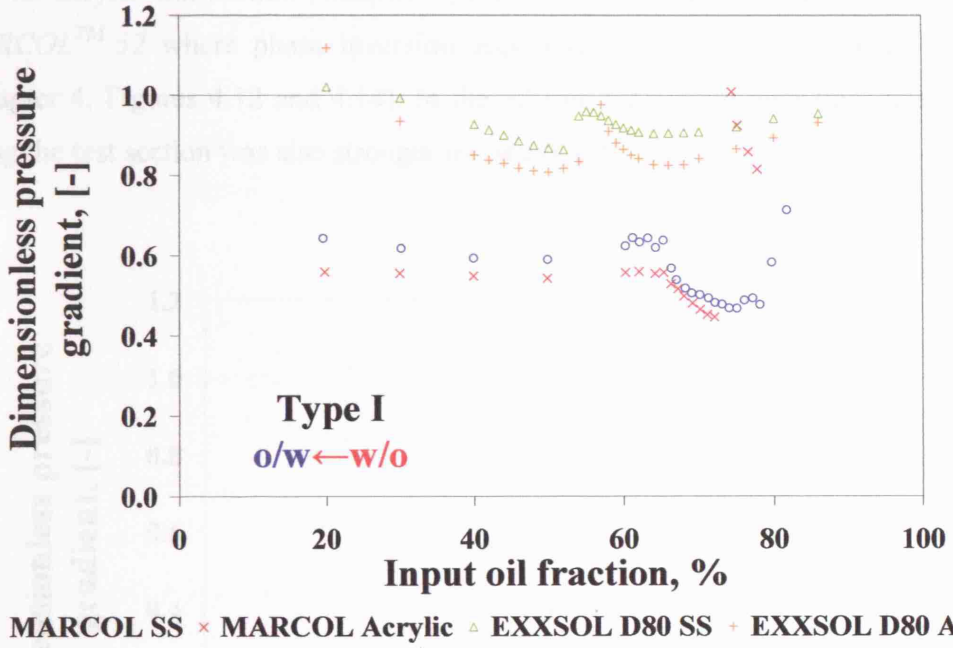

Figure 6.4 Effect of oil properties for Type I experiments at 4.0 m/s mixture velocity for the 60 mm ID SS and acrylic pipes (NTNU).

In Figure 6.5 dimensionless pressure gradient is shown for both oils for experiments that started from oil continuous mixtures (Type I) at 4.5 m/s mixture velocity in the 32 mm ID acrylic pipe. Measurements in this test sections were taken at approximately 320*D* downstream the test section inlet.

In the oil continuous region and especially at the higher oil fractions dimensionless pressure gradient is similar for the two oil types. At lower oil fractions dimensionless pressure gradient for *EXXSOL™ D80* increases and inversion happens at the maximum in the graph. In the case of *MARCOL™ 52*, dimensionless pressure gradient decreases just after inversion and reaches a minimum. The difference in

dimensionless pressure gradient between the two oils is larger in the water continuous region, where it is higher for *EXXSOL™ D80* than for *MARCOL™ 52*.

It can, also, be concluded from all experiments conducted that with the use of *EXXSOL™ D80* inversion was simultaneously happening in the whole length of the 60 mm ID acrylic test section (Chapter 4, Figure 4.9), while this was not the case for *MARCOL™ 52* where phase inversion appeared at different times along the pipe (Chapter 4, Figures 4.12 and 4.14). In the 32 mm ID acrylic pipe flow stratification along the test section was also stronger for *MARCOL™ 52*.

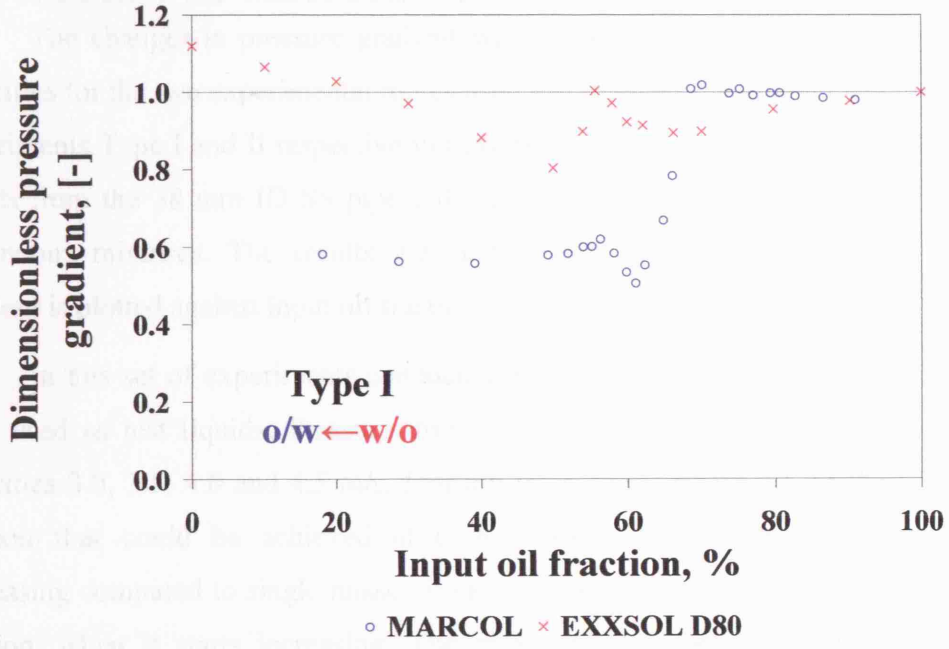

Figure 6.5 Effect of the oil properties for Type I experiments at 4.5 m/s mixture velocity in the 32 mm ID acrylic pipe (NTNU).

It can generally be concluded that the more viscous oils tend indeed to be more dispersed, as the inversion point was shifted to higher input oil fraction with increasing oil viscosity in all test sections used.

The most important difference appears to be that inversion with *EXXSOL™ D80* is preceded by a prominent peak in pressure gradient that is not seen with the use

of *MARCOL™ 52*. This can be explained as follows: at the same flowrate, the flow regime for the low-viscosity oil is generally in turbulence, while for the more viscous oil (*MARCOL™ 52* is 6.5 times more viscous than *EXXSOL™ D80*) the Reynolds number is expected to be lower, especially in the oil continuous region, but also slightly higher in the water continuous region. The higher turbulence/mixture velocity leads to a dispersion of finer droplets in the low viscosity oil, thus to a finer dispersion, whose viscosity appear to follow the description of emulsion behaviour. The oil viscosity is thus, the parameter affecting strongly the inversion point and the associated pressure gradient.

6.4 EFFECT OF MIXTURE VELOCITY

The changes in pressure gradient with input oil fraction at different mixture velocities for the two experimental routes used (oil to water continuous and vice versa-experiments Type I and II respectively) have been investigated in all test sections and results from the 38 mm ID SS pipe will be shown for experiments starting with oil continuous mixtures. The results are summarized in Figure 6.6, where pressure gradient is plotted against input oil fraction.

In this set of experiments conducted at UCL, tap water and *EXXSOL™ D140* were used as test liquids. Pressure drop measurements were performed at mixture velocities 3.0, 3.5, 4.0 and 4.5 m/s. Starting from single phase oil, or the highest oil fraction that could be achieved at each mixture velocity, pressure gradient is decreasing compared to single phase oil experimental value, until about 73% input oil fraction, when it starts increasing. The maximum pressure gradient is reached at differing oil fractions depending on mixture velocity; it is seen at 72% and 67% input oil fraction at 4.5 m/s and 3.0 m/s respectively. This maximum has been identified with the use of conductivity probes (as described in Section 4.5, Figures 4.16 and 4.17) to coincide with the occurrence of phase inversion; it actually appears at the oil volume fractions just after inversion to water continuous mixtures in the whole cross sectional area. After this, pressure gradient decreases to lower values as the fraction of water in the mixture is increasing. When the oil fraction is decreased to less than 60%, pressure gradient starts increasing again towards the single phase water value. The

peak in pressure gradient at inversion is less discernable and covers a broader range of input oil fractions at lower mixture velocities and more specifically at 3.0 m/s, while it becomes sharper with increasing mixture velocity.

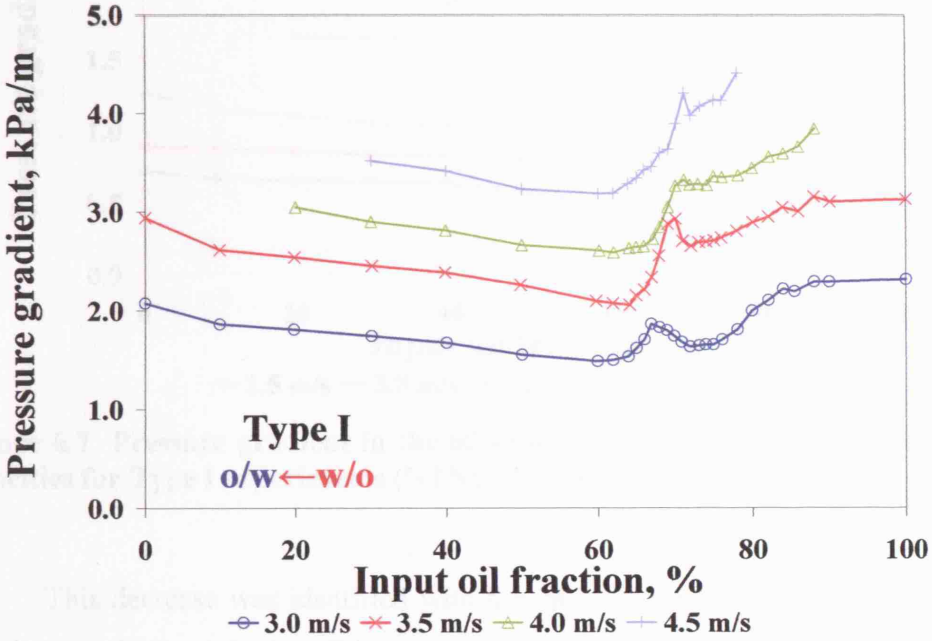

Figure 6.6 Pressure gradient in the 38 mm ID SS pipe at different mixture velocities for Type I experiments (UCL, *EXXSOL™ D140*).

In Figure 6.7 similar data obtained at NTNU in the 60 mm ID acrylic test section can be seen; *MARCOL™ 52* and tap water were used as test fluids.

Starting from high oil fractions, or single phase oil at the lower mixture velocities, pressure gradient is almost constant, or it increases slightly at higher velocities with decreasing oil fraction (decrease seen between 100 and 80% input oil fraction). At higher velocities, 3.5 m/s and especially 4.0 m/s, pressure gradient starts increasing at approximately 78% showing a maximum around 75% input oil fraction. A similar increase is not seen at lower velocities. A sharp decrease in pressure gradient is seen at approximately 75% input oil fraction for the higher mixture velocities and at slightly lower fraction (at about 73% oil) for the lower mixture velocities.

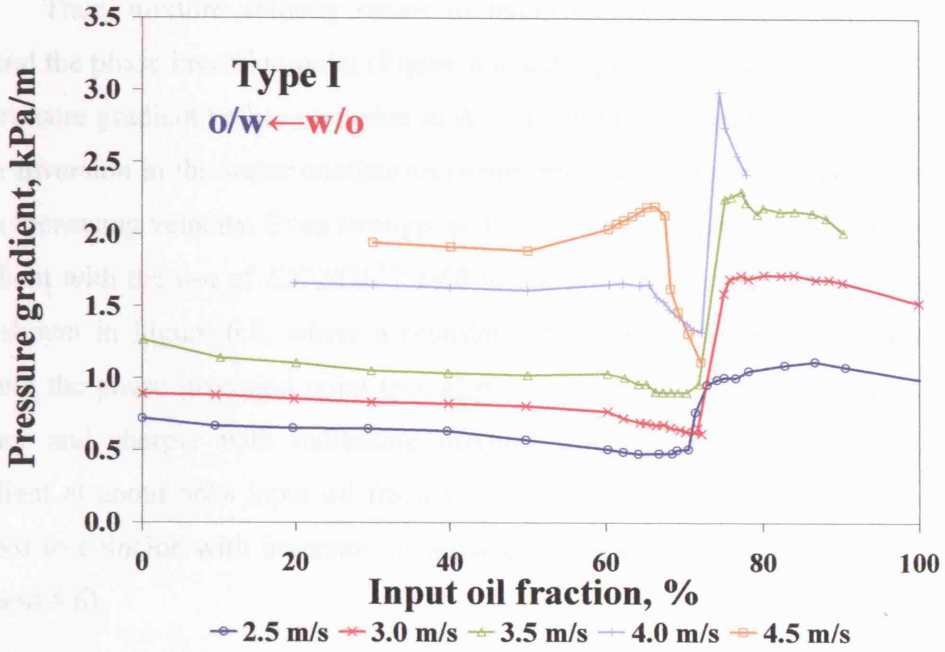

Figure 6.7 Pressure gradient in the 60 mm ID acrylic pipe at different mixture velocities for Type I experiments (NTNU, *MARCOL™ 52*).

This decrease was identified with the use of the ring probes to coincide with the change of the continuity of the system and inversion to water continuous mixtures. At 4.5 m/s mixture velocity this maximum and then decrease in pressure gradient are not observed, as the first experimental condition that could be achieved is 72% input oil fraction, which is after the inversion point (the mixture is already water continuous or there is at least some water wetting the pipe at the beginning of the experiment as identified with the use of the ring probes). After that decrease, pressure gradient increases again slightly at lower mixture velocities, or more significantly at the higher ones where it reaches a new maximum. This is identified to coincide with a further increase in the conductivity signal (Section 4.2, Figures 4.3 and 4.4). As the oil fraction further decreases, the pressure gradient values change only slightly towards the single phase water value. The new maximum seen at 4.0 m/s but mainly at 4.5 m/s mixture velocity at 66% and 67% input oil fraction respectively coincides with a significant increase in the conductivity signal obtained from the ring probes (Section 4.2, Figures 4.3 and 4.4).

Thus, mixture velocity seems to intensify the changes in pressure gradient around the phase inversion point (Figure 6.6 and Figure 6.7); both the relative increase of pressure gradient before inversion in the oil continuous region and the decrease just after inversion in the water continuous region become higher and sharper respectively with increasing velocity. Even stronger is the effect of mixture velocity on the pressure gradient with the use of *EXXSOL™ D80* in the same 60 mm ID acrylic pipe. Results are shown in Figure 6.8, where a prominent peak in pressure gradient can be seen around the phase inversion point (see also Ioannou *et al.*, 2005). This peak becomes higher and sharper with increasing mixture velocity. The maximum in pressure gradient at about 56% input oil fraction has been identified with the use of the ring probes to coincide with inversion to water continuous mixtures (Section 4.2, Figures 4.5 and 4.6).

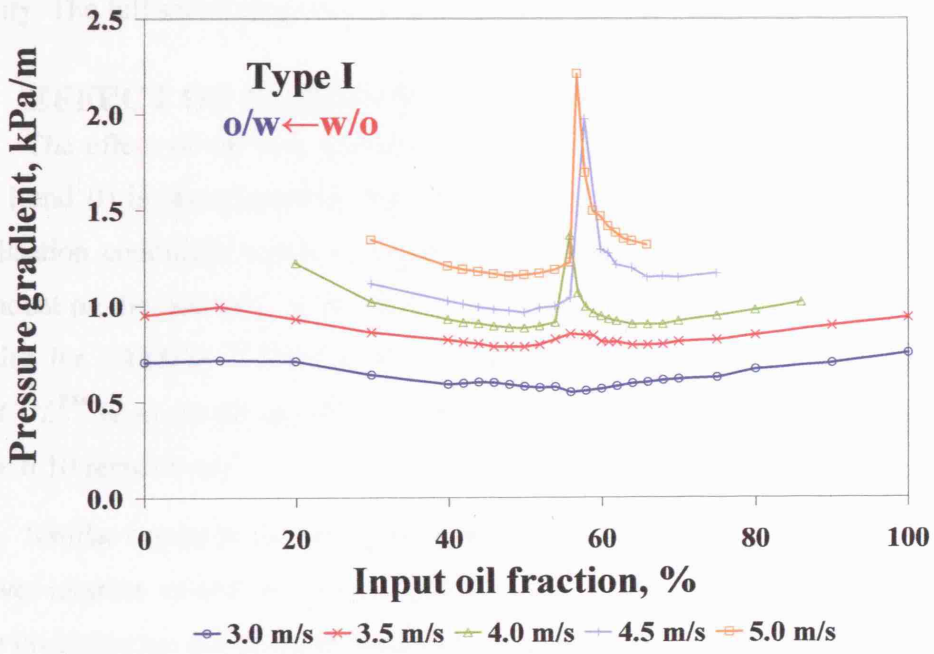

Figure 6.8 Pressure gradient in the 60 mm ID acrylic pipe at different mixture velocities for Type I experiments (NTNU, *EXXSOL™ D80*).

Increased mixture velocity is expected to result in more abrupt results: viscosity of emulsions and thus pressure gradient is very much dependent on drop size

and increases with decreasing drop size (Pal, 1996; Chen *et al.*, 2005). It is expected and was experimentally found (Section 5.4) that drop size decreases with increasing mixture velocity. The more dramatic changes in pressure gradient with phase inversion at increased velocities may thus be related to the smaller mean dispersed droplet diameters encountered.

Interestingly, the exact inversion point does not seem to depend strongly on mixture velocity (with the use of all types of oil). There was however, a slight tendency for inversion to occur at higher input oil fractions with increasing mixture velocity (for both Type I and II experiments) with the use of *EXXSOL™ D140* in the 38 mm SS pipe and *MARCOL™ 52* in all test sections.

Similar conclusions can be drawn for all test sections used and with all different oil types, as it was always found that more prominent effects on pressure gradient were seen around the area of phase inversion with increasing mixture velocity. The full set of experimental data can be found in Appendix C.

6.5 EFFECT OF DISPERSION INITIALISATION CONDITION

The effect of the two different routes in approaching inversion (experiments Type I and II) is investigated in this section. This will reveal whether the dispersion initialisation conditions result in a different inversion point or whether inversion is dependent on the "history" of the flow in the pipe. Results at 4.0 and 4.5 m/s mixture velocity for *EXXSOL™ D80* at the 60 mm ID SS pipe and 3.5 and 4.0 m/s for *MARCOL™ 52* at the 60 mm ID epoxy coated pipe will be shown in Figure 6.9 and Figure 6.10 respectively.

Similar results to the ones presented here have been obtained for both oil types at lower mixture velocities (where, however, the effects on pressure gradient around phase inversion are not so prominent) and at higher ones (where, however, the curves obtained were not complete due to limitations of the experimental set up and inversion was sometimes not reached or had already occurred at the start of the experiment as seen in Figure 6.7 at 4.5 m/s).

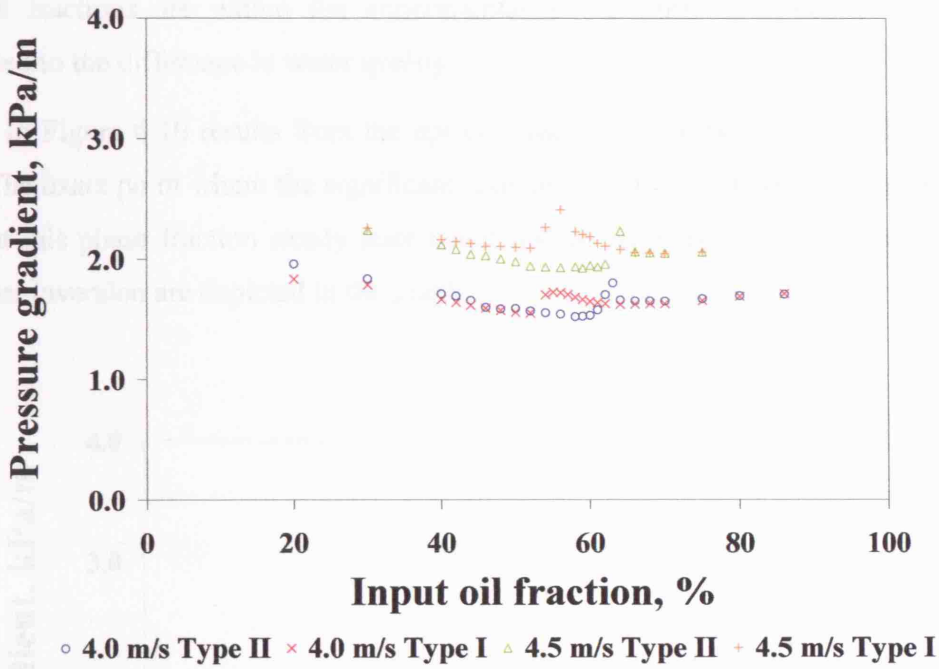

Figure 6.9 Pressure gradient in the 60 mm ID SS pipe for Type I (o/w←w/o) and II (o/w→w/o) experiments at 4.0 and 4.5 m/s mixture velocities (NTNU, *EXXSOL™ D80*).

Similar behaviour of pressure gradient was observed in the 60 mm ID SS pipe for both types of experiments (Figure 6.9). When starting from low oil fractions both at 4.0 and 4.5 m/s mixture velocity and increasing the oil fraction, pressure gradient decreases slightly and then it increases. A maximum occurs just before phase inversion. With further increase in the oil fraction pressure gradient decreases again initially and then remains almost constant or slightly increases approaching the single phase oil value. These peaks in pressure gradient around phase inversion appear at higher oil fractions for Type II experiments that started from water continuous mixtures (open symbols in Figure 6.9) than for Type I experiments. It can be said that the initial continuous phase tends to preserve its continuity longer resulting in a hysteresis in the appearance of inversion between the two experiment types. This has also been observed in literature for stirred vessels and has been attributed to the differences in behaviour of oil and water dispersions. Away from the inversion point pressure gradient was the same for both initial conditions used. Small discrepancies at

low oil fractions are within the experimental error, while they could be partly attributed to the difference in water quality.

In Figure 6.10 results from the epoxy coated SS pipe with 60 mm ID can be seen. The exact point where the significant change in conductivity occurs was left out since at this phase fraction steady state could not be achieved: instead points before and after inversion are depicted in the graph.

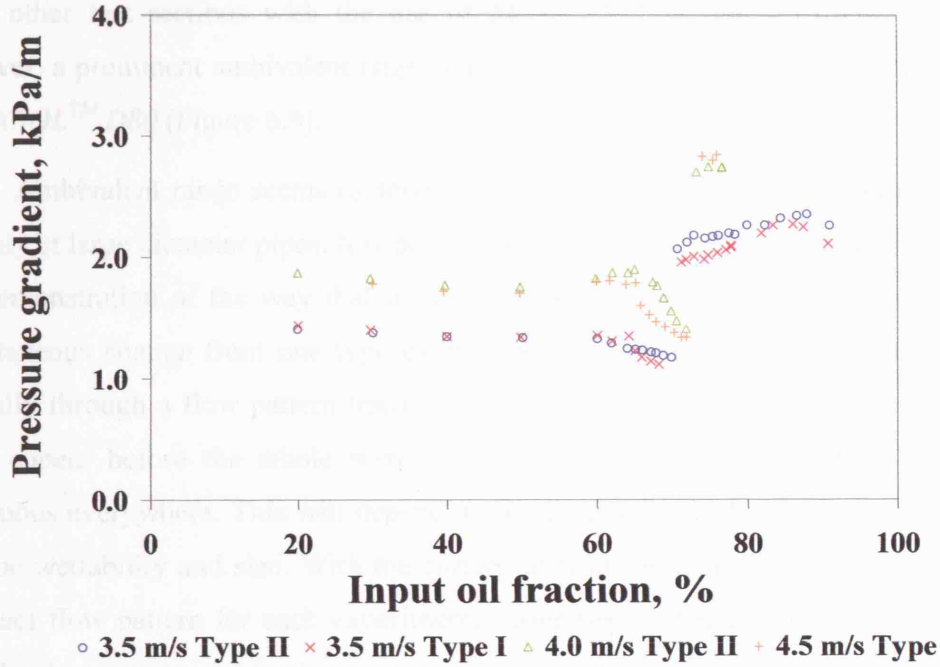

Figure 6.10 Pressure gradient in the 60 mm ID epoxy coated SS pipe for Type I (o/w←w/o) and II (o/w→w/o) experiments at 3.5 and 4.0 m/s mixture velocities (NTNU, *MARCOL*^{TM} *52*).

A different behaviour is seen for the epoxy coated SS pipe as compared to the SS pipe. Starting from water continuous mixtures, the pressure gradient at both mixture velocities decreases slightly, then at approximately 60% input oil fraction at 4.0 m/s mixture velocity it increases slightly but then decreases significantly soon after (63% input oil fraction) reaching a minimum at 72% oil fraction (at 3.5 m/s this happens at 70% input oil fraction). This decrease at 63% coincides with changes in the

conductivity signal from the ring probes that may imply partial change in phase continuity. Inversion to totally oil continuous mixtures results in a sudden and significant increase in pressure drop after 63% at 4.0 m/s mixture velocity or 70% at 3.5 m/s mixture velocity since the more viscous phase is now the continuous phase. Type I experiments yield the same trend in pressure gradient (differences are within experimental error) and the same inversion points. Important changes in pressure gradient are now seen at 73% (sudden decrease) and 63% (increase) input oil fraction. Negligible ambivalent range is thus observed in the 60 mm epoxy coated SS pipe, and in all other test sections with the use of *MARCOL™ 52* and *EXXSOL ™ D140.* However, a prominent ambivalent range was seen in the 60 mm ID pipes with the use of *EXXSOL™ D80* (Figure 6.9).

Ambivalent range seems to appear therefore only with the lower viscosity oil and only at large diameter pipes. It is possible that this appearance of ambivalent range is a demonstration of the way that inversion happens; whether for example it is an instantaneous change from one type of dispersion to another or whether it happens gradually through a flow pattern transition, where continuous layers of the dispersed phase appear before the whole mixture inverts and the dispersed phase becomes continuous everywhere. This will depend on the properties of the fluids as well as on the pipe wettability and size. With the current instrumentation, it is difficult to know the exact flow pattern for each experimental condition, especially for the systems at NTNU, where only average phase conductivity in a pipe cross section was measured. Thus, final conclusions on the origin of the ambivalent range and the effect of fluid and flow parameters on it cannot be drawn.

It is proposed that the existence of ambivalent range with the less viscous oil is related to the mechanism of coalescence and the fact that secondary dispersions are believed to exist at the region of inversion and right before the occurrence of the phenomenon in the whole cross section. In an oil continuous environment, the water droplets with have a greater propensity to form secondary dispersion with decreasing oil viscosity; this is attributed to the fact that colliding droplets of water will require less draining time for coalescence to occur in a less viscous continuous environment

($t_d \propto \mu_c$, Coulaloglou and Tavlarides, 1977; Davies, 1992; Dreher *et al.*, 1999) and thus, lead to higher coalescence efficiency. More effective collisions potentially mean that a larger amount of the continuous phase might be entrapped within the dispersed droplets, altering the effective dispersed phase fraction, something that might shift the inversion point with the use of *EXXSOL™ D80*.

Furthermore, the limits of the ambivalent range have been found to depend on the interfacial tension of the two immiscible liquids. More specifically, the lower the interfacial tension within the two liquids, the wider the ambivalent range (Luhning and Sawistowski, 1972; Clarke and Sawistowski, 1978; Norato *et al.*, 1998). This would indicate a broader ambivalent range for *EXXSOL™ D80* (lower interfacial tension) as compared to the other two types of oil studied which had almost negligible ambivalent range (almost the same interfacial tension with water). This finding was attributed to the fact that lower interfacial tension will promote the formation of new surfaces. Thus, a given dispersion morphology at constant velocity will remain stable over a wider range of dispersed phase volume fractions as the interfacial tension is decreased.

6.6 EFFECT OF PIPE DIAMETER

Two acrylic pipes with different diameters have been used with *EXXSOL™ D80* and *MARCOL™ 52*, so that the effect of pipe diameter on inversion can be examined. Results on pressure gradient at 4.0 m/s mixture velocity for Type I experiments with *MARCOL™ 52* are plotted in Figure 6.11. Pressure gradient has been made dimensionless by dividing the two-phase pressure gradient in each pipe with the respective experimental single phase oil value at the same mixture velocity. Measurements were taken at 175*D* and at 328*D* from the inlet in the large and in the small acrylic pipe respectively.

Starting from very high oil fractions in the large acrylic pipe, dimensionless pressure gradient appears to be increasing and reaches a maximum before it sharply decreases at 75% oil fraction; this decrease has been related to the formation of a water layer at the bottom of the pipe. In the small acrylic pipe, pressure gradient only slightly increases with decreasing oil fraction up to about 63% oil fraction where it sharply decreases as well. This decrease coincides with the change of the signal

obtained from the ring probes from zero (oil continuous flow) to positive (water continuous flow, or some water in contact with the ring probes).

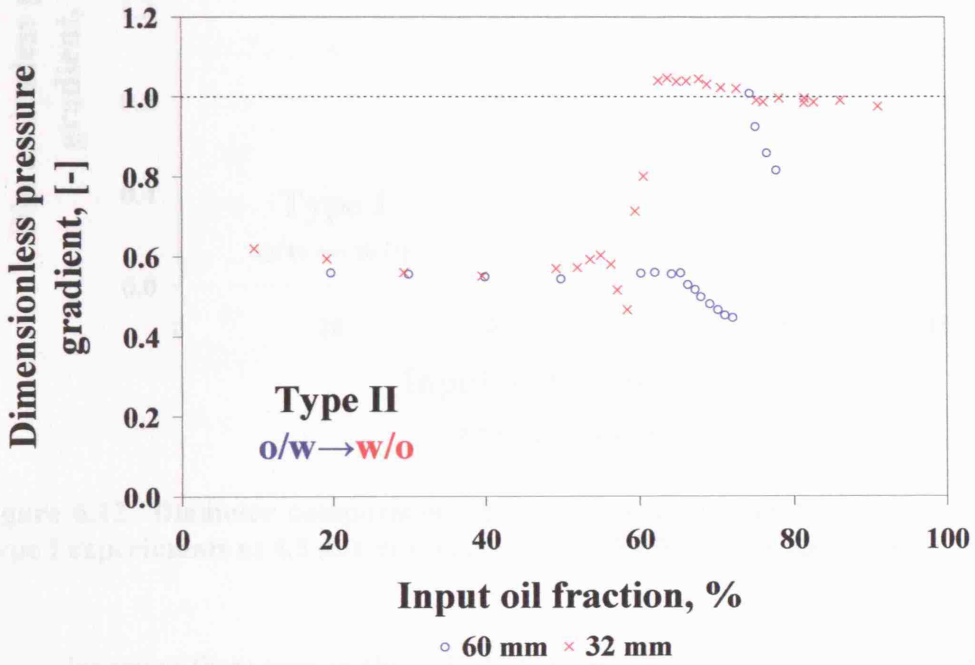

Figure 6.11 Diameter comparisons for the 32 and 60 mm ID acrylic pipes for Type II experiments at 4.0 m/s mixture velocity (NTNU, *MARCOL™ 52*).

In the 60 mm pipe inversion or wetting of water on the pipe wall seems to be happening at higher oil fraction (75%) than in the 32 mm pipe (63% input oil fraction) showing a rather delayed inversion in the latter case. Thus, the diameter of the pipe has an effect on the resulted pressure gradient and the phase inversion point. After inversion in both pipes dimensionless pressure gradient forms small peaks with decreasing oil fraction, while after 50% input oil fraction it is almost the same, showing small effect of diameter in the water continuous region.

Results from both pipes were also obtained with *EXXSOL™ D80* which can be seen in Figure 6.12 for Type I experiments at 4.5 m/s mixture velocity. Pressure gradient has been made dimensionless as above.

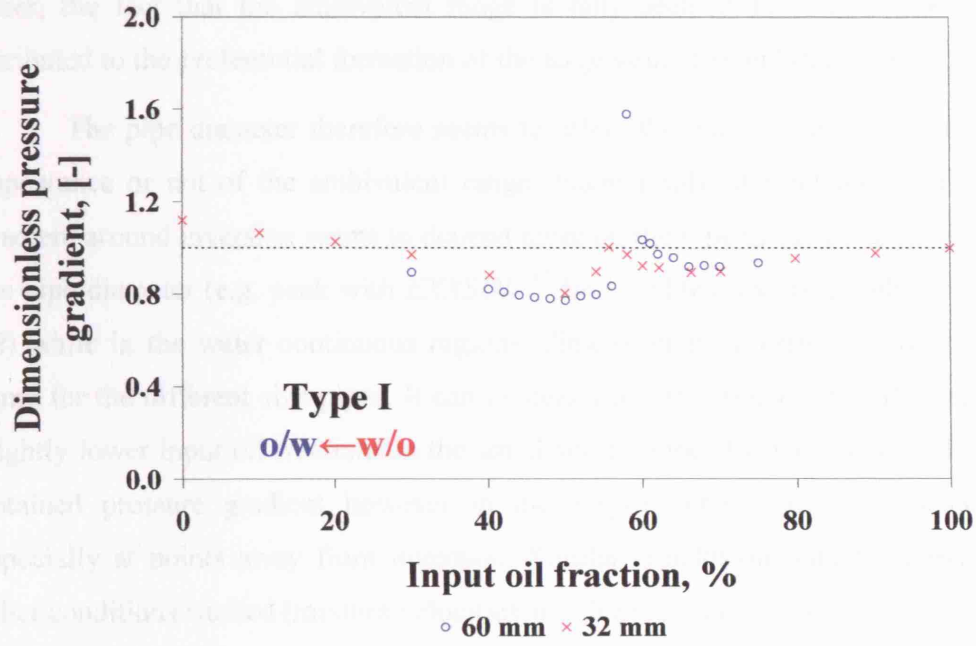

Figure 6.12 Diameter comparisons for the 32 and 60 mm ID acrylic pipes for Type I experiments at 4.5 m/s mixture velocity (NTNU, *EXXSOL™ D80*).

Inversion (here seen at about 56-58% input oil fractions in both pipes, resulted in a peak around the inversion point that was much sharper and extended over a smaller range of oil percentages in the 60 mm ID pipe than in the 32 mm ID pipe. The trends of pressure gradient are again the same. However, ambivalent range appeared in the large pipe but not in the small one. This means that in Type II experiments the phase inversion point is not the same in the two pipes. No ambivalent range was seen with the smaller diameter acrylic pipe (32 mm ID) with any of the oils used, leading to the conclusion that wettability is insignificant in smaller diameter pipes, where the narrow or negligible ambivalent range suggests that rewetting of the pipes is relatively fast. For the bigger pipes (60 mm ID) the effect of surface wettability is generally rather small in most cases, but can be significant depending on the type of oil used as explained above.

Furthermore, considering the theory that the ambivalent range is indeed related to the formation of secondary dispersions and large formations of one phase into the

other, the fact that the ambivalent range is only seen in the larger pipes can be attributed to the preferential formation of the large structures in larger pipes.

The pipe diameter therefore seems to affect the phase inversion point and the appearance or not of the ambivalent range. Interestingly, the behaviour of pressure gradient around inversion seems to depend more on the type of the oil used rather than the pipe diameter (e.g. peak with *EXXSOL™ D80*, sudden decrease with *MARCOL™ 52*) while in the water continuous regions, dimensionless pressure gradients are the same for the different size pipes. It can be concluded that phase inversion happens at slightly lower input oil fractions in the small acrylic pipe (Ioannou *et al.*, 2005). The obtained pressure gradient however in the acrylic pipes shows the same trend, especially at points away from inversion. Similar conclusions can be drawn for all other conditions studied (mixture velocities and dispersion initialisation condition).

6.7 EFFECT OF PIPE MATERIAL

The effect of pipe material on inversion and associated pressure gradient was investigated. Three pipes with the same internal diameter (60 mm) made from acrylic, SS and epoxy coated SS respectively were used with two different oils *EXXSOL™ D80* and *MARCOL™ 52*.

Experiments with *EXXSOL™ D80* were carried out in the acrylic and SS pipes. In general, measurements in the acrylic pipe for both types of experiments gave similar trends in pressure gradient to those in the SS pipe. Peaks in pressure gradient associated with phase inversion appeared at the higher mixture velocities (4.0, 4.5 and 5.0 m/s), while a difference on the phase inversion point between the two initial conditions (ambivalent range) was also observed in both pipes.

The pressure gradients for *EXXSOL™ D80* (non-dimensionalised as mentioned in Section 6.3), are shown in Figure 6.13 for both test sections and for experiments that started from oil continuous mixtures (Type I) at 4.5 m/s mixture velocity. Generally pressure gradient in the acrylic pipe was lower than that in the steel pipe away from the inversion point (especially in the water continuous region) for the same mixture velocity and initial conditions. Furthermore, in the acrylic pipe the increase in

pressure gradient was much higher and sharper and the peak around inversion was seen from lower mixture velocities than in the steel pipe.

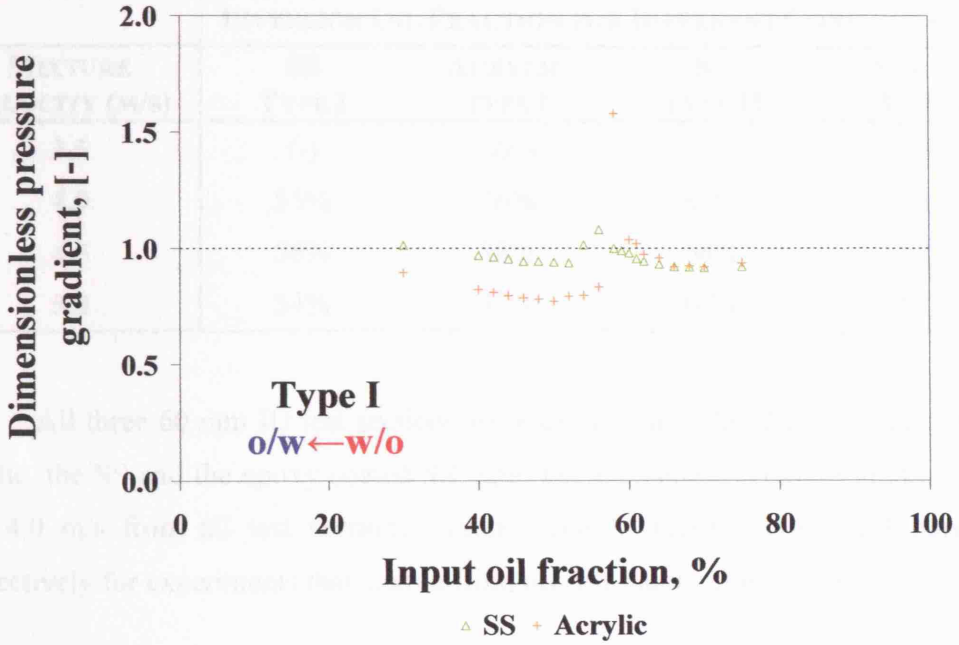

Figure 6.13 Comparison of non-dimensional pressure gradient in the SS and acrylic pipe with 60 mm ID at mixture velocity 4.5 m/s starting with oil continuous mixtures (NTNU, *EXXSOL™ D80*).

Table 6.1 summarises the points where inversion was seen in both pipes used and for both dispersion initialisation conditions. No peak was seen in the SS pipe at 3.5 m/s, while it was already present in the acrylic pipe at this velocity. For both types of experiments phase inversion happened at slightly lower dispersed phase fractions in the acrylic that in the steel pipe, but the differences are negligible.

These experimental findings agree with results from Pettersen *et al.* (2001) who used the same test fluids in 10 cm ID PVC and SS pipes and found that inversion was reached in somewhat higher oil fractions in PVC pipes compared to the steel one (their experiments started from oil continuous mixtures).

Table 6.1 Input oil fraction where inversion appeared for the 60 mm ID SS and acrylic pipes and for both initial conditions (Type I and II). Experiments conducted with the use of *EXXSOL™ D80*.

	Inversion Oil Fraction for Different Configurations			
Mixture velocity (m/s)	SS Type I	Acrylic type I	SS Type II	Acrylic Type II
3.5	(-)	56%	(-)	56%
4.0	55%	56%	63%	64%
4.5	56%	58%	64%	65%
5.0	54%	57%	67%	68%

All three 60 mm ID test sections were used with *MARCOL™ 52*; namely, the acrylic, the SS and the epoxy coated SS pipe. Dimensionless pressure gradient at 3.5 and 4.0 m/s from all test sections can be seen in Figure 6.14 and Figure 6.15 respectively for experiments that started from oil continuous flows (Type I).

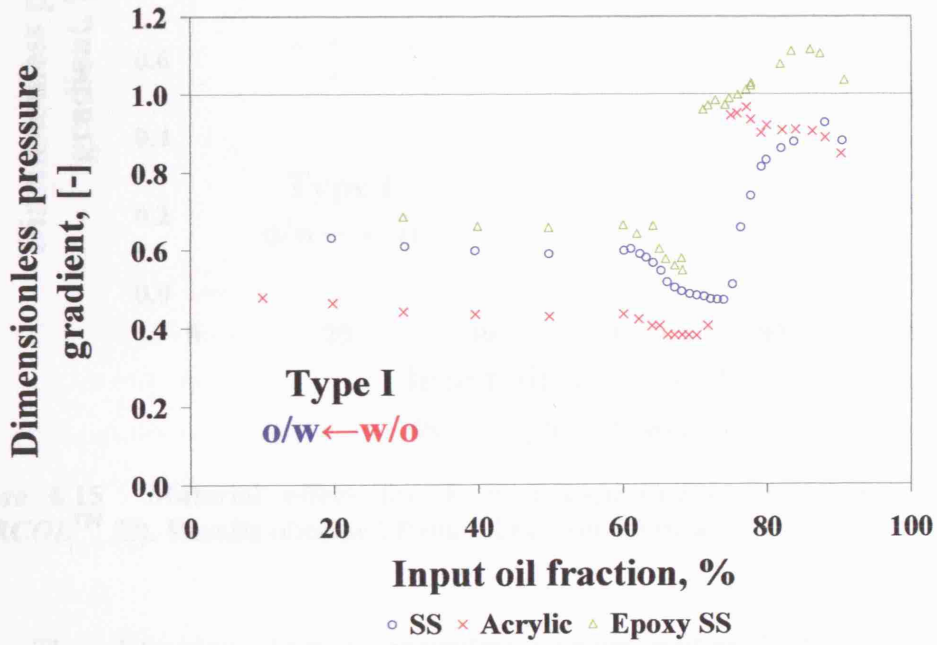

Figure 6.14 Material effect for Type I experiments at 3.5 m/s (NTNU, *MARCOL™ 52*). Results obtained from all 60 mm ID pipes.

In general, it seems that different pipe materials affect the dimensionless pressure gradient with most of the differences seen in the oil continuous region. In all cases, pressure gradient in the acrylic was higher than that in the steel pipe in the oil continuous region for the same mixture velocity and initial conditions until the inversion point was reached. In the water continuous region the situation inverted, with the pressure gradient in the SS pipe being higher than the respective pressure gradient in the acrylic pipe (this is not obvious from Figure 6.14 and Figure 6.15 of dimensionless pressure gradient). The epoxy coated pipe behaves more like the acrylic pipe and appears to be preferentially wetter by oil, since inversion is occurring at lower input oil fractions in this test section, while little drag reduction is seen in the oil continuous region.

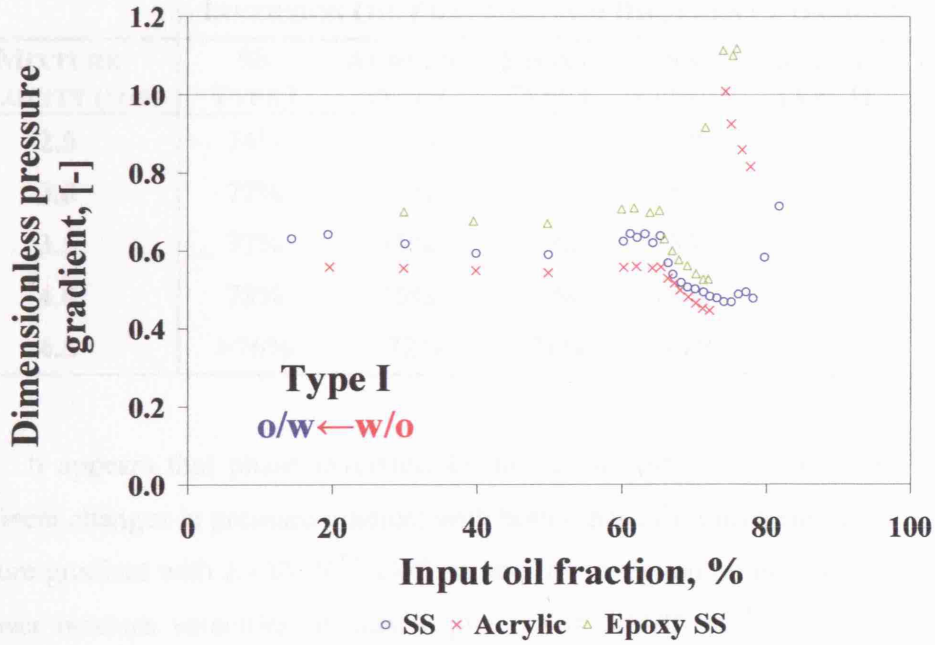

Figure 6.15 Material effect for Type I experiments at 4.0 m/s (NTNU, *MARCOL™ 52*). Results obtained from all 60 mm ID pipes.

The oil fraction where dimensionless pressure gradient is decreasing sharply occurs simultaneously with the change of the signal of the ring probes to positive and denotes the existence of water or water continuous dispersion in the pipe, thus the start of phase inversion from the oil continuous flows. This fraction varies slightly

depending on the pipe material for both mixture velocities seen in Figure 6.14 and Figure 6.15, while the epoxy coated SS pipe seems to result in pressure gradient values closed to the ones obtained by the acrylic pipe. There is also a tendency for inversion to occur at higher input oil fractions in the SS pipe, showing its preference to be wetted by water. Inversion happens at lower input oil fractions for the acrylic and the epoxy coated SS pipes.

Table 6.2 summarises the points where inversions appeared in all test sections used and for all mixture velocities using *MARCOL™ 52*. In practice, this is the point just before the continuity of the system inverts.

Table 6.2 Input oil fraction where inversion appeared for the 60 mm ID pipes and for both initial conditions (Type I and II). Experiments conducted with the use of *MARCOL™ 52*.

	INVERSION OIL FRACTION FOR DIFFERENT CONFIGURATIONS					
MIXTURE VELOCITY (M/S)	SS TYPE I	ACRYLIC TYPE I	EPOXY TYPE I	SS TYPE II	ACRYLIC TYPE II	EPOXY TYPE II
2.5	74%	73%	(-)	72%	74%	(-)
3.0	77%	75%	72%	75%	73%	72%
3.5	77%	75%	71%	75%	74%	70%
4.0	78%	75%	74%	78%	75%	72%
4.5	>76%	>72%	>71%	>74%	>75%	>73%

It appears that phase inversion in the acrylic pipe is accompanied by more prominent changes in pressure gradient with both types of oil investigated. The peak in pressure gradient with *EXXSOL™ D80* around the inversion point is sharper and seen at lower mixture velocities in acrylic pipe. With *MARCOL™ 52*, the decrease in pressure gradient at the point of the change of the continuity of the system is more sudden in the acrylic and epoxy coated SS pipes than in the SS pipe. The same results were obtained for Type II experiments that started from water continuous mixtures. With *MARCOL™ 52*, there is a tendency for water to wet the SS pipe up to higher input oil fractions, while inversion appears at lower velocities for the acrylic than for the SS pipe (consistent to the findings from the *EXXSOL™ D80*). Generally, dimensionless pressure gradient for *EXXSOL™ D80* is higher for the SS than for the

acrylic, while for *MARCOL*^{TM} *52* there is a very strong drag reduction in the oil continuous region in the SS pipe.

6.8 DRAG REDUCTION

The results presented above indicated that the dispersion pressure drop away from inversion is lower than single phase oil or water values, particularly for the more viscous oils. This drag reduction in unstable dispersions has been reported before in the literature (Pal, 1993; Angeli, 1996; Lovick, 2004). Pal (1993) attributed drag reduction to the modification of the turbulence of the carrier fluid due to the continuous breakage and coalescence of the dispersed droplets. Even though turbulence measurements were not done in the current study, it was shown in Chapter 5 that the velocity profiles of both continuous and dispersed phases are affected by the presence (number, size and type) of the dispersed phase droplets. In order to better illustrate the appearance of drag reduction in the systems studied here, the experimental friction factors (*f*) at different Reynolds numbers are shown in Figure 6.16 and are compared against predictions of the Blasius equation (Eq. 4.1). In this section, the Reynolds number of the mixture is calculated by using the Taylor equation for the dispersion viscosity that is given by:

$$\mu_m = \mu_c \left[1 + 2.5\varphi \frac{\mu_d + 0.4\mu_c}{\mu_d + \mu_c} \right] \tag{6.1}$$

where φ is the input dispersed phase fraction was used, μ is the viscosity, while the subscripts *m*, *c*, and *d* stand for mixture, continuous and dispersed phase. A sensitivity analysis was conducted using the obtained *in situ* oil fraction values in the 38 mm ID SS pipe, but negligible difference was seen in the calculated.

Drag reduction seems to depend on the pipe material (Figure 6.16); the acrylic pipe is exhibiting stronger drag reduction in the water continuous region (high Re) and this is decreasing with increasing velocity in the water continuous region (high Re).

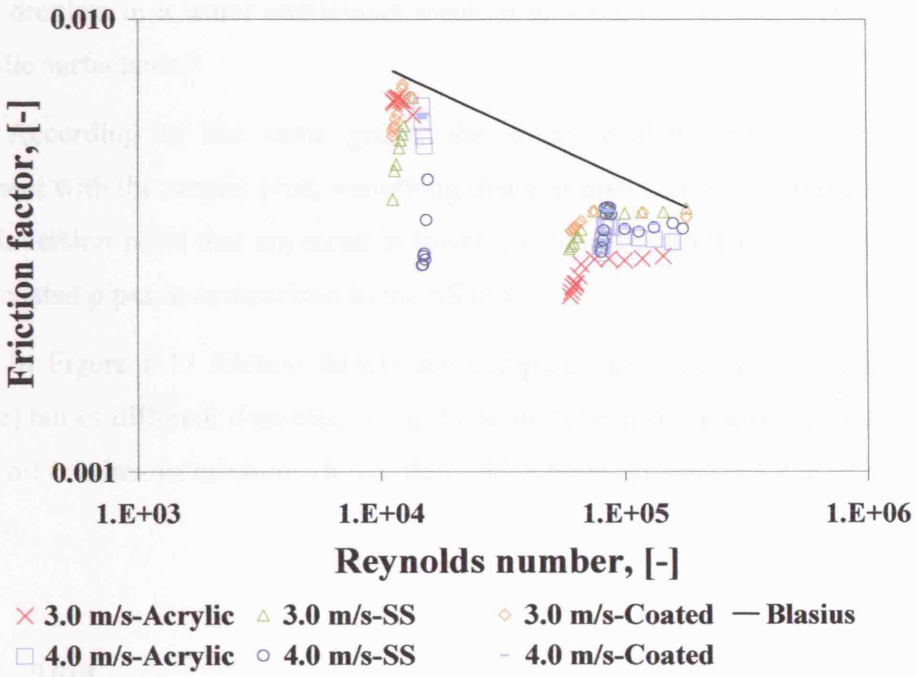

Figure 6.16 Drag reduction behaviour with the use of *MARCOL™ 52* in all 60 mm ID pipes.

On the other hand, the SS pipe is exhibiting stronger drag reduction in the oil than in the water continuous region (low Reynolds numbers) where friction factors are further decreasing with increasing velocity. The SS pipe results agree with the results from Pal (1993) who worked with SS pipes. He found that unstable water-in-oil emulsions exhibit stronger drag reduction; oil-in-water emulsions still exhibit drag reduction but to a lesser degree as also seen in the current findings for SS and epoxy coated pipes.

The fact that drag reduction increases with increasing velocity/turbulence can be explained by the increased number of coalescence and breakup events in the flow, causing suppression of the velocity/turbulence of the carrier fluid. The reduced drag reduction for oil-in-water emulsions might be explained by the hindered coalescence of the dispersed oil droplets in a bipolar continuous medium: resistance to oil drop coalescence can occur due to the electrical double layer around the drops in the water continuous phase. The possible presence of physical surfactants should also be considered in the breakage and coalescence events; these will inhibit coalescence of

the oil droplets in a water continuous medium as well, due to the orientation of the lipophilic surfactants.

According to the same graph, the epoxy coated pipe behaves more in agreement with the acrylic pipe, something that was also seen in the appearance of the phase inversion point that appeared in lower oil input fractions in the acrylic and the epoxy coated pipes in comparison to the SS pipe.

In Figure 6.17 friction factors are compared for pipes of the same material (acrylic) but of different diameter, using the same type of oil as test fluid (*MARCOL™ 52*). In oil continuous mixtures (lower Reynolds numbers) significant drag reduction is not seen.

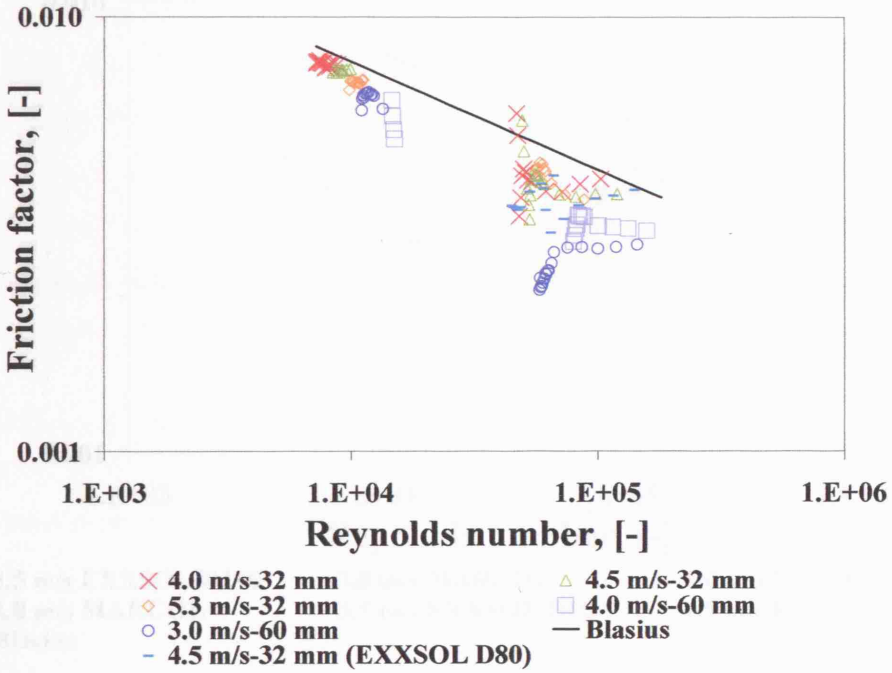

Figure 6.17 Drag reduction behaviour with the use of *MARCOL™ 52* in the 32 and 60 mm ID acrylic pipes.

When comparison is made for the same Reynolds numbers in the water continuous region (high Re) the large acrylic pipe is exhibiting stronger drag reduction, while the small acrylic results in friction factors closer to the smooth pipe

predictions. The pipe diameter appears therefore to be important. This can be explained bearing in mind that for oil-in-water dispersions and for the same Reynolds number, the dispersed phase fraction is higher in the large pipe than in the small acrylic pipe, enhancing coalescence and breakup and suppressing more the continuous phase (water) turbulence in the 60 mm ID pipe.

In Figure 6.18 comparisons of the friction factors between two types of oil (*EXXSOL™ D80* and *MARCOL™ 52*) used in the same pipe (SS 60 mm ID) are made. For *EXXSOL™ D80* in the 60 mm pipe only high Reynolds numbers have been obtained (due to the oil low viscosity), while some results obtained in the 38 mm ID SS pipe are also included.

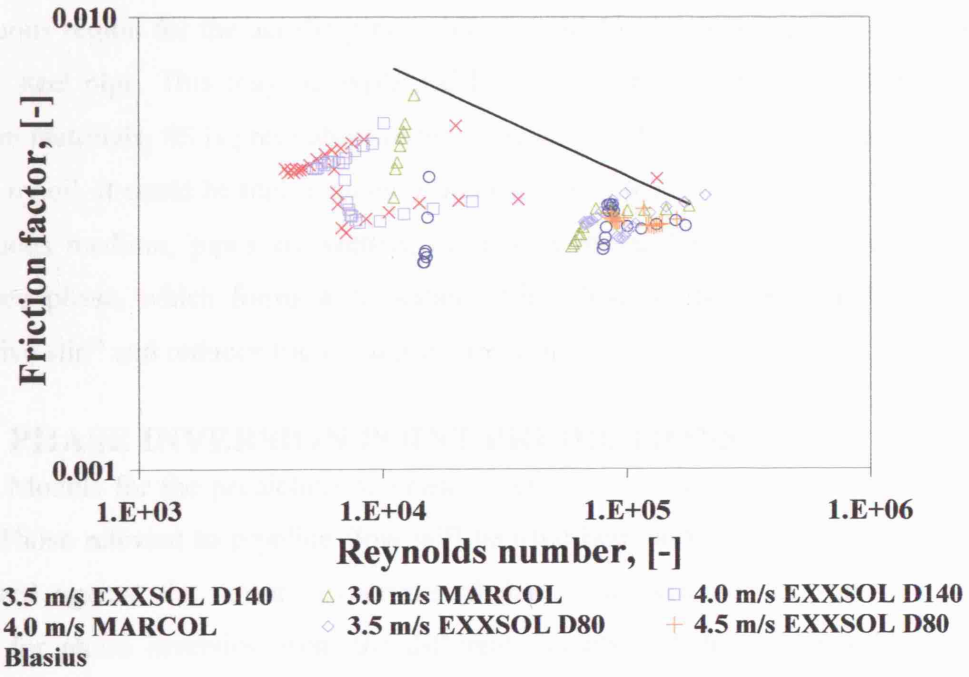

Figure 6.18 Drag reduction behaviour with the use of all types of oil in the SS pipes. *EXXSOL™ D140* is used in the 38 mm ID SS pipe, while *MARCOL™ 52* and *EXXSOL™ D80* are used in the 60 mm ID SS pipe.

At high Reynolds number, the type of oil does not seem to significantly affect drag reduction in the same pipe as friction factors are similar for both types of oil for

the same Reynolds number. This graph might explain as well why there is a big difference in the values obtained in Figure 6.3 and Figure 6.4 where a comparison between different types of oil has been attempted; for same mixture velocity the calculated Reynolds number for *EXXSOL™ D80* is much higher coinciding with the region where the pipe is not exhibiting strong drag reduction, whereas for *MARCOL™ 52* due to the high oil viscosity, Reynolds number is much lower coinciding with the region of strong drag reduction in the stainless steel pipes. Thus, there is stronger drag in the oil continuous region for the SS pipes the more viscous the oil is. A series of results obtained in the 32 mm ID acrylic pipe with the use of *EXXSOL™ D80* has also been included in Figure 6.17 to illustrate that the percent of drag reduction is not oil dependant in the acrylic pipe for high Reynolds numbers either.

The question that still remains is why drag reduction is higher in the water continuous region for the acrylic pipe, while it is higher in the oil continuous region for the steel pipe. This may be explained by bearing in mind the wettability of the different materials; SS is preferably wetted by water, while acrylic pipes are preferably wetted by oil. It could be that in an environment where the less preferable phase is the continuous medium, pipes are wetted, even on a molecular level, by the preferred dispersed phase, which forms a "lubricant" film close to the wall that leads to an "effective slip" and reduces frictional pressure drop.

6.9 PHASE INVERSION POINT PREDICTIONS

Models for the prediction of phase inversion point were discussed in Section 2.4.5. Those relevant to pipeline flow will be used here and their predictions will be compared against the current experimental data. The predicted critical oil holdup values for phase inversion from the different models and the experimental data is shown in Table 6.3. The variables involved in the correlations listed are explained in detail in Section 2.4.5.

The physical properties used in the calculations can be seen (first line of the Table 6.4). The experimental values of the inversion point for experiments that started from oil continuous mixtures can be seen as well. This is the point right before the change of the continuity of the system in case of the *MARCOL™ 52* and *EXXSOL™*

D80 also, while it is the point of inversion in the whole cross section area in the case of the *EXXSOL*^{TM} *D140* oil. Clearly all correlations fail to predict all sets of experimental findings; some predictions however are closer to some of the systems used. The model by Nädler and Mewes (1995) had two constants k_1 and k_2 while no range was suggested for values. In this work they were adjusted to better fit all experimental data but no pair of values was found to satisfy all 3 systems used.

The holdup value shown in Table 6.3 is for the pair of k_1/k_2 values that would better predict the inversion point for all systems. A sensitivity analysis was carried out to select these values (see Table 6.4).

All these models predict phase inversion irrespective of initial conditions and pipe size. Some consideration for the pipe diameter has been made in the model by Nädler and Mewes (1995). However, when flow is turbulent (as it is in the conditions studied here) and the pipe is smooth (where Blasius equation is used) the effects of diameter and mixture velocity are cancelled. Some considerations at the appearance of the ambivalent range have been made by Brauner and Ullmann (2002) and they will be discussed in Section 6.10.

Table 6.3 Empirical models for the prediction of phase inversion point tested against current experimental findings. The predicted and experimental critical oil holdup is calculated.

		CRITICAL OIL HOLDUP				
AUTHOR	MODEL	*EXXSOL™ D140* *D*=0.038 M ρ_o=828 kg/m^3 μ_o=5.7 mPa s	*EXXSOL™ D80* *D*=0.060 M ρ_o=800 kg/m^3 μ_o=1.7 mPa s	*EXXSOL™ D80* *D*=0.032 M ρ_o=800 kg/m^3 μ_o=1.7 mPa s	*MARCOL™ 52* *D*=0.060 M ρ_o=827kg/m^3 μ_o=11 mPa s	*MARCOL™ 52* *D*=0.032 M ρ_o=827kg/m^3 μ_o=11 mPa s
ARIRACHAKARAN (1989)[6.1]	$\varphi_w = \left(\frac{U_{ws}}{U_m}\right)_I = 0.5 - 0.1108 \log_{10}(\mu_o/\mu_r)$	58.3%	52.5%	52.5%	61.5%	61.5%
DECARRE& FABRE (2003) [6.1]	$\varphi = \frac{1}{1+\left[\left(\frac{\mu_c}{\mu_d}\right)^{1/6}\left(\frac{\rho_c}{\rho_d}\right)^{5/6}\right]}$	53.3%	47.6%	47.6%	56%	56%
BRAUNER& ULLMANN(2002)[6.2]	$\varphi_o = \frac{\tilde{\rho}\tilde{\nu}^{0.4}}{1+\tilde{\rho}\tilde{\nu}^{0.4}}$	64.2%	52%	52%	70%	70%
NÄDLER & MEWES (1995)	$\varphi_w^I = \frac{1}{1+k_1\left[\frac{C_o}{C_w}\frac{\rho_o^{(1-n_o)}}{\rho_w^{(1-n_w)}}\frac{\mu_o^{n_o}}{\mu_w^{n_w}}(DU_m)^{n_w-n_o}\right]^{1/k_2}}$	67.2%[6.3]	60.9%[6.3]	60.9%[6.3]	70.1%[6.3]	70.1%[6.3]
YEH *ET AL.* (1964)[6.1]	$\frac{\varphi}{1-\varphi} = \left(\frac{\mu_d}{\mu_c}\right)^{1/2}$	70.5%	56.6%	56.6%	76.8%	76.8%
EXPERIMENTAL		≈70%	≈56%	56%	≈73%	≈63%

[6.1] No diameter dependence.
[6.2] Simplified model; the other prediction model of Brauner and Ullmann will be examined in Section 6.10.
[6.3] for k_1=1.6 and k_2=1.2.

Table 6.4 Sensitivity analysis for the Nädler and Mewes model (1995) parameters.

SET-UP	K_1=1.8 K_2=1.2	K_1=2.16 K_2=1.2	K_1=1.3 K_2=1.2	K_1=1.0 K_2=0.35	K_1=1.0 K_2=1.2	K_1=3.0 K_2=1.2	K_1=1.0 K_2=-1.2	K_1=1.6 K_2=1.2	EXPERI-MENTAL
EXXSOL D140 D=0.038 M ρ_o=828 kg/m^3 μ_o=5.7 mPa s	70[6.4]	73.5	63	70	56	79	44	67	70
EXXSOL D80 D=0.060 M ρ_o=800 kg/m^3 μ_o=1.7 mPa s	67	68	56[6.4]	48	50	75	51	61	56
MARCOL D=0.060 M ρ_o=827kg/m^3 μ_o=11 mPa s	73	76[6.1]	66	79	60	81	41	70	73

As it can be concluded from Table 6.3, Yeh's *et al.* model (1964) predicts the inversion point well particularly with the low viscosity oils (*EXXSOL™ D80, EXXSOL™ D140)*. His equation is a direct relationship between phase holdup at inversion point and viscosity ratio of continuous and dispersed phase. His findings were supported by Selker and Sleicher (1965) that also found that the ambivalent limits depend primarily on the kinematic viscosity ratios of the two fluids. Similar results were obtained from the current experimental work conducted in many different pipes and with different fluids: the inversion point and the associated pressure gradient are mainly related to oil viscosity (and thus viscosity ratio) while the other parameters studied have a much weaker effect on the inversion point, even though they strongly affect the resulted pressure drop along the pipe. Especially in the small acrylic pipe (32 mm ID) there was no significant effect of the mixture velocity or dispersion initialisation conditions on inversion. This simplified model could be used for the prediction of the phase inversion point as a first approximation.

[6.4] Best fit.

6.10 AMBIVALENT RANGE PREDICTIONS

Ambivalent range was only seen in the 60 mm ID pipes both acrylic and SS with the use of *EXXSOL™ D80*. Figure 6.19 depicts the experimental phase inversion points for these cases and all conditions used.

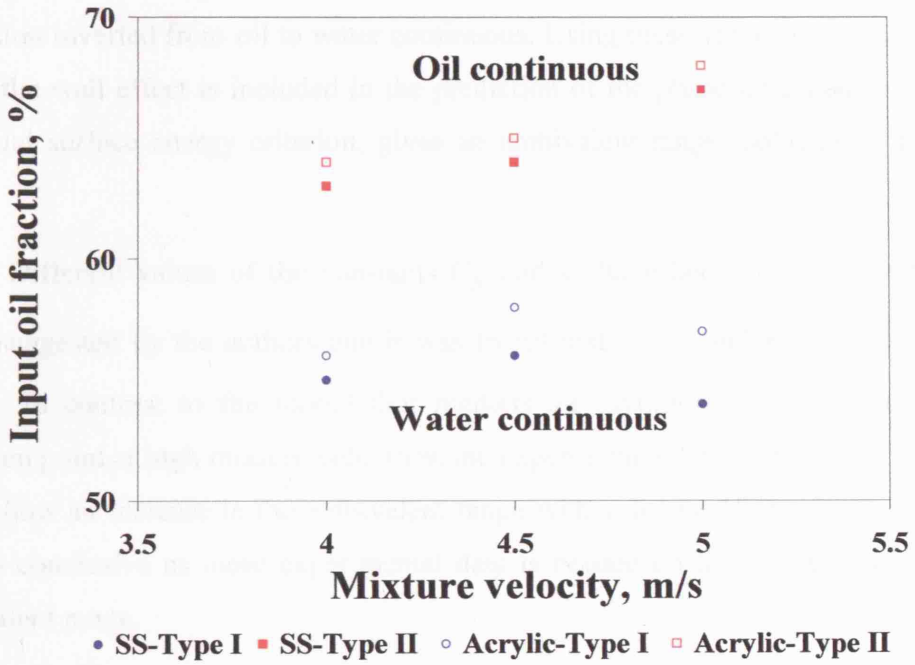

Figure 6.19 Experimental ambivalent range values in the steel and acrylic 60 mm ID pipes obtained with the use of *EXXSOL™ D80*.

The phase inversion points are taken as the volume fraction where the maximum in pressure gradient appeared (which in the acrylic pipe was found to be the point at the sharp change in conductivity). Only mixture velocities where the peak in pressure gradient because of inversion was clear are included. Phase inversion always happened in the SS pipe at lower input oil fractions than in the acrylic pipe, but the differences are not significant. Also, the ambivalent range seems to increase with increasing velocity but this trend might be due to the lack of a large number of results at higher velocities.

Brauner and Ullmann (2002) suggested that a possible reason for this hysteresis depending on the dispersion initialisation condition was the time needed after phase inversion for the new continuous phase to completely wet the pipe wall. As a result when a dispersion inverts from water to oil continuous, the pipe wall immediately after inversion would still be covered by a water layer and therefore behave as hydrophilic ($\theta=0^o$) while it would behave as hydrophobic ($\theta=180^o$) when the dispersion inverted from oil to water continuous. Using these values in Equation 2.17, where the wall effect is included in the prediction of the phase inversion point using the equal surface energy criterion, gives an ambivalent range (solid lines in Figure 6.20).

Different values of the constants $\tilde{C}_H$ and k_d have been attempted within the range suggested by the authors and it was found that $\tilde{C}_H=1$ and $k_d=5$ gave the best results. In contrast to the model that predicts an asymptotic value for the phase inversion point at high mixture velocities, the experimental data (dotted lines in Figure 6.20) show an increase in the ambivalent range with velocity. However, these results are not conclusive as more experimental data is needed on the effect of velocity on ambivalent range.

The model has been also applied to the small pipe in Figure 6.21. According to Brauner and Ullmann's (2002) considerations the effect of wettability of the pipe wall material should increase with decreasing pipe diameter and the ambivalent range in the small pipes should be larger (solid lines in Figure 6.21). The experimental results showed no effect of initial conditions on the phase inversion point in the small, 32 mm ID, acrylic pipe.

It is possible that these discrepancies arise because the models predict *in situ* volume fractions needed for phase inversion while the experimental results are presented against input oil fractions, although slip between the two phases is not expected to be high at these velocities (still above unity according to holdup finding with the use of *EXXSOL™ D140*).

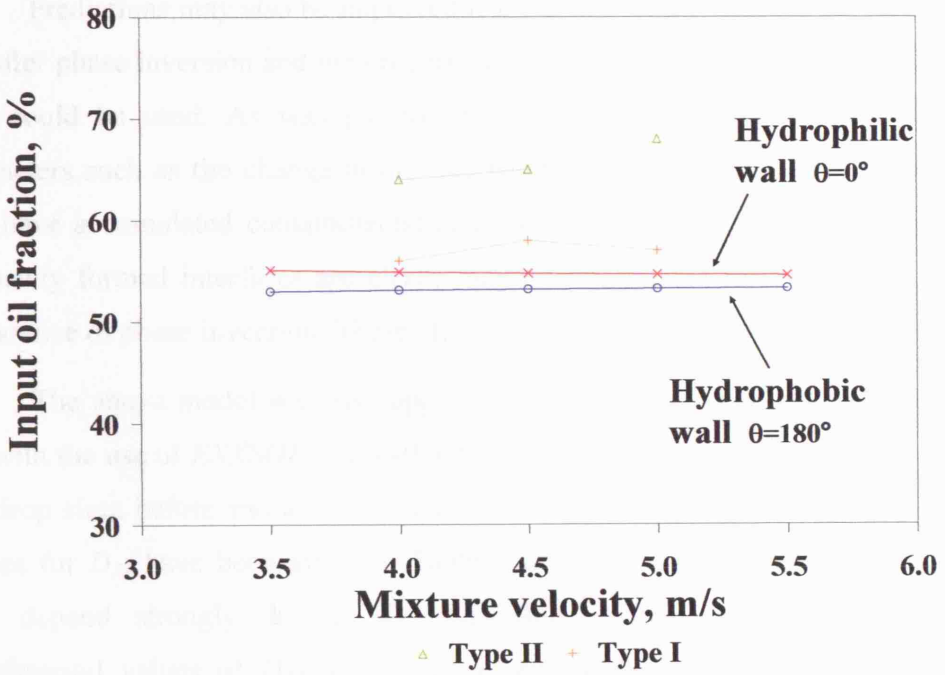

Figure 6.20 Comparison of experimental ambivalent range for the 60 mm ID acrylic test sections with the use of *EXXSOL™ D80* with the prediction of the model by Brauner and Ullmann (2002).

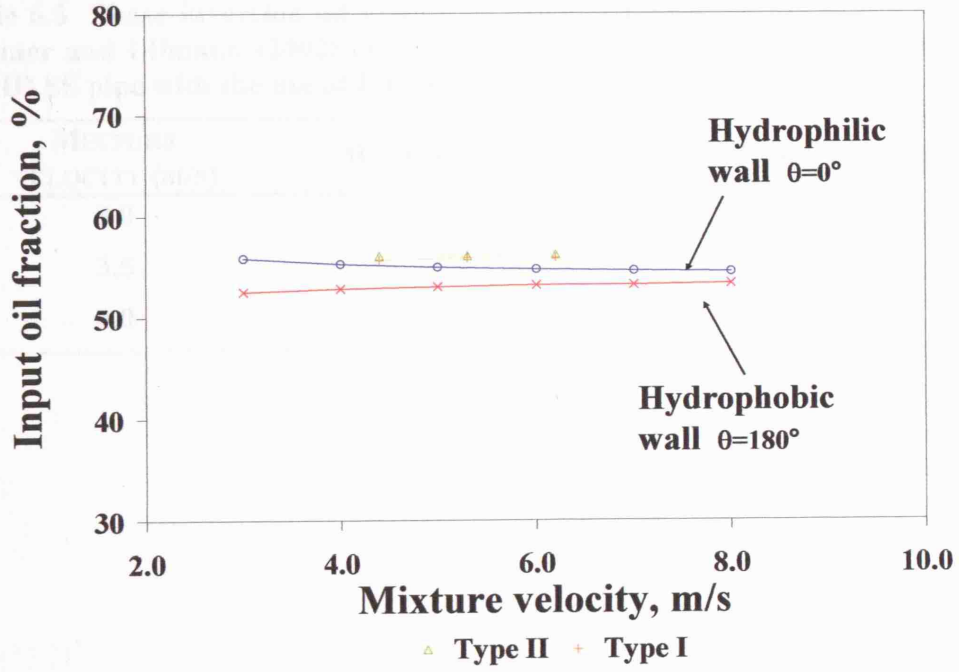

Figure 6.21 Comparison of experimental ambivalent range for the 32 mm ID acrylic test section with the use of *EXXSOL™ D80* with the prediction of the model by Brauner and Ullmann (2002).

Predictions may also be improved if the actual wall contact angle values before and after phase inversion and the properties of the recycled fluids rather than the fresh ones could be used. As was pointed out by Brauner and Ullmann (2002) other parameters such as the change in the interfacial tension before (where the interfaces may have accumulated contaminants) and immediately after phase inversion (where the newly formed interfaces are clean) may be responsible for the hysteresis in the appearance of phase inversion. These effects, however, are not readily included.

The above model was also applied to the stainless steel pipe with 38 mm ID and with the use of *EXXSOL™ D140*, where experimental measurements of *in situ* up and drop sizes before and after phase inversion are available at 3.0, 3.5 and 4.0 m/s. Values for D_{32} have been given in Table 5.2. The predicted phase inversion points (that depend strongly droplet size and thus mixture velocity) based on the experimental values of D_{32} do not agree well with experimental phase inversion points. Results are shown in Table 6.5.

Table 6.5 Phase inversion oil holdup as predicted with the use of the model by Brauner and Ullmann (2002) using the drop size experimental values for the 38 mm ID SS pipe with the use of *EXXSOL™ D140*.

MIXTURE VELOCITY (M/S)	HYDROPHILIC WALL	HYDROPHOBIC WALL
3.0	61.1%	56.0%
3.5	70.5%	66.6%
4.0	61.6%	58.4%

6.11 CONCLUSIONS

The effect of parameters on phase inversion and the associated pressure gradient was studied. The parameters considered were mixture velocity, dispersion initialisation conditions, pipe diameter and material and oil properties. The type of oil was found to have the most significant effect. In summary, the following were found:

- Phase inversion is accompanied by significant changes in pressure gradient. The exact behaviour will depend mainly on the pipe material and the type of oil used.
- Increasing mixture velocity will result in more abrupt changes in pressure gradient during inversion.
- The dispersion initialisation conditions (Type I vs Type II) affect the inversion point for the case of the less viscous oil in experiments in the large diameter pipes, both acrylic and SS pipes, where ambivalent range was found. No ambivalent range was seen in the smaller, 32 mm ID, acrylic pipe or with the use of the other two oils in any of the test sections.
- Pipe material was found to affect the pressure gradient during phase inversion, a behaviour that was related to the wetting characteristics of the pipe wall. A slight effect on the inversion point was also seen.
- The effect of change in the system's continuity is stronger in the acrylic pipe and inversion is seen to affect pressure gradient at lower mixture velocities.
- The phase inversion point as well as the pressure gradient behaviour during phase inversion were found to depend strongly on the type of oil used.

The effect of the different parameters on drag reduction was also investigated. More specifically:

- Acrylic pipes exhibit stronger drag reduction in the water continuous region, while the opposite is seen for the stainless steel and epoxy coated pipes.
- The type of oil does not seem to affect drag reduction for the same pipe in the water continuous region, but more viscous oils exhibit stronger drag reduction in the oil continuous region.
- Comparisons that were made for acrylic pipes of different diameters have revealed that drag reduction is higher for the larger acrylic pipe for the oil-in-water dispersions than in the 32 mm ID acrylic pipe and this was explained by the increased dispersed phase fraction in the larger pipe for the same Reynolds number.

Predictions of the phase inversion point based on literature correlations were compared against the current findings; the model by Yeh *et al.* (1964) was found to predict the inversion point in all experimental cases, verifying the importance of viscosity ratio to the prediction of inversion. The predictions of the ambivalent range based on the model by Brauner and Ullmann (2002) did not match the experimental data well.

Since the existing correlations in literature did not succeed in predicting the inversion characteristics, a new approach will be suggested in the following Chapter 7, based on the experimental findings presented before. The new mechanistic model will attempt to include the suggested mechanism for the occurrence of phase inversion in horizontal pipelines, also making considerations of the emulsion's viscosity and the phenomenon of drag reduction (described in Section 6.8) that was present in the current experimental results.

Chapter 7

Mechanistic predictive models of flow characteristics during phase inversion

7.1 OVERVIEW

The experimental findings in Chapter 4 indicate a potential mechanism for the occurrence of inversion in horizontal pipes at high mixture velocities. Based on these observations and measurements around the phase inversion point, new mechanistic models are suggested. These assume the formation of a layered structure prior to the occurrence of inversion. A review of the suggested correlations for the viscosity of emulsions is given first, and these correlations, in combination with the commonly used homogeneous model, will be used to predict pressure gradient in all experimental systems studied (Section 7.2). Previous work on the use of two and three fluid models will be presented (Section 7.3). New mechanistic models (the 2Layer and the 3Layer model) will then be introduced (Section 7.4) and the experimental results on pressure gradient will be compared against the predictions from the different models (Section 7.5).

7.2 HOMOGENEOUS MODEL

In this model, the two phases (which in the current work are believed to be fully mixed in most of the experimental conditions) are considered to form a

homogeneous mixture which is then regarded as one 'pseudo-fluid' with appropriately averaged properties. The pressure gradient is then calculated using single phase flow equations:

$$\frac{\Delta P}{l} = \frac{2f\rho_m U_m^2}{D} \tag{4.1}$$

where ΔP is the pressure gradient per unit length, l is the length, f is the Fanning friction factor, ρ_m is the mixture density, U_m is the mixture velocity, and D is the pipe diameter. The mixture velocity can be found from $\frac{Q_o + Q_w}{A}$ where Q_o and Q_w are the oil and water volumetric flowrates respectively, and A is the pipe cross sectional area. The friction factor is related to the Reynolds number as follows $f = C\mathrm{Re}^{-n}$, where Re is the mixture Reynolds number, and C and n are constants.

The above equations require the density of the homogeneous liquid which can be obtained from:

$$\rho_m = \rho_d\varphi + \rho_c(1-\varphi) \tag{2.4}$$

In this equation ρ_m, ρ_c and ρ_d are the mixture, continuous and dispersed phase densities respectively (kgm^{-3}) and φ the *in situ* holdup of the dispersed phase which is equal to the input dispersed phase holdup if no slip between the phases is assumed.

The viscosity of the mixture is more difficult to calculate. There is a large body of literature on the topic while a number of correlations originate from solid-liquid suspensions that have been suitably modified for liquid-liquid dispersions. Several investigators have studied the flow behaviour of oil-water dispersions in pipe viscometers, where the two fluids were premixed and pressure gradient of the mixture was measured during its flow in the pipe.

Viscosity is a measure of the ability of the fluid to transport shear from one location in the fluid to the other. According to Einstein's theory (1906, 1911) for the viscosity of suspensions, mixture viscosity, μ_m, is given as:

$$\mu_m = \mu_c(1+2.5\varphi) \qquad (2.1)$$

where μ_c is the viscosity of the continuous phase. This equation is valid regardless of the size of the particles. However, there are two important assumptions involved in its derivation: a) the suspension is very "dilute" so that the particles are far apart (isolated from one another) and b) the particles are considered to be "hard spheres", i.e. rigid and non-deformable. The latter is valid when the repulsive (due to electrical double layer) and attractive forces (due to van der Waals attraction) between particles are both negligible and the absorbed stabilizing layer thickness (δ), if any, is very small relative to the particle size (R), that is δ / R negligibly small.

According to Pal (1996) soon after the latter assumption is violated, the effect of particle size on viscosity is important and cannot be ignored. The *electroviscous effect* describes the case where viscosity of the dispersion is rising due to the presence of an electrical double layer on the surface of the particles. For dilute dispersions, the electroviscous effect is associated with the distortion of the electrical double layer from the spherical symmetry by the shear field. Viscosity shows a trend to increase as the droplet size is decreasing, as smaller droplets are more rigid, while the non-rigid and deformable spheres might have further effects on the rheological behaviour of the dispersions. It is expected that the deformable droplets might exhibit shear thinning and elastic effects even in dilute systems.

Thus, equations that refer to very dilute systems cannot be used for the current experimental systems, where concentrated dispersions are encountered, particularly close to phase inversion. Other available equations for the prediction of mixture viscosity such as the one proposed by Brinkman (1952) (Equation 7.4) imply a peak in viscosity at the inversion point. Another similar correlation used is that of Krieger and

Dougherty (1959) (Equation 7.9 below), which states that the viscosity must reach a maximum at the maximum packing of the dispersed phase (φ_m), called packing fraction. To use this equation in the current work it has been assumed that the maximum packing occurs at the inversion point.

A summary of the most important and used correlations for predicting dispersion viscosity that also take into account the dispersed phase fraction is given in Table 7.1. Brief literature review of emulsion viscosity correlations is given in Giulinger *et al.* (1988) and Pal and Rhodes (1989). In the following equations, μ is the viscosity, subscripts *o*, *w*, *c*, *d*, and *m* refer to oil, water, continuous phase, dispersed phase and mixture respectively, φ is the dispersed phase fraction, $[C]$ is the intrinsic viscosity, N_{Ca} is the capillary number (defined as the ratio of hydrodynamic over interfacial stress, $N_{Ca}=(\mu_c\dot{\gamma}R)/\sigma$, where $\dot{\gamma}$ is the shear rate) while the parameters in each equation are defined respectively in the most right column of Table 7.1.

Table 7.1 Literature correlations predicting emulsion viscosity.

AUTHOR	MODEL	REMARKS
Taylor (1932)	$\mu_m=\mu_c\left[1+2.5\varphi\left(\frac{0.4+\mu_d/\mu_c}{1+\mu_d/\mu_c}\right)\right]$ (6. 1)	
Leviton & Leighton (1936)	$\mu_m=\mu_c\exp\left[2.5\frac{0.4+\mu_d/\mu_c}{1+\mu_d/\mu_c}\left(\varphi+\varphi^{5/3}+\varphi^{11/3}\right)\right]$ (7. 1)	$\varphi<0.5$
Eiler (1941)	$\mu_m=\mu_c\left(1+\frac{1.25\varphi}{1-\alpha_g\varphi}\right)^2$ (7. 2)	$1.28<\alpha_g<1.30$
Mooney (1951)	$\mu_m=\mu_c\exp\left(\frac{2.5\varphi}{1-k\varphi}\right)$ (7. 3)	k Mooney's crowding factor. $1.35<k<1.91$
Brinkman (1952) Roscoe (1952)	$\mu_m=\mu_c(1-\varphi)^{-2.5}$ (7. 4)	Polydisperse system
Roscoe (1952)	$\mu_m=\mu_c(1-1.35\varphi)^{-2.5}$ (7. 5)	Particles of uniform size

AUTHOR	MODEL		REMARKS
Vermuelen *et al.* (1955)	$\mu_m = \frac{\mu_c}{1-\varphi}\left[1+\frac{1.5\varphi\mu_d}{\mu_c+\mu_d}\right]$	(7. 6)	$\phi < 1$
Laity& Treybal (1957)	$\mu_m = \frac{\mu_m}{\varphi}\left[1+\frac{6\varphi_o\mu_o}{\mu_m+\mu_o}\right]$ water more than 40%	(7. 7)	
	$\mu_m = \frac{\mu_o}{\varphi_o}\left[1-\frac{1.5\varphi_w\mu_w}{\mu_m+\mu_o}\right]$ water less than 40%	(7. 8)	
Krieger& Dougherty (1959)	$\mu_m = \mu_c\left(1-\frac{\varphi}{\varphi_m}\right)^{[C]\cdot\varphi_m}$	(7.9)	$[C]=-2.5$
Krieger& Dougherty With variable exponent	$\mu_m = \mu_c\left(1-\frac{\varphi}{\varphi_m}\right)^{[C]\cdot\varphi_m}$	(7.10)	-8.5<[C]<-2.5
Krieger& Dougherty With fractional exponent	$\mu_m = \mu_c\left(1-\frac{\varphi}{\varphi_m}\right)^{[C]\cdot(\varphi/\varphi_m)}$	(7.11)	$[C]=-2.5$
Furuse (1972)	$\mu_m = \frac{\mu_c(1+0.5\varphi)}{(1-\varphi)^2}$	(7.12)	
Barnea& Mizrahi (1976)	$\mu_m = \mu_c \exp\left[\frac{2.5\varphi}{1-\varphi}\left(\frac{0.4+\mu_d/\mu_c}{1+\mu_d/\mu_c}\right)\right]$	(7.13)	$\varphi < 0.33$
Bedeaux (1983)	$\frac{\mu_d-\mu_m}{\mu_d+1.5\mu_m}\varphi+\frac{\mu_c-\mu_m}{\mu_c+1.5\mu_m}(1-\varphi)=0$	(7.14)	
Pal&Rhodes (1989)	$\mu_m = \mu_c\left[1+\left(\frac{0.8415\varphi/(\varphi)_{\mu_r=100}}{1-0.8415\varphi/(\varphi)_{\mu_r=100}}\right)\right]^{2.5}$	(7.15)	$\varphi < 0.74$
Pal (2001)	$\mu_m/\mu_c\left[\frac{2(\mu_m/\mu_c)+5(\mu_d/\mu_c)}{2+5(\mu_d/\mu_c)}\right]^{3/2} = \left(1-\frac{\varphi}{\varphi_m}\right)^{-2.5\varphi_m}$	(7.16))	$N_{Ca}\to 0$
Pal (2003)	$\mu_m/\mu_c\left[\frac{(\mu_d/\mu_c)-(\mu_m/\mu_c)}{(\mu_d/\mu_c)-1}\right]^{3/2} = \left(1-\frac{\varphi}{\varphi_m}\right)^{-2.5\varphi_m}$	(7.17)	$N_{Ca}\to\infty$

Pal and Rhodes (1989) used a purely empirical approach to correlate viscosity data of emulsions (Equation 7.15). In this one $(\varphi)_{\mu_r=100}$ is the dispersed phase fraction at which the relative viscosity (defined as the viscosity of the mixture divided by the viscosity of the continuous phase) becomes 100. This value can be obtained in stable emulsions, but for pipeline flows it has to be extrapolated from relative viscosities at lower volume fractions. These are found by calculating the friction factor from pressure gradient data and then the Reynolds number from which mixture viscosity can be obtained.

Most of the correlations in Table 7.1 predict that the emulsion viscosity is increasing with increasing dispersed fraction. Based on the work conducted in both experimental facilities and with the three different types of oil used, it was concluded that different dispersions will not behave in the same way, especially close to inversion. More specifically, it was the less viscous oil (*EXXSOL^{TM} D80*) that exhibits a sharp peak in the pressure gradient at the inversion point regardless of the experimental route (Type I or II) followed. The more viscous oil (*MARCOL^{TM} 52*) would yield pressure gradient almost constant in the oil continuous region (especially for the acrylic pipes regardless of ID) irrespective of the dispersed phase fraction (behaviour also seen by Arirachakaran *et al.*, 1989), while for the SS pipe there was a reduced pressure gradient in the oil continuous region attributed to drag reduction. In the water continuous region with the use of the same oil, pressure gradient is more reduced in the acrylic test section, while it is again almost constant in all test sections with input oil fraction. Last, the *EXXSOL^{TM} D140* used with the 38 mm ID SS pipe has shown an intermediate behaviour, with some peak in pressure gradient close to inversion but this peak was always in the water continuous region.

However, drag reduction occurred in both oil and water continuous dispersed flows in all test sections used, especially with the use of *EXXSOL^{TM} D140* and *MARCOL^{TM} 52*. To account for this, a modified friction factor, f_d, is used as suggested by Rozentsvaig (1982):

$$f_d = \frac{f}{1 + y\varphi} \tag{7. 18}$$

where f is the friction factor of a fine emulsion with the dispersed phase concentration φ, and y is a concentration function constant, ranging from 0.5 to 1.125 in pipe flows as suggested by Rozentsvaig (1982). A combination of the modified friction factor as given by Eq. (7.18) with the viscosities predicted by equations in Table 7.1 will be used.

The homogeneous model was applied to the data from the experimental set up at UCL (*EXXSOL^{TM} D140* as test fluid). Results of the calculated pressure gradient obtained with various mixture viscosity predictions can be seen in Figure 7.1 plotted against input oil fraction.

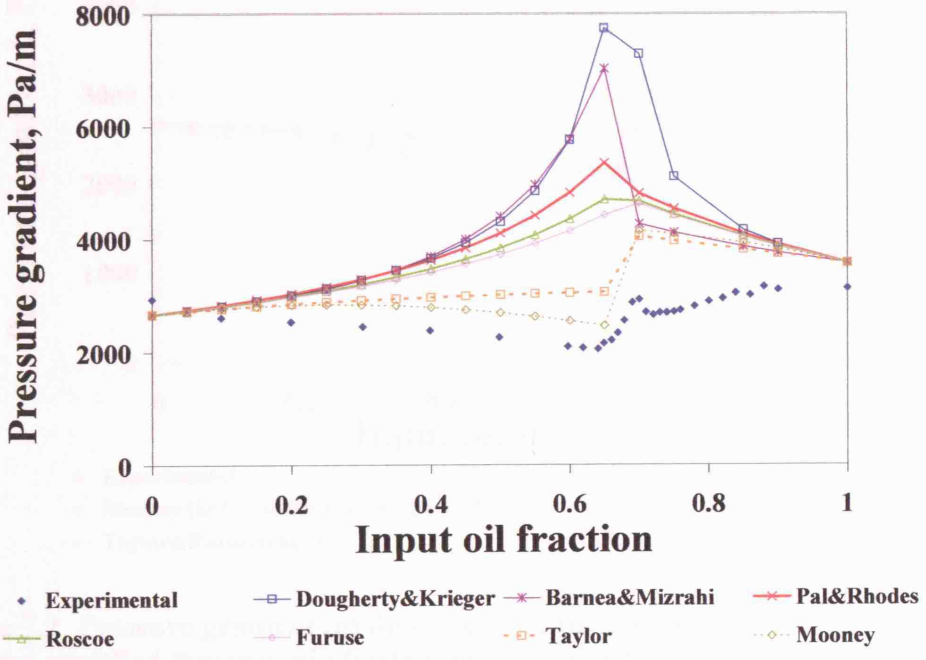

Figure 7.1 Pressure gradient predictions from the homogeneous model and various viscosity correlations against experimental data from the 38 mm ID SS pipe at UCL with the use of *EXXSOL^{TM} D140*. Results are obtained at 3.5 m/s mixture velocity. The phase inversion point was taken at φ_o=0.7 according to experimental findings.

Most correlations are overpredicting the pressure drop for this configuration, with predictions from Taylor (1932) and Mooney (1951) (with k = 1.91) giving the best agreement to the experimental values. Further analysis was conducted for these two models, and the predicted friction factor was modified according to Eq. 7.18. Results can be seen in Figure 7.2. Taylor's model with y = 0.7, yields values very close to the experimental findings in the water continuous region. However, the drag reduction in the oil continuous region cannot be predicted by any of the modified f_d. With the dotted line in each Figure the best fit(s) to the experimental values can be seen. Applying curve fitting methods for the results of Figure 7.2 it is found that Taylor & Rozentsvaig for y = 0.7 and y = 1.125 are the best approaches (with the latter being slightly better).

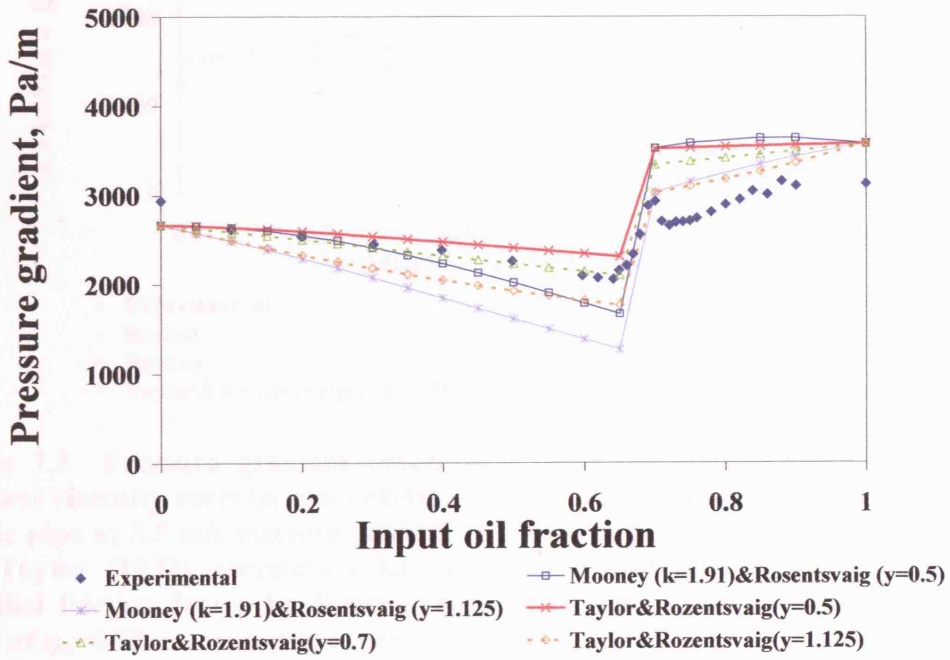

Figure 7.2 Pressure gradient predictions from the homogeneous model combined with the modified Rozentsvaig friction factor against experimental data. Analysis was conducted for the correlations of Taylor (1932) and Mooney (1951) for the facility at UCL with the use of *EXXSOL™ D140*. Results are obtained at 3.5 m/s mixture velocity. The phase inversion point was taken at φ_o=0.7 according to experimental findings.

The same analysis was conducted for the 60 mm ID acrylic section at NTNU with the use of *MARCOL™ 52* and results can be seen in Figure 7.3. Here, the modified friction factor by Rozentsvaig has been used again with Taylor's model. For $y = 1.125$ there is a very good agreement especially in the oil continuous region. This is due to the increased drag reduction in the acrylic pipe of the water continuous region, especially with the use of *MARCOL™ 52* as test fluid.

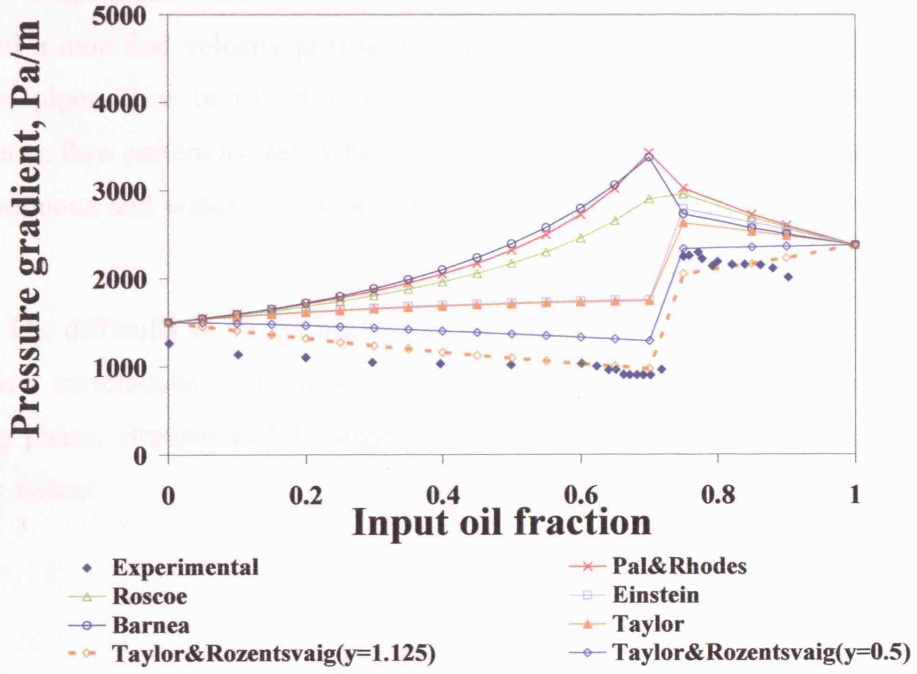

Figure 7.3 Pressure gradient predictions from the homogeneous model and different viscosity correlations against the experimental data from the 60 mm ID acrylic pipe at 3.5 m/s mixture velocity at NTNU with the use of *MARCOL™ 52*. The Taylor (1932) correlation has also been used in conjunction with the modified friction factor by Rozentsvaig (1982). The phase inversion point was taken at φ_o=0.75 according to experimental findings.

7.3 TWO-FLUID MODEL

In the two fluid model suggested by Taitel and Dukler (1976) for stratified gas-liquid flow, momentum balances were written for each one of the phases. Wall shear stresses were calculated based on single phase flow and equivalent diameters of the layers while for the calculation of the interfacial shear stress it was assumed that the

faster gas phase is flowing in a closed duct, and the slower liquid is flowing in an open channel. The interfacial height and hold up and the pressure gradient could thus be calculated. Since then there have been a number of developments of this model where it has been extended to three phase gas-liquid-liquid and to three-layer flows (Vedapuri *et al.*, 1997; Ghorai *et al.*, 2005).

Recently, Vedapuri *et al.* (1997) considered a 3-layer structure to predict water layer thickness in oil-water horizontal flows where a mixed layer is flowing in between single phase water and oil layers. Ghorai *et al.* (2005) took a step further and included a modified velocity profile in their three-phase (gas-liquid-liquid) stratified flow in pipes. The two-fluid model has been used for characterizing the dual continuous flow pattern as well, where the flow is split in two dispersed layers, namely oil continuous and water continuous (Jayawardena *et al.*, 2000; Lovick and Angeli, 2004).

The difficulty in measuring interfacial shear stress has resulted in a number of suggested correlations. For liquid-liquid annular flow where the core is the faster flowing phase, Brauner (1991) suggested the following equation for the interfacial friction factor:

$$f_i = BC''\left(\frac{D_c U_c \rho_c}{\mu_c}\right)^{-n} \tag{7.19}$$

which is used to calculate the shear stress by:

$$\tau_i = f_i\left(\frac{\rho_c U_c^2}{2}\right) \tag{7.20}$$

where f_i is the interfacial friction factor, D_c is the diameter of the core phase, U_c is the core phase average velocity, ρ_c is the core density, μ_c is the core viscosity, C'' and n

are constants which depend on the flow regime and B is an augmentation factor which accounts for interfacial waviness. Brauner (1991) suggested that in liquid-liquid flows the waviness at the interface would be very slight and B should take the value of 1. Neogi *et al.* (1994), however, used the same approach to model oil-water interfacial shear stress in three-phase, gas-oil-water flows and found from experimental data that the value of B could vary from 0.8 to 1. It has also been suggested (Taitel *et al.*, 1995) that a constant value of 0.014 can be used for the interfacial friction factor except when the wall friction factor of the faster phase is greater than 0.014; in this case this wall friction factor value should be used instead.

According to Hall (1992):

$$\tau_i = \gamma \tau_o \tag{7.21}$$

where τ_o is the oil wall shear stress and γ is a proportionality factor which must be less than 1. The term γ was calculated from the analytical solution of one-dimensional momentum equations for oil-water laminar stratified flow between parallel plates and was found to be closely related to the water/oil viscosity ratio. Roberts (1996) in his three-fluid model used γ equal to this viscosity ratio (Khor *et al.*, 1997), while Taitel *et al.* (1995) suggested that a constant value of 0.014 can be used for the interfacial friction factor except when the wall friction factor of the faster phase is greater than 0.014; in this case, this wall friction factor value is used instead.

7.4 MODEL DEVELOPMENT

INTRODUCTION

A two and a three fluid model are suggested based on the fluid models reviewed above to predict holdup and pressure gradient around the point of inversion, where a layered structure is believed to exist. As described in Section 4.5, when an experiment started for example from oil continuous mixtures (Type I experiment, Figure 4.16), and the oil fraction was gradually decreased (water fraction increased), phase inversion did not happen at one specific phase fraction, but an intermediate condition existed, where both phases could be present as continuous layers in the pipe

cross sectional area, even at the higher mixture velocities studied. It was found that just before phase inversion in the whole cross section, the phase that was about to become continuous (in this case water), forms a thin layer on the bottom of the pipe, detected by the flush hot-film probe (FP) as seen in Figure 4.16 at 70% input oil fraction. At that phase fraction, the cross sectional area is still dominated by an oil continuous mixture. If the water fraction is further increased, the thin water layer will still be wetting the lower part of the pipe, the bulk mixture in the pipe core will now invert to a water continuous mixture, and there is probably a thin oil layer on top. When the inversion process is complete and the conductivity values obtained from all conductivity probes have been stabilised in water continuous values, the thin oil layer will not be present anymore at the upper part of the pipe.

Similar conclusions can be drawn for a Type II experiment, seen in Figure 4.17; when the flush hot-film probe was located at the top of the pipe, its output voltage would indicate oil/oil continuous flow at lower input oil fractions (in this case at 71-72% oil) in comparison to the rest of the instrumentation used, while it took a further increase in the oil fraction for inversion towards oil continuous mixtures to occur in the whole cross sectional area (in this case at approximately 73% oil).

Two approaches are thus, suggested. Taking a Type I experiment into consideration, as described above, at the inversion point the major part of the cross sectional area will be occupied by an oil continuous mixture, while a thin water layer will have formed at the bottom of the pipe (2Layer). The upper part of the pipe though may be wetted by an oil layer without any drops in it, forming together with the oil continuous mixture and the newly formed single phase water layer, a 3Layer structure. After the bulk of the mixture inverts, this layer may persist for some fractions, giving again a 3Layer structure. In both 2Layer and 3Layer structures the mixture is considered oil continuous up to the point where large oscillations are detected with the local conductivity probe in the core of the pipe, at which point it is considered that oil has ceased being the continuous phase and the mixture is now water continuous.

THE MODEL

In the following, the 3Layer structure will be explained in detail, while the 2Layer approach is simply derived from it. It is assumed that oil is wetting the upper part of the pipe, an oil continuous mixed layer is occupying the biggest part of the pipe at the middle, while a fine water layer has just formed, wetting the lower part of the pipe.

The suggested 3Layer flow geometry can be seen in Figure 7.4.

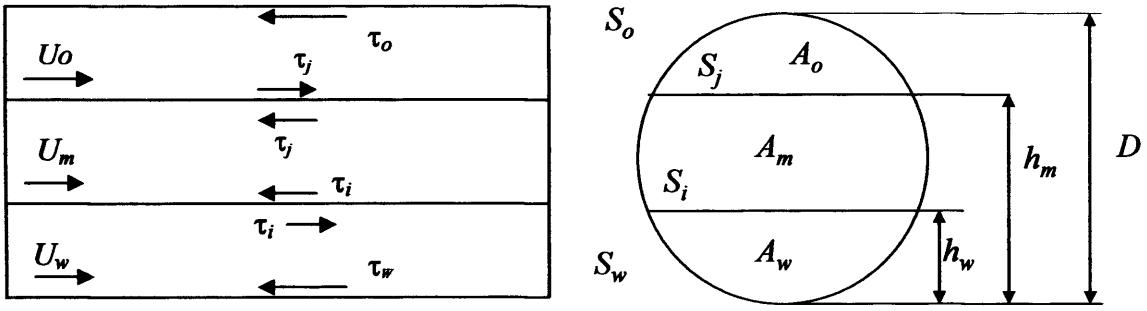

Figure 7.4 Schematic diagram of stratification of the flow around inversion point.

The oil continuous mixture in the middle of the pipe is considered a homogeneous dispersion with a uniform density and viscosity. General momentum balances for the three layers are as follows.

For the water layer at the bottom of the pipe:

$$-A_w(\frac{dp}{dx})-\tau_W S_W \pm \tau_i S_i = 0 = F1 \qquad (7.22)$$

For the mixed homogeneous layer in the middle of the pipe:

$$-A_m(\frac{dp}{dx}) - \tau_m S_m \mp \tau_i S_i \pm \tau_j S_j = 0 = F2 \qquad (7.23)$$

For the oil layer at the top of the pipe:

$$-A_o(\frac{dp}{dx}) - \tau_o S_o \mp \tau_j S_j = 0 = F3 \qquad (7.24)$$

where the subscripts *w*, *m* and *o* refer to water, mixed homogeneous, and oil layers respectively, A is the cross sectional area, S is the wetted perimeter, i and j refer to the mixed layer-water and mixed layer-oil interfaces respectively, τ , τ_i and τ_j stand for wall, interfacial layer-water and interfacial layer- oil shear stresses respectively, and (dP/dx) is the pressure gradient. Horizontal flow is considered. The signs of the interfacial tension terms in Equations 7.22-7.24 depend on the velocity of the layers and will be defined below.

ASSUMPTIONS

The main assumptions made for the 3Layer model are:

- The phase fractions in the mixed layer are equal to the input ones, as the single phase layers are not very thick and there is no significant slip.
- The two single phase layers are occupying that area of the pipe (closer to the wall) where there is low velocity. Thus, the mixed layer is flowing with higher velocity than the other two. So, it is the mixed layer that is dragging both water and oil phases. This assumption is used in order to write the interfacial stress terms in the momentum balances. This means that the terms that refer to interfacial stresses in Equation (7.23) for the mixed layer are both negative, while the

respective terms in Equations (7.22) and (7.24) are positive for both the water and the oil layers respectively.

- The density of the mixed layer will be given by Equation (2.4), while its viscosity will be given by Taylor's equation that was found to predict the experimental results well (Equation 6.2). As mentioned above, for a Type I experiment, the bulk mixture is considered oil continuous before inversion and water continuous after inversion.

CALCULATION OF WALL SHEAR STRESSES

For the individual phases, the single phase flow wall shear stress is:

$$\tau_x = f_x \frac{\rho_x U_x^2}{2} \text{ where } (x = w, o, m) \tag{7.25}$$

where U_x is the average velocity of the phase, defined as:

$$U_x = \frac{Q_x}{A_x} \tag{7.26}$$

The above equation will be used here for the oil wall and water wall shear stresses, with U_x being the average *in situ* velocity of the relevant phase. Friction factors from single phase flows are considered. So,

$$f_x = \frac{16}{\mathrm{Re}_x} \text{ for laminar flow} \tag{7.27}$$

$$f_x = \frac{0.079}{\mathrm{Re}_x^{0.25}} \text{ for turbulent flow} \tag{7.28}$$

For the calculation of Reynolds numbers, the hydraulic diameters have to be defined. As discussed above the mixed layer is assumed to flow faster than the single phase layers. The mixed layer can then be assumed to flow in a closed conduit and the two single phases in open channels. The hydraulic diameters for each layer are thus, found as follows:

$$D_m = \frac{4A_m}{S_m + S_{i1} + S_{i2}} \tag{7.29}$$

and

$$D_O = \frac{4A_O}{S_O} \tag{7.30}$$

$$D_w = \frac{4A_w}{S_w} \tag{7.31}$$

CALCULATION OF INTERFACIAL STRESSES

Even though assumptions have been made regarding the expected velocities of the single phase layers, the signs of the predicted interfacial stresses have been taken into consideration. Therefore:

$$\tau_i = f_i \frac{\rho_i (U_m - U_W)|(U_m - U_W)|}{2} \tag{7.32}$$

$$\tau_j = f_j \frac{\rho_j (U_o - U_m)|(U_o - U_m)|}{2} \tag{7.33}$$

where the interfacial friction factors have been evaluated using an approach similar to that by Brauner and Maron (1989) as follows:

$f_i = f_m$ and $\rho_i = \rho_m$, when $U_m > U_W$, while $f_i = f_W$ and $\rho_i = \rho_W$, when $U_m < U_W$.

Similarly,

$f_j = f_m$ and $\rho_j = \rho_m$, when $U_m > U_O$, while $f_i = f_O$ and $\rho_i = \rho_O$, when $U_m < U_O$.

MASS BALANCES

The mass balances for oil and water yield:

$$Q_W = Q_L + \varphi_{ml} Q_m \tag{7.34}$$

$$Q_O = Q_U + (1 - \varphi_{ml}) Q_m \tag{7.35}$$

where

φ_{ml} is the dispersed phase fraction (in the case considered, water) in the mixed layer,

Q_l= the volumetric flow rate of water in the lower (single phase water) layer, m^3/s,

Q_m = volumetric flow rate of the mixed layer, m^3/s.

Q_o = total volumetric flow rate of oil, m^3/s

Q_u= the volumetric flow rate of oil in the upper (single phase oil) layer, m^3/s, and

Q_w= total volumetric flow rate of water, m^3/s,

Dividing by the total pipe area:

$$U_{sw} = U_{sl} + \varphi_{ml} U_{sml} \tag{7.36}$$

$$U_{so} = U_{su} + (1 - \varphi_{ml}) U_{sml} \tag{7.37}$$

where:

U_{sw}= water superficial velocity, m/s,

U_{so} = oil superficial velocity, m/s,

U_{su} = upper (single phase oil) layer superficial velocity, m/s,

U_{sl} = lower (single phase water) layer superficial velocity, m/s and

U_{sml} = mixed layer superficial velocity, m/s.

Thus, there are five equations (7.22-24 and 7.35-36) containing seven unknowns, U_{sl}, U_{sml}, U_{su}, φ_{ml}, A_w, A_o and A_m. As stated before, for the 3Layer model it will be assumed that the dispersed phase fraction in the mixed layer is equal to the input dispersed phase fraction, while the velocity of the mixed layer will be considered equal to the continuous phase velocity that has been obtained experimentally with the use of a hot film anemometer by Hu (2005) (results shown in Figures 5.8 and 5.9). Its average value for conditions close to the inversion point (expected at about 70% input oil fraction) was found to be equal to:

$$U_{ml} = 1.1\left(U_{sw} + U_{so}\right) \tag{7.38}$$

where U_{ml} is the *in situ* mixed layer velocity. This is equal to the average velocity at the whole cross section area, without taking into account the velocity close to the pipe wall where measurements were not experimentally obtained anyway. This value is similar to the approach of Vedapuri *et al.* (1997) who obtained experimentally:

$$U_{ml} = 1.2\left(U_{sw} + U_{so}\right) \tag{7.39}$$

Table 7.2 gives a list of all geometric parameters involved in the equations above. The geometric parameters depend upon the thickness of the single phase oil, h_o, and water, h_w, layers. Comparing with the heights shown in Figure 7.4, it is $h_o = D - h_m$ and r is the pipe radius.

Table 7.2 Geometric parameters used in the three-layer model.

Geometric parameters	
$A_w = r^2 Arc\cos\left(\frac{r-h_w}{r}\right) - (r-h_w)\sqrt{(h_w(2r-h_w))}$	**(7. 40)**
$A_o = r^2 Arc\cos\left(\frac{r-h_o}{r}\right) - (r-h_o)\sqrt{(h_o(2r-h_o))}$	**(7. 41)**
$A_t = \pi r^2$	**(7. 42)**
$A_m = \pi r^2 - A_w - A_o$	**(7. 43)**
$S_w = 2r\arccos\left(\frac{r-h_w}{r}\right)$	**(7. 44)**
$S_o = 2r\arccos\left(\frac{r-h_o}{r}\right)$	**(7. 45)**
$S_m = 2\pi r - (S_o + S_w)$	**(7. 46)**
$S_i = 2(h_w(2r-h_w))^{1/2}$	**(7. 47)**
$S_j = 2(h_o(2r-h_o))^{1/2}$	**(7. 48)**

METHOD OF SOLUTION

Equations (7.22), (7.23) and (7.24) are the three equations required to be solved for the variables h_o and h_w. The method of solution is as follows:

1. Assume values for $h_o < r$ and $h_w < r/2$ (for a given set of inlet fluid flow rates. (The mixed layer is assumed still oil continuous).

2. Calculate geometric parameters using Equations 7.40-7.48.
3. Calculate velocities using Equations 7.36-7.38.
4. Calculate Reynolds numbers.
5. Compute frictions factors and shear stresses from Equations 7.25-7.33.
6. Substitute all these values in Equations 7.22-24.
7. If these are not satisfied, use secant method to update the values of h_o and h_w.

Repeat steps 1-6 until the residues of equations are less than the tolerance, which in the present work has been kept to approximately 10^{-10}.

Similar equations are used for the 2Layer structure, where one of the single phase layers that is assumed to exist in the 3Layer model is now ignored. For a Type I experiment the mixed layer is oil continuous, while a single phase water layer is assumed to form just before inversion to water continuous mixtures. In this case, the experimental value of velocity ratio was incorporated in the model. The momentum equations for such a flow structure would yield:

$$-A_w\left(\frac{dp}{dx}\right)-\tau_W S_W \pm \tau_i S_i = 0 = F1 \tag{7.49}$$

$$-A_m\left(\frac{dp}{dx}\right)-\tau_m S_m \mp \tau_i S_i = 0 = F2 \tag{7.50}$$

where the variables have the meaning defined above. The interfacial terms are defined from Equation 7.32 with the Brauner and Maron (1989) approach. The mass balances for the 2Layer model will yield:

$$Q_w = Q_L + \varphi_{ml} Q_m \tag{7.51}$$

$$Q_O = (1-\varphi_{ml}) Q_m \tag{7.52}$$

and by dividing with the total cross section area:

$$U_{sw} = U_{sl} + \varphi_{ml} U_{sml} \tag{7.53}$$

$$U_{so} = (1-\varphi_{ml}) U_{sml} \tag{7.54}$$

For the definition of the friction factor the approach of Rozentsvaig is used where y =1.125 as this value was found to fit the experimental results better when used in the homogeneous model. In this approach, the definition of velocity ratio (Equation 5.1) was introduced and its experimental value used, adding a 5th equation to the system as follows:

$$S = \frac{\varepsilon_o / \varepsilon_w}{\varphi_o / \varphi_w} = \frac{U_{os}}{U_{ws}} \frac{(\varphi_{ml} A_m + A_w)}{(1-\varphi_{ml}) A_m} \tag{7.55}$$

Equations 7.49-7.50 and 7.53-7.55 are 5 equations with 5 unknowns, thus the system can be solved to yield water layer height, entrained fraction φ_{ml}, pressure gradient and the velocities of the two phases, as follows:

1. A value for $h_w < r/2$ is assumed (the mixed layer is considered oil continuous).
2. The geometric parameters are calculated.
3. Equation 7.55 is used to obtain the entrained fraction.

4. Equations 7.53 and 7.54 are used to calculate velocities.
5. Reynolds number is calculated.
6. Compute frictions factors and shear stresses from Equations 7.25-7.33 (in this case the oil layer is ignored).
7. Substitute values in Equations 7.49 and 7.50.
8. If these are not satisfied, use secant method to update the values of h_w.

Repeat steps 1-7 until the residues of equations are less than the tolerance.

7.5 RESULTS AND DISCUSSION

The models have been applied to all experimental facilities and the heights of single phase water and oil layers, along with pressure gradient were calculated. Sensitivity analysis was conducted to check how the value of *in situ* mixture velocity (Equation 7.38) would affect the results.

It was found that the 3Layer model has solutions at the phase fractions around the phase inversion point with the assumptions made, verifying that such flow geometry can actually exist. In fact, at each mixture velocity, the model only gives results for this range of volume fractions. This implies that such a 3Layer geometry is possible around phase inversion, but not for dispersed phase fractions away from it. The range of fractions where the 3Layer model has a solution could be used to predict the width of the transitional regime between oil and water continuous flows. This range of fractions becomes wider with decreasing mixture velocity, showing that the single phase layers are preferably formed at lower velocities. For the experimental facility at UCL with the use of the 38 mm ID SS pipe and *EXXSOL*^{TM} *D140* the range of conditions that satisfy Equation 7.37 at 3.0 m/s mixture velocity is 0.2 to 0.4 dispersed water fraction, while at 4.5 m/s it is 0.25 to 0.4 dispersed water fraction. This range becomes smaller when higher *in situ* mixture velocity is used (i.e. when $U_{ml} = 1.11(U_{sw} + U_{so})$ at 4.5 m/s the 3Layer structure exists between 0.2 to 0.3 dispersed phase fraction. The 2Layer model could yield results in all experimental conditions studied with the use of the experimental values of holdup for the calculation of the phase fraction in the mixed layer.

In Figure 7.5 and Figure 7.6 results from the 2Layer and 3Layer models and the best fit that has been obtained from the homogeneous model (using Taylor's viscosity predictions in combination with Rozentsvaig' s modified friction factor) are compared with the experimental results at 3.0 and 3.5 m/s mixture velocity respectively in the 38 mm ID SS pipe with the use of *EXXSOL™ D140*. The graphs are divided in three regions: oil continuous, water continuous and the transitional region. Pressure gradient has been plotted against input oil fraction from 0.6 to 0.8, as it was found that it is only between this region that the 3Layer model actually has a solution.

To enhance the understanding on how the three regions in Figure 7.5 and Figure 7.6 were drawn, a schematic description of phase inversion can also be seen in Figure 7.5.

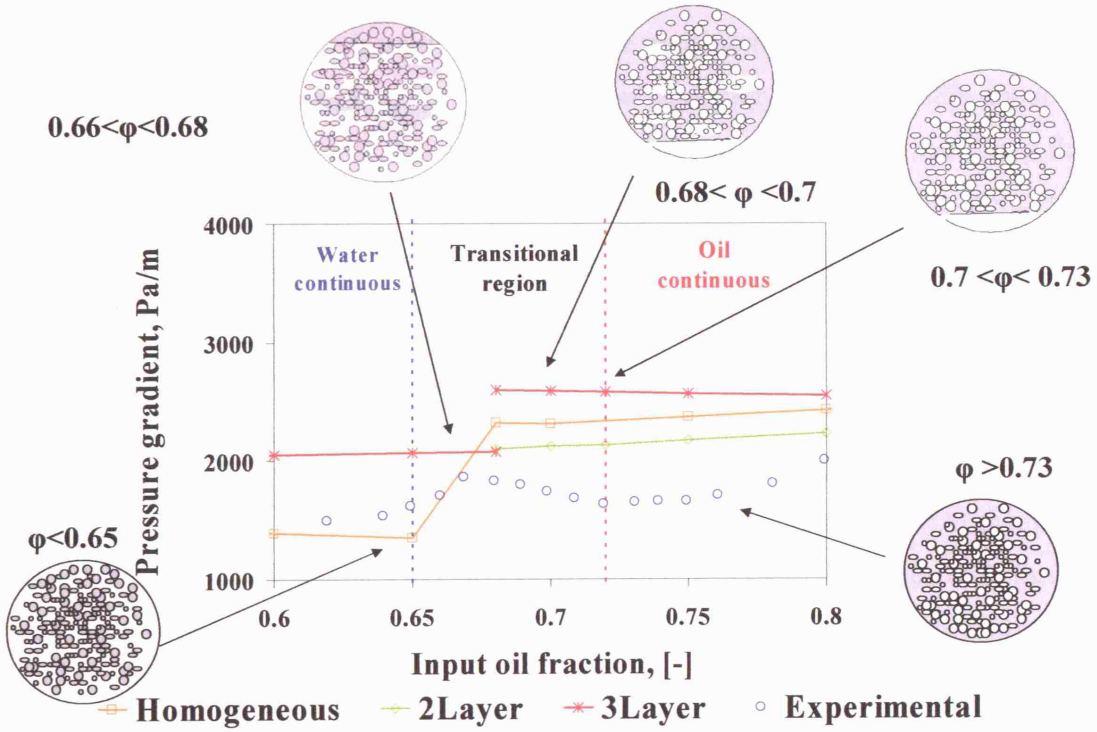

Figure 7.5 Predicted and experimental pressure gradient in the 38 mm ID SS pipe with the use of *EXXSOL™ D140* and schematic description of the phenomenon of phase inversion. Homogeneous, 2Layer and 3Layer model results against input oil fraction at 3.0 m/s mixture velocity. The mixed layer is considered water continuous up to 0.68 input oil fraction, where it inverts to oil continuous.

The schematic corresponds to the experimental observations (and not the 2 or 3Layer models). Starting from high input oil fractions, all conductivity probes are indicating fully dispersed oil continuous flow. This is true until approximately 73% input oil fraction. For input oil fractions higher that 73%, it is believed that the flow is best described by the homogeneous model, however the 2 and 3Layer models have also been applied, assuming that most of the pipe cross sectional area is occupied by the oil continuous mixture with some water possibly on the bottom of the pipe (2Layer model) and an additional single phase oil layer with no drops on top for the 3Layer model.

At 72% input oil fraction at this mixture velocity, the flush hot-film probe at the bottom of the pipe is indicating high voltage, implying that the bottom of the pipe is now wetted by water. The pipe core is still dominated from the oil continuous mixture. It is believed that from this point on, the transitional inversion region begins, and the flow can be described by a layered flow approach better. At 68% input oil fraction, large oscillations at the values of conductivity are recorded, indicating that some large water structures might be present within the oil continuous core, also verified by the large chord lengths recorded before inversion by the dual impedance probe (described in Section 5.4). With a slight decrease in the oil fraction, the conductivity values now indicate water continuous mixture in the whole pipe cross sections, while some oil might be left at the top of the pipe (seen in the schematic at 67% oil) and some oil formations in the water continuous mixture. The flow is still described better by a layered flow, but now the pipe is water dominated. At this point the velocity ratio increases in value and large chord lengths are measured. With further decrease, the large formations are not seen any more and the flow is water continuous with a uniform distribution of oil droplets at the whole cross section, described better from the homogenous model once more.

The predictive models have been applied for the whole range of volume fractions where they have a solution, and results are shown for all fractions around inversion. The 2Layer model did not give results with the current assumptions in the water continuous region. For the transition between oil and water continuous mixed

layers (at 68% input oil fraction) the experimentally found inversion point was used. In case the inversion point is not known, the Yeh *et al.* (1964) model can be used.

It is obvious from both Figures 7.5 and 7.6 that all models are overpredicting pressure gradient in the pipe especially in the area of the oil continuous flow, where a strong drag reduction was seen experimentally for the SS pipe. The 3Layer approach is overpredicting pressure gradient even in the water continuous region. From both graphs, it appears that the 2Layer approach (combined with the Taylor model for mixture viscosity and the Rozentsvaig model for a modified friction factor) is giving results closer to the experimentally obtained pressure drop in the oil continuous region at both mixture velocities.

In addition, in the region close to inversion it is the 2Layer model that gives in all cases predictions closer to the experimental results, while the homogeneous model yields good results in the water continuous region. Agreement with the experimental findings tends to be slightly better with increasing mixture velocity for all models.

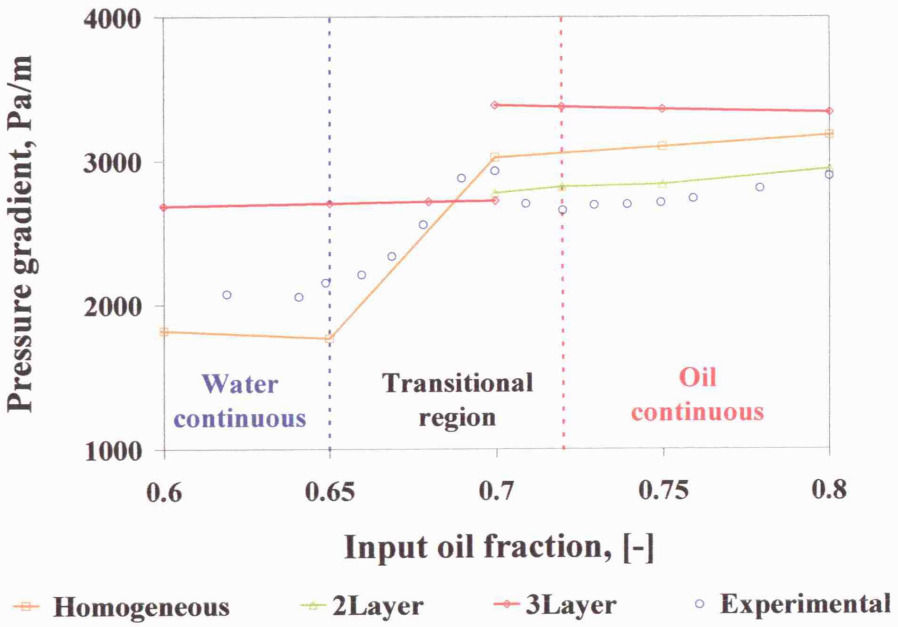

Figure 7.6 Predicted and experimental pressure gradient in the 38 mm ID SS pipe with the use of *EXXSOL™ D140*. Homogeneous, 2Layer and 3Layer model results against input oil fraction at 3.5 m/s mixture velocity. The mixed layer is considered water continuous up to 0.7 input oil fraction, where it inverts to oil continuous.

Table 7.3 summarises results obtained in the same experimental facility at different mixture velocities just before inversion (points identified experimentally) with the 2Layer and 3Layer models. The calculated heights with the 3Layer model for the single phase layers are about 10 mm for the single phase oil and 5 mm for the single phase water. It is believed that these values are not impossible close to inversion, as it might be that the newly formed, initially thin, water layer will gradually spread in the cross section (transitional oil continuous region), and water will eventually become the dominating phase in the cross section (transitional water continuous region). It is however, rather unlikely that both layers are single phase water (or oil) layer, since some oil (or water respectively) droplets should be expected for such layer thickness (verified from the dual impedance probe and the results from drop size measurements in Chapter 5, which indeed showed presence of drops).

As can be seen from Table 7.3 the heights of the single phase layers predicted by the 3Layer model at inversion point do not seem to depend on mixture velocity.

Table 7.3 Single phase layers height and pressure gradient predictions at inversion point and percentage error for pressure gradient predictions obtained by the 2Layer and 3Layer model.

	3Layer model		**2-layer model**	
Usm (m/s)	**3.0**	**3.5**	**3.0**	**3.5**
***hw* (mm)**	5.6	5.5	1.8	4.2
***ho* (mm)**	10.22	10.16	(-)	(-)
Predicted DP (kPa/m)	2.31	3.38	2.12	2.77
Experimental DP(kPa/m)	1.81	3.01	1.81	3.01
DP%error	+50%	+13%	+47%	-8%

Similar results were obtained for the 60 mm ID SS pipe at NTNU with the use of *MARCOL*^{TM}*52* and can be seen in Figure 7.7 for 3.5 m/s and Type I experiments (that started from oil continuous). In this experimental facility the instrumentation

available could not give any details of the flow structure. Thus, all models are applied for the input oil fractions where they provide results, while the transitional region is related to the start of the decrease in the experimental pressure gradient. The water continuous region is related to the increase in pressure gradient (that coincides with the second increase in the conductivity value recorded, as described in Section 4.2).

Again all models overpredict the pressure gradient in the oil continuous region within the transitional region, while the 2Layer model gives results closer to the experimental data. The predicted with the 3Layer single phase water and oil layer heights are about 8 mm and 17 mm respectively, with the oil layer always having twice the thickness of the water layer, which is not surprising regarding the very high oil fraction in the mixture (about 75%). In the water continuous region within and beyond the transitional region, the homogeneous model agrees well with the experimentally obtained values. The 3Layer model cannot be applied anyway beyond the oil input fractions shown in the graph.

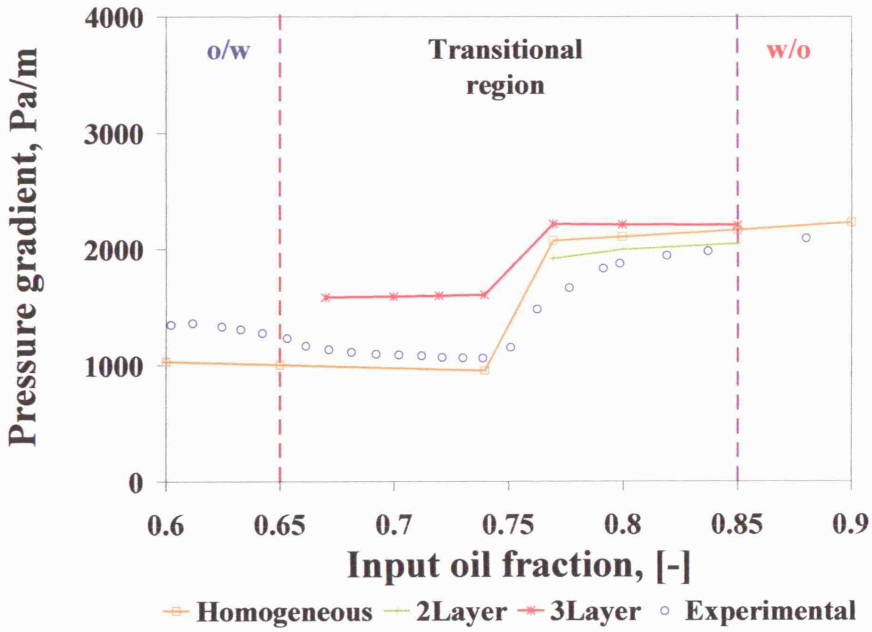

Figure 7.7 Predicted and experimental pressure gradient in the 60 mm ID SS pipe with the use of *MARCOL*^{TM}*52*. Homogeneous, 2Layer and 3Layer model results against input oil fraction at 3.5 m/s mixture velocity. The mixed layer is considered water continuous up to 0.75 input oil fraction, where it inverts to oil continuous.

Thus, the prediction of pressure drop by the 3Layer model does not agree very well with the experimental results as the predicted pressure gradient and the heights appear to be rather high. This could be due to the assumptions made:

a) The dispersed phase fraction is taken equal to the input; this would be a correct assumption if both single phase water and oil layers were sufficiently thin and there was no slip. It appears though that especially the oil layer is quite thick (thicker than the single phase water one) and if this is the case then, the *in situ* dispersed water phase fraction in the mixed layer would be expected to be higher than the input one, as less oil is in the mixed layer.

b) The *in situ* mixed layer velocity that was taken equal to 1.1 times the input mixture velocity based on experimental findings. Some sensitivity analysis was performed for the parameters of the UCL test section to investigate the effect of this value on the predicted pressure gradient and hold up. The height of the layers for all mixture velocities studied was found to be almost the same for the same phase fraction. In Figure 7.8 the pressure gradient predictions are plotted against dispersed phase fraction for different values of the *in situ* mixed layer velocity. It was found that as the mixed layer velocity increases the geometry of the three layers becomes less sustainable, and the region of volume fractions it can exist reduces. However, pressure gradient does not vary largely with *in situ* mixed layer velocity for mixture velocities 3.0 and 4.0 m/s.

Even though predictions from the 3Layer model are not satisfactory, the other two models applied in the current experimental flow facilities yielded good results, with the 2Layer model predictions being closer to the experimentally values. Not only the pressure but also the predicted water height have realistic values and imply that such layered structures can be proposed as a potential mechanism for inversion of oil/water dispersions in horizontal pipelines.

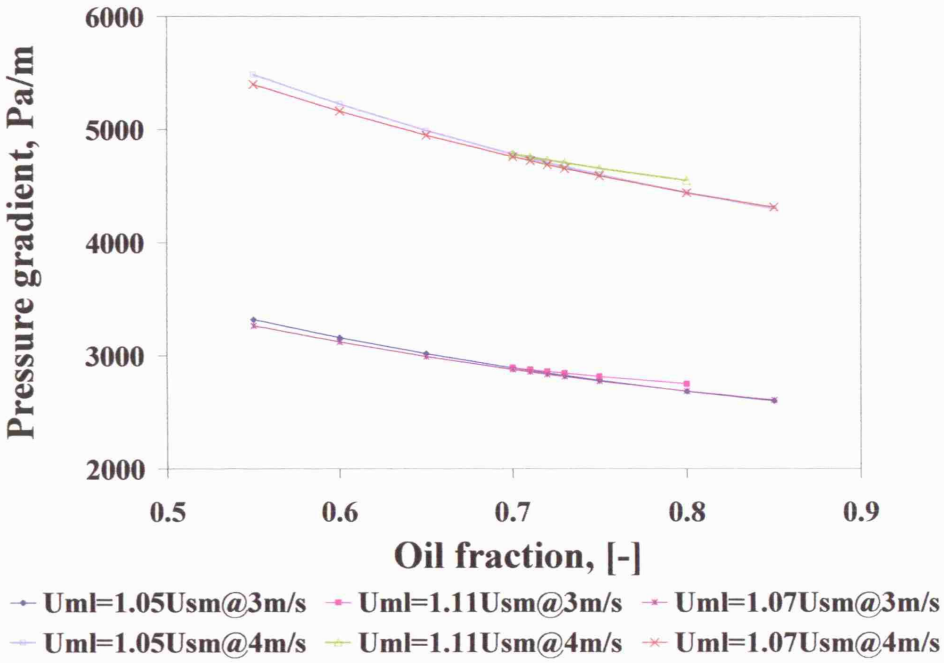

Figure 7.8 Sensitivity analysis for different values of the *in situ* mixed layer velocity for the 38 mm ID SS pipe with the use of *EXXSOL™ D140*.

7.6 CONCLUSIONS

The homogeneous model with various correlations for emulsion viscosity, and the new mechanistic 2Layer and 3Layer models have been applied for the prediction of pressure gradient around phase inversion. It was concluded that:

- The 3Layer suggested structure did not seem to predict the flow characteristics well. On the contrary, the homogenous model predicts reasonably well the pressure gradient of the experimental matrix while even better predictions can be made within the transitional region by using the 2Layer model.
- Some consideration should be made regarding the mixture viscosity and the drag reduction. It was found that Taylor's viscosity model that predicted mixture viscosity better than other models when combined with the modified friction factor by Rozentsvaig, yields good results.
- A layer structure is therefore suggested as a description tool for the flow characteristics of inversion in horizontal pipelines.

Chapter 8

Commercial feasibility study

8.1 OVERVIEW

The aim of this Chapter is to assess the business opportunity deriving from the developments achieved at the duration of this research project. An advanced diagnostic sensor that was designed and developed in-house to aid the investigations in liquid-liquid flows, has been proven to have unique advantages over other competing technologies, especially since it is able to handle opaque flows and materials and be permanently mounted on non-transparent pipes. At a time when the optimization of the oil production is of global focus, a great opportunity might arise from such a venture, also taking other chemical applications into account.

The commercial application of the newly developed dual impedance probe that obtains information on cross sectional phase distribution during two-phase flow, as well as drop velocity and dispersed drop size distribution was studied through the potential establishment of a spin-out company (called "Tri-Eye") that would develop and promote the product, first in the European market before entering others. The establishment of the company was scheduled for July 2006, thus the timeline that follows was adjusted accordingly. An executive summary of the spin out company can be found in Appendix E1, along with the proposed logo of the company. In the

following, the business concept is explained first (Section 8.2), and considerations regarding the intellectual property are then presented in Section 8.3. A suggested management team is presented in Appendix E4. The market analysis (Section 8.4) and the production strategy (Section 8.5) are also discussed in turn. A detailed development and marketing strategy is conducted in Section 8.6. Major competing technologies and methods are then compared and existing competitors are presented in Section 8.7. A detailed financing plan is suggested in Section 8.8, while the financial plan and exit strategy are given in Sections 8.9 and 8.10 respectively.

8.2 BUSINESS CONCEPT

VALUE PROPOSITION

The probe technology (called hereafter "Tri-Eye" technology) allows companies to reduce risk and costs when transporting oil/water mixtures through pipelines. Tri-Eye delivers savings to users through enhanced measurement benefits which provide economies of time, cost and accuracy.

CURRENT DEVELOPMENT STAGE

Tri-Eye technology is the result of a three year project performed in the Department of Chemical Engineering at University College London (UCL). An initial £50,000 was secured from EPSRC to conduct initial research and lab tests in the phase inversion field of interest, part of which was consumed towards the development and construction of the Tri-Eye technology. More specifically:

- Tri-Eye has completed laboratory testing and is ready to enter the field test stage.
- No company has yet been incorporated (planned for 2007).
- The Intellectual Property (IP) Rights to Tri-Eye belong to UCL. The technology has not yet been patented. Further steps have been made towards this direction and the founders are now in contact with the Technology Transfer Office (TTO) of UCL[8.1].

[8.1] In contact with Peter Sinden, Senior Technology Transfer Manager, UCL Ventures.

PRODUCT DESCRIPTION

The Tri- Eye probe consists of three parts (also described in Section 3.6.2):

- One/two traversing needles that are housed on the side of the pipe.
- An instrumentation box to acquire measurement readings that is then connected to a PC where logging and further processing is conducted.
- An associated software programme developed specifically for probe measurement activities, easily adjustable to the customer's needs.

This probe, which is based on impedance, is incorporated on the pipe. The needle(s) traverse the cross-section of the pipe in order to take measurements at any point at the pipe cross sectional area, obtaining detailed, accurate and local results.

Tri-Eye can be configured according to specific end-customer needs. Its software and after-sale support service provision will be bundled together and sold as a package to end-users.

UNIQUE BENEFITS TO END-USERS

Tri-Eye provides versatile measurement of critical variables in the transport of oil/gas/water mixtures.

- The technology can be used with plastic as well as steel pipes (or other non-transparent materials).
- It provides high accuracy even at high mixtures velocities, where mixture can be opaque.
- Three critical variables can be measured with just one apparatus.

These latter critical variables, which influence cost and risk, include:

- Phase distribution: the exact concentration of each of the two phases (oil/gas and water) in the pipe cross-sectional area (i.e. the way water

and oil/gas are spread physically through the pipe and the exact percentage of each phase at each point).

- Velocity profile: the speed at which the dispersed phase (oil or water droplets) is flowing through the pipe.
- Drop size: the size of the dispersed phase drops/bubbles (oil/gas or water) at any point in the pipe cross sectional area.

Of key additional importance is the fact that measurements are obtained online with the current technology: Tri-Eye can be permanently fixed on the side of the pipe, providing continuous measurement at any required point within the pipe. A more detailed description of the employed technology can be seen in Appendix E2.

Existing technologies provided by competitors are limited in functionality and range of measurements. Furthermore, competitor technology can only achieve accuracy under specific conditions. Based on the initial research, Tri-Eye believes that no competitor technology can provide easy, simultaneous measurement of these three variables through a single probe.

A market gap therefore exists for a comprehensive and reliable solution. By providing a single specialised product and specialised services, Tri-Eye will become a preferred supplier to the industry and the R&D market.

8.3 INTELLECTUAL PROPERTY

PATENT ISSUES

The Intellectual Property to Tri-Eye (the "IP") has yet to be secured and the founding team has started discussions with the UCL TTO[8.1]. After having completed a search in patent databases, there is no similar protected technology/apparatus. Thus, in order to secure the IP, one patent covering two aspects will be filed:

1. *The "method":* related to the way in which the electrical signal is eventually converted into a drop/bubble size distribution curve (the main scientific feature of the product). This is linked to the developed software, but mainly to the theory behind it (relating the

measured chord length of the dispersed droplets/bubbles to actual drop/bubble size readings - the Know-How). This will be the main defence against potential duplication by rivals.

2. *The "apparatus":* related to the actual configuration used together with the electrical circuit and logging system. This aspect of the patent will refer to the mechanical construction of the probe, the materials used in order to construct and mount the probe, along with the wiring and the circuit.

Patenting a technology is subject to prior due diligence. The process takes time and varies in costs. The TTO at UCL takes responsibility for related cost and other matters. The patent process diagram in Appendix E3 indicates time and cost of patenting (costs are shown exclusive of VAT and patent agent charges).

It should be mentioned here that the initial file application can be done within a week from submission and, as soon as this is done, the technology is fully protected in the whole of Europe. In case a US patent is not yet held, filing a patent in Europe still prevents replication in the US as a result of relative national legislation for intellectual properties rights. Production can therefore commence before the completion of the patenting process.

OWNERSHIP OF IP

Tri-Eye has arisen from research at University College London. It has been generated as a result of funding obtained by UCL and through the extensive use of UCL resources. The costs of the patent will be covered by the TTO of UCL. Costs for a patent do vary, but the estimated value is £50,000 (paid by UCL), an amount that will be then compensated through an equity stake in any future founded company. As a consequence, the IP rights belong to UCL, even in the event of hypothetical bankruptcy/liquidation.

However, people or companies who contribute to the creation of a spin-out company built around UCL technology will receive an equity stake in that company. The exact stake received depends on the individual's contribution in developing the

initial IP, their level of on-going involvement after the company has been formed and the number of people involved. Spin-out companies invariably require external investment and the level of capital committed to the company will also impact on the equity splits.

8.4 MARKET ANALYSIS

TARGET MARKET SEGMENTS

Within the broad market for multiphase flow analysis technologies, Tri-Eye targets two market segments: the oil industry segment and the food/beverage industry segment. The market research is focused on the oil industry segment with the food/beverage segment as a potential upside opportunity to be developed at a future stage.

Oil industry: A detailed industry analysis with the application of the Porter's five forces on a macrolevel has been conducted and can be found in Appendix E5. Tri-Eye targets R&D research centres studying multiphase characteristics of liquid/liquid and liquid/gas flows[8.2].

The company will target the oil industry segment for the following reasons:

- High segment attractiveness (see Appendix E5 for further details).
- The imperative and proven need for such a product.
- The background of the technology.
- Easily leveraged experience and expertise of the management team.

The company will target the market through both oil companies' in-house R&D centres and University Labs (which conduct either independent or funded from the oil industry research). Tri-Eye estimates market size for the product at **between**

[8.2] Interviews with industry experts (Dr Lee Rhyne, Chevron; Olga Saenko, NiPiNefteGas), have shown that the product will be used primarily by oil industry labs and R&D centres, but not at the oil field directly.

$29 million and $37 million. This number was derived from the total budget spent by the industry on oil production related research (see Appendix E6 for details)[8.3].

Food/beverage industry: Initial research has shown that the product has received interest in production procedures where droplet size and distribution are important for quality (taste and feel), shelf life and emulsion stability of products. This applies to mayonnaise, margarine and beer production[8.4], (an example of the latter is dissolving O_2 in Wort, a sugar solution to be fermented) as well as dissolving CO_2 back into beer before bottling. As a consequence, there is potential commercial interest from brewery equipment designers.

MARKET DRIVERS

The size of the flow analysis market is driven by oil industry investments in R&D. These investments are related strongly to production and revenues by oil companies. In recent years, this R&D expenditure trend has been upward as a result of existing oil well production optimisation, increased supply to new growing economies (i.e. China, India), and by the strong performance of oil prices. According to the US Energy Information Administration, the crude oil price has increased from $30 to $60 per barrel over the last 3 years (and is further increasing daily).

The market size has been found with a top down approach starting with the evaluation of the global oil industry R&D budget and calculating which percentage of this budget is spent on flow analysis related instrumentation. Figure 8.1 summarises assumptions and approaches used to calculate the global number of probes sold in the target market each year and the respective lump sum, while the detailed derivation is described in Appendix E6.

MARKET GROWTH RATE AND SHARE

The analysis of the characteristics of the probe in comparison to competing products has demonstrated that the company has a superior technology/product to the

[8.3] The market size estimate does not include independent research usage incurred by University Labs – a potential upside.

[8.4] Interview with Mr Willem van Waesberghe, MSc, MBA and Mr Gary Freeman, senior engineer, Heineken and Brewing Research International.

nearest competitors[8.5]. Therefore, the Tri-Eye team believes that the product will be differentiated and gain market share rapidly.

The aim is to reach 15% of the total flow analysis market. This total has been estimated to be 2,211 instrument units at the beginning of 2007 and will grow by 2% each year (see Table 8.1). This market share will be achieved within 6 years, assuming a continuous steady growth. From the third year of production onwards, a company expansion has been planned in order to increase probe production and meet market share targets.

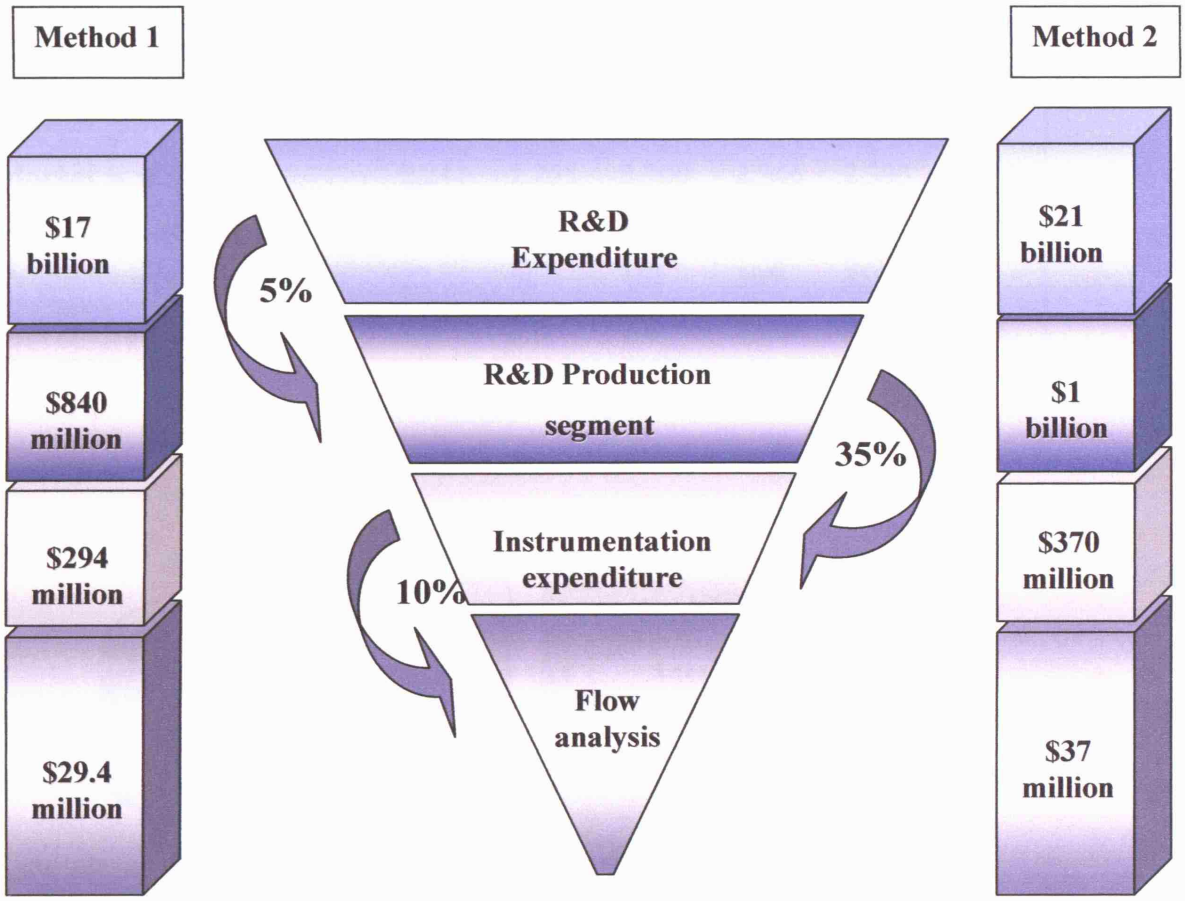

Figure 8.1 The instrumentation for multiphase flow market top-down analysis. Assumptions and details can be found in Appendix E6.

[8.5] Internet research, Survey Results.

The projection of market growth and market share are shown in Table 8.1.

A key element for the market analysis was also the survey that was conducted revealing the frequency in which people involved in the field might purchase instrumentation related to flow analysis (Figure 8.2 summarises the results). The answers to these questions are biased to some extent as some of the people in the sample are only involved in theoretical aspects of multiphase flow, which practically means that they have never bought such equipment, raising the respective percentage up to 12%. The results are shown in the graph below and are discussed in Appendix E7.

Table 8.1 Tri-Eye market share (in number of probes).

Year	2007	2008	2009	2010	2011	2012
Market growth rate	2%	2%	2%	2%	2%	2%
Market size	2,211	2,255	2,300	2,346	2,393	2,441
Production growth rate (%)	100	100	200	10	10	10
Production (units)	22	68	161	305	359	366
Market Share (%)	1.0	3.0	7.0	13.0	15.0	15.0

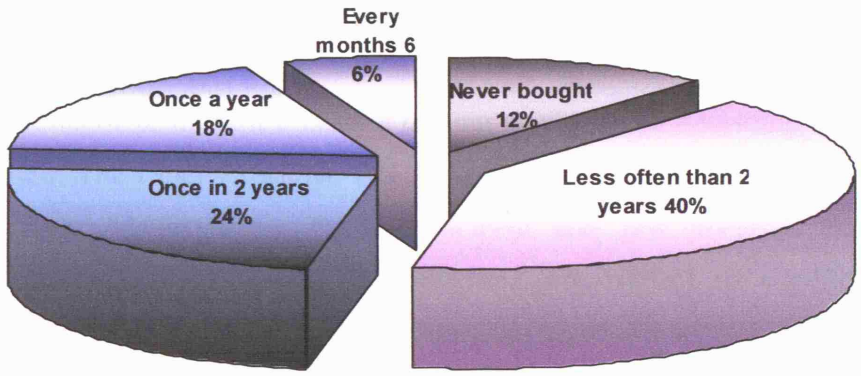

Figure 8.2 Flow analysis related instrumentation purchase frequency. Results obtained from the conducted survey within professionals in the oil industry and researchers at universities in different countries.

Justification of the proposed market share forecasts: Based on Tri-Eye's survey results:

- Very positive feedback on the equipment capabilities was received.
- Analysis of competing products has also confirmed a Tri-Eye advantage.
- The operational life of probes is 1-2 years, indicating a high replacement rate. The low cost structure allows providing probes at a very competitive price.

Therefore, Tri-Eye believes its market share growth rates to be reasonable.

8.5 PRODUCTION STRATEGY

Tri-Eye will be produced in-house at UCL premises (lab and offices)[8.6] in order to keep costs down, mitigate IP theft threats and generate synergies with after-sales support services. For the first three years of operation the Tri-Eye team envisages hiring three staff:

- 2 technical staff to manufacture Tri-Eye.
- 1 R&D technician to work on software application improvement and a more comprehensive interface.

The Management Team will oversee staff activities and take responsibility for initial after-sales support.

In terms of equipment a lathe, a milling machine and a welding machine will be purchased. The Chief Executive Officer (CEO) will take particular responsibility for production related issues. Staff, equipment and raw materials required to manufacture Tri-Eye are widely available and not subject to significant price fluctuations or shortages (see Appendix E5 for industry analysis).

Tri-Eye will continue to maintain a strong R&D focus within the production unit in order to improve products according to feedback obtained from the customers. This is fundamental to sustaining a competitive advantage.

[8.6] Confirmed by TTO UCL

COST STRUCTURE

Tri-Eye is a high margin, premium product as illustrated in the cost structure diagram (Figure 8.3). Three Tri-Eye style probes have already been constructed and used in the laboratory.

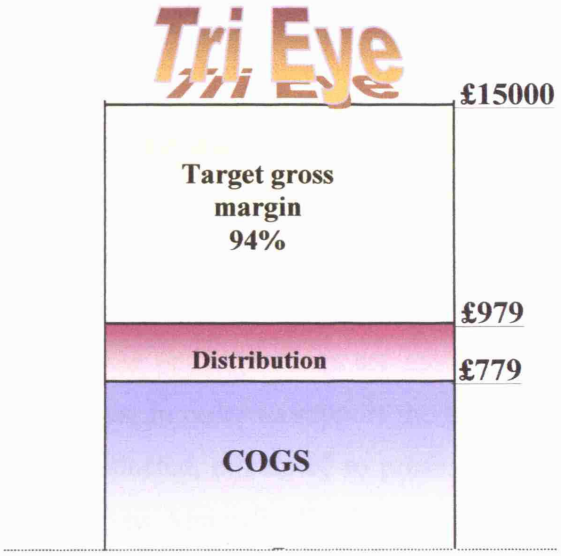

Figure 8.3 Tri-Eye cost structure diagramme and gross margin.

BESPOKE MANUFACTURING

Tri-Eye believes that this production strategy is appropriate for tailor made technology production as a few of Tri-Eye's characteristics may have to be re-adjusted according to specific end-user needs:

- *Probe length and diameter:* related to the implementation of the probe on the customer system.
- *Probe implementation method*: to enable the easy implementation of the technology on the pipe test section with less disturbance to normal activities.

Further details on Tri-Eye's production cost structure can be found in the financial model inAppendix E8: Gross margin analysis.

8.6 DEVELOPMENT & MARKETING STRATEGY

OVERVIEW

The timeline for creation and delivery of Tri-Eye to the market is outlined over the first one and half years. This forms the context and backdrop to the marketing strategy (Figure 8.4).

THE POSITIONING

Development of the Customer base: Tri-Eye's target customers are in-house labs of oil companies and external research centres all over the world that require the Tri-Eye technology to understand important flow characteristics. Tri-Eye's technology is needed in order to be able to predict the fluid mechanics (most important feature of which is pressure drop). These understandings are incorporated into design strategies and risk management policies. In order to support the company's positioning towards customers a survey was conducted, circulated to professionals in the oil industry and researchers at universities (see Appendix E7 for detailed analysis and summarising graphs). The results indicate that:

- Customers purchase probes for use approximately every 2 years.
- Customers become aware of up to date technology through either technical scientific conferences, tech magazines or from direct approaches from suppliers.

Customer Procurement decisions: Oil companies execute procurement decisions through their preferred list of suppliers (suppliers who have proved the attractiveness of their products through successful tests). Therefore, it is critical for the company to be on the preferred list of suppliers. Once the customers have used the products and are comfortable with them, it is relatively easier for suppliers to be re-selected. Universities do not have such strict criteria. Tri-Eye management team thus

plans to start selling the product to universities immediately with the founding of the company, also due to the fact that Tri-Eye has been proven to work on labs.

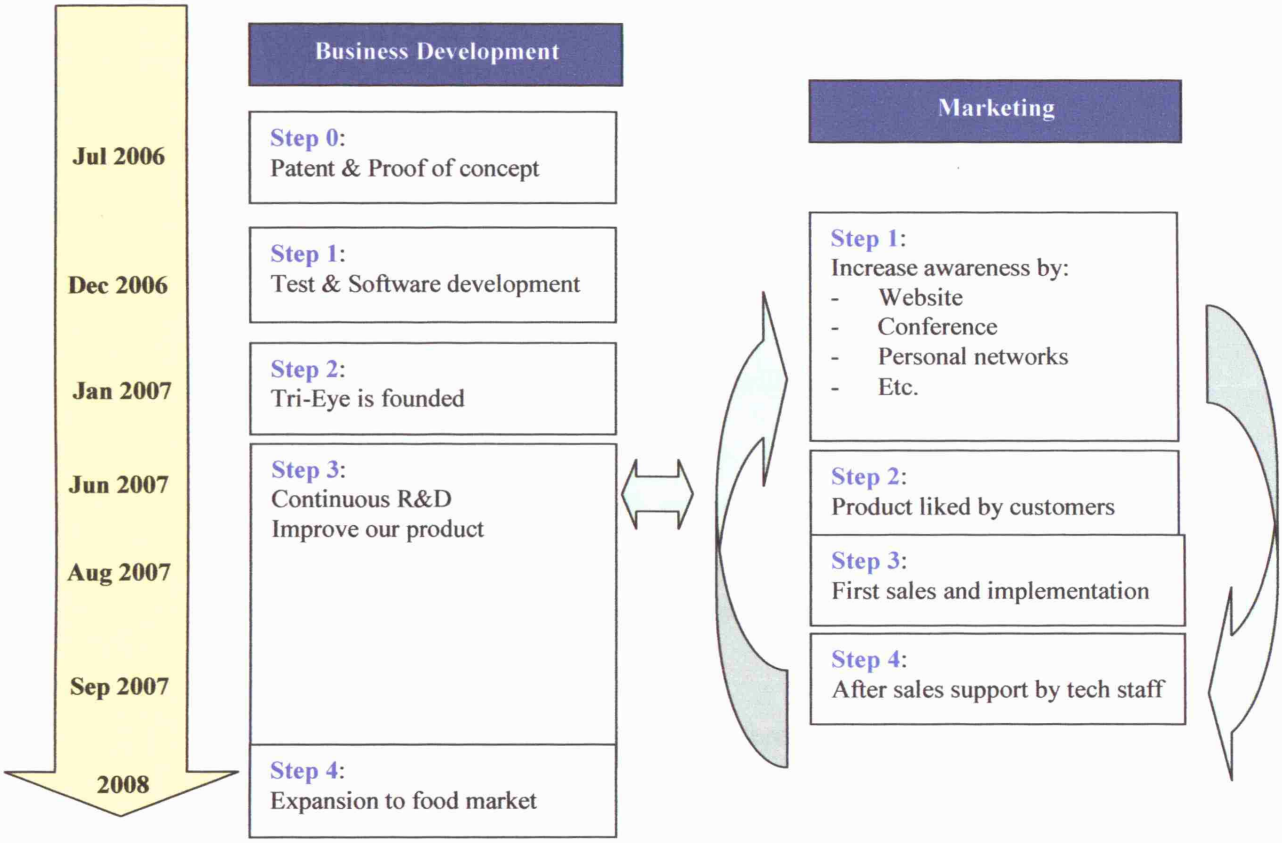

Figure 8.4 Tri-Eye's Business Timeline.

Further Development of the Capabilities: Tri-Eye needs to pass a trial test in order to achieve proof of concept. The company is currently examining two options: performance of the required tests in Kazakhstan using the Kazakhstan National Oil company's facility (through existing personal contacts of one of the suggested management team members) or use of a test facility in Norway (more expensive but more easily accessible). Tri-Eye aims to complete this phase within 6 months after raising the required amount of money through the first round of financing.

Consolidation of Competitive Position: Having already conducted a preliminary survey, Tri-Eye has confirmed its competitive advantage against existing

products and some universities have shown interest in purchasing the product. Section 8.7 contains further details on these issues[8.7].

CONQUERING THE MARKET

Product: Tri-Eye will compete on its functionality and accuracy of measurement based on proprietary technology.

Price: Tri-Eye targets an initial price of £15,000. This is based on competitor pricing and a target margin of 94%. Tri-Eye will discount its products for customers representing universities and academic institutions as such customers are sensitive to price.

Promotion: After the Test-Phase Tri-Eye will promote awareness of the products through the following channels:

- *Websites:* Tri-Eye team shall establish the company website with detailed information on the product. They shall link the website to popular websites for buyers of these technology products (such as Global Spec).
- *Conferences:* There are few major conferences related to flow analysis technology. All of the potential buyers attend these events and the team could have a chance to open a booth for explaining the products. Examples of conferences: SPE (Society of Petroleum Engineers), the International Conference of Multiphase Flow, European Meeting of Multiphase flow etc.
- *Personal networking:* The Tri-Eye team is in contact with several oil companies about their products through personal professional networks. They plan to reach other oil companies through these networks. The team plans to visit the premises of the personal connections in the industry and the academia to directly explain the merits of the products and perform trials. They will start from the big oil companies and other companies who have already demonstrated some interest.

[8.7] Market analysis questionnaire, see Appendix E7.

- *Publications:* There are several magazines/journals, which are related to the products and exposed to the potential buyers. Tri-Eye team will advertise in respectable tech magazines (International Journal of Multiphase Flow, Journal of Instrumentation, Chemical Engineering Science) etc, while at the same time scientific papers with results obtained from the probe on a lab basis will be published raising awareness.

Place: Tri-Eye will market and sell directly to end users using own in-house resources (i.e. the Management Team). A distributor will not be used at this stage because the direct relationship with end users will help the management team understand more about market potential and the potential improvement of the products. Tri-Eye will also use own resources for after-sales support, which the team believes will increase the chances of the customers repurchasing the products (more focused service).

8.7 COMPETITION

OVERVIEW

Tri-Eye competitors are the major diversified instrumentation suppliers for the oil industry. The universe of manufacturers is global and fragmented with around 30 manufacturers of related technology. Three companies stand out in particular:

- *Mettler Toledo:* American private company supplying research centres.
- *DANTEC Dynamics:* Danish private company supplying various industrial centres.
- *Forschungszentrum Rossendorf:* German private company making probes using an intrusive technique similar to Tri-Eye.

The first two companies make extensive chemical process related instrumentation including some visual analysis technology for particle/droplet characterisation. These companies benefit from strong and established R&D departments, credibility and established customer bases. They also have substantial financial resources and significant assets to bring new technology to the market.

None of these competitor firms appear to make a probe that holds all three features of Tri-Eye technology, instead manufacturing probe technologies for each one of the three different results that can be obtained by Tri-Eye. In addition, their associated measurement techniques are inferior (see below in Weaknesses of competitor technologies).

Competition in the flow analysis technology market is based on product feature and functionality rather than price. Industry players therefore prioritise innovation as a source of competitive advantage. Further analysis of the competitive industry structure is included in Appendix E9.

WEAKNESSES OF COMPETITOR TECHNOLOGIES

The most important technologies currently used for two phase (oil/water and gas/water) flow measurement are that of image analysis and light scattering methods. This technique works by capturing images of particles, bubbles or drops using high resolution cameras together with short pulse laser illumination to freeze the motion. Software then measures the particle size and shape and calculates the size distribution (see Appendix E9 for more details on competing technologies).

The disadvantage of such a technology is that it can only be used with transparent vessels/pipes and cannot work with stainless steel pipes, which are the majority of oil/water pipelines, or other non-transparent materials. Another disadvantage is that these systems can only be used where diluted mixtures are in place. Also, they cannot function in the case of high mixture velocities or high percentages of dispersed phases (oil or water). Some optical probes that can be used in-line and are intrusive in the flow like Tri-Eye's technology are made of tips that are very sensitive to fouling.

WHAT MAKES TRI-EYE DIFFERENT?

The weaknesses of the competitors are Tri-Eye's strengths. Not only can the product work at high mixture velocities, but it can obtain on-line real time results in any kind of pipe material, while at the same time it can conduct all three measurements (phase and drop size distribution and velocity profiles) at any point at the pipe cross sectional section, taking more accurate and local measurements. A value

curve has been drawn (Figure 8.5*)* in order to better illustrate Tri-Eye's differentiated features.

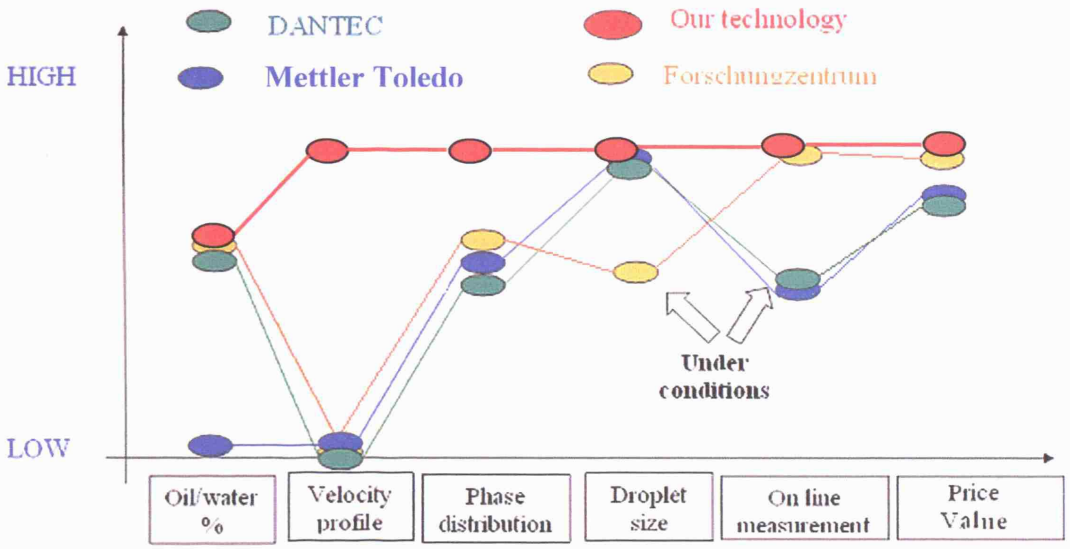

Figure 8.5 Value curve for Tri-Eye. Comparisons have been made only to the main competitors. Note: "Under Conditions" = only in dilute systems, transparent vessels and low mixture velocity.

STRATEGY FOR SECURING COMPETITIVE ADVANTAGE

Tri-Eye technology will gain competitive advantage on the basis of product differentiation protected by IP. The company will thus secure competitive advantage in three ways:

Specialisation: Specialise in the processing and interpretation of oil/water and water/gas systems and the continuous development of the apparatus and software. The goal is to be the best at creating customer value with the Tri-Eye technology and to develop a reputation of high reliability as soon as possible.

Adjustment to/selection of customers: Focus on customers that suffer from limitations because of their current use of technologies. At the same time, Tri-Eye will adjust the technology and the prices to the needs and the budgets available. The Tri-Eye team will work closely with customers on the development of specially designed

measurement systems in all areas of flow measurement and characterisation. Valuable research time and money can be saved when measurement instrumentation is optimized hand-in-hand with end-users for the application concerned.

Bespoke probe crafting: The optimisation process involves the design and manufacture of special components - either through the modification of standard products or the development of completely new ones - or the design, manufacture and installation of a complete integrated measurement system, which may include automatic traverse mechanisms.

8.8 FINANCING PLAN

USE OF PROCEEDS

The funding needs for Tri-Eye are summarised in Table 8.2 and are divided into two stages:

- Proof of concept: (June 2006-January 2007) GBP 220,000
- Commercial start: GBP 150,000 for the first year (January 2007-December 2007)

Table 8.2 Tri-Eye's funding needs for the two suggested rounds.

Items	Proof of Concept (GBP)	Commercial start (GBP)
Budgeted items	0	106,747
Patent registration	50,000	0
Test in Norway oil facilities	150,000	0
Travel costs	10,000	21,626
R&D (software)	10,000	21,626
Total	**220,000**	**150,000**

Commercial start includes purchase of materials, purchase of machinery, 6 month labour costs, overheads and company registration costs. A significant amount, GBP 43,253 is allocated for ad-hoc R&D, travel budget and contingency budget. The whole list of items is reported in Table 8.3.

Table 8.3 Start up use of proceeds (GBP).

Assumption	GBP
Machinery	1,883
Labour	82,500
Overheads	4,750
Start up costs	5,000
Materials	12,614.4
Travel	21,626
R&D	21,626
Total	**150,000**

FINANCING

Tri-Eye's management team envisages two financing rounds: one right before proof of concept and the other right before commercial start. The source of financing and respective amount are summarised in Table 8.4.

1ST FINANCING ROUND

It is expected that the five founding members of the suggested management team will contribute GBP 100,000 pro-rata amount. UCL will fund patent registration costs for GBP 50,000 in return for an equity stake. In addition, the management team will apply for UCL grant funding of GBP 25,000 to support commercialisation of technology.

The management team plans to obtain funds for GBP 45,000 from VC investors in return for stake in the enterprise. The equity structure will be split between 3 parties: the Founders, UCL and VC investors. The split in Equity structure is pro-rata to cash contributions to the enterprise.

Table 8.5 summarises further details.

The issue value of the shares will be 1 pound, so that the funds raised from the 1st round will be £195,000. This will be sufficient to support the project during the proof of concept stage.

Table 8.4 Financing plan.

Source	Seed Financing (GBP)	Commercial start (GBP)
Founders	100,000	150,000
UCL (patent registration funds)	50,000	
UCL (grant)	25,000	
VC investors	45,000	
Total	**220,000**	**150,000**

Table 8.5 Equity structure.

Name	Number of shares	Stake %
Founders	99,450.00	51%
UCL	50,700.00	26%
VC investors	44,850.00	23%
Total	195,000.00	100%

2ND FINANCING ROUND

During the second round, the estimated funding needs of GBP 150,000 will be requested from existing shareholders (Founders, UCL, VC investors). Relevant size of equity stakes and valuation of enterprise (pre-money, at the 2nd round) will be done after the successful completion of proof of concept stage.

8.9 FINANCIAL MODEL

Tri-Eye founding and management team has prepared a 6 year financial model which is included in Appendix E10-11. The projected period is from 2007 to 2012. By year 2012, the management team plans to reach production of 366 units (Table 8.6). The assumed market price per probe is GBP 15,000.

BASE CASE

In the base case, which assumes that Tri-Eye reaches projected sales volumes, achieve price targets and maintain cost consistency, the company will generate revenues of GBP 6.4 million by year 2012. Profit after tax will stand at GBP 4.2 million. Further financial data are presented in Appendix E11.

Table 8.6 Production plan.

Year	2007	2008	2009	2010	2011	2012
Number of units produced	22	68	161	305	359	366

SENSITIVITY ANALYSIS

Extensive sensitivity analysis demonstrated that the project is quite healthy and resistant to significant adverse conditions that may occur to sales volume or decreases in price. Table 8.7 shows Net Profit Value[8.8] (NPV) (75% discount rate) and Internal Rate of Return[8.8] (IRR) for the project assuming different combination of events (changes in Sales and Price), Terminal Value factor is 1. For detailed sensitivity tables see Appendix E10.

Table 8.7 Sensitivity analysis.

Scenarios	NPV	IRR
Sales volume (0%), Price (0%)	**645,110**	**188%**
Sales volume (-30%), Price (-20%)	**221,148**	**119%**
Sales volume (-40%), Price (-20%)	**144,935**	**105%**
Sales volume (-50%), Price (-30%)	**19,147**	**79%**
Sales volume (-60%), Price (-40%)	**-89,051**	**53%**

8.10 EXIT STRATEGY

OVERVIEW

Both sale to a strategic investor or an IPO within 3-5 years are exit opportunities that Tri-Eye envisages. Tri-Eye currently favours a trade sale as the optimal exit route.

- Acquisition of 100% of the company by either a flow analysis technology firm or a large, diversified technology company such as GE

[8.8] IRR: The rate of return that would make the present value of future cash flows plus the final market value of an investment or business opportunity equal the current market price of the investment or opportunity.

NPV: The present value of an investment's future net cash flows minus the initial investment. If positive, the investment should be made (unless an even better investment exists), otherwise it should not.

or Honeywell is the preferred option. A competitive action would allow synergies to be added to the company's valuation as well as premium developed through a competitive process

- A flotation on AIM or the London Stock Exchange could also be considered.

POSSIBLE EXIT VALUES

Tri-Eye has carried out an exit valuation analysis for the company in 2012. As there is lack of comparable quoted flow analysis technology companies, the Tri-Eye management team has presented a spread of multiples (Table 8.8) and associated IRRs for illustrative purposes.

Table 8.8 Exit in 2012: Company value and IRR.

Exit multiples	1	2	3	4	5	6	7
Company value (GBP million)	4.29	8.58	12.86	17.15	21.44	25.73	30.02
IRR	188%	189%	190%	191%	192%	193%	194%

8.11 CONCLUSION

Based on the above analysis it can be concluded that the newly developed instrument offers an exciting business opportunity to address a number of increasingly urgent issues regarding aspects of multiphase flow. Similar technologies might exist in the market but the high margin that this product offers along with its wide application and high accuracy makes it ideal for commercialisation. However, further investment will be needed for the business start - up, and for the continuous research and development in order to build a sustainable market position.

Chapter 9

Conclusions and Recommendations

9.1 OVERVIEW

Phase inversion in dispersed liquid-liquid flows in horizontal pipelines was investigated. The emphasis was on understanding the effect of parameters, such as mixture velocity, oil properties and pipe diameter and material on its appearance. New data regarding pressure drop, hold-up, drop size and flow patterns provide insights on how inversion is occurring at horizontal pipelines A number of probes were used to identify phase continuity at a point or over the whole pipe cross section. Based on experimental findings, mechanistic models based on layered structure of the phases were suggested for the description of the mixture behaviour near and at the inversion point.

A summary of the main experimental and theoretical conclusions is given below (Section 9.2), followed by recommendations or future studies (Section 9.3).

9.2 CONCLUSIONS

Experiments have been conducted at the experimental facility in the Department of Chemical Engineering at UCL and in the Department of Energy and Process Engineering at NTNU to investigate the phenomenon of inversion of highly dispersed oil/water mixtures in horizontal stainless steel, epoxy coated stainless steel

and acrylic pipelines of different diameters. Two experimental routes were followed: starting from oil or water continuous mixtures where the fraction of the dispersed phase was increased in small intervals until phase inversion point and beyond. This would reveal any hysterisis on the phenomenon. A variety of probes was used especially at UCL (namely local conductivity probe, flush probe, wetting probe, ring probes) that provided local and average information on phase continuity and the appearance of phase inversion in a pipe cross section or along the pipe. Pressure drop and holdup data were obtained. The velocity of the dispersed phase as well as dispersed phase droplet size distribution were also studied.

AT THE OCCURRENCE OF INVERSION

The use of the glue-on flush probe together with the traversing conductivity probe and the ring probes in the UCL facility has revealed that phase inversion does not happen simultaneously at the whole pipe cross sectional area (depending also on the properties of oil used), but gravitational effects result in more localised inversions. The use of many ring probes along the acrylic test sections also gave interesting results. More specifically:

- Phase inversion in horizontal pipelines is accompanied by large changes in the recorded pressure gradient along the pipe. The pressure gradient curve depends strongly on the oil properties and it was found that it was preceded by a large peak with the use of the less viscous *EXXSOL^{TM} D80*, while different behaviour was seen with the other two types of oil, with no peak appearing for the more viscous *MARCOL^{TM} 52*. The change in pressure gradient at inversion was still significant.
- An ambivalent behaviour was seen for the less viscous *EXXSOL^{TM} D80*, and not with the more viscous oils. This might be due to the fact that the less viscous oils have a greater propensity to form secondary dispersion.
- The change of the rheological characteristics of the mixture during phase inversion and thus, the abrupt change in the resulted pressure in

the system can affect significantly the flowrates. This at NTNU enhanced inversion.

- Inversion was found to occur over a range of input oil fractions for the UCL facility, while in was seen in one value of dispersed phase fraction at NTNU. This might be due to the operational characteristics in each system.
- The conductivity experiments showed that at the beginning of phase inversion there is a formation of a single phase layer of the phase that is about to become the continuous, at the respective side of the pipe (upper or lower depending on gravity). This resulted in the suggestion of a mechanism for inversion, where a structure of two or three layers exists before the systems inverts.

FLOW ANALYSIS OF CONCENTRATED DISPERSIONS AND INVERSION

- There is a decrease at the value of velocity ratio at the inversion point for Type II experiments. The difference in velocity ratio before and after inversion becomes less with increasing mixture velocity.
- Velocity ratio was found to be more that 1 in most conditions studied.
- Most dispersed phase both in oil and water continuous mixtures was found at the core of the pipe. If the upper and lower parts of the pipe are compared, in water continuous mixtures more dispersed oil droplets were detected at the upper part of the pipe, while in oil continuous mixtures more water droplets were found at the lower part of the pipe.
- Drop size and phase distributions became more homogenous while smaller droplets were encountered with increasing mixture velocity.
- There was a significant increase of the dispersed drop size at the input oil fraction just before inversion at all mixture velocities studied, showing an extremely enhanced coalescence just before inversion.

EFFECT OF PARAMETERS ON PHASE INVERSION

The effect of mixture velocity, pipe diameter and material of construction, oil properties and dispersion initialisation conditions on phase inversion point and the accompanying pressure gradient were studied. These efforts have revealed that:

- Phase inversion is accompanied by significant changes in pressure gradient. The exact behaviour will depend mainly on the pipe material of construction and the properties of the fluid used.
- Increasing mixture velocity will result in more abrupt changes of pressure gradient at inversion.
- The dispersion initialization conditions seem to be able to affect strongly the inversion point for the less viscous oil and in large diameter pipes. No ambivalent range was seen in the 32 mm ID acrylic pipe or by using *EXXSOL™ D140* or *MARCOL™ 52* in any of the test sections.
- Pipe material was found to affect the inversion point, a behaviour that was related mainly to wetting characteristics. The epoxy coated SS pipe was found to behave similarly to the acrylic pipe.
- Phase inversion is seen to affect pressure gradient at lower mixture velocities in the acrylic than in the steel pipes.

The effect of different parameters on drag reduction was also investigated. It was found that pipe diameter, pipe material and type of dispersion would strongly affect drag reduction, while the type of oil did not have a large effect. More specifically:

- Acrylic pipes exhibit stronger drag reduction in the water continuous region, while the opposite is seen for the stainless steel and epoxy coated pipes.

- The type of oil does not seem to affect drag reduction for the same pipe in the water continuous region, but more viscous oils exhibit stronger drag reduction in the oil continuous region.
- Comparisons that were made for acrylic pipes of different diameters at same Reynolds number have revealed that drag reduction is higher for the larger acrylic pipe in the water continuous region and this was explained by the increased dispersed phase fraction in the larger pipe for the same Reynolds number.

CONCLUSIONS FROM THEORETICAL STUDIES

- Using the experimentally measured droplet sizes, the equal surface energy criterion of phase inversion did not seem to be applicable.
- The empirical correlation by Yeh *et al.* (1964) was found to predict the experimental findings satisfactorily, as long as no ambivalent range was present, in all experimental set ups used.
- The homogeneous model combined with the Taylor's prediction for emulsion viscosity and the modified friction factor by Rozentsvaig has been found to predict well the experimental pressure gradient.
- The introduced 2Layer and 3Layer flow structure can be applied to predict flow characteristics around the area of phase inversion. The 3Layer model overpredicts the pressure gradient (in comparison to the experimental values), while the 2-Layer model was found to predict the flow characteristics better, especially in the oil continuous region. The homogeneous model can be applied in both oil and water continuous regions with good agreement to the experimental values.

9.3 RECOMMENDATIONS

The obtained theoretical and experimental results helped towards the understanding of inversion at horizontal flows. However, further work would allow a deeper insight that will reveal all aspects of inversion. Regarding further experimental

work few parameters can yet be studied, while some improvements can be considered for the current experimental facility at UCL. More specifically:

- In the present study tap water and different model oils were used as test liquids. Thus, the presence of natural oil surfactants could not be accounted for. Therefore, the use of added surfactants in different quantities will vary the surface tension and enable its controlled study on phase inversion.
- Ionic strength is a parameter least studied in the literature of inversion. It is also expected to have great effect on the appearance of inversion due to its effect on breakup and coalescence of the dispersed phase droplets. The ionic strength of the tap water was not considered in this work. Thus, the use of ASME seawater is suggested.
- Parameters like oil properties and pipe material of construction and diameter were widely studied in this study. However, further investigation can contribute to set up a database towards the broader understanding of these parameters on phase inversion point and the way that inversion is occurring at horizontal pipelines. Considerations of crude oil on phase inversion experiments should also be particularly interesting.
- More drop size and phase distributions results should be obtained using the new dual impedance probe already developed.
- The effect of bends on phase inversion and drop size can be studied.
- It is believed that secondary dispersions strongly affect the appearance of inversion. Thus, considering the difficulty in obtaining droplet size results of secondary dispersions, a visual system should be implemented for this purpose.
- The constructed new electronic boxes allow the use of more than one ring probes; many more channels can now be logged in and the use of many probes simultaneously is enabled. This way, experiments on the

identification of the exact location of inversion downstream can now be conducted (information about occurrence of inversion along the pipe has already been obtained in this work from the NTNU facility).

IMPROVEMENTS TO THE CURRENT FACILITY

- Separation has to be further improved. A suggested solution would be to keep using the current separator vessel by keeping the height of the interface of the two liquids in the separator vessel low, so that oil in the outlet will be fully separated. The use of a second large water vessel is suggested in which water will flow right after the first separator, where it will be allowed to settle for some time. Fresh water can be continuously supplied to the water supply tank. This way the pumped water will be of excellent quality at all times during the experimental procedure.
- A very useful tool, the ring probes have been developed and used successfully in this study. However, a new design with edges from stainless steel flanges is believed to make the connection to the stainless steel section with the help of the tri-clamps use easier (the probes are described in detail in Chapter 3). The design has been submitted for construction.

At the duration of this project, a new system has been designed and constructed (the "small rig"), but was not used. The test section is made of acrylic with a 14 mm internal diameter, while 2 ring probes have also been designed and constructed in the 5 m long test section. Instead of the centrifugal pumps that have been used in this study, vein pumps that are believed to introduce low shear to the flow have been employed. This will allow easier study of the inversion phenomenon with variation of more parameters, as less liquid quantities are needed, while the separation is enhanced due to the special design of the separator vessel

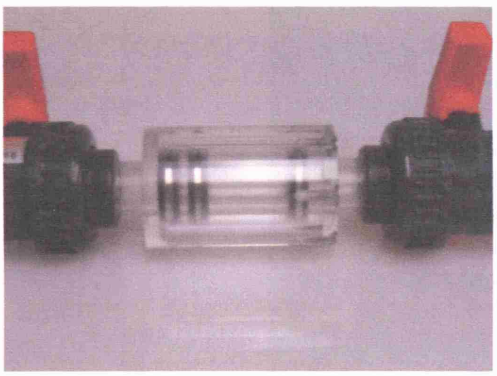

(a)

(b)

Figure 9.1 (a) Small test rig ring probes (b) The new test section beam that will support the test section.

Figure 9.2 Storage and supply oil and water vessels and the flowmeter sections that allows for smaller or larger flowrates.

Figure 9.3 The new vertical tank especially designed for enhanced separation.

Future work should also involve theoretical consideration of inversion. More specifically:

- Improvements of the suggested mechanistic models should be done to include the long structures that are seen to exist in the flow just before and after inversion (current findings are based on homogeneous mixed layer properties). Different combinations of layered structure just before inversion could also be investigated.
- Secondary dispersions should be taken into consideration.
- Numerical simulations should be done to predict the flow developments and the exact inversion point along the test sections.

References

Agterof, W. G. M., Vaessen, G. E. J., Haagh, G. A. A. V., Klahn, J. K., and Janssen, J. J. M., Prediction of emulsion particle sizes using a computational fluid dynamics approach, *Colloids and Surfaces B-Biointerfaces*, Vol. 31 (1-4), pp. 141-148, 2003.

Al-Wahaibi, T., Investigations on the transition between stratified to non stratified horizontal oil-water flows, *PhD* thesis, University College London, 2006.

Andreussi, P., Di Donfrancesco, A., and Messia, M., An impedance method for the measurement of liquid hold-up in two-phase flow, Int. *Int. J. Multiphase Flow,* Vol. 14, pp. 777-787, 1988.

Angeli, P., Liquid-liquid dispersed flows in horizontal pipes, *PhD Thesis, Imperial College London,* 1996.

Angeli, P., Hewitt, G.F., Pressure gradient in horizontal liquid-liquid flows, *Int. J. Multiphase Flow,* Vol. 24, pp. 1183-1203, 1998.

Angeli, P., and Hewitt, G.F., Flow structure in horizontal oil-water flow, Int. *J. of Multiphase Flow,* 26, pp.1117-1140, 1999.

Angeli, P., and Hewitt, G., Drop size distributions in horizontal oil-water dispersed flows, *Chem. Eng. Sc.,* Vol. 55, pp. 3133-3143, 2000.

Arashmid, M., and Jeffreys, G.V., Analysis of the phase inversion characteristics of liquid-liquid dispersions, *AIChE J.*, Vol. 26 (1), pp. 51-55, 1980.

Arirachakaran, S., Oglesby, K.D., Shoulam, O., and Brill, J.P., An investigation of oil water flow phenomena in horizontal pipes, *SPE Proc. Prod. Operation* Symp., SPE 18836, pp. 155-167, 1989.

Barnea, E., and Mizrahi, J., On the "Effective" Viscosity of Liquid-Liquid Dispersions, *Ind. Eng. Chem. Fundam.*, Vol.15 (2), pp. 120-125, 1976.

Beretta, A., Ferrari, P., Galbiati, L., Andreini, P.A., Horizontal Oil-Water Flow in Small Diameter Tubes. Pressure Drop, *Int. Comm. Heat Mass Transfer*, Vol. 24, No. 2, pp. 231-239, 1997.

Bouchama, F., van Aken, G.A., Autin, A.J.E., Koper, G.J.M., On the mechanism of catastrophic inversion in emulsions, *Colloids and Surfaces A: Physicochem. Eng. Aspects 231*, pp. 11-17, 2003.

Brauner, N., and Maron, D., Two phase liquid-liquid stratified flow, *PCH PhysicoChemical Hydrodynamics,* Vol. 11 (4), pp. 487-506, 1989.

Brauner, N., Two phase liquid-liquid annular flow, *Int. J. Multiphase Flow*, Vol. 17, pp. 59-76, 1991.

Brauner, N., and Maron, D., Pattern Transition in 2-phase liquid-liquid flow in horizontal tubes, *Int. J. Multiphase Flow*, Vol. 18, pp. 123-140, 1992.

Brauner, N., and Ullmann, A., Modelling of phase inversion phenomenon in two-phase pipe flows, *Int. J. Multiphase Flow*, Vol. 28, pp. 1177-1204, 2002.

Brinkman, H. C., The Viscosity of Concentrated Suspensions and Solutions, *J. of Chem. Phy.*, Vol. 20 (4), 571, 1952.

Brooks W. B., and Richmond, H. N., Phase inversion in non-ionic surfactant-oil water systems- I. the effect of transitional inversion on emulsion drop sizes. *Chem. Eng. Sci.* 49 (7), pp. 1053-1064, 1994.

Calabrese, R. V., Chang, T. P. K., and Dang, P. T., Drop Breakup in Turbulent Stirred-Tank Contactors Part I: Effect of Dispersed –Phase Viscosity, *AIChE J.*, Vol. 32 (4), pp. 667-676, 1986.

Chapman, F.S., and Holland, F. A., Liquid mixing and processing, pp. 208-210, Reinhold, 1966.

Charles, M. E., Govier, G. W., and Hodgson, G. W., The horizontal pipeline flow of equal density oil-water mixture, *Can. J. Chem. Eng.*, Vol. 39, pp. 27-36, 1961.

Charles, M. E., and Lilleleht, L. U., Correlation of Pressure Gradients for the Stratified Laminar-Turbulent Pipeline Flow of Two Immiscible Liquids, *Can. J. Chem. Eng.*, pp. 46-49, February, 1966.

Charles, M. E., and Redberger, P. J., The Reduction of Pressure Gradient in Oil Pipelines by the Addition of Water: Numerical Analysis of Stratified Flow, *Can. J. Chem. Eng.*, Vol. 40, pp. 70-75, April, 1962.

Chupin, G., An experimental investigation of multiphase gas-liquid pipe flow at low liquid loading, *Dr. Ing. Thesis*, NTNU, Trondheim, 2004.

Clarke, S. I., and Sawistowski, H., Phase inversion of stirred liquid/liquid dispersions under mass transfer conditions, *Trans. IChemE*, Vol. 56, pp. 50-55, 1978.

Collins, S. B., and Knudsen, J. G., Drop size distribution produced by turbulent pipe flow of immiscible liquids, *AIChEJ.*, Vol. 6, pp. 1072-1080, 1970.

Coulaloglou, C. A., and Tavlarides, L. L., Description of interactions processes in agitated liquid-liquid dispersions, *Chem. Eng. Sci.*, Vol. 32, pp. 1289-1297, 1977.

Cox, A. L., A study of horizontal and downhill two-phase oil-water flow, *M. S. Thesis.* The University of Texas, 1985.

Davies, G. A., Mixing and coalescence phenomena in liquid-liquid systems in science and practice of liquid-liquid extractions (ed. Thornton, J.D.), Vol. 1, pp. 244-342, Clarendon Press, Oxford, 1992.

Decarre, S., Ecoulements triphasiques en conduite horizontale, *Ph. D. thesis,* Institut National Polytechnique de Toulouse, France, 1997.

Deshpande, K. B., and Kumar, S., A new characteristic of liquid-liquid systems – inversion holdup of intensely agitated dispersions, *Chem. Eng. Sci.,* Vol. 58, pp. 3829-3835, 2003.

Dickinson, E., Shape Polydispersity in Concentrated Colloidal Dispersions, *J. of Colloid and Interface Science*, Vol. 83 (1), pp 305-306, 1981.

Dickinson, E., Thermodynamic Aspects of Emulsion Phase Inversion, *J. of Colloid and Interface Science*, Vol. 87 (2), pp. 416-423, 1982.

Dreher, T. M., Glass, J., O'Connor, A. J., and Stevens, G. W., Effect of Rheology on Coalescence Rates and Emulsion Stability, *AIChE J.*, Vol. 45 (6), pp.1182-1190, 1999.

Efthimiadou, I., and Moore, I. P. T., Phase inversion of liquid-liquid dispersions produced between parallel shearing plates, *Chem. Eng. Sci.*, Vol. 49, pp. 1439-1449, 1994.

Efthimiadou, I., Kocianova, E., and Moore, I. P. T., Behaviour of concentrated liquid-liquid dispersions in the tube flow and in static mixers, Proc. The 1994 ICHEME Research Event, Vol. 2, pp. 1020-1022, 1994.

Fakhr-Din, S. M., Phase inversion and drop size measurements in agitated liquid-liquid systems, *Ph. D.*, University of Manchester, 1973.

Ghorai, S., Suri, V., and Nigam, K. D. P., Numerical modeling of three-phase stratified flow in pipes, *Chem. Eng. Sci.*, Vol. 60, pp. 6637-6648, 2005.

Gilchrist, A., Dyster, K. N., Moore, I. P. T., Nienow, A. W., Delayed phase inversion in stirred liquid-liquid dispersions, *Chem. Eng. Sci.*, Vol. 44 (10), pp. 2381-2384, 1989.

Gillies, R.G., Sun, R. and Shook, C.A., Laboratory Investigation of Inversion of Heavy Oil Emulsions, *Can. J. of Chem. Eng.*, Vol. 78, pp. 757-763, 2000.

Giulinger, T. R., Grislingas, and A. K., Erga, O., Phase inversion behaviour of water-kerozene dispersions, *Ind. Eng. Chem. Res.*, Vol. 27 (6), pp. 978-982, 1988.

Groeneweg, F., Agterof, W. G. M., Jaeger, P., Janssen, J. J. M., Wieringa, J.A., Klahn, J.K., On the mechanism of the inversion of emulsions, *Trans IChemE*, Vol. 76, Part A, January 1998.

Guzhov, A. I., Grishan, A.L., Medredev, V. F., and Medredeva, O. P., Emulsion formation during the flow of two immiscible liquids in a pipe, *Neft Khoz*, Vol. 8, pp. 58-61, 1973 (in Russian).

Guzhov, A. I., and Medvedev, V. F., Pressure losses in flow of two mutually immiscible liquids, *Int. Chem. Eng.*, Vol. 11, No. 1, pp.104-106, 1971.

Hanzevack, E. L., and Demetriou, G. D., Effect of velocity and pipeline configuration on dispersion in turbulent hydrocarbon-water flow using laser image processing, *Int. J. Multiphase Flow*, Vol. 15, pp. 985-996, 1989.

Hinze, J. O., Fundamentals of the hydrodynamic mechanism of splitting in dispersion processes, *AIChE J.*, Vol. 1, pp. 289-295, 1955.

Hogsett, S., and Ishii, M., Local two-phase flow measurements using sensor techniques, *Nuclear Engineering and Design*, Vol. 175, pp. 15-24, 1997.

Hu, B., Ioannou, K., Matar, E. S., Hewitt, G. F., Angeli, P., Theoretical prediction with PBE of phase inversion in dispersed two-phase liquid systems, 3rd International Symposium on Two-phase Flow Modelling and Experimentation, Pisa, 2004.

Hu, B., and Angeli, P., Phase inversion and associated phenomena in oil-water vertical pipeline flow, *Can. J. of Chem. Eng.*, Vol.84 (1), pp. 94-107, 2006.

Hu, B., Matar, O. K., Hewitt, G. F., and Angeil, P., Population balance modelling of phase inversion in liquid-liquid pipeline flows, *Chem. Eng. Sci.*, Vol. 61 (15), pp. 4994-4997, 2006(a).

Hu, B., Angeli, P., Matar, O. K., Lawrence, C. J., Hewitt, G. F., Evaluation of drop size distribution from chord length measurements, *AIChE J.*, Vol. 52 (3), pp.931-939, 2006 (b).

Ioannou, K., Nydal, O. J., Angeli, P., Phase inversion in dispersed liquid-liquid flows, *Experimental Thermal and Fluid Science*, Vol. 29 (3), pp. 331-339, 2005.

Ioannou, K., Bin, H., Matar, O. K., Hewitt, G. F., Angeli, P., Phase inversion in dispersed liquid-liquid pipe flows, *Proc. 5th Int. Conf. on Multiphase Flow*, May 30-June 4, 2004.

Jayawardena S. S., Alkaya, B., Redus, C. L., and Brill, J. P., A new model for dispersed multi-layer oil-water flows, In *Proc. of BHR 2000, Multiphase Technology, Banff, Canada*, pp. 77-89, 2000.

Karabelas, A. J., Droplet size spectra generated in turbulent pipe flow of dilute liquid-liquid dispersions, *AIChE J.,* Vol. 24, pp. 170-180, 1978.

Klahn, J. K., Janssen , J. J. M., Vaessen, G. E. J., de Swart, R., Agterof, W. G. M., On the escape process during phase inversion of an emulsion, *Colloids and Surfaces A: Physicochem. Eng. Aspects*, Vol. 210, pp. 167-181, 2002.

Krieger, I. M., and Dougherty, T. J., A Mechanism for Non-Newtonian Flow in Suspensions of Rigid Spheres, *J. of Rheology*, Vol. 3 (1), pp.137-152, 1959.

Kubie, J., and Gardner, G.C., Drop sizes and drop dispersion in straight horizontal tubes and helical coils, Chem. Eng. Sci., Vol. 32, pp. 195-202, 1977.

Kumar, S., Kumar, R., and Gandhi, K. S., Influence of the wetting characteristics of the impeller on phase inversion. *Chem. Eng. Sci.*, Vol. 46, pp. 2365–2367, 1991.

Kumar, S., On phase inversion characteristics of stirred dispersions, *Chem. Eng. Sci.*, Vol. 51 (5), pp.831-834, 1996.

Lilleby, K., User manual for the Multiphase Flow lab, NTNU, Trondheim, 2001.

Liu, L., Matar, O.K., Perez de Ortiz, E.S., Hewitt, G.F., Experimental investigation of phase inversion in a stirred vessel using LIF, *Chem. Eng. Sci.*, Vol. 60 (1), pp. 85-94, 2005.

Liu, L., Matar, O., Lawrence, C. J., and Hewitt, G. F. Laser-induced fluorescence (LIF) studies of liquid–liquid flows. Part I: Flow structures and phase inversion, *Chem. Eng. Sci.*, 61, pp. 4007-4021, 2006a.

Liu, L., Matar, O., and Hewitt, G. F., Laser-induced fluorescence (LIF) studies of liquid–liquid flows. Part II: Flow pattern transitions at low liquid velocities in downwards flow, *Chem Eng. Sci.*, 2006b.

Lovick, J., Horizontal oil-water flows in the dual continuous flow regime, *PhD Thesis*, University College London, University of London, 2004.

Lovick, J., and Angeli, P., Experimental studies on the dual continuous flow pattern in oil-water flows, *Int. J. Multiphase Flow*, Vol. 30 (2), pp. 139-157, 2004.

Luhning, R. W., and Sawistowski, H., Phase inversion in stirred liquid-liquid systems, *Proc. Int. Solvent Extr. Conf., The Hague, Society of Chemical Industry,* London, pp. 873-887, 1971.

Luo, H., and Svendsen, H. F., Theoretical Model for Drop and Bubble Breakup in Turbulent Dispersions, *AIChE Journal*, Vol, 42 (5), pp. 1225-1233, 1996.

Luo, Y. S., Chen, T. K., Cai, J. Y., Frictional pressure loss and phase inversion point for oil-water emulsion in vertical tube, *In Proceedings*: Int. Symposium on Multiphase Fluid, non Newtonian Fluid&Physicochemical Fluid Flows, 3.53-3.58, 1997.

Manfield, P. D., Lawrence, C. J., and Hewitt, G. F, Drag reduction with additives in multiphase flow, *Multiphase Sci. and Tech.*, Vol. 11, pp.197-221, 1999.

Martinez, A. E., Intevep, S. A., and Arirachakaran, S, Shoham, O., and Brill, J.P., Prediction of Dispersion Viscosity of Oil/Water Mixture Flow in Horizontal Pipes, *SPE Proc. Prod. Operation Symp.*, SPE 18221, pp. 427-438, 1988.

McClarey, M.J., and Mansoori, G.A., Factors affecting the phase inversion of dispersed immiscible liquid-liquid mixtures, *AIChEJ Symposium Series*, Vol. 4, pp. 134-139, 1978.

Nädler, M., The pressure losses in multiphase flow of oil, water and gas in horizontal pipes, *PhD Thesis*, University of Hanover. Fortschritt-Berichte VDI, Reihe 7: Strömungstechnick No. 296, 1995.

Nädler, M., and Mewes, D., The effect of gas injection on the flow of immiscible liquids in horizontal pipes, *Chem. Eng. Technol.*, Vol. 18, pp. 156-163, 1995a.

Nädler, M., and Mewes, D., Intermittent Three-Phase Flow of Oil, Water and Gas in Horizontal Pipes, Proc. *Of the 5th International Offshore and Polar Engineering Conference*, The Hague, The Netherlands, June 11-16, pp. 72-80, 1995b.

Nädler, M., and Mewes, D., Flow induced emulsification in the flows of two immiscible liquids in horizontal pipes, *Int. J. Multiphase Flow*, Vol. 23, No. 1, pp.55-68, 1997.

Nixon, A.J., The influence of fat crystals on droplet coalescence in liquid-liquid food dispersions, *M Phil Thesis*, University of Birmingham, 1998.

Nienow, A. W., Pacek, A. W., Moore, I. P. T., Homer, J., "Fundamental studies of phase inversion in stirred vessels", *Proc. Euro. Conf. on Mixing, IChemE Symposium Series*, No. 136, pp. 171-178, 1994.

Norato, M.A., Tsouris, C., Tavlarides, L. L. Phase inversion studies in liquid-liquid dispersions, *Can. J. Chem. Eng.*, Vol. 76, pp. 486-494, 1998

Oglesby, K. D., An experimental study on the effects of oil viscosity, mixture velocity, and water fractions on horizontal oil-water flows, *MS Thesis*, The University of Tulsa, 1979.

Overbeek, J. Th. G., Verhoeckx, G. J., De Bruyn, P. L., and Lekkerkerker, N. W., On understanding microemulsions II. Thermodynamis of droplet-Type microemulsions, *J. of Colloid and Interface Science*, Vol. 119(2), pp. 422-441, 1986.

Owen, D. G., An experimental and theoretical analysis of equilibrium annular flows , *PhD Thesis*, University of Birmingham, Birmingham, pp.248-252, 1986.

Pacek, A. W., Nienow, A. W., Moore, I. P. T., On the structure of turbulent liquid-liquid dispersed flows in an agitated vessel, *Chem. Eng. Sci.*, Vol. 49(20), pp. 3485–3498, 1994.

Pacek, A. W., and Nienow, A. W., A problem for the description of turbulent dispersed liquid-liquid systems, *Int. J. Multiphase Flow*, Vol. 21(2), pp. 323–328, 1995.

Pan, L., Jayanti, S., and Hewitt, G.F., Flow patterns, phase inversion and pressure gradient in air-oil-water flow in horizontal pipe, *in: Proc.* 2nd Int. Conference on Multiphase Flow, Kyoto, Japan, 1995.

Pal, R., Bhattacharya, S. N., and Rhodes, E., Flow behaviours of oil-in-water emulsions, *Can. J. Chem. Eng.*, Vol. 64, pp. 3-10, 1986.

Pal, R., Pipeline flow of unstable and surfactant-stabilized emulsions, *AIChEJ.*, Vol. 39, (11), pp. 1754-1764, 1993.

Pal, R., Viscous behavior of concentrated emulsions of two immiscible Newtonian fluids with interfacial tension, *J. of Colloid and Interface Sci.*, Vol. 263, pp. 296-305, 2003.

Pal R. and Rhodes, E., Viscosity/Concentration Relationships for Emulsions, *J. of Rheology*, Vol. 33 (7), pp. 1021-1045,1989.

Perry, R.H., and Green, D., Perry's chemical engineering handbook 6th edition, McGraw Hill, New York, 1985.

Pettersen, B.H., Langsholt, M., and Ødegård, J., Pressure drop and wall wetting; the effect of pipe wall material in multiphase flow, *Proc.* 10th International Conference of Multiphase Flow, Cannes, France, 13-15 June, pp. 177-192, 2001.

Quinn, J. A., and Sigloh, D. B., Phase inversion in the mixing of immiscible liquids, *Can. J. Chem. Eng.,* Vol. 41, pp. 15–18, 1963.

Rice, O.K., The thermodynamics of non-uniform systems, and the interfacial tension near a critical point, *J. Phys. Chem.*, Vol. 64, pp. 976-983, 1960.

Roscoe, R., the viscosity of suspensions of rigid spheres, British journal of applied physics, pp. 267-269, 1952.

Ross, S., and Kornbrekke, R.E., Change of Morphology of a Liquid-Liquid Dispersion as a Stohastic Process, *J. of Colloid and Interface Sci.*, Vol 81 (1), pp. 58-68, 1981.

Ruckenstein, E., Thermodynamic Approaches to Microemulsions, *J. of Colloid and Interface Sci.*, 204, pp. 143-150, 1998.

Russell, T.W.F., Hodgsen, G.W., and Govier, GW., Horizontal pipeline flow of mixtures of oil and water, *Can. J. Chem.* Eng., 1959.

Russell, T.W.F., and Charles, M.E., The Effect of the Less Viscous Liquid in the Laminar Flow of Two Immiscible Liquids, *Can. J. of Chem. Eng.*, Vol. 37, pp. 18-24, February, 1959.

Salager, J.L., in "Encyclopedia of Emulsion Science", P.Becher, Ed., Vol. 3, p. 79, Dekker, New York, 1983.

Sajjadi, S., Zerfa, M., & Brooks, B.W., Morphological change in drop structure with time for abnormal polymer/water/surfactant dispersions, *Langmuir*, 16, pp. 10015-10019, 2000.

Sajjadi, S., Zerfa, M., & Brooks, B.W., Dynamic behaviour of drops in oil/water/oil dispersions, *Chem. Eng. Sci.*, Vol. 57, pp. 663-675, 2002.

Scott, G.M., A study of two-phase liquid-liquid flow at variable inclinations. *M Sc. Thesis*, The University of Texas, 1985.

Selker, A.H., and Sleicher, C.A. Jr., Factors affecting which phase will disperse when immiscible liquids are stirred together, *Can. J. Chem. Eng.*, Vol. 43, pp. 298-301, 1965.

Serizawa, A. and Kataoka, I., Dispersed flow- I. Paper presented at the 3rd Int. Workshop on Two Phase Flow Fundamentals. Imperial College London, 1992.

Sevik, M., and Park, SH., The splitting of drops and bubbles by turbulent fluid flow, J. Fluid Eng., *Transactions of the ASME*, March, pp. 54-59, 1973.

Simmons, M. J. H., and Azzopardi, B. J., Drop size distributions in dispersed liquid-liquid pipe flow, *Int. J. Multiphase Flow*, Vol. 27, pp. 843-859, 2001.

Simmons, M. J., Zaidi, S. H., and Azzopardi, B. J., Comparison of laser-based drop-size measurement techniques and their application to dispersed liquid-liquid pipe flow, *Optical Engineering*, Vol. 39 (2), pp. 505-509, 2000.

Shi, H., Cai, J. Y., and Jepson, W.P., Oil- Water distributions in large diameter horizontal pipelines, Multiphase Flow and Heat Transfer, *In Proc.* Of the Fourth International Symposium, Aug. 22-24, Xi'an, China, 1999.

Sleicher, C.A., Jr., Maximum stable drop size in turbulent flow, AICHeJ., Vol. 8, pp. 471-477, 1962.

Soleimani, A., Lawrence, C.J., and Hewitt, G.F., Effect of mixers on flow pattern and pressure drop on horizontal oil-water pipe flow, Int. Symp. On liquid-liquid Two Phase Flow and Transport Phenomena, Turkey, 1997.

Soleimani, A., Lawrence, C. J., and Hewitt, G.F., Spatial Distribution of Oil and Water in Horizontal Pipe Flow, *SPE Journal*, Vol. 5 (4), pp. 394-401, 2000.

Soleimani, A., Phase Distribution and Associated Phenomena in Oil-Water Flows in Horizontal Tubes, *PhD Thesis*, Imperial College London, 1999.

Su, H. T., and Hanzevack, E. L., A model of drop size distribution and maximum drop size in two phase liquid-liquid flow, *AIChE* Annual Meeting, Washington DC, 1998.

Taitel, Y., Barnea, D., and Brill, J. P., Stratified three-phase flow in pipes, *Int. J. Multiphase Flow*, Vol. 21, pp. 53-60, 1995.

Taylor, G. I., the Viscosity of a Fluid Containing Small Drops of Another Fluid, 1932

Tidhar, M., Merchuk, J. C., Sembira, A. N., Wolf, D., Characteristics of a motionless mixer for dispersion of immiscible fluids - II Phase inversion of liquid-liquid systems, *Chem. Eng. Sci.,* vol. 41, pp. 457- 462, 1986.

Trallero, J.L., oil water flow patterns in horizontal pipes, PhD Thesis, The University of Tulsa, 1995.

Trallero, J. L., Sarica, C., and Brill, J. P., A Study of Oil/Water Flow Patterns in Horizontal Pipes, *SPE Journal*, Vol. 12 (3), pp. 165-172, 1997.

Treybal, RE., Liquid Extraction, 1st Edition, McGraw Hill, New York, 1951.

Tsouris, C., and Tavlarides, L. L., Breakup and coalescence models for drops in turbulent dispersions, *AICheJ*, Vol. 40 (3), pp. 395-406, 1994.

Utvik, O. H., Valle, A., Rinde, T., Pressure Drop, Flow Pattern and Slip for a Multi-Phase Crude Oil-water-Hydrocarbon Gas System, *Proc. 3rd Int. Conf. Multiphase Flow*, Lyon, 1998.

Vaessen, G. E. J., and Stein, H. N., The Applicability of Catastrophe Theory to Emulsion Phase Inversion, *J. of Colloid and Interface Science*, Vol. 176, pp.378-387, 1995.

Vaessen, G. E. J., Visschers, M., Stein, H. N., Predicting Catastrophic Phase Inversion on the Basis of Droplet Coalescence Kinetics, *Langmuir*, Vol. 12, pp. 875-882, 1996.

Valentas, K. J., Bilous, O., Amundson, N. R., Analysis of breakage in dispersed phase systems, *Ind. Eng. Chem. Fundamentals*, Vol. 5, pp. 271-279, 1966.

Valle, A., and Kvandal, H.K., Pressure drop and dispersion characteristics of separated oil-water flows, Int. Symp. on Two Phase Flow Modelling and Experimentation, Rome, 1995.

Valle, A., and Utvik, O.H., Pressure drop, flow pattern and slip for two phase crude oil-water flow, Int. Symp. on Liquid-Liquid two Phase Flow and Transportation Phenomena, Turkey, 1997.

Valle, A., Multiphase pipeline flows in hydrocarbon recovery, *Multiphase Sci&Tech,* Vol. 10, pp. 1-139, 1998.

Wang, C.Y., and Calabrese, R. V., Drop Breakup in Turbulent Stirred-Tank Contactors Part II: Relative Influence of Viscosity and Interfacial Tension, *AIChE J.*, Vol. 32 (4), pp. 657-666.

Watanabe, K., Yanuar, Ohkido, K. and Mizunuma, H., Drag reduction in flow through square and rectangular ducts with highly water repellent walls, *In Proc. ASME FED* Summer meeting on Turbulence Modification and Drag Reduction, FRD-237, Vol. 2, pp. 115-119, 1996.

Watanabe, K., Yanuar, and Udagawa, H, Drag reduction of Newtonian fluid in a circular pipe with a highly water-repellent wall, *J. Fluid Mech.,* Vol. 381, pp. 225-238, 1999.

Ward, J. P., and Knudsen, J.G., Turbulent flow of unstable liquid-liquid dispersions: drop sizes and velocity distributions, *AIChE J.*, Vol. 13, pp. 356-365, 1967.

Yeh, G.C., Haynie, Jr., F.H., Moses, R.A., Phase volume relationship at the point of phase inversion in liquid dispersions, *AIChE J.*, Vol. 10 (2), pp. 260-265, 1964.

Yeo, L.Y., Matar, O.K., Perez de Ortiz, E.S., Hewitt, G.F., Simulation studies of phase inversion in agitated vessels using a Monte Carlo technique, *J. of Colloid & Interface Sci.*, Vol. 248, pp. 443-454, 2002.

Zaldivar, J. M., Alos, M. A., Molga, E., Hernandez H., and Westerterp, K. R., The effect of phase inversion during semibatch aromatic nitrations, *Chem. Eng. And Proc.*, Vol. 34, pp. 529-542, 1995.

Appendix A

Physical properties

BACKGROUND

Surface tension is a measurement of the cohesive energy present at an interface. The molecules of a liquid attract each other. The interactions of a molecule in the liquid are balanced by an equal attractive force in all directions. Molecules surface of a liquid experience an imbalance of forces as indicated below.

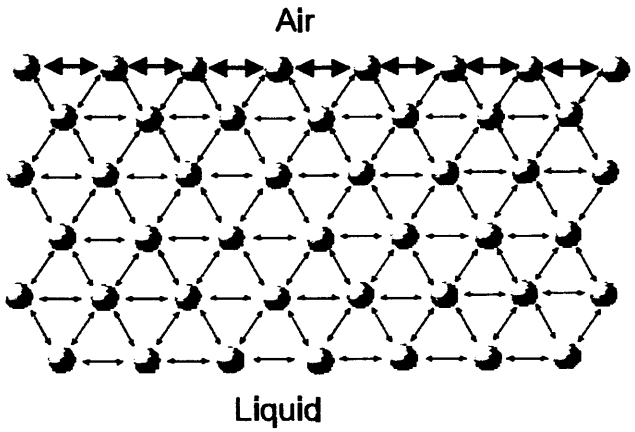

Figure A.1 Molecules' forces.

The net effect of this situation is the presence of free energy at the surface. The excess energy is called *surface free energy* and can be quantified as a measurement of energy/area. It is also possible to describe this situation as having a line tension or surface tension which is quantified as a force/length measurement. The common units for surface tension are dynes/cm or mN/m. These units are equivalent. This excess energy exists at the interface of two fluids. If one of the fluids is the vapour phase of a liquid being tested the measurement is referred to as *surface tension.* If the surface investigated is the interface of two liquids the measurement is referred to as *interfacial tension.* In either case the more dense fluid is referred to herein as the 'heavy phase' and the less dense fluid is referred to as the 'light phase'. Solids also may be described to have a surface free energy at their interfaces but direct measurement of its value is not possible through techniques used for liquids.

Polar liquids, such as water, have strong intermolecular interactions and thus high surface tensions. Any factor which decreases the strength of this interaction will lower surface tension. Thus an increase in the temperature of this system will lower surface tension. Any contamination, especially by surfactants, will lower surface tension. Therefore researchers should be very cautious about the issue of contamination.

HOW IS SURFACE TENSION MEASURED?

The following is a short introduction to the concepts involved in the measurement of surface and interfacial tensions. Included is an introduction to the methods that could be used for these measurements along with so involved and some practical advice.

Table A.1. Measuring techniques for surface and interfacial tension.

Surface tension		Interfacial tension	
Static	**Dynamic**	**Static**	**Dynamic**
Ring method	Drop volume	Plate method	Drop volume
Plate method	Bubble volume	Spinning drop	
Pendant drop		Pendant drop	

- Du Nouy Ring

A platinum/iridium ring is used. This should be cleaned regularly after use and treated carefully to avoid deformation. Dimensions: R(ring) = 9.545mm, r (wire)= 0.185mm.

A good way to store the ring is to immerse it in ethanol by first hanging it on a hook attached to a lid which is then attached to a beaker filled half-full with ethanol. Then before using the ring again, it should be flushed with pure ethanol and water, or burn it with a Bunsen burner for a short time (glowing yellow-red for a few seconds).

- Wilhelmy Plate

Platinum/iridium micro-roughened plate is supplied in a plastic box. Should be cleaned regularly after use and treated carefully to avoid deformation. Dimensions: Width = 19.6mm, Thickness = 0.1mm. The same cleaning procedure as for the Du Nouy ring.

The devices should be calibrated every 6 months. Since this is being done rather often, there was no need of re-calibration.

- Temperature Probe

Sigma70, the system used to yield surface tension and interfacial tension results, is equipped with temperature measuring capabilities. When the probe is connected the programme will automatically provide temperature readings.

The probe is hung on a balance and brought into contact with the liquid interface tested. The forces experienced by the balance as the probe interacts with the surface of the liquid can be used to calculate surface tension. The forces present in this situation depend on the following factors: size and shape of the probe, contact angle of the liquid/solid interaction and surface tension of the liquid. The size and shape of the probe are easily controlled. The contact angle is controlled to be zero (complete wetting). This is achieved by using probes with high surface energies. The probes used are made of a platinum/iridium alloy which insures complete wetting and easy and reliable cleaning.

The mathematical interpretation of the force measurements depends on the shape of the probe used.

In these measurements the Du Nouy Ring has been used in all cases.

This method utilizes the interaction of a platinum ring with the surface being tested. The ring is submerged below the interface and subsequently raised upwards. As the ring moves upwards it raises a meniscus of the liquid. Eventually this meniscus tears from the ring and returns to its original position. Prior to this event, the volume, and thus the force exerted, of the meniscus passes through a maximum value and begins to diminish prior to the actually tearing event. The process is shown in Figure A.2 and Figure A.3.

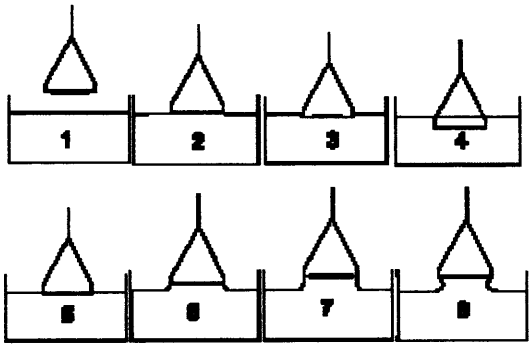

Figure A.2 Process of measuring surface tension.

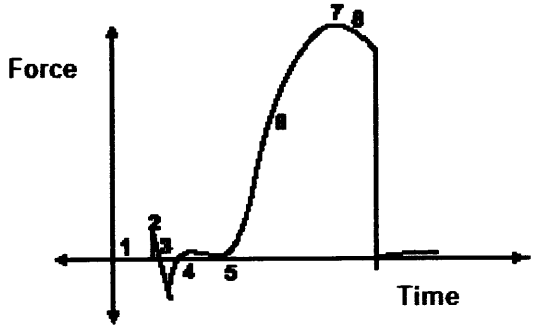

Figure A.3 Forces in the different stages of measuring surface tension.

1. The ring is above the surface and the force is zeroed.
2. The ring hits the surface and there is a slight positive force because of the adhesive force between the ring and the surface.

3. The ring must be pushed through the surface (due to the surface tension) which causes a small negative force.
4. The ring breaks through the surface and a small positive force is measured due to the supporting wires of the ring.
5. When lifted through the surface the measured force starts to increase.
6. The force keeps increasing until
7. The maximum force is reached
8. After the maximum there is a small decrease of in the force until the lamella breaks.

The calculation of surface or interfacial tension by this technique is based on the measurement of this maximum force. The depth of immersion of the ring and the level to which it is raised when it experiences the maximum pull are irrelevant to this technique. The original calculations based on the ring technique were based on theories which apply to rings of infinite diameter and do not consider an additional volume of liquid which is raised due to the proximity of one side of the ring to the other. This additional liquid lifted is diagrammed below as the shaded portion:

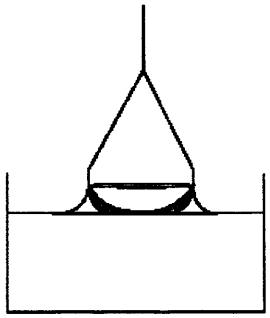

Figure A.4 Liquid miniscus forming on the Du Nouy Ring.

Mathematical corrections which compensate for this extra liquid have been produced. The software used in this case (KSV) utilizes the corrections.

PENDANT DROP SHAPE ANALYSIS

Another method that was used to obtain results with *MARCOL*^{TM}*52* was that of the pendant drop. The shape of a drop of liquid hanging from a syringe tip is determined from the balance of forces which include the surface tension of that liquid. The surface or interfacial tension at the liquid interface can be related to the drop shape through the following equation:

$\gamma = \rho\Delta\, g\, R_0^{\,2}/\beta$

$dx/ds = \cos\phi$

$dz/ds = \sin\phi$

$d\phi/ds = 2 + \beta z - \sin\phi/x$

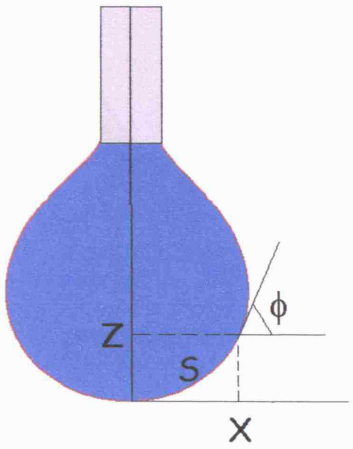

Figure A.5 Pendant drop analysis.

where γ = surface tension

$\rho\Delta$ = difference in density between fluids at interface

g = gravitational constant

R_0 = radius of drop curvature at apex

β = shape factor that can be defined through the Young-Laplace equation expressed as 3 dimensionless first order equations as shown in the figure above.

Modern computational methods using iterative approximations allow solution of the Young-Laplace equation for β to be performed. Thus for any pendant drop where the densities of the two fluids in contact are known, the surface tension may be measured based upon the Young-Laplace equation.

Contact Angles

WHAT IS CONTACT ANGLE?

Contact angle, θ, is a quantitative measure of the wetting of a solid by a liquid. It is defined geometrically as the angle formed by a liquid at the three phase boundary where a liquid, gas and solid intersect as shown below:

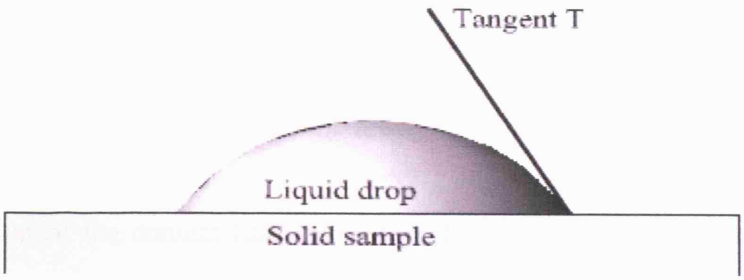

Figure A.6 Definition of contact angle

It can be seen from this figure that low values of θ indicate that the liquid spreads, or wets well, while high values indicate poor wetting. If the angle θ is less than 90 the liquid is said to wet the solid. If it is greater than 90 it is said to be non-wetting. A zero contact angle represents complete wetting.

The values of "static" contact angles, where the drop is not in motion, are found to depend on the recent history of the interaction. When the drop has recently expanded the angle is said to represent the 'advanced' contact angle. When the drop has recently contracted the angle is said to represent the 'receded' contact angle. These angles fall within a range with advanced angles approaching a maximum value and receded angles approaching a minimum value.

If the three phase (liquid/solid/vapor) boundary is in actual motion the angles produced are called Dynamic Contact Angles and are referred to as 'advancing' and 'receding' angles. The difference between 'advanced' and 'advancing', 'receded' and 'receding' is that in the static case motion is incipient in the dynamic case motion is actual. Dynamic contact angles may be assayed at various rates of speed. Dynamic contact angles measured at low velocities should be equal to properly measured static angles.

HYSTERESIS

The difference between the maximum (advanced/advancing) and minimum (receded/receding) contact angle values is called the contact angle hysteresis. A great deal of research has gone into analysis of the significance of hysteresis. It has been

used to help characterize surface heterogeneity, roughness and mobility. Briefly, for surfaces which are not homogeneous there will exist domains on the surface which present barriers to the motion of the contact line. For the case of chemical heterogeneity these domains represent areas with different contact angles than the surrounding surface. For example when wetting with water, hydrophobic domains will pin the motion of the contact line as the liquid advances thus increasing the contact angles. When the water recedes the hydrophilic domains will hold back the draining motion of the contact line thus decreasing the contact angle. From this analysis it can be seen that, when testing with water, advancing angles will be sensitive to the hydrophobic domains and receding angles will characterize the hydrophilic domains on the surface.

For situations in which surface roughness generates hysteresis the actual microscopic variations of slope in the surface create the barriers which pin the motion of the contact line and alter the macroscopic contact angles. There has been a great deal of research investigating the significance of hysteresis and you are recommended to the papers cited at the end of this note for further details.

Contact angle can also be considered in terms of the thermodynamics of the materials involved. This analysis involves the interfacial free energies between the three phases and is given by the Young equation:

$\gamma_{lv} \cos \theta = \gamma_{sv} - \gamma_{sl}$

where γ_{lv} ,γ_{sv} and γ_{sl} refer to the interfacial energies of the liquid/vapor, solid/vapor and solid/liquid interfaces.

UTILIZATION OF CONTACT ANGLE DATA:

The primary focus of contact angle studies is in assessing the wetting characteristics of solid/liquid interactions. Contact angle is commonly used as the most direct measure of wetting. Other experimental parameters may be derived directly from contact angle and surface tension results. Some examples are:

Work of Adhesion: Defined as the work required to separate the liquid and solid phases, or the negative free energy associated with the adhesion of the solid and liquid phases. Used to express the strength of the interaction between the two phases.

Work of Cohesion: Defined as the work required to separate a liquid into two parts, it is a measure of the strength of molecular interactions within the liquid.

It is given by: $Wc = 2\gamma$

Work of Spreading: the negative free energy associated with spreading liquid over solid surface.

Also referred to as Spreading Coefficient; it is given as: $Ws = \gamma (\cos\theta - 1)$

Wetting Tension: A measurement of force/length defined as: $\tau = Fw/P = \gamma LV \cos\theta$.

This value, wetting force normalized for length, also represents the product of the cosine of the contact angle and the surface tension. It is most helpful in situations, such as multicomponent systems, where surface tension at the interface may not equal equilibrium surface tension.

How is contact angle measured?

GONIOMETRY

Analysis of the shape of a drop of test liquid placed on a solid is the basis for goniometry. The basic elements of a goniometer include a light source, sample stage, lens and image capture. Contact angle can be assessed directly by measuring the angle formed between the solid and the tangent to the drop surface. The assignment of the tangent line which will define the contact angle is a factor which can limit the reproducibility of contact angle measurements. Conventional goniometry relies on the consistency of the operator in the assignment of the tangent line. This can lead to significant error, especially subjective error between multiple users. The KSV Instruments' CAM 200 used is using computer analysis of the drop shape to generate consistent contact angle data. The software can fit the Young-Laplace equation to the shape of the drop utilizing all points on the drop profile. Where this curve intersects the baseline the tangent may be assigned. The angle between this tangent and the baseline is the contact angle.

KSV CAM 200

This is a computer controlled and user programmable video based instrument designed for the measurement of:

- Surface and Interfacial tension
- Static Contact Angles
- Dynamic Contact Angles
- Surface Free Energy of Solids

The CAM 200 includes a CCD video camera, a frame grabber, an adjustable sample stage and a LED light source. The open design and modular construction should allow you to adapt your instrument to a wide variety of applications. In addition to the basic measuring unit the KSV CAM 200 can be equipped with:

- Automated Dispenser
- Environmental measuring chamber
- Interfacial measuring chamber
- Thermostated measuring chamber
- Tilt stage
- High speed imaging

References:

KSV Instruction manual, Sigma 70, August 2001, KSV Instruments Ltd.

Appendix B

Drop size, velocity and distribution

These results are complimentary to discussion of Chapter 5 regarding dispersed drop velocity, size and distribution in the pipe cross sectional area. Chord lengths have been obtained for both Type I and Type II experiments at some of the experimental conditions and the results are shown.

Following in Figure B.1 results obtained at 4.0 m/s starting from oil continuous mixtures have yield similar results to the ones discussed in Paragraph 5.4 and area weighted distributions can be seen below.

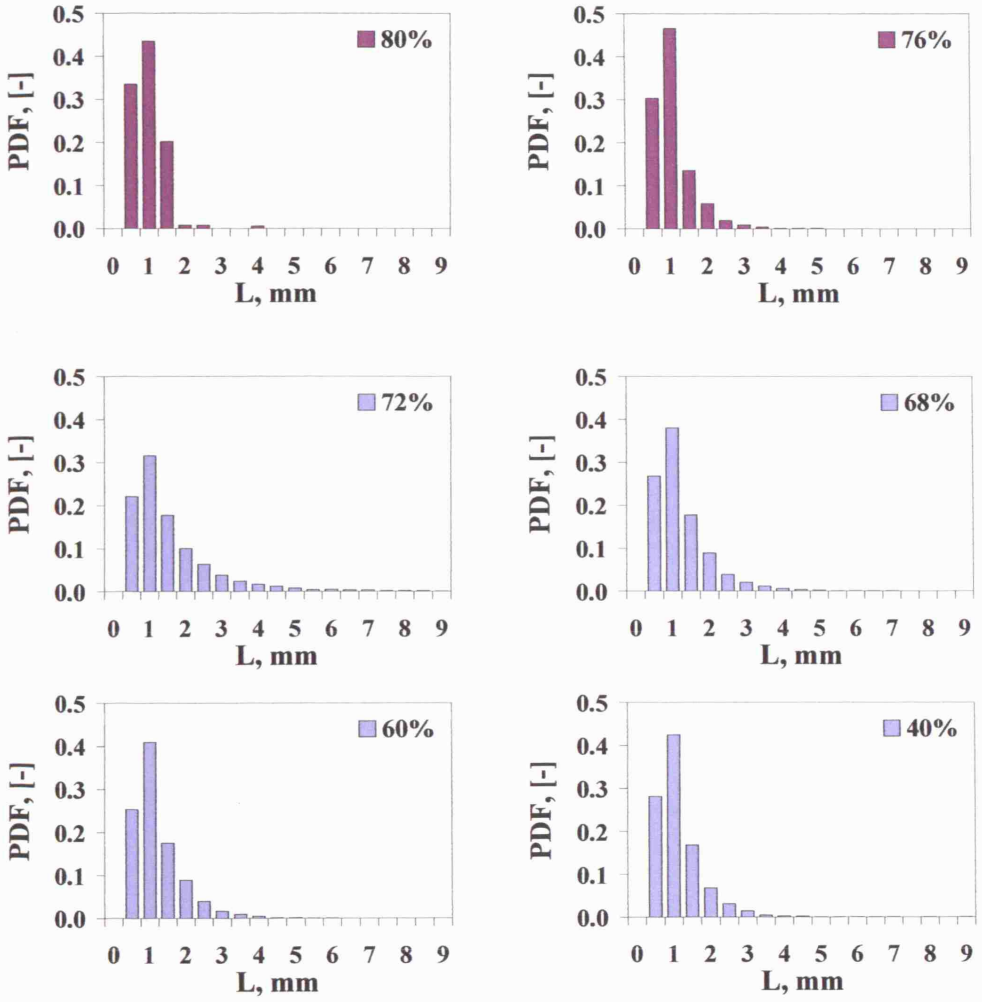

Figure B.1 Chord length (L) distributions averaged for the whole cross section at 4.0 m/s mixture velocity and for different input oil fractions (40 - 76%) starting from oil continuous mixtures. Light (blue) colour represents water continuous flows, while dark (magenta) represents oil continuous flows.

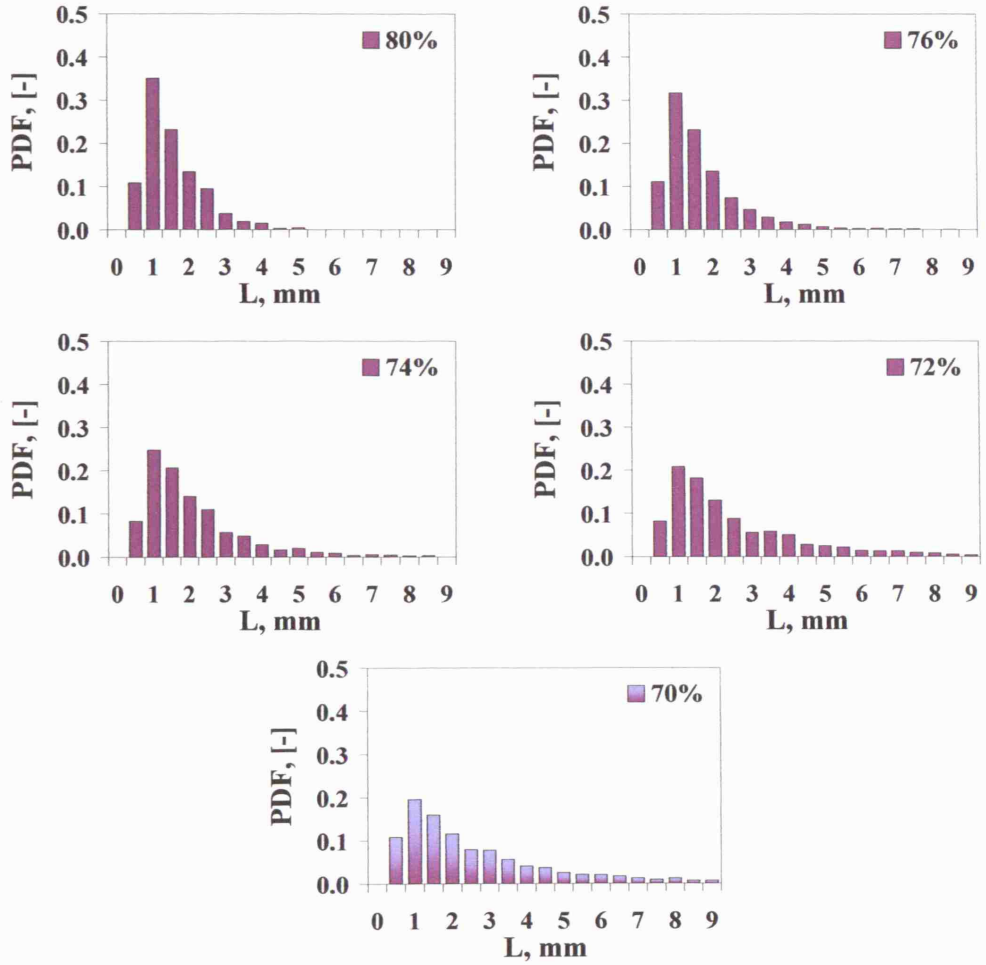

Figure B.2 Chord length (*L*) distributions averaged for the whole cross section at 3.0 m/s mixture velocity and for different input oil fractions (40 - 76%) starting from oil continuous mixtures. Light (blue) colour represents water continuous flows, while dark (magenta) represents oil continuous flows.

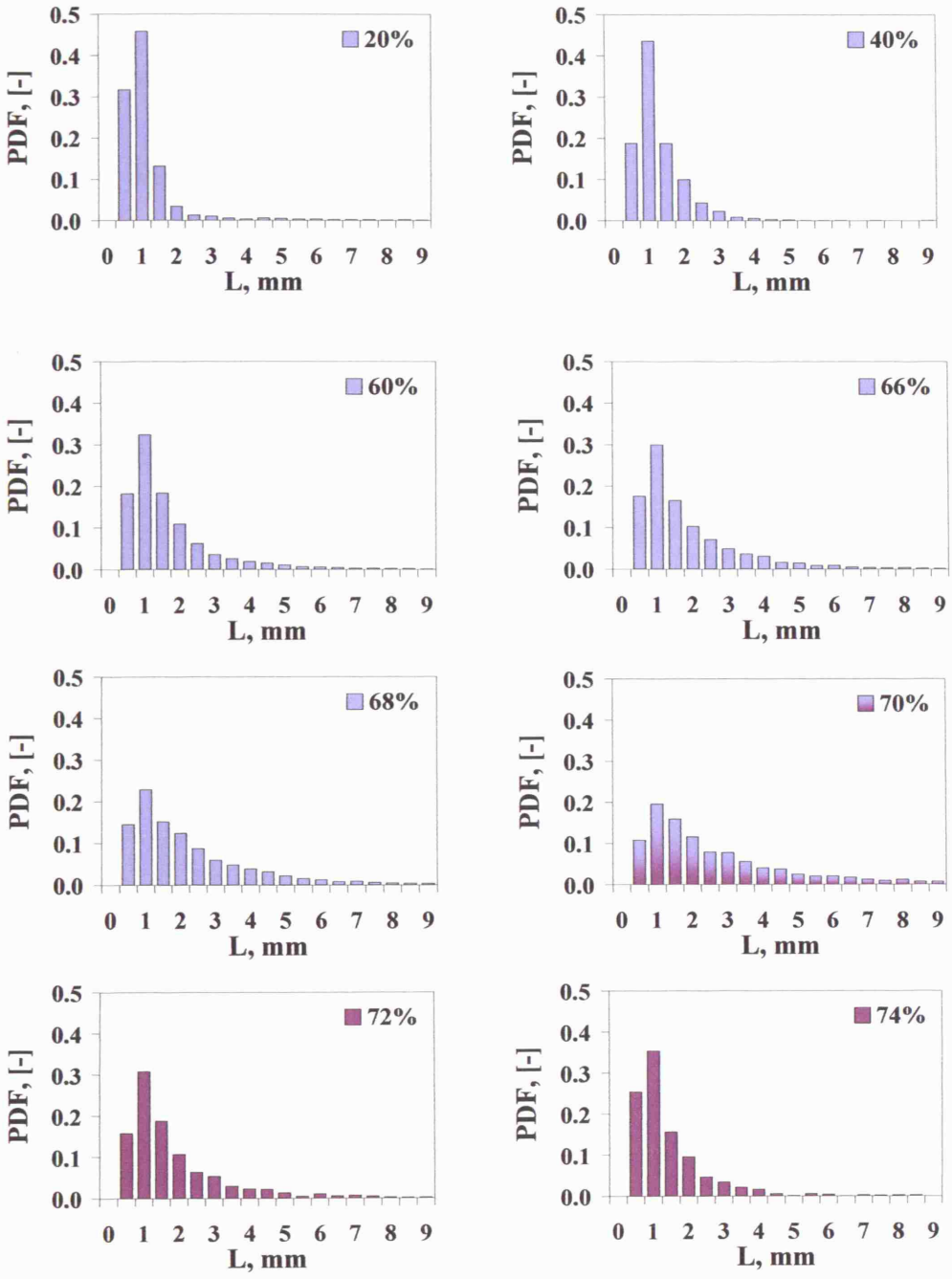

Figure B.3 Chord length (*L*) distributions averaged for the whole cross section at 3.0 m/s mixture velocity and for different input oil fractions (40 - 76%) starting from water continuous mixtures. Light (blue) colour represents water continuous flows, while dark (magenta) represents oil continuous flows.

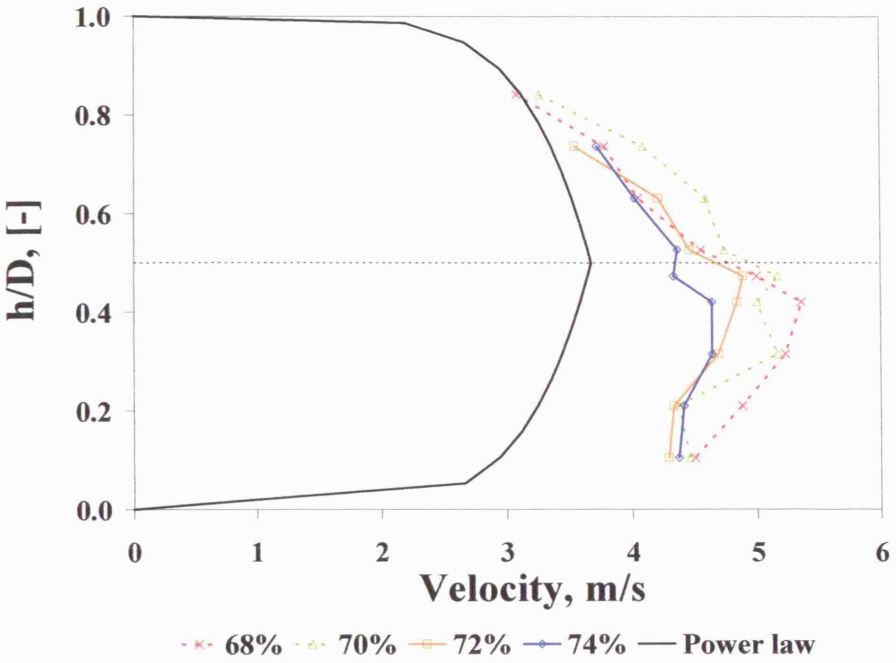

Figure B.4 Drop velocity profile at the inversion point (dotted lines) and the oil continuous region (solid lines) at 3.5 m/s mixture velocity for different input oil fractions.

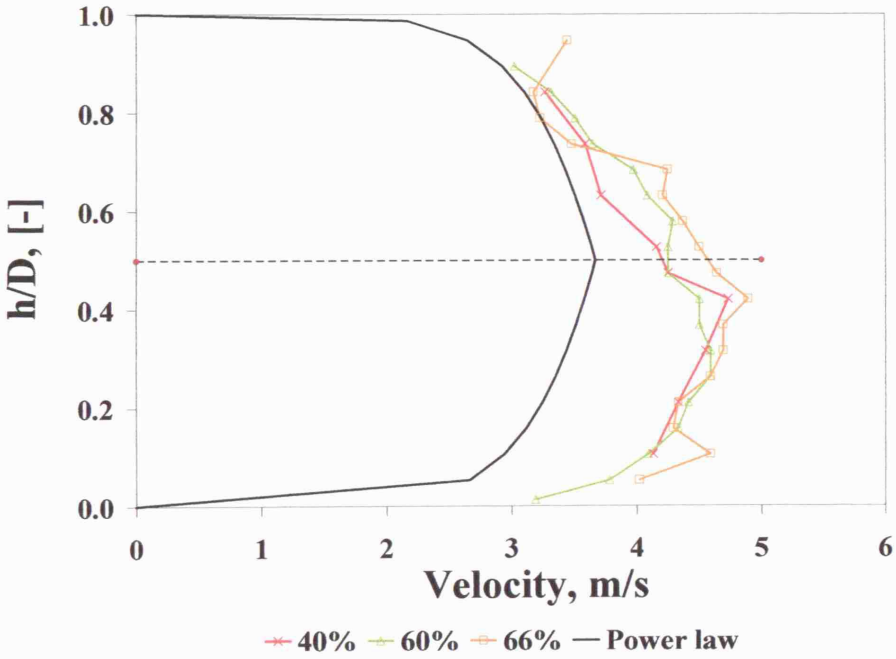

Figure B.5 Oil drop velocity profile it the water continuous region at 3.5 m/s mixture velocity for different input oil fractions.

Appendix C

Effect of parameters on phase inversion

The present is the Appendix to Chapter 6, where an extensive investigation on the effects of various parameters on the phase inversion point and the associated pressure gradient was conducted. All experimental results of pressure drop obtained in all test sections used and with all experimental fluids used are included.

Experiments Type I have started from oil continuous mixtures and the oil fraction was gradually decreased, while keeping the mixture velocity constant. Experiments Type II have started from water continuous mixtures and the water fraction was gradually decreased, while keeping the mixture velocity constant.

In the graphs that follow, results obtained at all test sections using all type of oil will be given at all mixture velocities studied and pressure gradient will be plotted against input oil fraction. More detailed comparisons of the effect of the different parameters are shown in Chapter 6 and will not be included in the present.

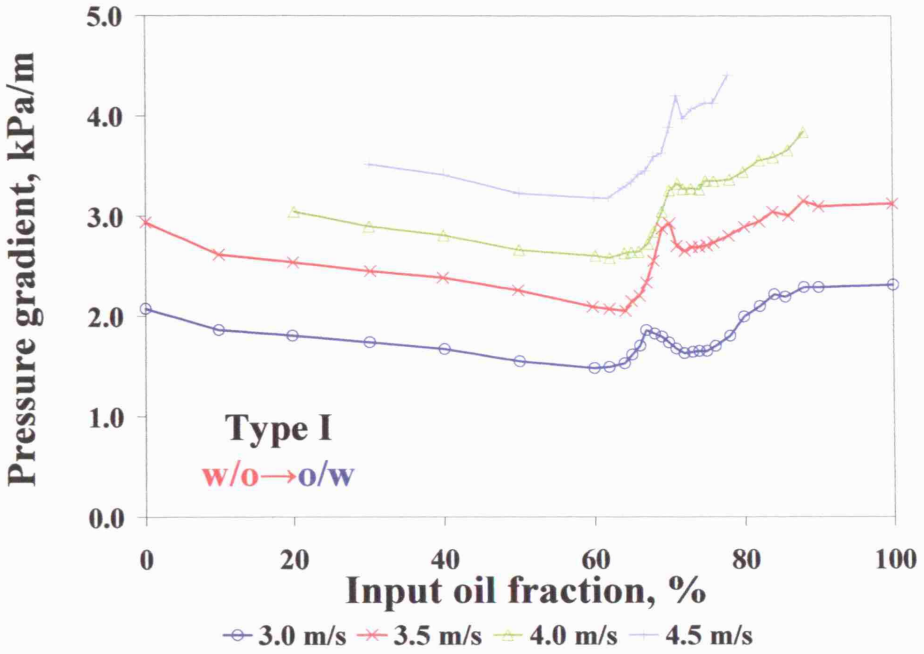

Figure C.1 Pressure gradient in the 38 mm ID SS pipe at different mixture velocities for Type I experiments (UCL, *EXXSOL™ D140*).

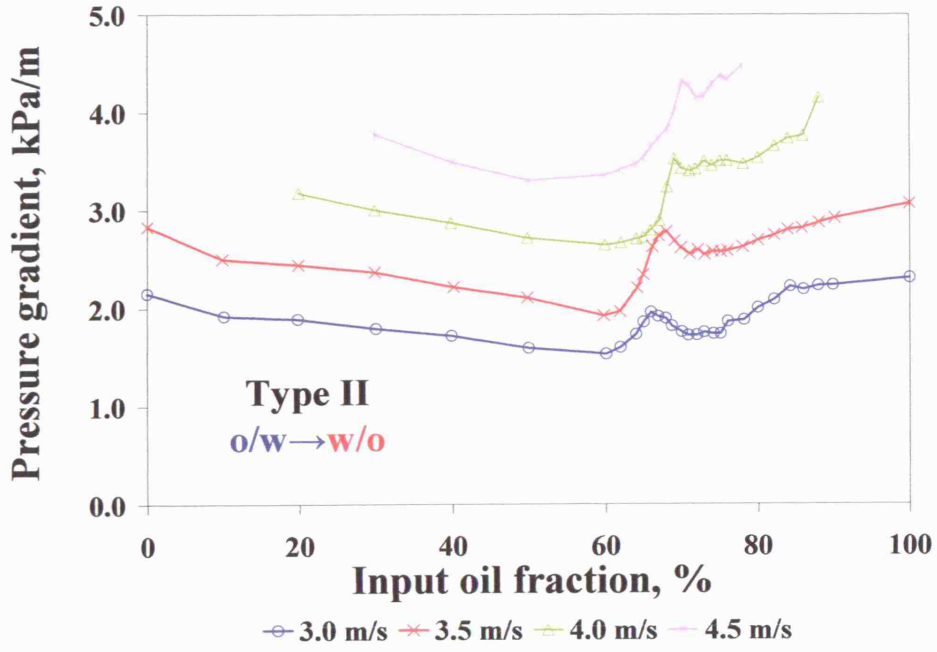

Figure C.2 Pressure gradient in the 38 mm ID SS pipe at different mixture velocities for Type II experiments (UCL, *EXXSOL™ D140*).

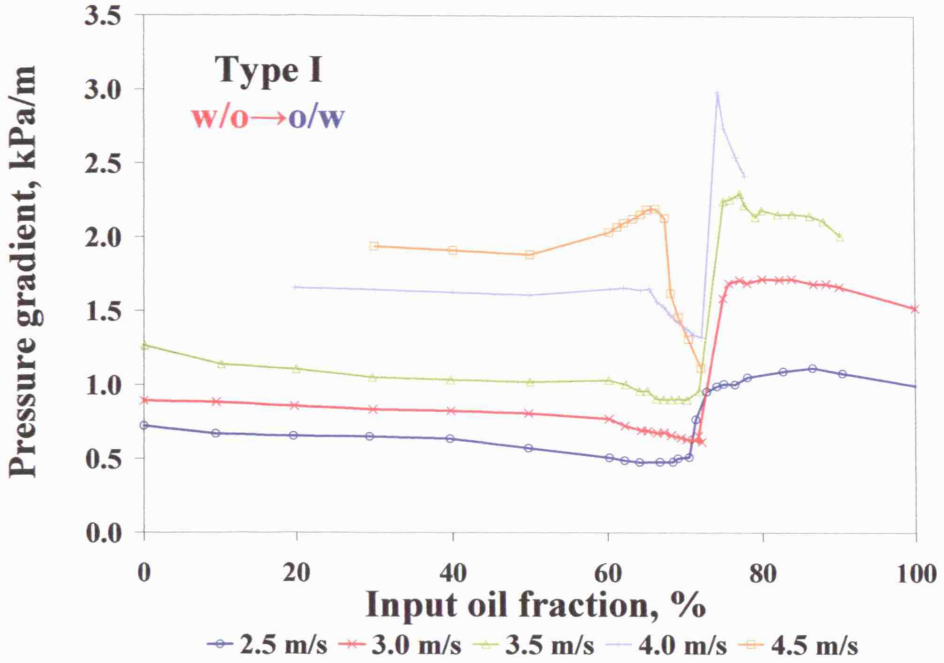

Figure C.3 Pressure gradient in the 60 mm ID acrylic pipe at different mixture velocities for Type I experiments (NTNU, *MARCOL*^{TM} *52*).

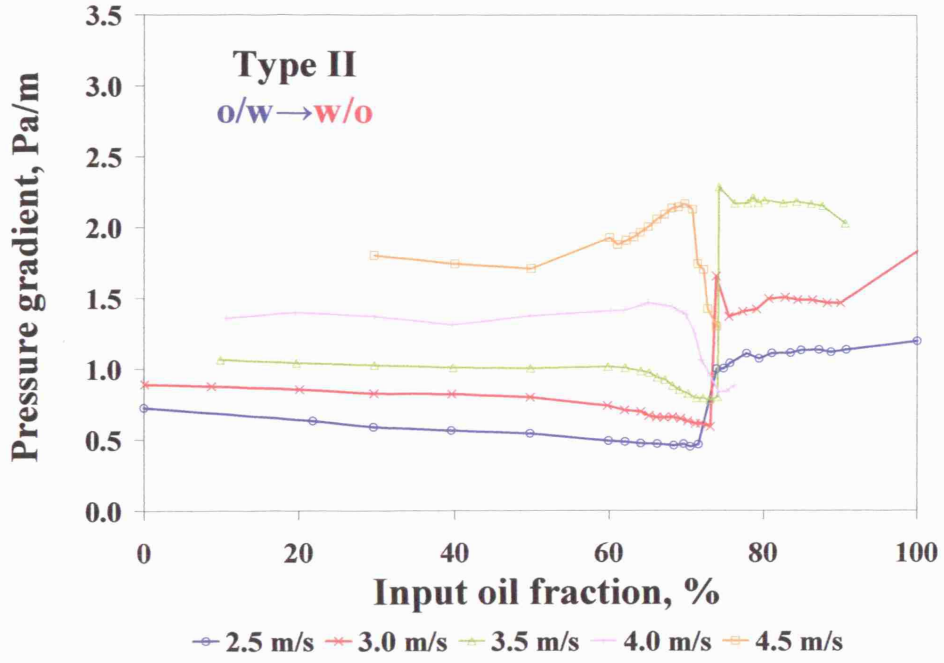

Figure C.4 Pressure gradient in the 60 mm ID acrylic pipe at different mixture velocities for Type II experiments (NTNU, *MARCOL*^{TM} *52*).

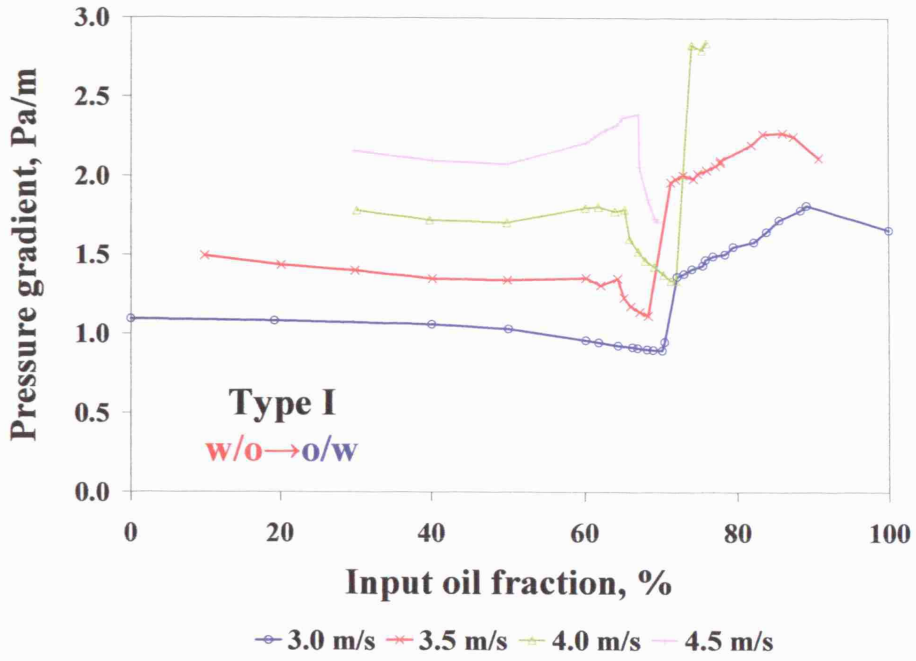

Figure C.5 Pressure gradient in the 60 mm ID epoxy coated SS pipe at different mixture velocities for Type I experiments (NTNU, *MARCOL™ 52*).

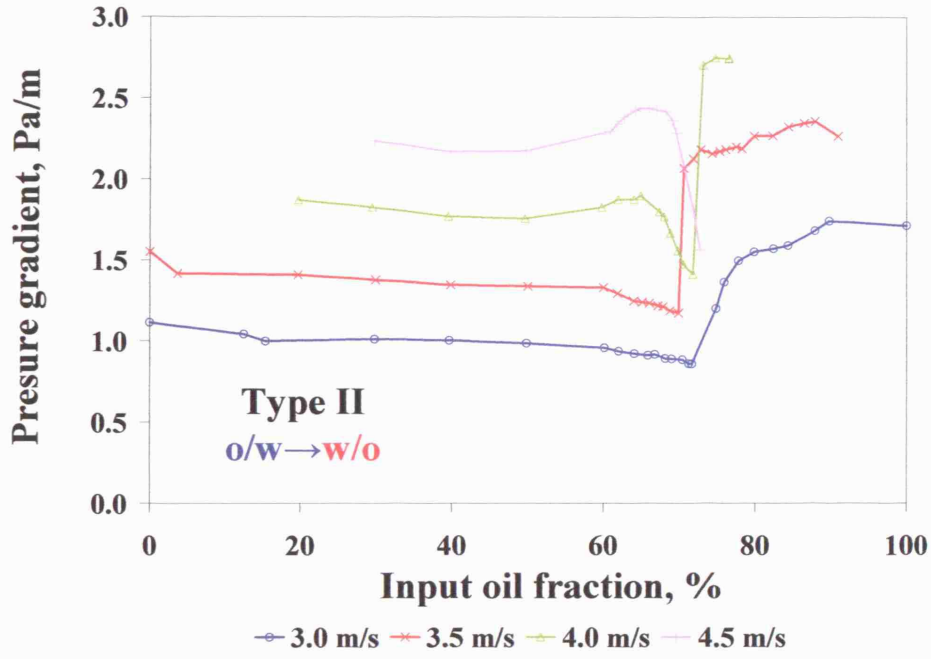

Figure C.6 Pressure gradient in the 60 mm ID epoxy coated SS pipe at different mixture velocities for Type II experiments (NTNU, *MARCOL™ 52*).

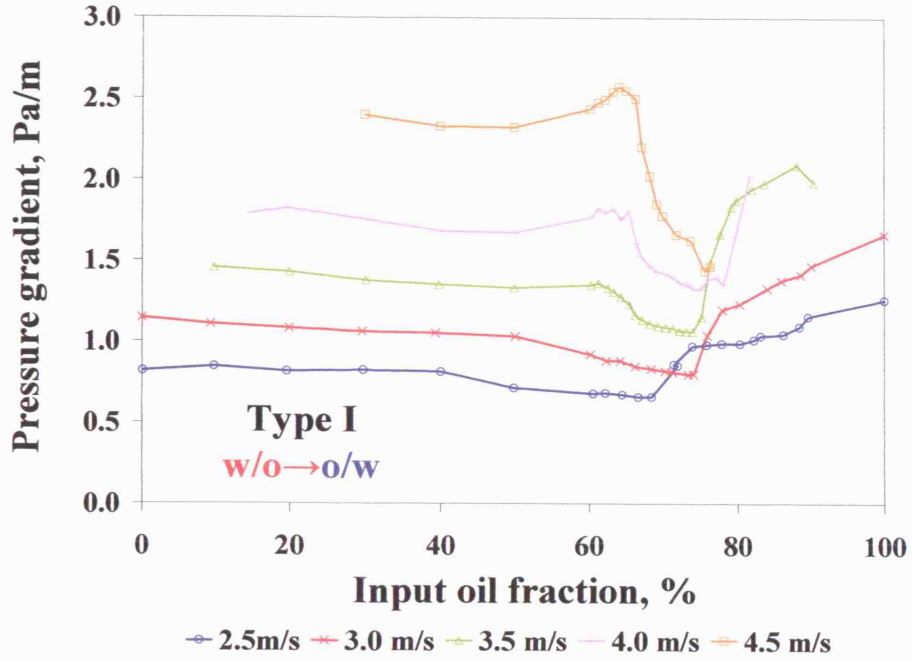

Figure C.7 Pressure gradient in the 60 mm ID SS pipe at different mixture velocities for Type I experiments (NTNU, *MARCOL*^{TM} *52*).

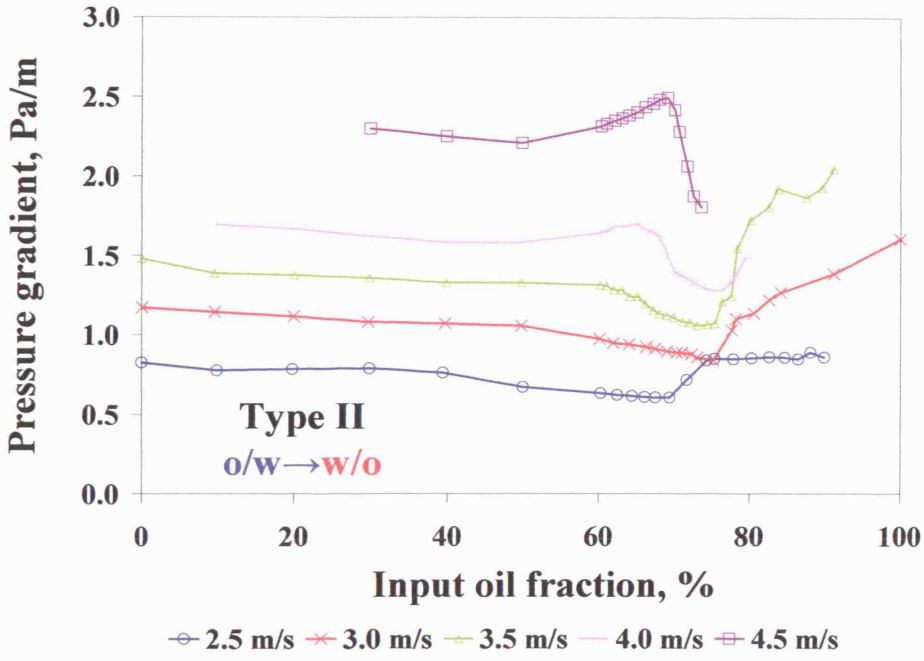

Figure C.8 Pressure gradient in the 60 mm ID SS pipe at different mixture velocities for Type II experiments (NTNU, *MARCOL*^{TM} *52*).

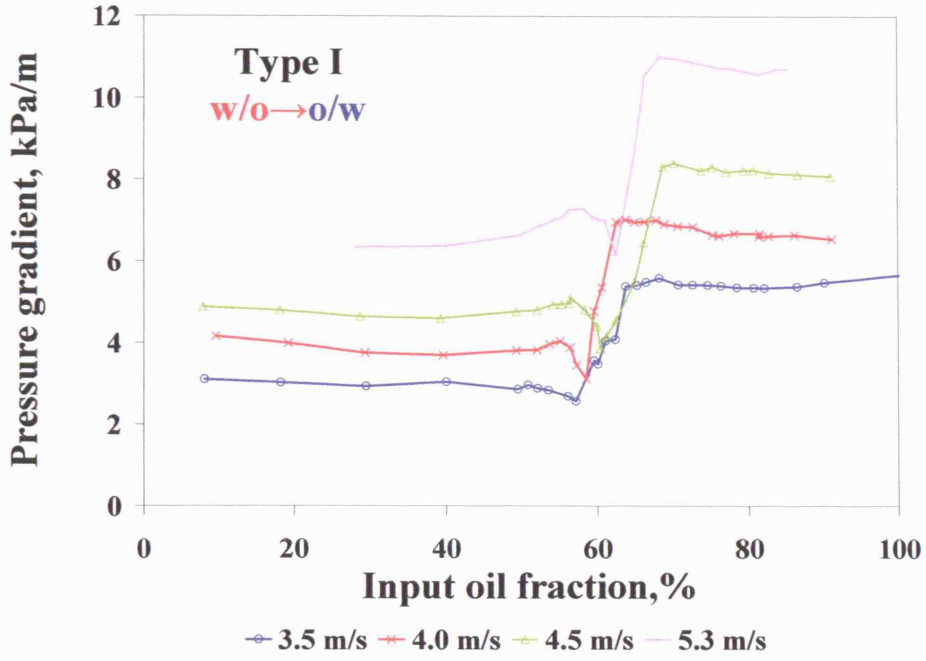

Figure C.9 Pressure gradient in the 32 mm ID acrylic pipe at different mixture velocities for Type I experiments (NTNU, *MARCOL™ 52*).

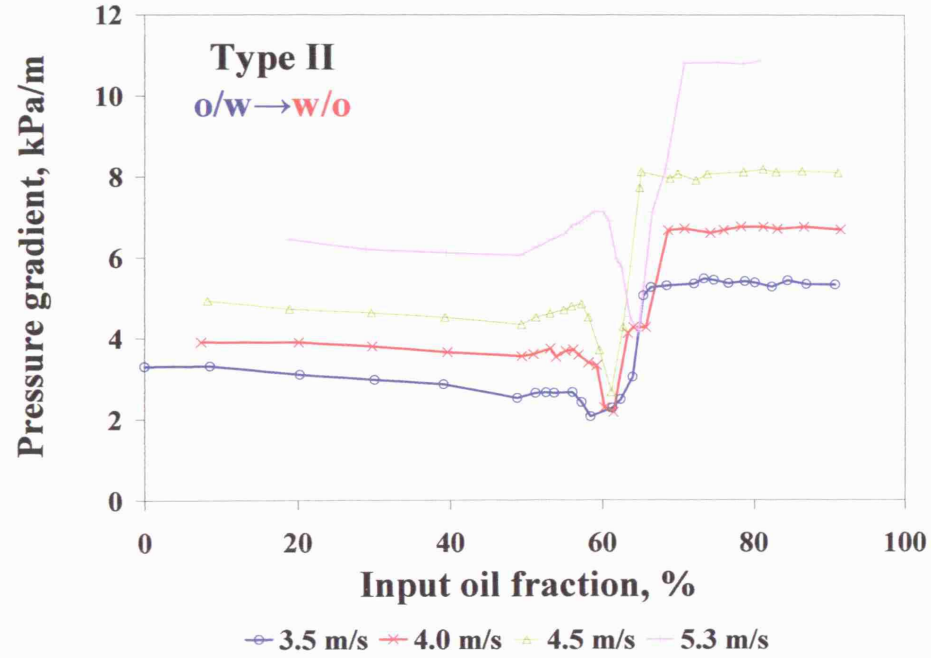

Figure C.10 Pressure gradient in the 32 mm ID acrylic pipe at different mixture velocities for Type II experiments (NTNU, *MARCOL™ 52*).

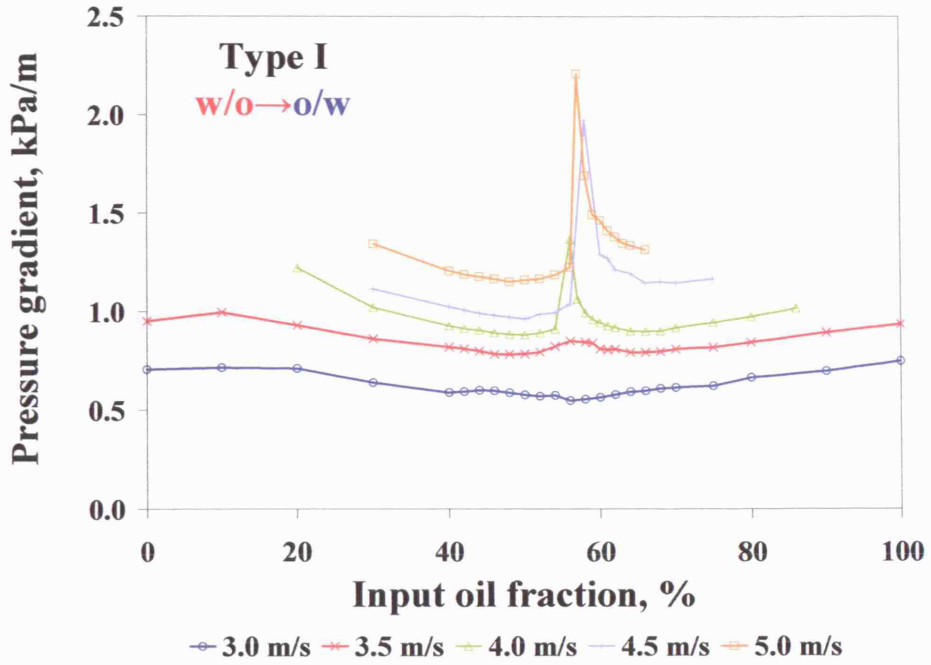

Figure C.11 Pressure gradient in the 60 mm ID acrylic pipe at different mixture velocities for Type I experiments (NTNU, *EXXSOL™ D80*).

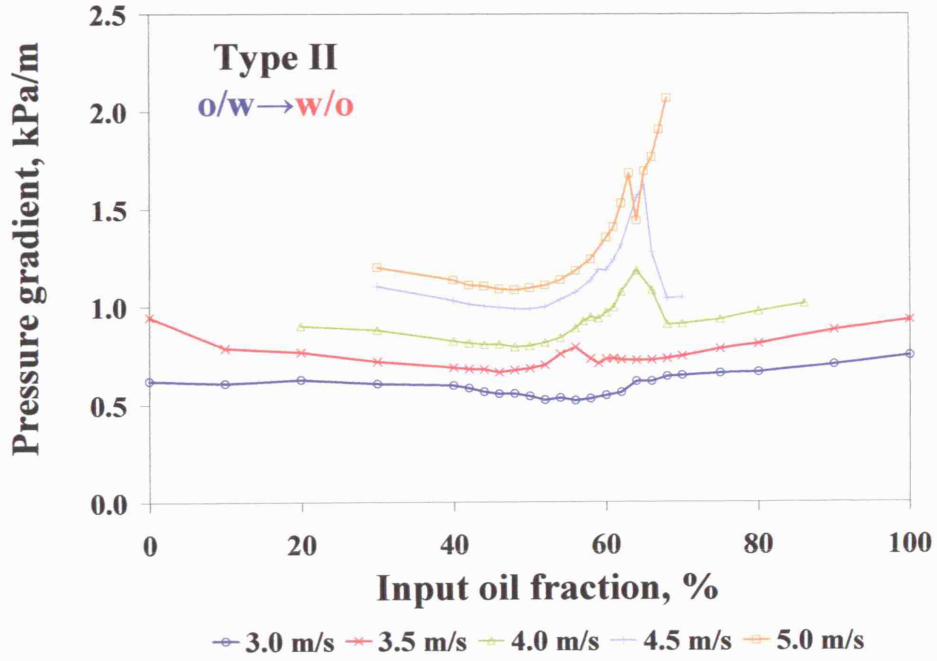

Figure C. 12 Pressure gradient in the 60 mm ID acrylic pipe at different mixture velocities for Type II experiments (NTNU, *EXXSOL™ D80*).

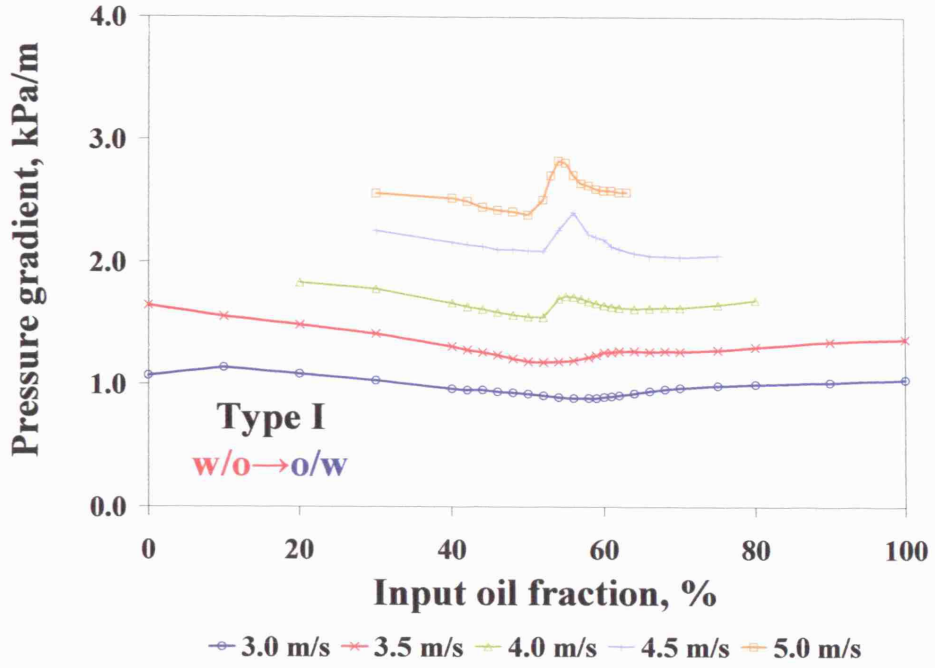

Figure C.13 Pressure gradient in the 60 mm ID SS pipe at different mixture velocities for Type I experiments (NTNU, *EXXSOL™ D80*).

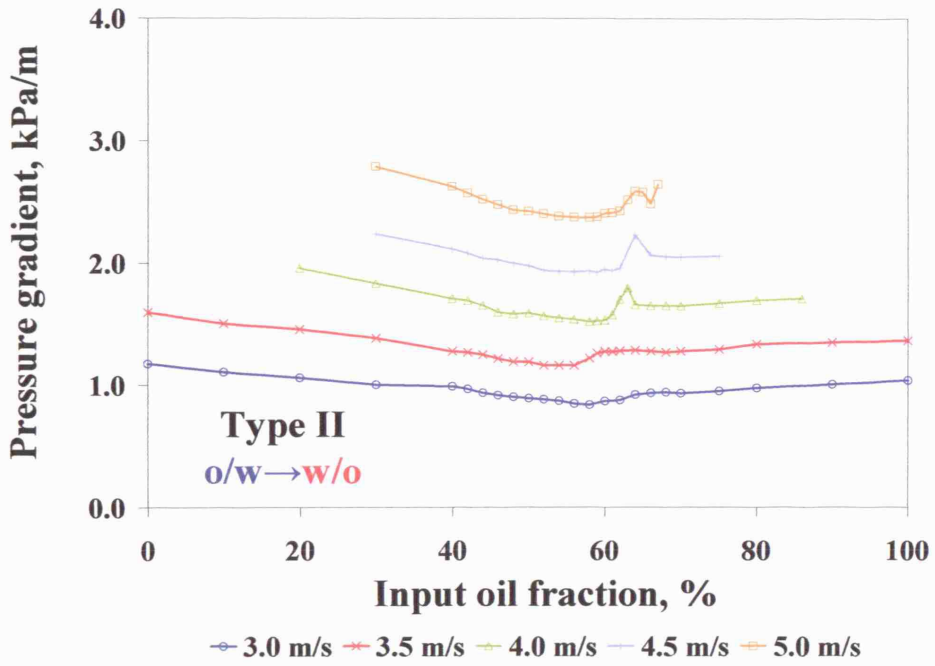

Figure C.14 Pressure gradient in the 60 mm ID SS pipe at different mixture velocities for Type I experiments (NTNU, *EXXSOL™ D80*).

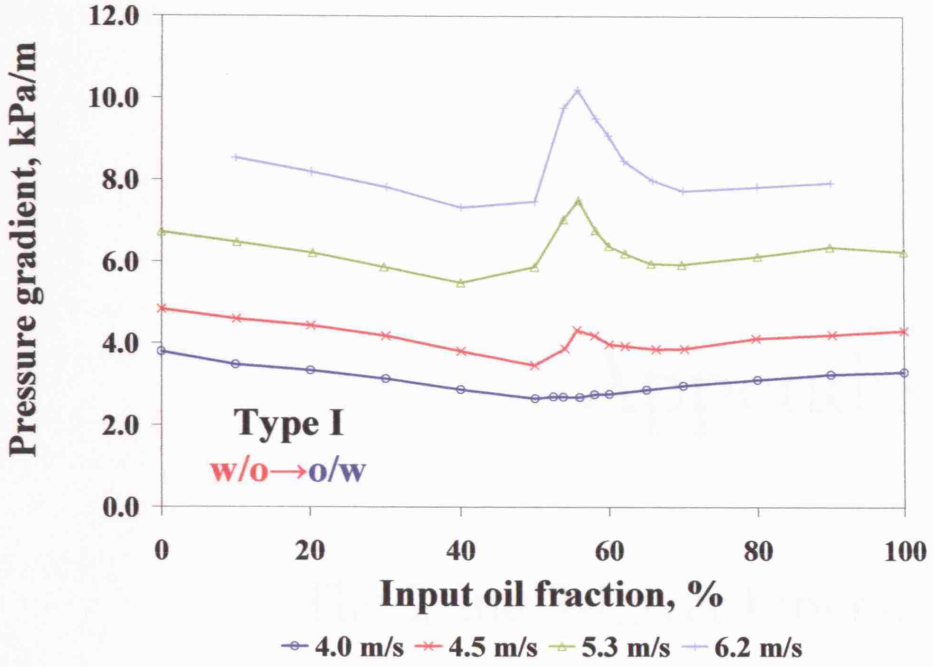

Figure C.15 Pressure gradient in the 32 mm ID acrylic pipe at different mixture velocities for Type I experiments (NTNU, *EXXSOL™ D80*).

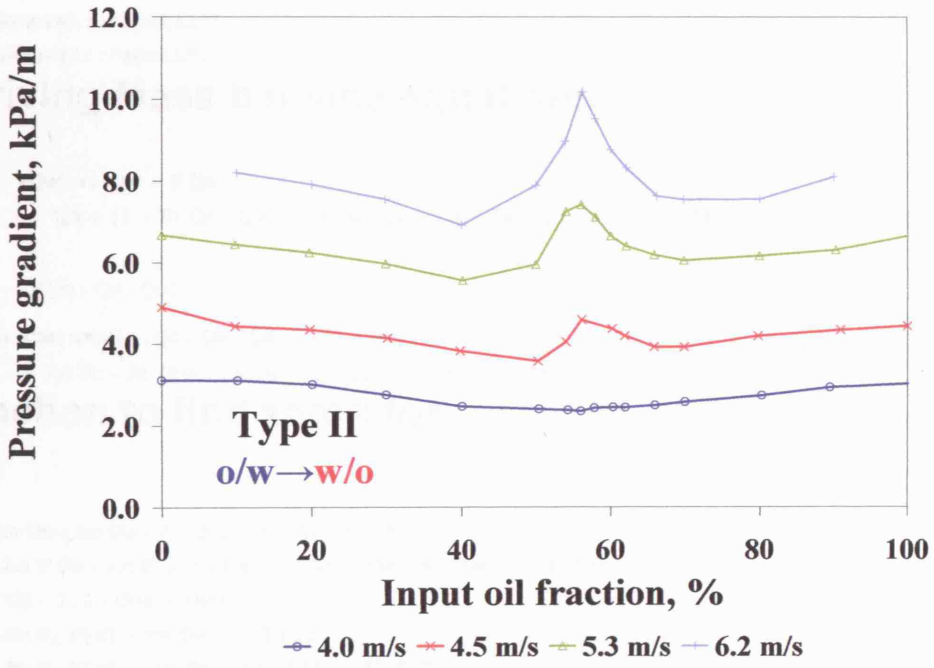

Figure C.16 Pressure gradient in the 32 mm ID acrylic pipe at different mixture velocities for Type II experiments (NTNU, *EXXSOL™ D80*).

Appendix D

The 2 and 3-Layer Programmes

3Layer

```
Off[General::"spell1"]
Off[General::"spell"]
```

Deriving Mass balance equations

```
exp0 = {Qwt == Qw + F Qm,
  Qot == Qo + (1 - F) Qm, Qw = Uw Aw, Qm == Am Um, Qo == Ao Uo , Uos = Qot / At, Uws = Qwt / At}
```

$$\left\{Qwt == F\,Qm + Qw,\ Qot == (1 - F)\,Qm + Qo,\ Qw == Aw\,Uw,\ Qm == Am\,Um,\ Qo == Ao\,Uo,\ Uos == \frac{Qot}{At},\ Uws == \frac{Qwt}{At}\right\}$$

```
Eliminate[exp0, {Qo, Qw, Qm, Qot, Qwt}]
```

$$Am\,Um == -Ao\,Uo + At\,Uos - Aw\,Uw + At\,Uws \;\&\&\; Ao\,F\,Uo == At\,F\,Uos + Aw\,Uw - Aw\,F\,Uw - At\,Uws + At\,F\,Uws \;\&\&\; At \neq 0$$

Function to find zeros for

```
M1 = Am Um + Ao Uo - At Uos + Aw Uw - At Uws;
M2 = -Ao F Uo + At F Uos + Aw Uw - Aw F Uw - At Uws + At F Uws;
Emp = Um - 1.1 (Uos + Uws);
F1 = -Aw ∂x P[x] - τw Sw + τi1 Si1;
F2 = -Am ∂x P[x] - τm Sm - τi1 Si1 - τi2 Si2;
F3 = -Ao ∂x P[x] - τo So + τi2 Si2;
```

Physical Properties and other inputs

$$\text{slphys}=\{\rho m\to (1-E)\rho o+E\rho w,\ \mu m\to \mu o(1-E)^{-2.5},\ \mu o\to 0.0055,\ \mu w\to 0.001,\ \rho o\to 828,\ \rho w\to 1000,\ E\to 0.27,\ g\to 9.81,\ d\to 0.038,\ Us\to 2.55,\ Ue\to 0.95,\ tol\to 10^{-12}\};$$

Geometry

$$\text{subgeom}=\{r\to d/2,$$

$$Aw\to r^2\,\text{ArcCos}\left[\frac{r-hw}{r}\right]-(r-hw)\sqrt{(hw\,(2r-hw))},$$

$$Ao\to r^2\,\text{ArcCos}\left[\frac{r-ho}{r}\right]-(r-ho)\sqrt{(ho\,(2r-ho))},$$

$$Am\to \pi r^2-Aw-Ao,$$

$$Sw\to 2r\,\text{ArcCos}\left[\frac{r-hw}{r}\right],$$

$$At\to \pi r^2,$$

$$So\to 2r\,\text{ArcCos}\left[\frac{r-ho}{r}\right],$$

$$Sm\to 2\pi r-(So+Sw),$$

$$Si1\to 2\,(hw\,(2r-hw))^{1/2},$$

$$Si2\to 2\,(ho\,(2r-ho))^{1/2}\};$$

Friction Factors and Shear stresses

$$f[d\_,U\_,\rho\_,\mu\_]:=0.079\left(\frac{dU\rho}{\mu}\right)^{-0.25}/;\text{Abs}\left[\frac{dU\rho}{\mu}\right]\geq 2000$$

$$f[d\_,U\_,\rho\_,\mu\_]:=16\Big/\left(\frac{dU\rho}{\mu}\right)/;\text{Abs}\left[\frac{dU\rho}{\mu}\right]<2000$$

$$f[d1\_,d2\_,U1\_,U2\_,\rho1\_,\rho2\_,\mu1\_,\mu2\_]:=f[d1,U1,\rho1,\mu1]\ /;U1>U2$$

$$f[d1\_,d2\_,U1\_,U2\_,\rho1\_,\rho2\_,\mu1\_,\mu2\_]:=f[d2,U2,\rho2,\mu2]\ /;U2>U1$$

$$\text{subshear}=\{\tau w\to f[dw,Uw,\rho w,\mu w]\frac{\rho w\,Uw^2}{2},$$

$$dw\to (4Aw)/Sw,$$

$$\tau m\to f[dm,Um,\rho m,\mu m]\frac{\rho m\,Um^2}{2},$$

$$dm\to (4Am)/(Sm+Si1+Si2),$$

$$\tau o\to f[do,Uo,\rho o,\mu o]\frac{\rho o\,Uo^2}{2},$$

$$do\to (4Ao)/So,$$

$$\tau i1\to \left(f[dw,dm,Uw,Um,\rho w,\rho m,\mu w,\mu m]\frac{\rho m\,(Um-Uw)^2}{2}\text{Sign}[Um-Uw]\right),$$

$$\tau i2\to \left(f[dw,dm,Uo,Um,\rho o,\rho m,\mu o,\mu m]\frac{\rho m\,(Um-Uo)^2}{2}\right)\text{Sign}[Um-Uo]\};$$

Solution

Initial Guess

```
sub1 = {ho → 0.009, hw → 0.001, Um → 3.85`};
sub2 = {Uo → 2.8, Uw → 1.2, P'[x] → -3405};
```

tolerance

```
tol = 10^-10;
n=0;
While[(((Abs[M1]+Abs[M2]+Abs[Emp]+Abs[F1]+Abs[F2]+Abs[F3] //. Flatten[{subgeom, subshear, subphys}] /. Flatten[{sub1, sub2}]) > tol) && (n<500)),
 sub1=FindRoot[{M1, M2, Emp} //. Flatten[{subgeom, subshear, subphys}] /. sub2, {ho, 0.001}, {hw, 0.001}, {Um, 3.85}];
 sub2=FindRoot[{F1, F2, F3} //. Flatten[{subgeom, subshear, subphys}] /. sub1, {Uo, 2.1, 2.2}, {Uw, 0.9, 0.95}, {P'[x], -3100, -3200}]; n++]
n
```

500

Output solution

Results

```
Flatten[{sub1, sub2}]
Flatten[{{ho → 0.010164799825618017`, hw → 0.005533367965891737`, Um → 3.8500000000000005`},
  {Uo → 2.7766287078610947`, Uw → 2.526758936715087`, P'[x] → -3706.8490546725716`}}]
```

Values of Mass balance and momentum balance expressions

```
{M1, M2, Emp, F1, F2, F3} //. Flatten[{subgeom, subshear, subphys, sub1, sub2}]
```

2Layer

```
Off[General::"spell1"]
Off[General::"spell"]
```

Deriving Mass balance equations

```
exp0 = {Qwt == Qw + F Qm, Qot == (1 - F) Qm,
  Qw = Uw Aw, Qm == Am Um , Uos = Qot / At, Uws = Qwt / At}
```

$$\left\{Qwt == F\,Qm + Qw,\ Qot == (1 - F)\,Qm,\ Qw == Aw\,Uw,\ Qm == Am\,Um,\ Uos == \frac{Qot}{At},\ Uws == \frac{Qwt}{At}\right\}$$

```
Eliminate[exp0, {Qw, Qm, Qot, Qwt}]
```

$$Am\,Um == At\,Uos - Aw\,Uw + At\,Uws \;\&\&\; F\,Uos == -\frac{Aw\,Uw}{At} + \frac{Aw\,F\,Uw}{At} + Uws - F\,Uws \;\&\&\; At \neq 0$$

Function to find zeros for

```
Rozentsvaig = 1.1250;

M1 = Am Um - At Uos + Aw Uw - At Uws;
M2 = +At F Uos + Aw Uw - Aw F Uw - At Uws + At F Uws;
F1 = -Aw ∂x P[x] - τw Sw + τil Sil;
F2 = -Am ∂x P[x] - τm Sm - τil Sil;
M3 = Uos/Uws (F Am + Aw)/((1 - F) Am) - Holdup;
```

Physical Properties and other inputs

```
subphys = {ρm → (1 - F) ρo + F * ρw, μm → μo (1 + 2.5 F ((μw + 0.4 μo) / (μo + μw))), μo → 0.0055, μw → 0.001,
   ρo → 828, ρw → 1000, g → 9.81, d → 0.038, Uos → 1.8, Uws → 1.2, tol → 10^-12, Holdup → 1.03};

ρ[Um_, Uw_, ρm_, ρw_] := ρm /; Um > Uw;
ρ[Um_, Uw_, ρm_, ρw_] := ρw /; Uw > Um;
```

Geometry

```
subgeom = {r → d/2,
   Aw → r^2 ArcCos[(r - hw)/r] - (r - hw) √(hw (2 r - hw)),
   Am → π r^2 - Aw,
   Sw → 2 r ArcCos[(r - hw)/r],
   At -> π r^2,
   Sm → 2 π r - Sw,
   Sil → 2 (hw (2 r - hw))^(1/2)};
```

Friction Factors and Shear stresses

$$f[d\_, U\_, \rho\_, \mu\_] := \frac{0.079\left(\frac{dU\rho}{\mu}\right)^{-1/4}}{1+\text{Rozentsvaig F}} \;/;\; \text{Abs}\left[\frac{dU\rho}{\mu}\right] \geq 2000$$

$$f[d\_, U\_, \rho\_, \mu\_] := \frac{16/\left(\frac{dU\rho}{\mu}\right)}{1+\text{Rozentsvaig F}} \;/;\; \text{Abs}\left[\frac{dU\rho}{\mu}\right] < 2000$$

```
f[d1_, d2_, U1_, U2_, ρ1_, ρ2_, μ1_, μ2_] := f[d1, U1, ρ1, μ1] /; U1 > U2
f[d1_, d2_, U1_, U2_, ρ1_, ρ2_, μ1_, μ2_] := f[d2, U2, ρ2, μ2] /; U2 > U1
subshear = {τw → f[dw, Uw, ρw, μw] ρw Uw^2/2,
   dw → (4 Aw) / Sw,
   τm → f[dm, Um, ρm, μm] ρm Um^2/2,
   dm → (4 Am) / (Sm + Si1),
   do → (4 Ao) / So,
   τi1 → (f[dw, dm, Uw, Um, ρw, ρm, μw, μm] ρ[Um, Uw, ρm, ρw] (Um - Uw)^2/2)};
totsub = Flatten[{subgeom, subshear, subphys}]
sub1 = Table[{hw, FindRoot[{M1, M2, M3} //. totsub, {Um, 4.0, 5.1}, {F, 0.1, 0.8}, {Uw, 0.5, 1.5}, MaxIterations → 200]},
   {hw, 0.0007, 0.0008, 0.00001}] // TableForm
Do[sub1 = FindRoot[{M1, M2, M3} //. totsub, {Um, 4.0, 5.1}, {F, 0.1, 0.8}, {Uw, 0.5, 1.5}, MaxIterations → 200];
 Print[{hw, F /. sub1, Solve[(F1 //. totsub /. hw → 0.0008 //. sub1) = 0, P'[x]], Solve[(F2 //. totsub /.
       hw → 0.0008 //. sub1) = 0, P'[x]]}], {hw, 0.00236, 0.00237, 0.000001}]
{AccuracyGoal→Automatic, Compiled→True, DampingFactor→1, Jacobian→Automatic, MaxIterations→15, WorkingPrecision→16}
```

Original Method

```
FindRoot[{M1, M2, M3, F1, F2} //. totsub, {hw, 0.002366, 0.002367}, {Um, 4.0, 5.1}, {F, 0.39, 0.9}, {Uw, 3.0, 4.5},
 {P'[x], -3000, -4000}, MaxIterations→ 6000, WorkingPrecision→ 32, DampingFactor→ 0.005]
{M1, M2, M3, F1, F2} //. totsub //. %
```

Appendix E

Commercial feasibility study

The following is complimentary work conducted for the understanding of the commercialisation potential of the newly developed instrumentation within this research for use in multiphase flow applications. The possibility of the development of a spin-out company (the "Tri-Eye") is considered. The main aspects are seen in Chapter 8, while the following summarises additional information regarding the market analysis and the general characteristics of the company, as well as the competition sector. The establishment of the spin-out company was scheduled for July 2006 and thus, all analyses were conducted respectively.

APPENDIX E1: THE EXECUTIVE SUMMARY

Industry & Business Area	Advanced diagnostic sensor for use within research & development activities of the oil and food industries.
Business Concept	Commercialisation of flow analysis technology and accompanying software that delivers savings to users through enhanced measurement benefits and thus economies of time, cost and accuracy. The technology, its software and after-sale support service provision will be bundled together and sold as a package to end-users.

Project Status

The technology ("Tri-Eye") is the result of a three year project performed at the Department of Chemical Engineering at University College London (UCL). Laboratory testing has been completed.

The core technology is to be protected by patent (for both apparatus & method). No company has yet been incorporated.

The intellectual property rights belong to UCL.

Product & Technology

Tri-Eye allows measurement of critical variables in the transport of oil/gas/water mixtures. These critical variables, which influence cost and risk, include:

- Phase distribution: the exact concentration of each of the two phases in the pipe cross-sectional area (i.e. the way water and oil/gas are spread through the pipe).
- Velocity profile: the speed at which the dispersed phase (oil/gas or water) is flowing through the pipe.
- Drop size: the size of the drops/bubbles of the dispersed phase (oil/gas or water).

Tri-Eye provides continuous measurements through a sensor and traversing mechanism housed permanently on the side of a pipe, an instrumentation box to process measurement readings, and an associated software programme.

Opportunity

There is a large existing market for flow analysis technologies in the oil industry (in-house/out-sourced research & development). There is also potential in the food (beer & margarine) production sectors.

Tri-Eye estimates current market size in the oil sector at between $29 million and $37 million. The market is stable and growing in line with long-term positive oil production and oil price fundamentals.

Existing technology provided by competitors is limited in functionality, range of measurements and accuracy.

Customers

In-house R&D units of state-owned and private oil companies.

University labs and other research centres serving the oil industry or carrying out independent research.

Beer and edible oil/margarine production companies (potential).

Competition

The market is global and fragmented, with firms competing on product differentiation. Tri-Eye estimates that there are circa 30 competitors that include Mettler Toledo, DANTEC Dynamics and Forschungszentrum Rossendorf.

None offer a directly comparable comprehensive technology.

Requirements

Tri Eye requires a total of £195,000 over two stages. Stage 1 is pre-seed funding of £45,000 and stage 2 is commercialisation (£150,000)

Financials

Income Statement

Years	2007	2008	2009	2010	2011	2012
Revenue	335,725	1,072,718	2,616,004	5,092,069	6,158,440	6,451,
Cost of sales	(46,580)	(60,876)	(132,526)	(267,364)	(290,959)	(301,1
Gross profit	289,145	1,011,842	2,483,479	4,824,704	5,867,481	6,150,
Marketing & Distribution Costs	(14,650)	(24,820)	(45,712)	(79,024)	(93,549)	(97,76
Administrative expenses	(187,706)	(143,585)	(147,911)	(151,973)	(156,147)	(160,4
Profit from operations	86,789	843,438	2,289,855	4,593,707	5,617,785	5,891,
Net Financing Cost	2,554	8,767	28,917	71,419	131,229	195,2
Profit before tax	89,343	852,204	2,318,772	4,665,126	5,749,014	6,087,
Corporate income tax expense	(26,803)	(255,661)	(695,632)	(1,399,538)	(1,724,704)	(1,826
Profit after tax	62,540	596,543	1,623,141	3,265,588	4,024,310	4,260,

Exit

Tri-Eye envisage sale to a strategic investor such as GE, Honeywell or Mettler Toledo within 5 years from start of commercial operations.

Management Team[E.1]

Karolina Ioannou – CEO (UCL, Chemical Engineer)
Sarah Germana'– COO (UCL, Hydraulic Engineer)
Hiroyoshi Koizumi – CFO (LBS, Corporate Banker)
Sanzhar Shalkarbekov – CMO (LBS, Corporate Banker)
Michael Webster – CMO (LBS, Investment Banker)

[E.1] CEO: Chief Executive Officer
CFO: Chief Financial Officer
CMO: Chief Marketing Officer
COO: Chief Operating officer.

Tri-Eye

Because "seeing" is believing...

Figure E.1 Tri-Eye's Logo.

APPENDIX E2: PRODUCTS & TECHNOLOGY

SCIENTIFIC BACKGROUND:

This technology is based on electrical impedance tomography: this is simply the inverse of the problem of determining conductivity or permittivity of interior to exterior measurements (further discussion on the technology used can be found in Section 3.6.2).

Impedance probes measure the differences in capacity and/or the resistance between two phases. If the sensors are in contact with oil (or alternatively air) the resistance value is large and no signal can be recorded. If the sensors are in contact with water then a high signal is recorded. These probes are used extensively in research in different configurations. Tri-Eye was designed for the needs of this PhD project (developed at UCL over a number of years both in terms of mechanical design and software development) through the monitoring and analysis of droplet size and phase distribution in a stainless steel pipe that does not allow visual observations. An example of the configuration is depicted in Figure 3.27. The materials were chosen so that the probe requires low maintenance and can be used extensively without changes.

Tri-Eye has been created in order to obtain phase distribution data throughout the pipe's cross-sectional area, providing information also on velocity profile and drop size distribution of the dispersed phase in a specific point at the pipe cross section. A code and software have been developed and pictures of the phases flowing through the

pipe (like the one shown in Figure E.2) can be obtained. The probe can traverse the pipe cross sectional area and obtain detailed information at any point. The innovation breakthrough is also demonstrated through Tri-Eye's ability to be used at high mixture velocities and more importantly, even in stainless steel pipes, since the technology can be implemented even on conductive materials.

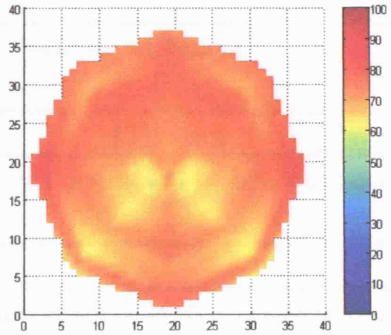

Figure E.2 Tomographic image obtained by the Tri-Eye.

TRI-EYE PRODUCTS:

If required, two different Tri-Eye products can be supplied to the customer:

- A probe that can obtain only phase distribution data/images. This can be sold at a lower price, since the accompanying software is half the software needed and the construction of the probe is simpler (single).
- A probe that can obtain all three characteristic results at the full price.

Both probes will use the same traversing mechanism (dual probe).

APPENDIX E3: PATENT PROCESS & COSTS

Figure E.3 summarises the patent process steps. The respective time frame and the cost are also included.

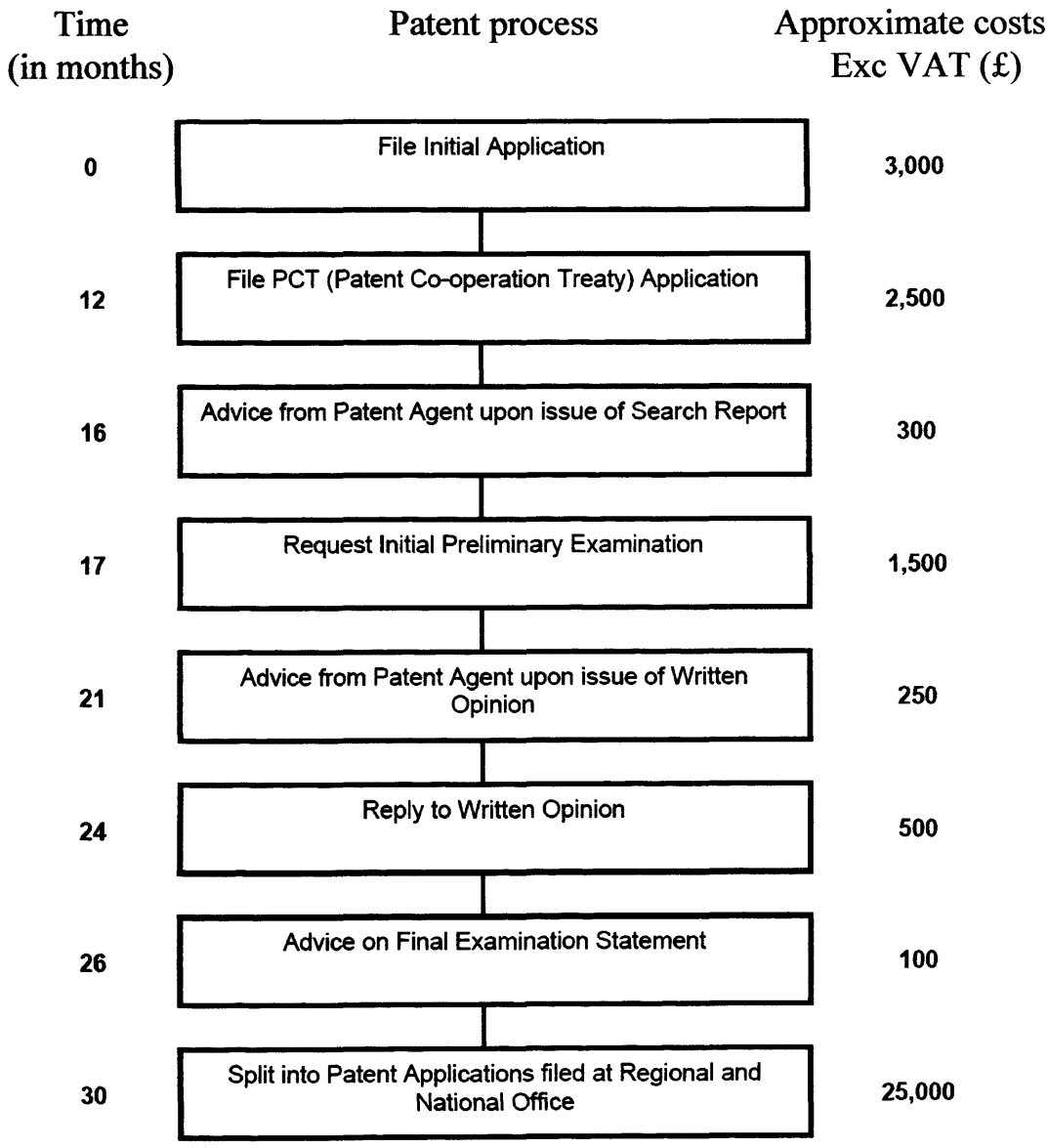

Figure E.3 Stages of filing a patent in the European market and the respective costs.

APPENDIX E4: MANAGEMENT TEAM

The team contains diverse skills and experience and is composed of individuals from both UCL and London Business School. All have a strong belief in the future of this opportunity and a personal friendship and commitment to work together towards building a highly successful business.

Table E.1 Tri-Eye's Management Team.

Karolina Ioannou	**CEO**	UCL – Chemical Engineer
Sarah Germana'	**COO**	UCL – Hydraulic Engineer
Hiroyoshi Koizumi	**CFO**	London Business School – Corporate Banker
Sanzhar Shalkarbekov	**CMO**	London Business School – Corporate Banker
Michael Webster	**CMO**	London Business School – Investment Banker

Most members of the Management Team have previous experience in the oil industry. Further details on the Management Team's education and experience are included below:

KAROLINA IOANNOU (CEO)

Education:

- Diploma in Chemical Engineering, Graduated with 78/100 in 2002, Aristotle University of Thessaloniki, Polytechnic School, Greece.
- New Venture Development, London Business School 2006.

Current Position:

- PhD student in Chemical Engineering, UCL, Project title: "Phase inversion in dispersed liquid-liquid pipe flows".
- Teaching fellow, responsible for Process Heat Transfer lecture, Engineering Experimentation and Transport Processes tutorials.

Karolina is involved in experimental studies concerning phase inversion in pipelines. During her research at UCL she designed and tested several measuring instruments for oil/water mixture characterisation. She is one of the authors of research publications in this field. Recently she was invited to NTNU, where she

performed research on different oil/water systems in difficult regime conditions. She speaks English, Greek, German and Italian.

SARAH GERMANA' (COO)

Education:

- Diploma in Hydraulic Engineering, University of Roma Tre, Rome.
- B.Eng. Civil and Environmental Engineering (96/110) in 2004.
- New Venture Development, London Business School 2006.

Current Position:

- MPhil student in Chemical Engineering, UCL, Project title: "Characterisation of reactive liquid binders in granulation processes".

Sarah has an engineering background in hydraulic instrumentation design and mechanical construction. While working in SEICO srl she developed skills in apparatus design for waste to energy plants. Her current project work is focused on the development of a new micro-mechanistic technology MFB (the Micro Force Balance) for liquid particles characterised in granulation processes.

SANZHAR SHALKARBEKOV (CMO)

Education:

- Bachelors in International Finance, Kazakh State Academy of Management. Graduated with Honours in 1999.
- MBA, London Business School, United Kingdom.

Work Experience:

- McKinsey & Company, Russia, Associate.
- European Bank For Reconstruction and Development, UK, Associate, Natural Resources team.

Sanzhar has several years of corporate & project finance experience with the oil industry. He combines a solid financial background with extensive knowledge of debt financing of emerging market oil & gas companies.

HIROYOSHI KOIZUMI (CFO)

Education:

- BA in Economics in Keio University, Tokyo, Japan. Graduated in 1997.
- MBA, London Business School, United Kingdom.

Work Experience:

- Mizuho Corporate Bank, LTD, Japan, Vice President, Power Team, Project Finance Division.
- Fuji Bank Ltd, Japan, Senior Credit Officer, Export Finance Team.

Hiroyoshi has worked for seven years as a project finance banker. His business experience covers different areas as cash flow modelling, assessment of critical financial problems and creation of new settlement administration procedures. Most recently he was an Adviser to the Japanese Ministry of Economy.

MICHAEL WEBSTER (CMO)

Education:

- MPhil in European Studies, Queens College, University of Cambridge.
- BAHons, War Studies, King's College, London. Graduated in 1995.
- MBA, London Business School, United Kingdom.

Work Experience:

- SEECAP Privatisation & Restructuring Advisory, Serbia & Montenegro, Co-founder.
- Citigroup, UK, European Investment Banking Division.
- Dept. of Political Affairs, United Nations Secretariat, New York.

Michael has six years of experience in corporate & project finance as well as company restructuring & privatisation in emerging markets. His sector experience encompasses energy, utilities & industrial manufacturing. Combining financial knowledge with extensive experience of working with both public and private sector organisations, he will take a lead CMO role.

APPENDIX E5: INDUSTRY ANALYSIS

MICRO LEVEL

The common characteristics of the competitive players are as follows:

- They are both small and big companies having strong R&D departments.
- Their margins are expected to be high and their profits can be reinvested in R&D for development of their products.
- Most of the companies sell their products directly to the end users.

Tri-Eye will compete in this industry with a strong technology, which will provide value for customers in terms of both quality and price.

MACRO LEVEL

Porter's Five Forces framework has been used to analyse the industry for Flow Analysis Instrumentation in general and the Tri-Eye probe. Figure E.4 shows the Five Forces diagramme for this industry. Each of the forces is discussed in turn below.

Threat of substitutes

Low: It must be noted that there is no standard and/or widely adopted technology for droplet size measurement even though image analysis is the technique most used. To date, developed probes are only capable of being mounted on pipe walls. Tri-Eye is an intruding technique that obtains results at specific points in the pipe cross sectional area. Thus, the threat of substitutes is assessed as relatively low.

Threat of new entry

Low: Since the core technology of our Tri-Eye probe will be protected by patent, this aspect of the industry is favourable already. There are few companies in the field, which have special technology for flow analysis and are all very specialized companies addressing specialized audiences. It requires several years and significant R&D investment for new entrants to reach the current technology level and thus Tri-Eye team concludes that this is another discouraging factor for potential new entrants.

Buyer power

Medium: Major buyers are oil companies who need to understand flow characteristics in order to better predict oil/water flows and reduce their costs. Despite

the fact that significant growth is expected in the market, the number of actual buyers will probably not increase much, potentially making current buyer power even stronger. Of course, where a supplier has an attractive technology, buyer exploitation of their power would be lessened. In the target market, price is not an issue but instead product versatility. The issue of how value created is split between the patent holder and the buyer is largely a contractual negotiation.

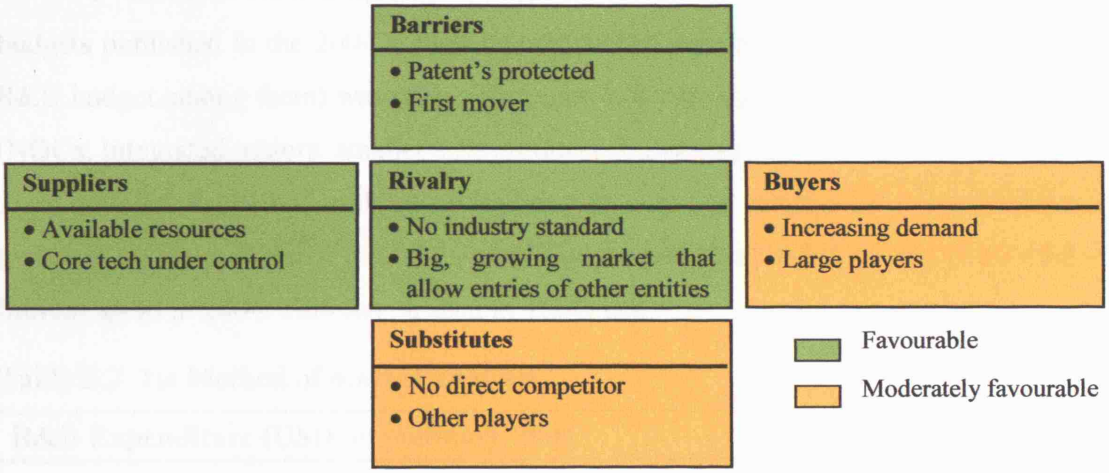

Figure E.4 Five Forces Analysis of the flow analysis instrumentation industry within the oil market segment.

Supplier power

Low: Capital, equipment and human resources are all available from a variety of sources. The most important input into the industry, i.e. the technology and the tacit knowledge related to it, is restricted to a few people, making supplier power rather favourable as well.

Rivalry

Low: This is currently low as there are no direct competitors to Tri-Eye's technology. There are some 30 companies in this industry. However, each company produces similar products, while most of them are focusing on image analysis methods that are very different and only used in limited applications. Thus, competition takes place in the limited area of the flow analysis industry.

APPENDIX E6: MARKET SIZE & ASSUMPTIONS

As a similar kind of analysis could not be found in order to estimate the market potential for similar technologies by 3rd parties and selling reports of competitor companies were not available, the following detailed analysis has been carried out.

The first step was the estimation of the *global* oil industry R&D budget with two different approaches:

1st method: As a sample the 6 larger oil companies and their respective R&D budgets published in the 2004 annual reports (with ConocoPhillips having the lowest R&D budget among them) was taken. There are 120 primary oil companies worldwide (NOCs, Integrated majors, smaller size producers). Bearing in mind the lowest budget spent by ConocoPhillips and by multiplying it with the number of primary firms (reduced by the number of the oil "sisters") gave us a proxy R&D budget (US$ 16.8 billion) spent in 2004. This can be seen in Table E.2.

Table E.2 1st Method of market analysis.

R&D Expenditure (USD, in millions), 2004	R&D budget
Exxon Mobil	$649
BP	$439
RD Shell	$553
Total	$492
Chevron	$242
ConocoPhillips	$126
There are 120 main oil players in the world (incl. 6 above)	
Min budget spent by 6 companies above	$126
Number of oil companies	114
Market size for 114 companies	$14,364
Market size for 6 companies	$2,501
Global R&D Budget	**$16,865**

2nd method: According to research published by Dr Don Paul of Chevron[E.2], the oil industry spends nearly 2% of its revenues on R&D. In order to derive a proxy number for global oil industry revenues, the global oil consumption (in tonnes) has

[E.2] http://www.oilonline.com/news/features/oe/20021105.and_anot.9965.asp

been multiplied by the average crude oil price in 2004. Both numbers have been provided by BP Statistical Review of World Energy, June 2005. Therefore, global R&D budget (US$ 21.1 billion) is calculated to be equal to 2% of generated revenues. This estimate is shown in Table E.3.

Table E.3 2nd Method of market analysis.

Estimate of Oil Industry Revenues 2004	
OPEC production (mln tonnes)	1588.20
Non-OPEC production (mln tonnes)	1720.79
Former Soviet Union production (mln tonnes)	558.88
Global Oil Production (mln tonnes)	3867.86
Global Inventory Stock (mln tones)	100.76
Global Consumption (mln tonnes)	3767.10
Crude Oil Prices ($/tonne)	$280.48
Global Revenues ($, mln)	$1,056,605.44
Global R&D Budget (2% of revenues)	**$21,132.11**

Table E.4 Estimate of Market size (in million $).

	1st method	**2nd method**
Global R&D Budget:	**16,800.00**	**21,100.00**
Production related R&D (5%)	**840.00**	**1,055.00**
Wage (50%)	**420.00**	**527.50**
Consumables (15%)	**126.00**	**158.25**
Instrumentation (35%)	**294.00**	**369.25**
Multiphase equipment market size (10%)	**29.40**	**36.93**

The second step is to calculate the percentage of the total R&D budget spent on flow analysis related instrumentation. This is conducted based on the annual published reports of the oil companies, as well as assumptions driven by personal interviews with people in the industry and a special questionnaire that has been specially prepared

for the comprehension of the market needs (see Appendix E.7 for Questionnaire analysis). More specifically:

1. 5% of the total R&D budget is allocated to oil production related research, where Tri-Eye is applicable[E.3].
2. The allocated global R&D budget is split into 3 main components [E.3,4]: (1) Wages (50%), (2) Instrumentation (35%) and (3) Consumables (15%).
3. Based on the conducted survey with scientists who are involved in fluid analysis research, instruments similar to the product will comprise nearly 10% of Instrumentation budget on average.

Based on the assumptions above, the estimated market for the product will be as follows:

Table E.5 Estimate of number of product units (in million $).

Industry average price per probe	**$15,000**	**$15,000**
Number of probes	**1,960**	**2,462**
Average number of probes (average of both)	**2,211**	

APPENDIX E7: MARKET ANALYSIS QUESTIONNAIRE

In order to better understand the needs of the market, a special questionnaire was prepared and circulated to a controlled test group of people with a technical background in multiphase flow. The questionnaire was completed by 17 people in the United Kingdom, United States, Norway and Greece. The group comprised both academics (professors and research students) as well as industry professionals from Chevron, Statoil, Scandpower and SINTEF. The sample group comprises scientists familiar with the significance, but also the difficulties of obtaining experimental results accurately in the actual pipe cross sectional area. (The questionnaire can be found at the following link: http://forms.london.edu/form.asp?id=4494).

[E.3] Interview with industry expert Dr Lee Rhyne, Chevron.
[E.4] Source: Dr Panagiota Angeli, Senior Lecturer, UCL, Prof. Stef Simmons, UCL.

A key finding of this survey was the frequency in which people involved in the field might purchase instrumentation that is related to flow analysis. (The answers to these questions are biased to some extent as some of the people in the sample are only examining theoretical aspects of multiphase flow, raising the respective percentage of people that have never bought such instrumentation up to 12%). The results are shown in Figure E.5.

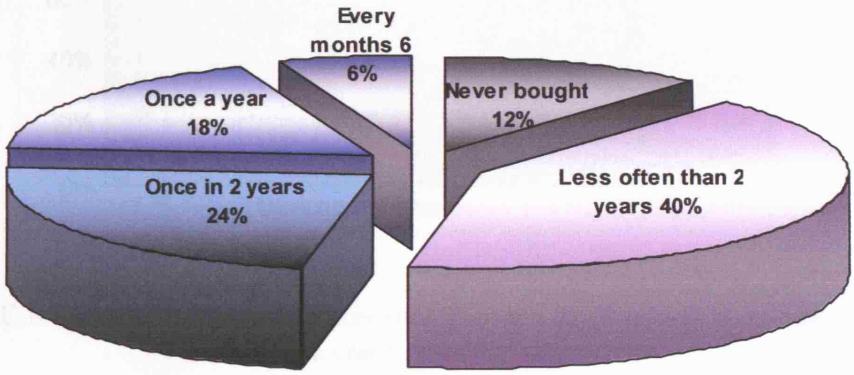

Figure E.5 Flow analysis related instrumentation purchase frequency as obtained from the results of the conducted survey.

PRODUCT FEATURE SIGNIFICANCE

One of the main objectives of this survey was to understand the significance of all three characteristic results that can be obtained from Tri-Eye and the value delivered to the potential customers. The test group was asked to answer within the range of 1 to 5, with 1 being less interesting and 5 being very interesting.

The majority of people (slightly more that 71%) that completed the questionnaire indicated that drop size distribution is a very interesting feature – assessing it with a 5. This fact re-assures the belief that drop size is one of the hardest and most controversial measurements that can be obtained in multiphase flow experiments and thus, Tri-Eye's strongest selling feature. Phase distribution is the

second most important measurement within the sample, while velocity profile is the third one in their preference.

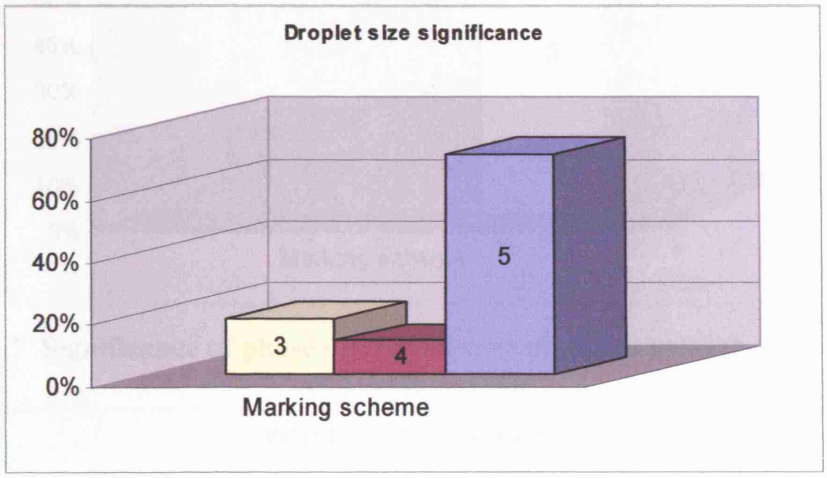

Figure E.6 Significance of drop size distribution as obtained from the results of the conducted survey.

PRICING

Furthermore, it is worth mentioning the difference in the monetary evaluation of such equipment. People working in the industry mentioned that price for instrumentation is not an issue. Moreover, people from academia indicated that they would value the product with a premium in comparison to equipment they have bought in the past; of course their budget is more limited.

OTHER PRODUCTS

It is the limitation of existing instrumentation that places Tri-Eye higher than that of the competitors. More specifically, the existing instrumentation does not satisfy the need of the customers as it is difficult to obtain results in higher mixture velocities and turbulent flows (an example of a dispersed flow and high mixture velocity is shown in Figure E.9b, while these are technologies only be applied in plastic pipes and only under specific conditions can accurate results be obtained (usually the degree of dispersion is a restriction parameter; existing instrumentation can operate better in flows depicted in Figure E.9a).

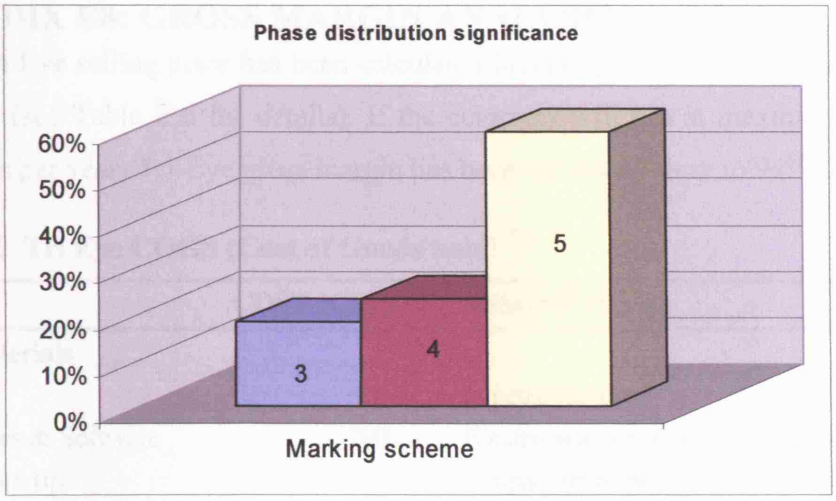

Figure E.7 Significance of phase distribution as obtained from the results of the conducted survey.

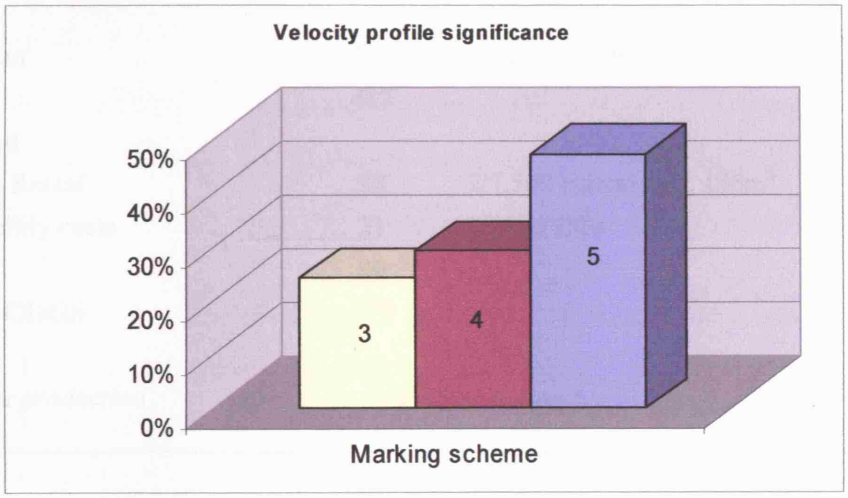

Figure E.8 Significance of velocity profile as obtained from the results of the conducted survey.

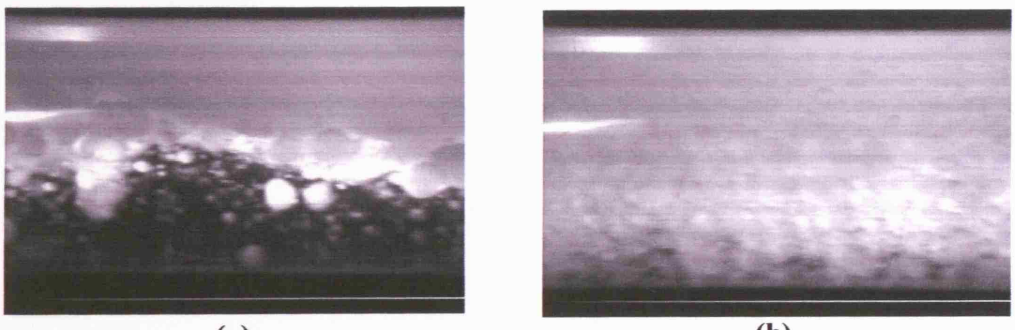

(a) **(b)**

Figure E.9 (a) Low velocity/stratified flow (b) High velocity/dispersed flow

APPENDIX E8: GROSS MARGIN ANALYSIS

Tri Eye selling price has been calculated including: raw materials, Labour and Overhead (see Table E.6 for details). If the company will run at maximum capacity (96 probes per year) Tri-Eye gross margin has been estimated close to 94%.

Table E.6 Tri Eye COGS (Cost of Goods Sold) [E.5].

ITEMS	COST (GBP)	ASSUMPTION
Raw Materials		
Steel	42	1 metre required
Electronics & Software	200	Electronics box & associated software
Aluminium tip	6	Forms part of probe tip
Platinum Wire	15	Forms part of probe tip
	263	
Labour		
Technician	417	2 employed fulltime (2 x £20k)
	417	
Overhead		
Facilities Rental	78	£ 7,500 annual rent, 150m^2
Other facility costs	21	£2,000 Bills
	99	
PROBE COGS	**779**	
Maximum production capacity	*96*	*probes per year*

[E.5] Tri-Eye has used direct costing, allocating total labour and overhead costs to each probe produced.

APPENDIX E9: COMPETITION

COMPETING TECHNOLOGIES

Optical/light scattering methods: The Phase Doppler Method is based upon the principles of light scattering interferometry. Measurements are made at a small, non-intrusive optical probe volume defined by the intersection of two laser beams. As a particle passes through the probe volume, it scatters light from the beams into a multi-detector receiving probe, strategically located at an off-axis collection angle. The phase shift between the Doppler burst signals from different detectors is proportional to the size of the spherical particles (representing companies: TSI, DANTEC). Two or more detectors collect the light scattered by single particles passing through the measurement volume. Very often they are referred to as Particle Dynamics Analysis (PDA) or as Phase Doppler Particle Analyser (PDPA).

Imaged analysis (photographic) methods: the general idea is that flash photographs of the flow are taken, and then analysed to obtain element size. Usually, a short flash of light from a laser illuminates a screen, which acts as a bright background behind the subject spray. The short pulse from the laser freezes the motion of the droplet, allowing blur-free visualisation of drop size and shape. Images from the digital camera are transferred to a computer and high-speed real-time particle sizing software analyses the images obtained in order to build up a drop size distribution. By double-pulsing the laser in a technique similar to PIV, particle size vs. velocity distributions may also be measured (company: Oxford Lasers).

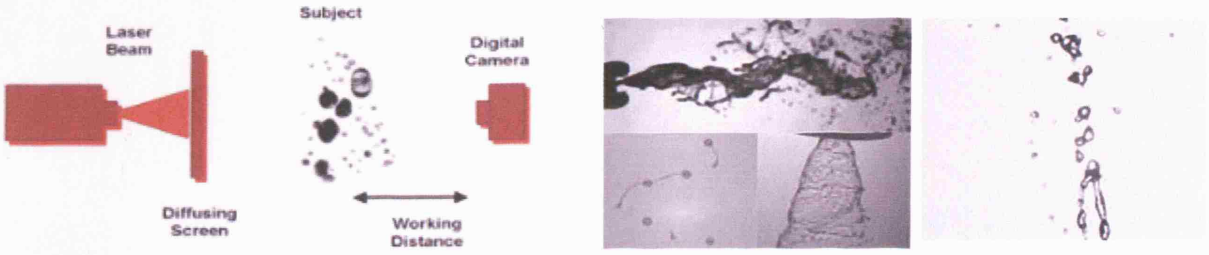

Figure E. 10 Image analysis methods.

Impingement Coating Technique: if a plate coated with soft magnesium oxide is held in a droplet flow, then holes are made in the magnesium oxide film by the impinging droplets. The size of the holes is slightly greater than that of the droplets. This method is not in use any more but has been used extensively in the past.

Electrical methods: if a droplet impinges an electrically charged wire, there is an instantaneous withdrawal of charge from the wire that can be recorded electronically (Tri-Eye). The use of electrical methods is very commonly used for obtaining tomographic images, and more specifically the Electrical Capacitance Tomography, which allows the concentration distribution of dielectric materials inside closed vessels to be viewed, measured and captured at high frame rates (Process Tomography Ltd). Other methods used are the electrical resistance tomography (Industrial Tomography Systems Ltd.) and electromagnetic Tomography that is mostly used in medicine.

There are some 30 companies producing flow analysis instrumentation. Leading players are listed below.

Table E. 7 Some competitors of Tri-Eye.

COMPANY	TECHNOLOGY	ADVANTAGES	PRICE (GBP' 000)	Tri-Eye's answer
DANTEC DYNAMICS (DK)	PDA: Particle Dynamic Analysis	Size, velocity and concentration of spherical particles, droplets or bubbles (analysis of strays)	**£80**	• System can only be applied in pipes under conditions. • Not applicable in opaque systems.
DANTEC DYNAMICS (DK)	LDA:Laser Doppler Anemometry	Velocity and turbulence profiles Non intrusive measurement High spatial and temporal resolution, no calibration	**£18**	• Does not give droplet size distribution
Oxford Lasers (UK)	Image analysis	Drop size distributions	**£45-50**	• System can only be applied in pipes under conditions. • Not applicable in opaque systems
TSI (US)	Scattering method (PDA)	Drop size distribuition/Velocity profiles	**£70**	• System can only be applied in pipes under conditions. • Not applicable in opaque systems
Kaiku (UK)	Impedance spectroscopy	Hold-up Change of chemical composition Non intrusive	**£15**	• Only working when mounted on a non-conductive material
Forschungszentrum Rossendorf (DE)	Optical tomography	Cross sectional images of temporal and time integral time distribution, non invasive technique,	**n.a.**	• Void up to 10%, oprical probe can easily be fouled, rays can be interrupted
Forschungzentrum Rossendorf (DE)	Conductivity Probes	Flow distributions	**18**	• Large tip/very disruptive/works in gas water flows/limited range/not traversing, no drop size
Mettler Toledo Lasentec® FBRM® and PVM® (US)	Scattering method (PDA)	Phase distribution/ drop size analysis	**70**	• Only applied in limited applications.

APPENDIX E10: SENSITIVITY ANALYSIS

NPV Analysis		Terminal Value Factor												
5,914,304.41		1.00	1.50	2.00	2.50	3.00	3.50	4.00	4.50	5.00	5.50	6.00	6.50	7.00
Discount Factors	20%	5,914,304	6,412,957	6,911,610	7,410,263	7,908,915	8,407,568	8,906,221	9,404,874	9,903,526	10,402,179	10,900,832	11,399,485	11,898,137
	25%	4,630,583	4,990,306	5,350,029	5,709,752	6,069,475	6,429,198	6,788,921	7,148,644	7,508,367	7,868,089	8,227,812	8,587,535	8,947,258
	30%	3,667,614	3,930,460	4,193,306	4,456,152	4,718,998	4,981,844	5,244,690	5,507,536	5,770,382	6,033,228	6,296,074	6,558,920	6,821,766
	35%	2,935,265	3,129,612	3,323,959	3,518,306	3,712,654	3,907,001	4,101,348	4,295,695	4,490,042	4,684,389	4,878,736	5,073,083	5,267,430
	40%	2,371,242	2,516,528	2,661,814	2,807,100	2,952,386	3,097,672	3,242,958	3,388,244	3,533,530	3,678,816	3,824,102	3,969,388	4,114,675
	45%	1,931,792	2,041,516	2,151,241	2,260,965	2,370,690	2,480,415	2,590,139	2,699,864	2,809,589	2,919,313	3,029,038	3,138,763	3,248,487
	50%	1,585,723	1,669,383	1,753,043	1,836,703	1,920,363	2,004,024	2,087,684	2,171,344	2,255,004	2,338,664	2,422,324	2,505,984	2,589,644
	55%	1,310,493	1,374,850	1,439,207	1,503,564	1,567,921	1,632,277	1,696,634	1,760,991	1,825,348	1,889,705	1,954,062	2,018,418	2,082,775
	60%	1,089,597	1,139,518	1,189,440	1,239,361	1,289,283	1,339,205	1,389,126	1,439,048	1,488,969	1,538,891	1,588,813	1,638,734	1,688,656
	65%	910,805	949,833	988,861	1,027,889	1,066,917	1,105,945	1,144,973	1,184,001	1,223,029	1,262,057	1,301,085	1,340,113	1,379,141
	70%	764,955	795,691	826,428	857,165	887,901	918,638	949,375	980,111	1,010,848	1,041,585	1,072,321	1,103,058	1,133,795
	75%	645,110	669,485	693,860	718,235	742,610	766,984	791,359	815,734	840,109	864,484	888,859	913,234	937,609
	80%	545,966	565,423	584,879	604,336	623,793	643,249	662,706	682,162	701,619	721,076	740,532	759,989	779,446
	85%	463,431	479,058	494,685	510,312	525,939	541,566	557,193	572,820	588,446	604,073	619,700	635,327	650,954
	90%	394,319	406,944	419,569	432,193	444,818	457,442	470,067	482,692	495,316	507,941	520,566	533,190	545,815
	95%	336,132	346,388	356,643	366,899	377,155	387,411	397,667	407,923	418,179	428,434	438,690	448,946	459,202

IRR Analysis	Terminal Value Factor												
	1.00	1.50	2.00	2.50	3.00	3.50	4.00	4.50	5.00	5.50	6.00	6.50	7.00
188%	188%	189%	189%	190%	190%	191%	191%	192%	192%	193%	193%	194%	194%

IRR Analysis		Sales volume change (%)												
	188%	-80%	-70%	-60%	-50%	-40%	-30%	-20%	-10%	0%	10%	20%	30%	40%
Price change (%)	-50%	1%	24%	41%	55%	67%	78%	88%	97%	106%	115%	123%	132%	140%
	-45%	7%	30%	47%	61%	74%	85%	96%	106%	116%	125%	134%	143%	151%
	-40%	12%	36%	53%	68%	81%	93%	104%	114%	125%	134%	144%	153%	162%
	-35%	17%	40%	58%	74%	87%	100%	111%	122%	133%	144%	154%	163%	173%
	-30%	21%	45%	64%	79%	93%	106%	119%	130%	142%	153%	163%	173%	183%
	-25%	25%	50%	69%	85%	99%	113%	126%	138%	150%	161%	172%	183%	194%
	-20%	29%	54%	73%	90%	105%	119%	133%	146%	158%	170%	181%	193%	204%
	-15%	33%	58%	78%	95%	111%	125%	139%	153%	166%	178%	190%	202%	214%
	-10%	37%	62%	82%	100%	116%	131%	146%	160%	173%	186%	199%	211%	224%
	-5%	40%	66%	86%	105%	121%	137%	153%	167%	181%	194%	207%	221%	233%
	0%	43%	69%	91%	109%	127%	143%	159%	174%	188%	202%	216%	230%	243%
	5%	46%	73%	95%	114%	132%	149%	165%	180%	195%	210%	225%	239%	253%
	10%	49%	76%	98%	118%	137%	155%	171%	187%	203%	218%	233%	248%	262%
	15%	52%	80%	102%	123%	142%	160%	177%	194%	210%	226%	241%	257%	272%
	20%	55%	83%	106%	127%	147%	166%	183%	200%	217%	233%	250%	265%	281%
	25%	57%	86%	110%	132%	152%	171%	189%	207%	224%	241%	258%	274%	291%

APPENDIX E11: BASE CASE PROJECTIONS

Income Statement	**2007**	**2008**	**2009**	**2010**	**2011**	**2012**
Revenue	335,725	1,072,718	2,616,004	5,092,069	6,158,440	6,451,180
Cost of sales	(46,580)	(60,876)	(132,526)	(267,364)	(290,959)	(301,123)
Gross profit	289,145	1,011,842	2,483,479	4,824,704	5,867,481	6,150,057
Marketing & Distribution Costs	(14,650)	(24,820)	(45,712)	(79,024)	(93,549)	(97,767)
Administrative expenses	(187,706)	(143,585)	(147,911)	(151,973)	(156,147)	(160,436)
Profit from operations	86,789	843,438	2,289,855	4,593,707	5,617,785	5,891,854
Net Financing Cost	2,554	8,767	28,917	71,419	131,229	195,267
Profit before tax	89,343	852,204	2,318,772	4,665,126	5,749,014	6,087,121
Corporate income tax expense	(26,803)	(255,661)	(695,632)	(1,399,538)	(1,724,704)	(1,826,136)
Profit after tax	62,540	596,543	1,623,141	3,265,588	4,024,310	4,260,985

Balance Sheet						
	2007	**2008**	**2009**	**2010**	**2011**	**2012**
Assets						
Non-current Assets						
Property, plant and equipment	1,883	1,695	1,506	1,318	1,130	942
Goodwill	0	0	0	0	0	0
Deferred tax	0	0	0	0	0	0
	1,883	1,695	1,506	1,318	1,130	942
Current Assets						
Inventories	339	1,082	2,639	5,137	6,212	6,508
Trade and other receivables	27,594	88,169	215,014	418,526	506,173	530,234
Cash and cash equivalents	196,197	850,152	2,568,878	5,987,902	10,089,096	14,377,327
	224,130	939,403	2,786,531	6,411,565	10,601,482	14,914,069
Total assets	226,013	941,098	2,788,038	6,412,883	10,602,611	14,915,010
Equity and Liabilities						
Capital and Reserves						
Issued ordinary share capital	150,000	150,000	150,000	150,000	150,000	150,000
Issued preferred share capital	0	0	0	0	0	0
Share premium	0	0	0	0	0	0
Retained earnings	62,540	659,084	2,282,224	5,547,812	9,572,122	13,833,107
	212,540	809,084	2,432,224	5,697,812	9,722,122	13,983,107
Non-Current liabilities						
Long term debt	0	0	0	0	0	0
Differed tax	141	191	214	217	205	182
	141	191	214	217	205	182
Current Liabilities						
Interest bearing loans and borrowings	0	0	0	0	0	0
Trade and other payables	0	4,017	7,796	15,087	17,927	18,642
Tax payable	13,331	127,806	347,804	699,767	862,358	913,080

	13,331	131,823	355,600	714,854	880,285	931,722
Total equity and liabilities	226,013	941,098	2,788,038	6,412,883	10,602,611	14,915,010
Retained Earnings						
Opening retained earnings	0	62,540	659,084	2,282,224	5,547,812	9,572,122
Net profit for the year	62,540	596,543	1,623,141	3,265,588	4,024,310	4,260,985
Preference dividends	0	0	0	0	0	0
Ordinary dividends	0	0	0	0	0	0
Closing retained earnings	62,540	659,084	2,282,224	5,547,812	9,572,122	13,833,107

Cash Flow (Direct method)

	2007	2008	2009	2010	2011	2012	
Sales		308,131	1,012,143	2,489,159	4,888,557	6,070,793	6,427,119
Raw material cost		(6,225)	(15,534)	(43,646)	(84,488)	(106,214)	(112,691)
Labour cost		(40,694)	(42,067)	(86,659)	(178,083)	(182,981)	(188,013)
Marketing & Distribution cost		(14,650)	(24,820)	(45,712)	(79,024)	(93,549)	(97,767)
Administrative salary costs		(127,169)	(131,461)	(135,404)	(139,128)	(142,954)	(146,885)
Other administrative costs		(46,037)	(2,103)	(2,166)	(2,226)	(2,287)	(2,350)
Rent and rates		(14,500)	(9,833)	(10,152)	(10,431)	(10,718)	(11,013)
Tax paid during the year		(13,331)	(141,137)	(475,610)	(1,047,572)	(1,562,125)	(1,775,438)
Interest on cash		2,554	8,767	28,917	71,419	131,229	195,267
Cashflow from Operations	48,080	653,955	1,718,726	3,419,024	4,101,194		4,288,231
Capex (new production line)		(1,883)	0	0	0		0
Cashflow from Investments	(1,883)	0	0	0	0		0
Nominal value of ordinary shares issued		150,000	0	0	0	0	0
Nominal value of preference shares issued		0	0	0	0	0	0
Nominal value of preference shares redeemed		0	0	0	0	0	0
Premium on ordinary shares issued		0	0	0	0	0	0
Preference dividend paid		0	0	0	0	0	0
Ordinary dividend paid		0	0	0	0	0	0
Cashflow from Financing	150,000	0	0	0	0	0	
Net Cash Flow	196,197	653,955	1,718,726	3,419,024	4,101,194	4,288,231	